Progressive orogenic deformation and metamorphism along the Combin Fault and Dent Blanche Basal Thrust in the Swiss-Italian Western Alps

Dissertation
zur
Erlangung des Doktorgrades (Dr. rer. nat.)
der
Mathematisch-Naturwissenschaftlichen Fakultät
der
Rheinischen Friedrich-Wilhelms-Universität Bonn

vorgelegt von
FREDERIK KIRST
aus
Bonn

Bonn 2014

Angefertigt mit Genehmigung der Mathematisch-Naturwissenschaftlichen Fakultät der Rheinischen Friedrich-Wilhelms-Universität Bonn.

1. Gutachter: PD Dr. Thorsten Nagel
2. Gutachter: Prof. Dr. Thorsten Geisler-Wierwille
Tag der Promotion: 06.02.2015
Erscheinungsjahr: 2015

„I will not live under a shadow of fear,
never be crippled by chaos and doubt,
fall prey to your madness.

I am not shattered,
out of the ashes I rise
knowing that nothing is stronger than faith,
finding hope in our hopeless lives.“

- John Petrucci -

Abstract

In the Western Alps of Switzerland and Italy, a stack of oceanic and continental units assembled during Late Cretaceous – Paleogene Alpine subduction, exhumation, and accretion. In the study area in the southern Valais and northern Aosta regions, oceanic units from the Piemont-Ligurian (South-Penninic) domain, the Combin zone and Zermatt-Saas zone, and continental units from the Adriatic continental margin, the Dent Blanche nappe, represent the structurally highest units of this nappe pile. These are separated from each other by two major Alpine tectonic contacts, the Combin Fault and the Dent Blanche Basal Thrust (DBBT). Structural and petrological analyses of shear zones along the two contacts were performed to deduce the structural evolution of the tectonic units and the sequence of deformation in the tectonic context of the Western Alps.

At Lago di Cignana in the western Valtournenche of Italy, (U)HP rocks of the upper Zermatt-Saas zone are exposed and overlain by greenschist-facies rocks of the Combin zone and the lower Dent Blanche nappe. Structural analyses revealed a progressive structural evolution from (U)HP to greenschist-facies conditions related to Paleogene syn- to post-exhumational deformation. Early exhumation of the Zermatt-Saas zone after the peak of (U)HP metamorphism at ca. 43 Ma occurred during normal-sense top-E shearing under eclogite- to upper greenschist-facies conditions. Exhumation to mid-crustal levels and juxtaposition with the overlying Combin zone occurred along greenschist-facies top-SE shear zones. Strain was mainly localized along the uppermost Zermatt-Saas zone and top-SE structures along the Combin Fault have been partly obliterated by subsequent deformation. Top-SE shearing was followed by a phase of pure shear deformation affecting units in the footwall and hanging wall of the Combin Fault. This phase was followed by top-NW shearing associated with renewed thrusting along the DBBT which continued until low-grade greenschist-facies conditions. A phase of dominant pure shear deformation after juxtaposition of the Combin and Zermatt-Saas zones may have led to the development of conjugate top-SE and top-NW shear zones on a regional scale within the Combin zone. This offers an explanation for contradicting views regarding the nature of the Combin Fault and the Combin zone, i.e. whether they represent thrust-related or normal-sense shear zones.

Whereas deformation under (U)HP conditions can be well studied within rocks of the Zermatt-Saas zone, the overlying Combin zone and lower Dent Blanche nappe show a strong greenschist-facies overprint which largely obliterated early HP-related deformation and metamorphism. The Becca d'Aver continental sliver (BACS) in the western Valtournenche of Italy represents a continental fragment from the former Piemont-Ligurian/Adriatic ocean-continent transition and is structurally located at the Combin/Dent Blanche boundary. Prograde blueschist-facies assemblages are partly preserved within metasediments of the BACS and yield peak conditions around 1.7 GPa and 500° C. Petrological, microstructural, and thermodynamic investigations suggest that prograde metamorphism was linked to progressive breakdown of lawsonite, associated water release, and fluid-mediated element transfer and mineral growth. Kinematic indicators suggest top-NW shearing during prograde metamorphism and SE-directed subduction. Deformation structures within the BACS and the underlying Combin zone suggest a common structural evolution and complex kinematics on the

retrograde path related to greenschist-facies top-(W)NW and top-(E)SE shearing. The last ductile deformation was related to top-NW shearing which evolved into brittle NW-SE extension.

Most of the deformation observed in the study area occurred under greenschist-facies conditions and variably affected the northwestern and southeastern realms. The overall sequence of deformation and structural evolution of the tectonic units has been deduced from analyses of shear zones along the Combin Fault and DBBT and partly within the Combin zone. The main stage of nappe stacking and ductile top-(N)W shearing between ca. 48 and 44 Ma (D1) was related to exhumation of the Dent Blanche nappe and Combin zone, formation of greenschist-facies mylonites along the DBBT, and a pervasive greenschist-facies overprint. This phase was followed by transpressional to orogen-parallel top-(S)W shearing between ca. 43 and 40 Ma (D2). Top-(S)W shearing especially affected the northwestern Combin Fault and occurred during ongoing exhumation of the Combin zone. The DBBT was probably characterized by continuing top-W shearing during early stages of this phase. Normal-sense top-SE shearing between ca. 39 and 37 Ma (D3) affected the northwestern Combin zone but only very locally the DBBT. Top-SE shear senses are subordinate in the southeastern realm and can locally be observed along the Combin Fault and at higher structural levels within the Combin zone. Top-SE shearing is held responsible for juxtaposition of the Combin zone and underlying (U)HP rocks of the Zermatt-Saas zone at crustal levels. It was followed by renewed top-NW shearing and folding from ca. 35 Ma onwards (D4) as a result of reactivation of the DBBT as out-of-sequence thrust. This phase was followed by brittle NW-SE extension after ca. 30 Ma (D5) due to updoming of the Vanzone antiform southeast of the study area.

This study suggests that progressive orogenic deformation and metamorphism are recorded within shear zones along the Combin Fault and DBBT. However, early stages of the Alpine orogenic cycle have been largely obliterated by subsequent greenschist-facies deformation and retrogression. The proposed structural evolution suggests that the Combin zone and Dent Blanche nappe experienced a common retrograde evolution and penetrative top-(N)W shearing after an early blueschist-facies imprint and subduction-related top-NW shearing. Subsequent exhumation of the Zermatt-Saas zone from (U)HP depths occurred during normal-sense top-E shearing. Juxtaposition with the overlying Combin zone at crustal levels occurred along greenschist-facies top-SE shear zones. The relative chronology between greenschist-facies top-NW and top-SE shearing is often difficult to establish. Structural observations suggest that top-NW and top-SE shear zones may have partly overlapped in space and time due to a large pure shear component during greenschist-facies deformation, especially around 36 Ma during the transition from normal-sense shearing to renewed thrusting. A late phase of top-NW shearing due to out-of-sequence reactivation of the DBBT affected units in the study area before the onset of brittle deformation.

Contents

- CHAPTER 1 -

- CHAPTER 2 -

- CHAPTER 3 -

- CHAPTER 4 -

- CHAPTER 5 -

List of figures

List of tables

- CHAPTER 1 -

Introduction

1.1 Progressive deformation and metamorphism in Alpine-type orogens

Alpine-type orogeny is the result of subduction of oceanic lithosphere underneath an active continental margin, subsequent subduction of continental crust, and final collision between two converging continental lithospheric plates. Growth of the orogen mostly occurs as a result of accretion of crustal or even lithospheric units to the active continental margin. These units may be detached from the downgoing plate at an early stage and immediately be accreted to the orogen or they may be subducted to great depths and experience metamorphism. Subduction zones are tectonic settings that are characterized by low geotherms and therefore (ultra)high-pressure ((U)HP) metamorphism (e.g. Agard et al., 2009; Fig. 1.1a). Subducted and exhumed units often experience clockwise pressure/temperature (PT) paths with blueschist- and eclogite-facies metamorphism on the prograde path during subduction and a retrograde path during exhumation which can either be cold, isothermal, or show further heating (Fig. 1.1b). An often discussed topic in the case of Alpine-type orogens is the exhumation of (ultra)high-pressure rocks, especially the mechanisms, rates, and kinematics of processes bringing deeply-subducted rocks back to the earth's surface (e.g. Froitzheim et al., 2003; Yamato et al., 2008; Warren et al., 2008; Agard et al., 2009; Husson et al., 2009; Kylander-Clark et al., 2012). Progressive underthrusting of oceanic and continental units and contemporaneous exhumation and accretion along the active continental margin leads to stacking of tectonic units derived from different paleogeographic domains. Tectonic units which have been transported over long distances are called "nappes" in Alpine geology and are separated from each other by tectonic contacts. Orogenic deformation is therefore often localized along such tectonic boundaries so that ductile shear zones at deeper crustal and lithospheric levels form preferentially along first-order nappe boundaries. Tectonic contacts and associated shear zone may also be reactivated, overprinted, or cut by shear zones that form during subsequent deformational events. Deformation can thus occur during all stages of the orogenic cycle and can be associated with compressional, extensional, or strike-slip tectonics. Different geodynamic scenarios have been proposed for the spatial and temporal distribution of shortening and extension in orogens from crustal- to lithospheric scale deformation modes (e.g. Lister and Forster, 2009; Beltrando et al., 2007a) to buoyancy-driven relative movement of individual crustal units (e.g. Wheeler et al., 2001; Froitzheim et al., 2003). The relationship between orogenic deformation and metamorphism can often be used to attribute deformational events to metamorphic conditions on the prograde or retrograde path. Late pervasive retrogression and deformation, however, can also obliterate earlier deformation phases and metamorphic stages so that reconstruction of the tectonic history may be hindered.

Deformation along ductile shear zones results in the formation of planar (foliations) and linear (stretching lineations) fabric elements (e.g. Lister and Williams, 1979; Lloyd et al., 1992). Their formation, however, does not occur instantaneously but is usually the product of progressive deformation during prolonged shear zone activity or even subsequent deformation phases. Two

theoretical endmember geometries for two-dimensional flow in ductile shear zones exist. The first one, simple shear (Fig. 1.2a), is characterized by rotation of lines parallel to the principle strain axes, i.e. the principle stretching and shortening axes, away from their original position (Fossen, 2010). This mechanism is therefore also referred to as rotational or non-coaxial deformation. The second geometry, pure shear (Fig. 1.2b), is a perfect coaxial deformation and is characterized by constant parallelism between the principle strain axes and the original position of marker lines during all stages of progressive deformation (Fossen, 2010). Any mixture of the two geometries is called general shear or subsimple shear (Fig. 1.2c).

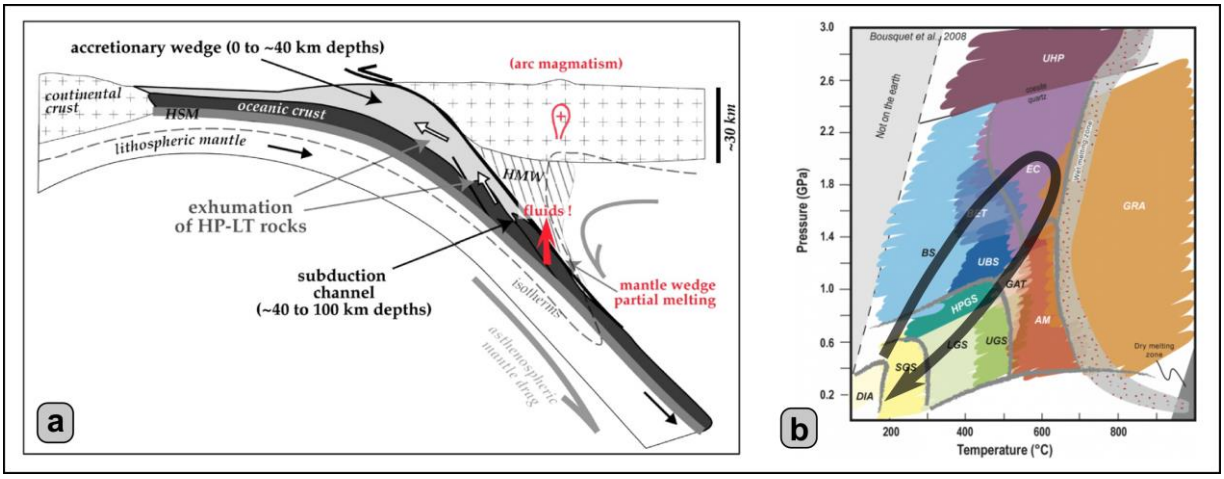

Figure 1.1: a) Schematic cross-section through a subduction zone showing features like accretionary wedge formation, detachment of crustal slivers from the downgoing plate, fluid-release at depth, and arc magmatism; from Agard et al. (2009). b) Metamorphic facies diagram with an exemplary clockwise PT-path; DIA: Diagenesis, SGS: Sub-greenschist facies, LGS: lower greenschist facies, UGS: upper greenschist facies, HPGS: high-pressure greenschist facies, BS: blueschist facies, UBS: upper blueschist facies, BET: blueschist/eclogite facies transition, EC: eclogite facies, UHP: ultrahigh-pressure metamorphism, GAT: garnet amphibolite facies, AM: amphibolite facies, GRA: granulite facies; modified from Bousquet et al. (2008).

An important step for the reconstruction of the structural evolution of tectonic units is the determination of the kinematics and the bulk shear sense along tectonic contacts and shear zones, i.e. the transport direction of a distinct unit. This direction, and therefore the vergence of shearing in ductile shear zones, can be inferred from kinematic indicators such as asymmetrically deformed minerals, shear bands, and oblique foliations (e.g. Platt and Vissers, 1980; Lister and Snoke, 1984; Passchier and Trouw, 2005). These are most abundant in simple shear zones since their formation largely depends on the degree of rotational (non-coaxial) deformation. The kinematics within pure shear zones on the other hand are more complicated and less well understood since they are by definition devoid of relative movement between adjacent blocks. Overall pure shear may, however, be localized into smaller conjugate simple shear zones. Pure shear deformation can be an important process leading to changes in shear zone or nappe geometry. The geometry of deformation within a particular shear zone, i.e. the degree of rotation, can be approximated by the relative abundance of asymmetric or symmetric deformation structures. More detailed information can often be obtained by texture analysis, i.e. the measurement of crystallographic preferred orientations, (e.g. Schmid and Casey, 1986; Leiss et al., 2000; Pleuger et al., 2009). Metamorphic conditions during deformation can be constrained by the occurrence of diagnostic minerals and assemblages which have grown, been deformed, or overprinted. Also, deformation mechanisms, recrystallization mechanisms of quartz (e.g.

Stipp et al., 2002), and the degree of ductility can be used to infer the metamorphic grade during shearing. Deformation can also increase and channelize fluid flow and thus trigger and enhance metamorphic reactions (e.g. Terry and Heidelbach, 2006; Konrad-Schmolke et al., 2011a).

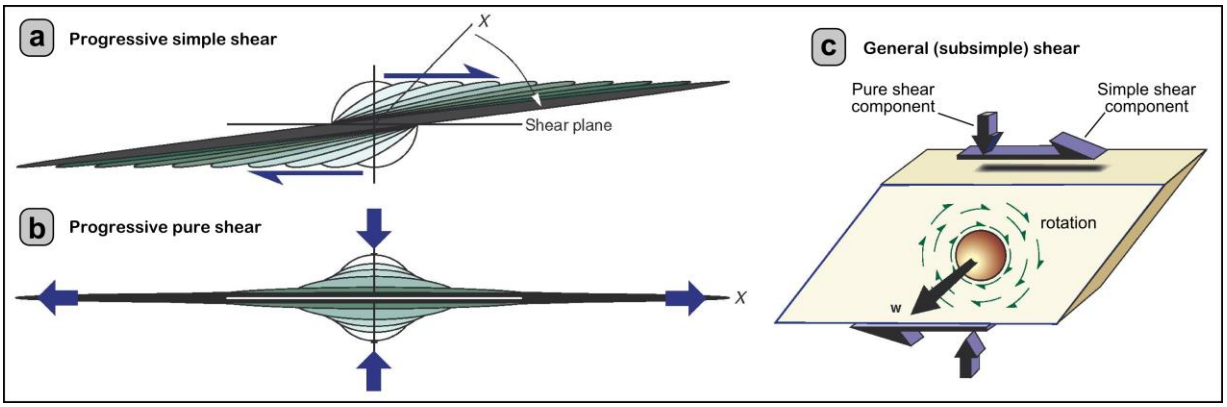

Figure 1.2: Principle geometries of progressive simple shear (a), pure shear (b), and general (subsimple) shear; from Fossen (2010).

Analyses of the kinematics, geometry, and distribution of shear zones in Alpine-type orogens are necessary for reconstructing the structural evolution of tectonic units and the relative chronology of shearing events during progressive orogenic deformation. In the context of this thesis, the term "progressive orogenic deformation" means that deformation does not occur during a singular event but occurs and evolves progressively in the course of shear zone development and subsequent shearing events over the entire orogenic cycle. Information about the metamorphic evolution of tectonic units and the metamorphic grade of deformation structures and PT-conditions during shearing events can help to establish the sequence of deformation and reconstruct the tectonometamorphic evolution for tectonic units.

1.2 The study area in the Swiss-Italian Western Alps

The European Alps (Fig. 1.3) are the classic example for Alpine-type orogens and the result of subduction of oceanic basins and continental crust and subsequent collision of the European and Adriatic continental margins. The study area is located in the southern Valais and northern Aosta regions of Switzerland and Italy, respectively, roughly between the Rhône valley in the north and the Aosta valley in the south (Fig. 1.3). This area has been the site of many studies dealing with the structural, metamorphic, and geochronological evolution of the exposed tectonic units since the famous works of Argand (e.g. Argand, 1916). Often addressed topics are the geodynamic evolution, tectonic and paleogeographic reconstructions (e.g. Froitzheim et al., 1996; Marchant and Stampfli, 1997; Dal Piaz, 1999; Rosenbaum and Lister, 2005; Beltrando et al., 2010a; Handy et al., 2010; Gasco et al., 2013) and the overall geometry and structure of the Western Alps (Escher et al., 1993; Escher & Beaumont, 1997; Schmid et al., 1996; Schmid and Kissling, 2000; Schmid et al., 2004). Other important topics include the grade and distribution of metamorphism in the Western Alps (e.g. Bousquet et al., 2004 and references therein; Bousquet et al., 2008), especially (U)HP-metamorphism (see Beltrando et al., 2010b for a review), the age of subduction-related metamorphism (see Berger and Bousquet, 2008 for a review), and the influence of rift-inheritance and pre-orogenic paleogeography on Alpine orogeny (e.g. Froitzheim and Manatschal, 1996; Beltrando et al., 2010c;

Beltrando et al., 2014). In this section, only a rough geological and tectonic overview is given. More detailed descriptions are given in chapters 2 – 4.

Figure 1.3: Overview map of the European Alps with location of the study area in southern Switzerland (southern Valais region) and northern Italy (northern Aosta region).

In the Western Alps, continental and oceanic units derived from different paleogeographic domains are exposed (Figs. 1.4 and 1.5). These were assembled during Late Cretaceous – Paleogene subduction, exhumation, and accretion along the Adriatic continental margin. Subsequent collision of the European and Adriatic plates and associated backfolding strongly modified the geometry of the nappe stack (e.g. Escher et al., 1993; Fig. 1.5a). The Late Cretaceous paleogeographic configuration before the onset of SE-directed Alpine subduction (Fig. 1.5c) was characterized from southeast to northwest by the Adriatic continental margin (Austroalpine domain), the Piemont-Ligurian ocean (South-Penninic domain), the Briançonnais continental spur (Middle-Penninic domain), the Valais basin (North-Penninic domain), and the European continental margin (Sub-Penninic domain) (e.g. Stampfli et al., 2002; Schmid et al., 2004; Handy et al., 2010).

In the study area, two major Alpine tectonic contacts, the Combin Fault and the Dent Blanche Basal Thrust (DBBT), are exposed (Figs. 1.5a and 1.6). The DBBT separates the continental Dent Blanche nappe in the hanging wall from the mainly ocean-derived Combin zone in the footwall. The Combin Fault separates the Combin zone from the continental St. Bernhard nappe system in the northwest and the ophiolitic Zermatt-Saas zone in the southeast. The Dent Blanche nappe is the structurally highest unit in the Western Alps together with the Sesia nappe from which it is separated by erosion. The Dent Blanche/Sesia nappe system is probably derived from one or more continental fragments which were separated from the Adriatic continental margin during Jurassic rifting (Froitzheim et al., 1996; Dal Piaz et al., 2001; Babist et al., 2006). The Dent Blanche/Sesia nappe system comprises several subunits consisting of Paleozoic basement and Permo-Mesozoic cover sequences (e.g. Gardien et al., 1994; Monjoie et al., 2005; Babist et al., 2006; Manzotti, 2011). The Alpine metamorphic overprint increases from northwest to southeast so that the Dent Blanche nappe experienced Alpine blueschist-facies metamorphism (e.g. Ballèvre et al., 1986; Manzotti et al., 2014) whereas rocks of the Sesia nappe display abundant eclogite-facies assemblages (e.g. Lardeaux and Spalla, 1991). The peak of the

Alpine high-pressure imprint in the Sesia nappe has been dated at ca. 70 – 65 Ma (e.g. Inger et al., 1996; Rubatto et al., 1999). The Dent Blanche nappe shows a strong pervasive greenschist-facies overprint, especially along shear zones (Oberhänsli and Bucher, 1987; Manzotti et al., 2014).

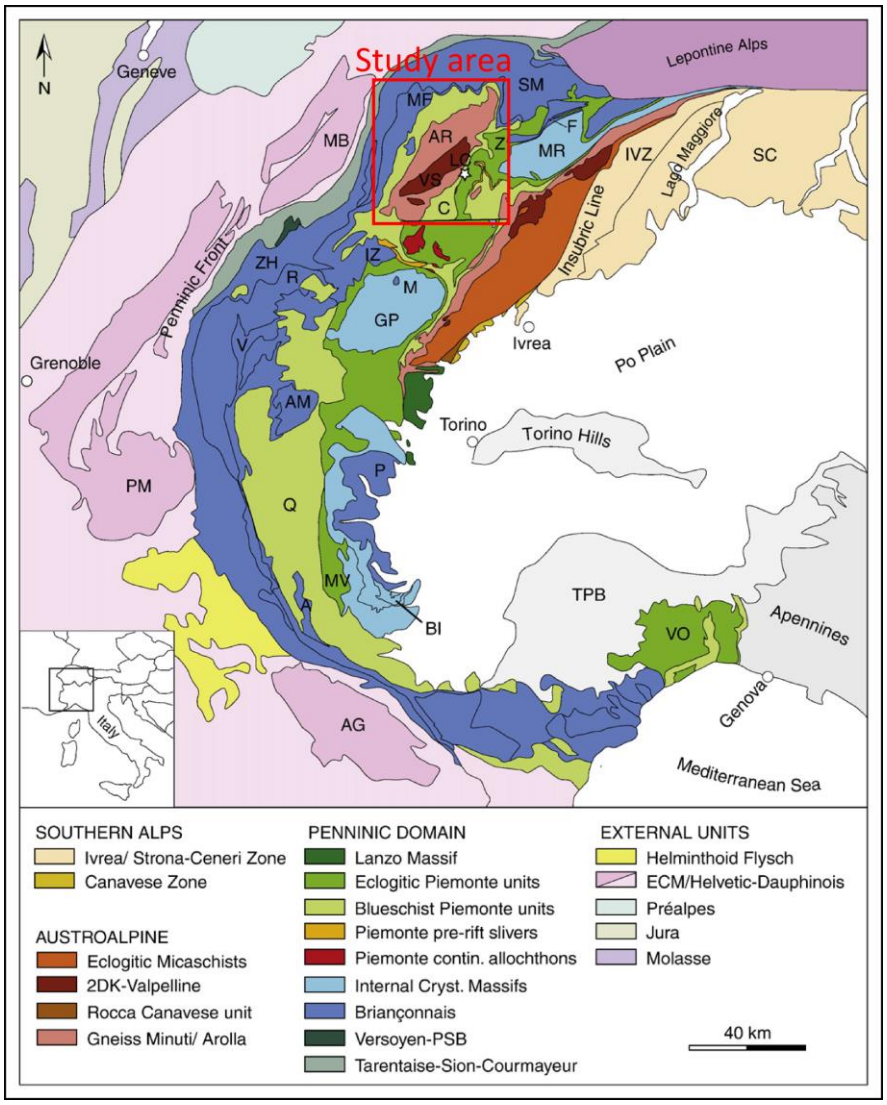

Figure 1.4: Tectonic map of the Western Alps with location of the study area; modified from Beltrando et al. (2010a).

The Combin zone in the footwall of the Dent Blanche nappe comprises the ophiolitic Tsaté nappe and the Cimes Blanches and Frilihorn nappes of continental affinity. The Tsaté nappe probably represents a former accretionary wedge at the Adriatic continental margin and consists of Jurassic to Cretaceous calcschists, metabasites, and serpentinites from the Piemont-Ligurian oceanic domain (Sartori, 1987; Marthaler and Stampfli, 1989). The Cimes Blanches and Frilihorn nappes consist of successions of Permo-Mesozoic sediments comprising conglomerates, quartzites, marbles, and dolomites which occur as thin dismembered sheets along the base and structurally higher up in the Combin zone (Sartori, 1987; Vannay and Allemann, 1990). They may represent sheared-off cover sequences from the Briançonnais continental spur or from more internal continental crust, e.g. the Dent Blanche/Sesia nappe system (Pleuger et al., 2007). The Combin zone reached greenschist- to blueschist-facies conditions during Alpine subduction and accretion (Kienast, 1973; Ballèvre and Merle, 1993; Reddy

et al., 1999; Bousquet, 2008) between ca. 62 – 48 Ma (Agard et al., 2002; Reddy et al., 2003) and experienced a pervasive greenschist-facies overprint (Ballèvre and Merle, 1993; Negro et al., 2013).

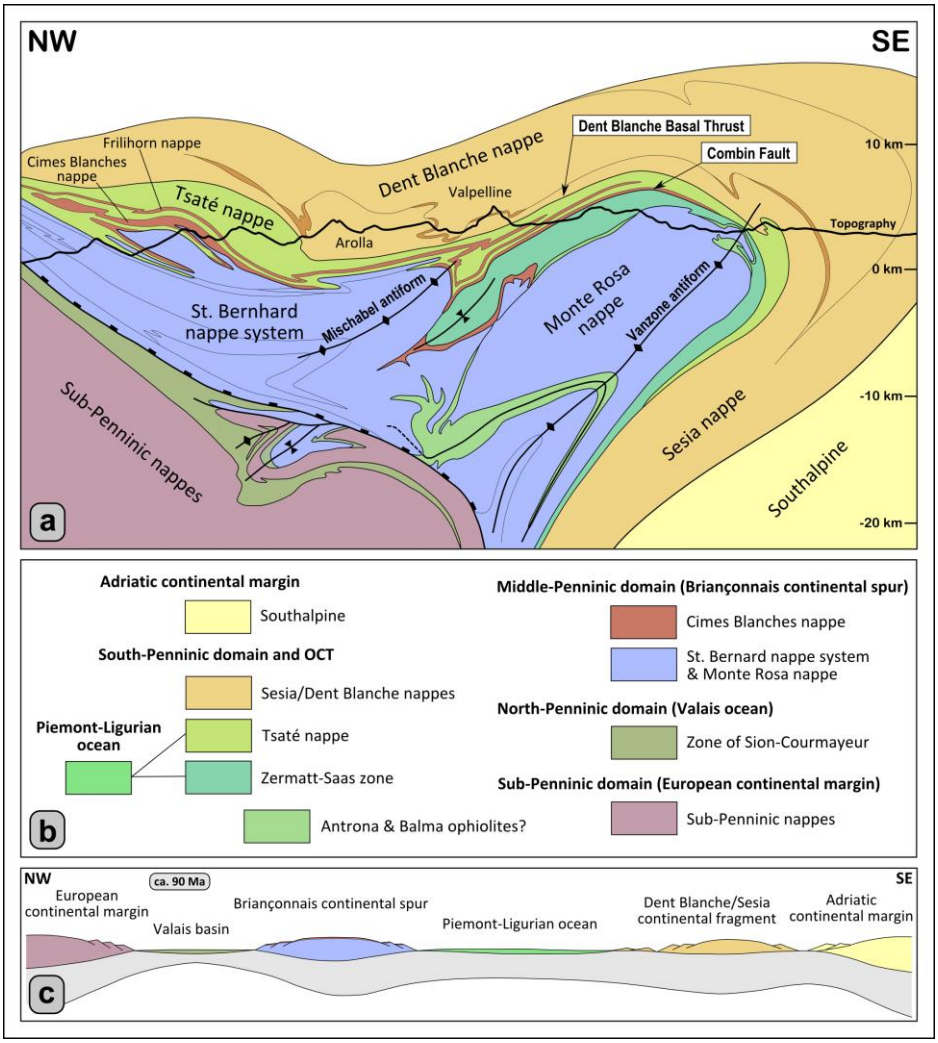

Figure 1.5: a) Cross-section through the nappe stack of the Western Alps; after Escher et al. (1993); trace of cross-section is indicated in figure 1.6. b) Key with assumed paleogeographic affiliations of tectonic units; note that the paleogeographic origin of the Antrona and Balma ophiolites in contact with the Monte Rosa nappe as well as the Monte Rosa nappe itself is still a matter of discussion; participitation in that discussion is beyond the scope of this thesis. c) Schematic paleogeographic configuration during the Late Cretaceous before the onset of Alpine subduction.

The Zermatt-Saas zone in the footwall of the southeastern segment of the Combin Fault is also derived from the Piemont-Ligurian oceanic domain and consists of metabasalts, metagabbros, metaultramafics, and metasediments. Metabasic rocks yield Jurassic protolith ages around ca. 164 Ma (Rubatto et al., 1998). The Zermatt-Saas zone experienced Paleocene – Eocene (U)HP metamorphism with ages between ca. 54 – 41 Ma (Bowtell et al., 1994; Rubatto et al., 1998; Amato et al., 1999; Lapen et al., 2003; Mahlen et al., 2005; De Meyer et al., 2014) and subsequent greenschist-facies retrogression between ca. 42 – 38 Ma (Amato et al., 1999; Cartwright and Barnicoat, 2002; De Meyer et al., 2014). Several continental fragments occur on top of the Zermatt-Saas zone which may represent continental outliers within the Piemont-Ligurian oceanic domain and also show an Alpine eclogite-facies imprint (Dal Piaz et al., 2001; Beltrando et al., 2010; Weber et al., accepted). The northwestern Combin zone is underlain by the continental St. Bernhard nappe system which is derived from Briançonnais

continental crust. It consists of Paleozoic basement and Mesozoic cover rocks which experienced an Alpine greenschist- to blueschist-facies overprint (Bearth, 1963; Sartori, 1990).
The geometry of the internal part of the Paleogene nappe stack in the Swiss-Italian Western Alps has been strongly modified by collision-related backfolding and formation of the Vanzone antiform after ca. 32 Ma (Escher et al., 1993; Pettke et al., 1999; Fig. 1.5a).

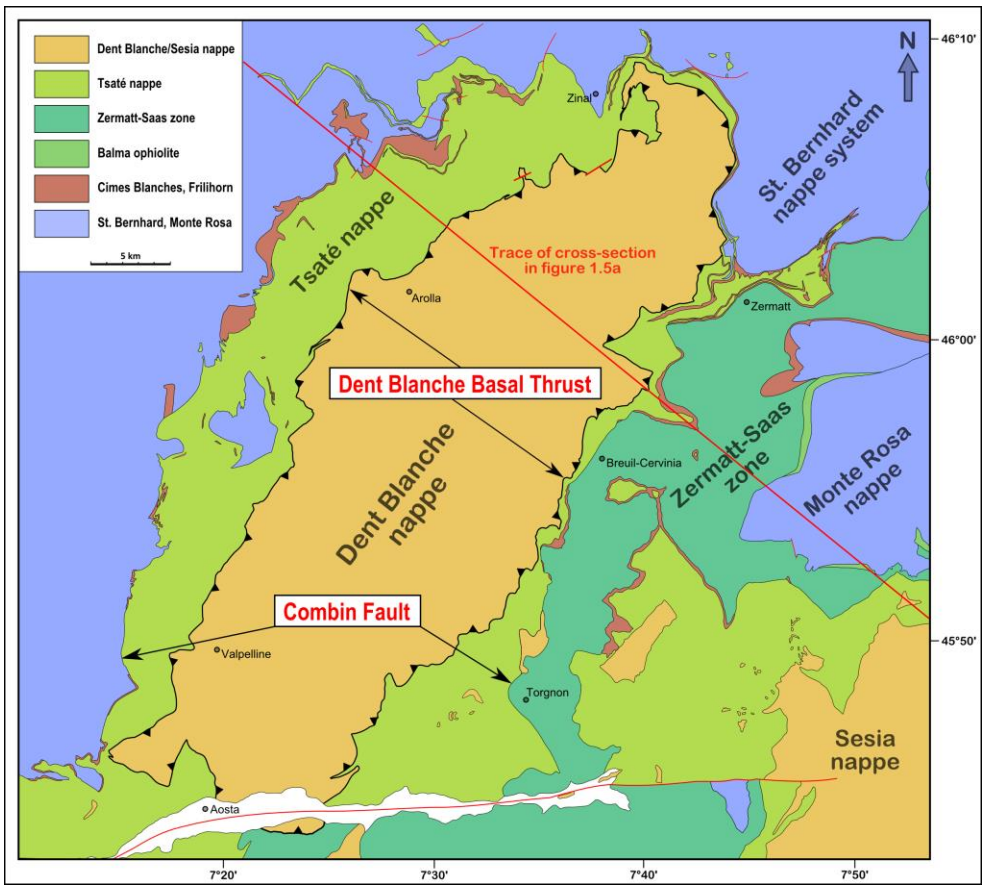

Figure 1.6: Tectonic map of the study area and adjacent areas; after Steck et al. (1999); the Dent Blanche Basal Thrust separates the Dent Blanche nappe in the hanging wall from the Combin zone in the footwall; the Combin Fault separates the Combin zone from the St.Bernhard nappe system in the northwest and the Zermatt-Saas zone in the southeast.

1.3 Research question, methods, and organization of the thesis

In this thesis, a structural model and sequence of deformation for the Swiss-Italian Western Alps is presented. This model is based on kinematic and geometric analyses of shear zones and deformation structures in outcrop and thin-section along two major Alpine tectonic contacts, the Combin Fault and the Dent Blanche Basal Thrust. Additional petrological investigations are used to constrain metamorphic conditions and processes during the structural evolution of the Combin zone and the Dent Blanche nappe. These new structural and metamorphic data are discussed in the context of the tectonic evolution of the Western Alps. The methods applied in this thesis include structural field work and collection of mostly oriented samples, analyses of microstructures in thin-section, measurement of quartz textures with x-ray texture goniometry, petrological and mineralogical investigations via electron microprobe analyses, x-ray fluorescence analysis (XRF), and thermodynamic modelling. 378 samples were taken along the two boundary zones and within the Combin zone (see table of samples and map with sample locations in appendix). Oriented samples were cut parallel to the xz-plane of the finite strain ellipsoid for further microstructural analyses. Some samples were prepared for

petrological and mineralogical investigations. All electron microprobe analyses were carried out with the Jeol JXA-8200 superprobe at the Steinmann-Institut. X-ray texture goniometry on quartz mylonites was carried out at Geowissenschaftliches Zentrum, University of Göttingen. Thermodynamic modelling (equilibrium phase diagram modelling, pseudosection modelling) was performed with the THERIAK-DOMINO software package (De Capitani and Petrakakis, 2010) which uses minimization of the Gibbs free energy to calculate stable mineral assemblages and/or compositions for defined PT-conditions.

The large difference in peak pressures between the eclogite-facies Zermatt-Saas zone in the footwall (ca. 2.3 – 3.0 GPa: Bucher et al., 2005; Angiboust et al., 2009) and the greenschist- to blueschist-facies Combin zone (ca. 1.2 GPa: Bousquet, 2008) in the hanging wall led many authors to suggest that the Combin Fault and the overlying Combin zone are large normal-sense shear zones accommodating exhumation of (U)HP rocks in its footwall (Ballèvre & Merle, 1993; Reddy et al., 1999; Wheeler et al., 2001). However, this straight-forward interpretation has been questioned by several authors on the basis of structural observations which do not support a normal-sense shear zone character for the Combin zone in many places (Ring, 1995; Froitzheim et al., 2006; Pleuger et al., 2007). The difference in metamorphic grade is greatest at Lago di Cignana in the Western Valtournenche of Italy where UHP-rocks of the Zermatt-Saas zone, which experienced peak conditions of $\geq$ 3.2 GPa and $\leq$ 600° C (Reinecke, 1998; Groppo et al., 2009; Frezzotti et al., 2011), are exposed and overlain by strongly retrogressed rocks of the Combin zone and the Dent Blanche nappe. Therefore, this locality is ideal for studying the kinematics and geometry of shearing during and after exhumation of rocks from great depths. Chapter 2 of this thesis deals with the structural evolution of the Penninic units at Lago di Cignana and aims at constraining their progressive orogenic deformation from (U)HP to greenschist-facies conditions. The Combin Fault and DBBT are well exposed in this area. Analyses of deformation structures in outcrop and thin-section are used to determine bulk shear senses and approximate 2D strain geometries, i.e. relative amounts of simple and pure shear. Texture analysis on quartz mylonites is also used to infer the kinematics and geometry of deformation and to estimate temperature conditions during texture formation. A model is presented which explains the structural record in the context of syn- to post-exhumational orogenic deformation and the tectonic evolution of the Western Alps.

The Combin zone and lower Dent Blanche nappe show a strong greenschist-facies overprint which has largely obliterated an earlier Alpine high-pressure imprint. Although blueschist-facies relics have been reported from the Combin zone, metamorphic conditions and the structural evolution during early subduction and accretion of this unit are poorly constrained. Especially units and lithological associations of the Piemont-Ligurian/Adriatic ocean-continent transition were involved in early subduction and experienced high-pressure metamorphism and associated deformation. Chapter 3 of this thesis focuses on the metamorphic and structural evolution of a continental fragment, the Becca d'Aver continental sliver (BACS) in the western Valtournenche of Italy, which is interpreted to be derived from this paleogeographic domain. The BACS is structurally located close to the Combin/Dent Blanche boundary, partly exhibits high-pressure metamorphic assemblages, and therefore holds crucial information about conditions and processes during subduction and exhumation of continental margin units. Petrographic and mineralogical analyses were performed on

metasediments from the BACS to gain information on mineral compositions of prograde and retrograde phases. Equilibrium phase diagram modelling and garnet isopleth thermobarometry are used to attribute mineral assemblages and compositions to specific PT-conditions on the prograde and retrograde path. Phase relations and inclusion patterns are studied in detail to gain information on the role of fluid-mediated mineral growth. (Micro)structural observations from the BACS and the underlying Combin zone are used to deduce kinematics during their tectonometamorphic evolution.

Previously published works already suggested that the structural evolution of the Combin zone and the Dent Blanche nappe are closely related (Oberhänsli and Bucher, 1987; Pleuger et al., 2007). As mentioned before, contradicting views exist on the nature of the Combin Fault and the Combin zone whether they mainly represent normal-sense or thrust-related shear zones (e.g. Ring, 1995; Reddy et al., 1999; Froitzheim et al., 2003; Pleuger et al., 2007). Although the nature of the DBBT is less controversial in that it is generally interpreted as a major thrust (e.g. Mazurek, 1986; Wust and Silverberg, 1989; Pleuger et al., 2007), more comprehensive work on deformation and shearing events along the DBBT and its relationship with the underlying Combin zone is needed. The overall structural evolution of the Combin zone and Dent Blanche nappe as well as the sequence of deformation along the Combin Fault and DBBT is still not well-constrained. Chapter 4 of this thesis deals with the kinematics, geometry, and distribution of greenschist-facies shear zones along the Combin Fault and DBBT in the study area. The presented structural evolution contributes to the discussion on the nature of shear zones and the sequence of deformation and is discussed in the context of the tectonic evolution of the Western Alps. Deformation structures in outcrop and thin-section from exemplary subareas along the two tectonic contacts and within the Combin zone give information on the vergence of shearing. Especially overprinting relations and correlations within and between subareas are used to deduce a relative chronology of shearing events. Conditions during shearing are approximated by the degree of ductility and quartz recrystallization mechanisms. Pseudosection modelling was performed for one mylonite sample from the northwestern DBBT to gain more detailed information on PT-conditions during retrograde shearing along the DBBT. Finally, structural observations and interpretations are used to constrain regional similarities and differences between fault segments and the geometry and distribution of greenschist-facies shear zones in the study area. The new findings are discussed in the context of previously published data and models to clarify some of the open questions regarding the tectonic evolution of the Swiss-Italian Western Alps.

During my PhD project, I also worked on the following two topics which for the reasons outlined are not included in this thesis.

To date, there are no protolith ages available for the Tsaté nappe north of the Aosta valley. Determination of such ages was originally part of this project. As such, metagabbroic rocks from two localities northwest of the Dent Blanche nappe, at Aiguilles Rouges d'Arolla and east of Val de Zinal, were collected. However, zircons of appropriate size could not be found within these rocks. Electron microprobe analyses of two metagabbro samples (FD306, FD377) can be found in the appendix.

The Alpine tectonometamorphic evolution of the Etirol-Levaz slice in the western Valtournenche of Italy is still poorly constrained. The age of peak metamorphism has been dated at ca. 47 – 45 Ma with Rb-Sr and U-Pb geochronology (Dal Piaz et al., 2001; Beltrando et al., 2010). However, age constraints for the prograde path and therefore the early subduction history of this continental

fragment have not been determined yet. I collected several samples suitable for Lu-Hf garnet geochronology from within the Etirol-Levaz slice and helped characterize them via electron microprobe analyses, LA-ICPMS analyses, and thermodynamic modelling. Lu-Hf garnet dating was performed as part of a master project (Faßmer, 2014) and the results will be presented in a stand-alone paper.

Chapters 2 – 4 of this thesis contain the aforementioned studies on the evolution of the tectonic units and contacts in the chosen areas. All chapters and sections were written by me. An earlier version of chapter 2 was revised by Thorsten Nagel (University of Bonn) and Bernd Leiss (University of Göttingen) who made suggestions regarding the content and language. Chapter 5 summarizes the key points of this thesis and contains a list of references used in this thesis as well as the acknowledgements and a short C.V.. The appendix contains a list of conference abstracts, electron microprobe analyses, a table of all samples taken in the field, and a map with sample locations.

- CHAPTER 2 -

Structural evolution of the Penninic units at Lago di Cignana (Western Alps, Italy): constraining progressive orogenic deformation from (ultra)high-pressure to greenschist-facies conditions

2.1 Abstract

In the Western Alps, a stack of oceanic and continental units derived from different paleogeographic domains experienced progressive orogenic deformation during Alpine subduction, exhumation, and accretion. Structural analyses of the Penninic units at Lago di Cignana (Valtournenche, Italy) revealed a continuous evolution from (ultra)high-pressure to greenschist-facies conditions related to Paleogene, syn- to post-exhumational deformation. Early exhumation of the oceanic Zermatt-Saas zone following (ultra)high-pressure metamorphism at ca. 43 Ma occurred during dominant top-E shearing under eclogite- to upper greenschist-facies conditions. Subordinate conjugate top-W shear senses suggest internal deformation and differential exhumation of (ultra)high-pressure rocks. Exhumation to mid-crustal levels and juxtaposition with the overlying Combin zone occurred during greenschist-facies normal-sense top-SE shearing. Strain was mainly localized along the uppermost Zermatt-Saas zone since top-SE shear senses are scarce in the hanging wall of the Combin Fault. Top-SE structures have also partly been obliterated by subsequent deformation. Top-SE shearing was followed by a phase of pure shear deformation affecting units in the footwall and hanging wall of the Combin Fault. Coaxial deformation is indicated by greenschist-facies symmetric fabrics, conjugate shear bands, boudinage, and orthorhombic quartz textures. It was followed by bulk top-NW shearing associated with renewed thrusting along the Dent Blanche Basal Thrust which continued until low-grade greenschist-facies conditions.

2D kinematic and geometric analyses in the area around Lago di Cignana suggest that normal-sense top-(S)E shearing along the top of the Zermatt-Saas zone accompanied exhumation of this unit from eclogite- to greenschist-facies conditions and was followed by a phase of dominant pure shear deformation partly obliterating exhumation-related deformation structures. On a regional scale, a significant pure shear component may have led to the development of conjugate top-SE and top-NW shear zones within the Combin zone which offers an explanation for contradicting views regarding the sequence of deformation and the nature of the Combin Fault and the Combin zone, i.e. whether they represent thrust-related or normal-sense shear zones.

2.2 Introduction

Deformation in Alpine-type orogens results from cycles of subduction and accretion, exhumation, and continental collision. Continental and oceanic units can be subducted to and exhumed back from (ultra)high-pressure ((U)HP) depths. During subsequent nappe stacking, crustal units that experienced such extreme conditions are juxtaposed with lower-pressure units along major tectonic contacts and shear zones. Deformation structures associated with initial exhumation from (U)HP conditions are often obliterated by later deformation phases associated with nappe stacking and continental collision. Accordingly, it is often controversial whether observed structures resulted from exhumation-related deformation or merely represent younger deformation phases. A classic example for oceanic (U)HP conditions and the discussion of exhumation-related deformation is the Zermatt-Saas zone in the Swiss-Italian Western Alps with its associated UHP sliver, the Lago di Cignana unit (e.g. Reinecke, 1991; Forster et al., 2004; Groppo et al., 2009). These units are derived from the oceanic South-Penninic paleogeographic domain (Fig. 2.1a) which experienced a Paleogene cycle of subduction, exhumation, and collision. The Zermatt-Saas zone is situated in the footwall of the Combin Fault, a major Alpine shear zone, the significance of which for the exhumation of the underlying (U)HP rocks has been controversially discussed in the literature. The large difference in metamorphic grade between the eclogite-facies Zermatt-Saas zone in the footwall and the greenschist- to blueschist-facies Combin zone in the hanging wall has led many authors to interpret the Combin Fault as a top-SE normal fault that accommodated exhumation of Zermatt-Saas (U)HP rocks (e.g. Ballèvre and Merle, 1993; Reddy et al., 1999; Wheeler et al., 2001; Reddy et al., 2003). This interpretation has been questioned by several authors due to the occurrence of abundant greenschist-facies top-NW kinematic shear senses along the Combin Fault and within the Combin zone. Ballèvre and Merle (1993) suggested that a Combin normal fault was overprinted by post-exhumational top-NW thrusting erasing earlier top-SE structures which was then followed by late-stage top-SE backfolding. Ring (1995) proposed that the Combin Fault represents an Eocene out-of-sequence thrust also overprinted by later top-SE backshearing. Froitzheim et al. (2006) and Pleuger et al. (2007) interpreted the Combin Fault as an extraction fault that formed due to extraction and subsequent out-of-sequence thrusting of the Dent Blanche nappe. Reddy et al. (2003) proposed on the basis of synkinematic Ar-Ar and Rb-Sr ages that top-SE shearing within the Combin zone was dominant during exhumation of the Zermatt-Saas zone but also overlapped and was partly coeval with the activity of top-NW shear zones due to a significant pure shear component. Whereas the nature of the Combin Fault is still a matter of discussion, the Dent Blanche Basal Thrust (DBBT) separating the continental Dent Blanche nappe from the underlying Combin zone is considered to undoubtedly represent a major Alpine thrust of probably Eocene age (e.g. Mazurek, 1986; Oberhänsli and Bucher, 1987; Pleuger et al., 2007). Both these major Alpine shear zones are exposed in the area around Lago di Cignana in the western Valtournenche of Italy. This locality has been the site of many studies since the first recognition of UHP metamorphism within oceanic rocks of the Zermatt-Saas zone (Reinecke, 1991). UHP conditions within metabasic and metasedimentary lithologies are evident from the occurrence of coesite (Reinecke, 1991) and microdiamond (Frezzotti et al., 2011). Due to the rare opportunity to study UHP oceanic crust, numerous studies have been carried out on the petrological and geochronological evolution of these rocks.

Studies dealing with structural aspects of this area comprise the work of Van der Klauw et al. (1997) who linked deformation structures to the exhumation path and Ballèvre and Merle (1993), Ring (1995), and Reddy et al. (2003) who included the Lago di Cignana area in their regional studies.

In this chapter, I present structural data from the Lago di Cignana area to reconstruct the structural evolution of the exposed tectonic units. I describe deformation structures from the upper Zermatt-Saas zone to the lower Dent Blanche nappe and especially focus on deformation along the Combin Fault to clarify its nature. My observations constrain the structural evolution of the Penninic units at Lago di Cignana during Paleogene progressive orogenic deformation from (U)HP to greenschist-facies conditions. Finally, I discuss their tectonic evolution in the framework of the Western Alps.

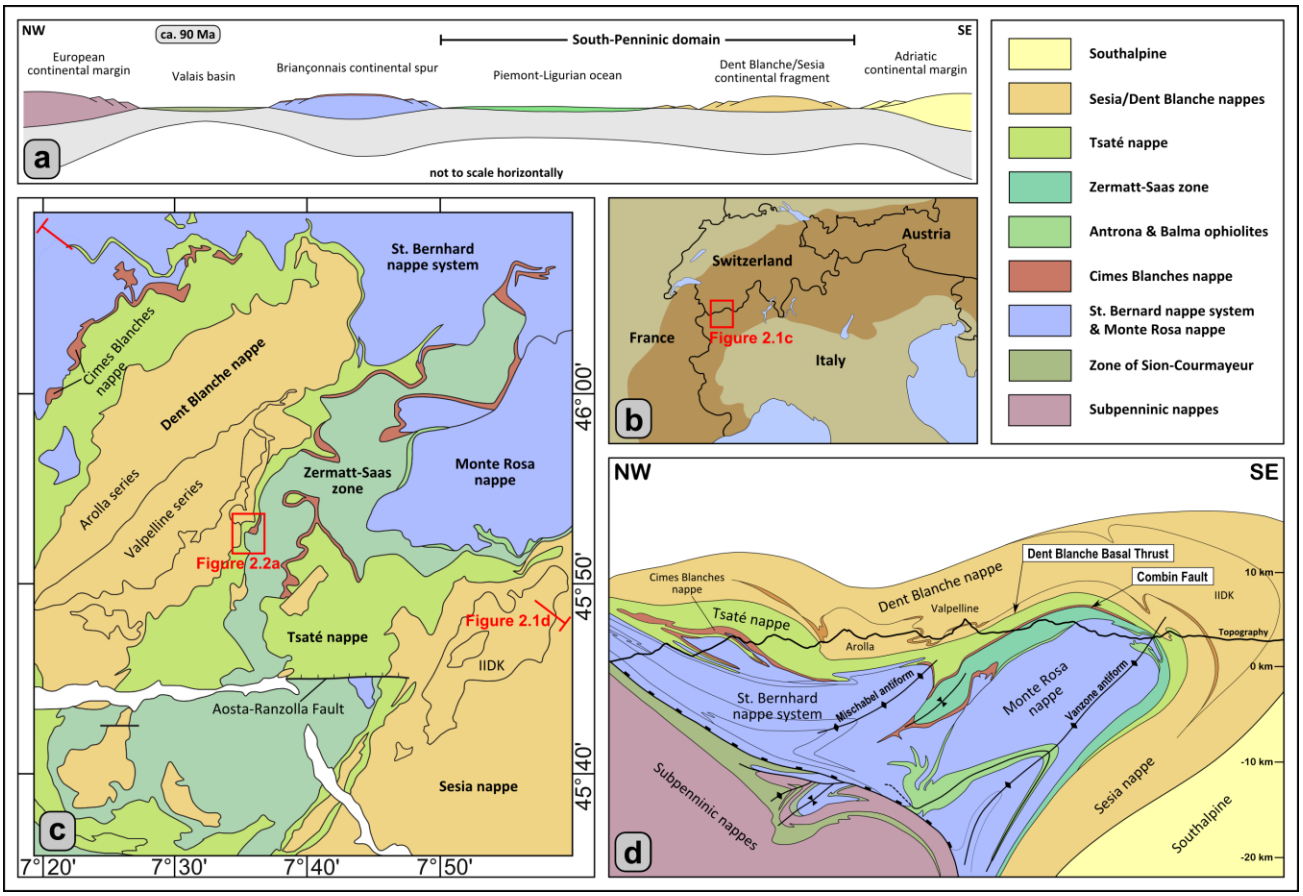

Figure 2.1: a) Late Cretaceous paleogeography before the onset of Alpine subduction; the South-Penninic paleogeographic domain comprises the Piemont-Ligurian oceanic realm from which the Zermatt-Saas zone and Tsaté nappe are derived and continental fragments that later became the Dent Blanche/Sesia nappe system. b) Sketch map of the European Alps with location of the tectonic map. c) Tectonic map of the Penninic units in the Swiss-Italian Western Alps after Steck et al. (1999) and Pleuger et al. (2007) with location of the geological map in figure 2.2a. d) Schematic cross-section through the Western Alps; not to scale vertically or horizontally; after Escher et al. (1993) and Pleuger et al. (2007).

2.3 Geological setting

The Swiss-Italian Western Alps consist of a stack of continental and oceanic units derived from different paleogeographic domains (Fig. 2.1a). During the Late Cretaceous, before the onset of Alpine subduction, these included from northwest to southeast the European continental margin, the Valais oceanic basin

(North-Penninic units), the Briançonnais continental spur (Middle-Penninic units), the Piemont-Ligurian oceanic domain including several continental fragments (South-Penninic units and Dent Blanche/Sesia nappe system), and the Adriatic continental margin (Southern Alps). In the course of SE-directed subduction during the Late Cretaceous - Paleogene, crustal slices of these different paleogeographic units were progressively accreted to the Adriatic margin.

The study area is located in the Italian Western Alps (Figs. 2.1b and c) where units of the South-Penninic paleogeographic domain are exposed. The structurally highest unit is the Dent Blanche/Sesia nappe system which is interpreted to originate from one or more continental fragments derived from the Adriatic continental margin and stranded inside the Piemont Ligurian oceanic domain during Jurassic rifting (Froitzheim et al., 1996; Dal Piaz et al., 2001; Babist et al., 2006). The Dent Blanche nappe in the northwest is separated from the Sesia nappe in the southeast by erosion. Both units consist of Paleozoic basement and remnants of Permo-Mesozoic cover sequences. The Dent Blanche nappe is subdivided into two pre-Alpine basement units, the Arolla and Valpelline series. The Arolla series consists of Permian granitoids and gabbros (Bussy et al., 1998; Monjoie et al., 2005) whereas the Valpelline series comprises pre-Alpine amphibolite- to granulite-facies metasediments (Gardien et al., 1994). Permo-Mesozoic cover rocks, often referred to as Roisan zone (Ballèvre and Kienast, 1987), comprise breccias, marbles, and quartzites. They occur on top of the Arolla series and along major shear zones (e.g. Manzotti, 2011). The Alpine overprint within the Dent Blanche/Sesia nappe system increases from northwest to southeast which is consistent with SE-directed subduction and accretion of the units. The Dent Blanche nappe reached blueschist-facies conditions of ca. 1.6 GPa and 520° C and shows a pervasive greenschist-facies overprint along shear zones (Ballèvre et al., 1986; Oberhänsli and Bucher, 1987; Manzotti et al., 2014). The Sesia nappe experienced eclogite-facies conditions around 2.0 GPa and 550° C (e.g. Lardeaux and Spalla, 1991; Regis et al., 2014). High-pressure metamorphism in the Sesia nappe occurred during the Late Cretaceous at ca. 70 – 65 Ma (e.g. Inger et al., 1996; Rubatto et al., 1999) but started as early as ca. 85 Ma with several distinct pressure peaks (Rubatto et al., 2011; Regis et al., 2014). Babist et al. (2006) suggested that the Sesia nappe was mainly exhumed between 55 – 45 Ma. The basal tectonic contact of the Dent Blanche nappe towards the underlying Combin zone is the Dent Blanche Basal Thrust (DBBT). The Combin zone comprises (1) the Tsaté nappe, a mélange of Jurassic to Cretaceous calcschists, metabasites, and serpentinites derived from the Piemont-Ligurian oceanic domain, and (2) the Cimes Blanches and Frilihorn nappes which consist of successions of Permo-Mesozoic sediments with continental affinity comprising quartzites, meta-arkoses, marbles, and dolomites (Vannay and Allemann, 1990). These sediments occur as thin dismembered sheets along the base (Cimes Blanches nappe) and structurally higher up (Frilihorn nappe) in the Combin zone. Their origin is still debated and they have been interpreted to represent sheared-off cover sequences of the St. Bernard nappe system (e.g. Vannay and Allemann, 1990) or the Dent Blanche/Sesia nappe system (Pleuger et al., 2007). The Combin zone reached Alpine greenschist- to blueschist-facies conditions (Reddy et al., 1999) with peak estimates around 1.2 GPa and 450° C (Bousquet, 2008) and has been interpreted as an accretionary wedge that formed at the Adriatic continental margin during Alpine subduction (Sartori, 1987; Marthaler and Stampfli, 1989). $^{40}Ar/^{39}Ar$ white mica ages obtained by Reddy et al. (2003) indicate that accretion took

place between 60 - 48 Ma which coincides with ages between 62 - 55 Ma obtained by Agard et al. (2002) from in-situ $^{40}Ar/^{39}Ar$-dating of phengites within carpholite-bearing metasediments of the Schistes Lustrés complex south of the Aosta valley. The Combin zone is underlain by the Zermatt-Saas zone in the southeast and the St. Bernard nappe system in the northwest and its basal contact is the Combin Fault. The Zermatt-Saas zone is also derived from Piemont-Ligurian oceanic lithosphere and consists of Jurassic ophiolites (metabasalts, metagabbros, metaultramafics, and metasediments) which experienced high- to ultrahigh-pressure metamorphism in the Paleocene - Eocene. U-Pb geochronology on magmatic zircons from metagabbros yielded protolith ages around 164 Ma (Rubatto et al., 1998). A large spread of available HP ages between ca. 54 and 41 Ma (Bowtell et al., 1994; Amato et al., 1999; Lapen et al., 2003; Mahlen et al., 2005; De Meyer et al., 2014; Weber et al., accepted) suggests that the Zermatt-Saas zone consists of several ophiolite slivers that were assembled in a subduction channel. Peak metamorphic conditions commonly reached 2.5 – 3.0 GPa and 550° – 600° C (Bucher et al., 2005). Ultrahigh-pressure metamorphism has been reported for metasediments and eclogites at Lago di Cignana in the western Valtournenche of Italy (Reinecke, 1998; Groppo et al., 2009; Frezzotti et al., 2011). Peak metamorphic conditions for these rocks have been calculated at $\geq$ 3.2 GPa and $\leq$ 600° C (Groppo et al., 2009; Frezzotti et al., 2011) and the age of metamorphism has been dated with various geochronometers. U-Pb SHRIMP dating on whole zircons and zircon rims by Rubatto et al. (1998) yielded ages of 44.1 ± 0.7 Ma. Amato et al. (1999) reported a Sm-Nd garnet age of 40.6 ± 2.6 Ma for a UHP eclogite whereas Lapen et al. (2003) obtained a garnet-omphacite-whole rock isochron age of 48.8 ± 2.1 Ma with the Lu-Hf method for the same sample. Gouzu et al. (2006) reported an age of ca. 44 – 43 Ma for phengite inclusions in garnet dated with the $^{40}Ar/^{39}Ar$ step-heating method. I therefore consider the age of peak-metamorphism within UHP rocks at Lago di Cignana to have occurred around 43 Ma. The Zermatt-Saas zone partly shows a greenschist-facies overprint at the Lago di Cignana area which has been dated at 38 ± 2 Ma by Amato et al. (1999) with Rb-Sr whole rock-phengite chronometry. The Zermatt-Saas zone is folded around the underlying Monte Rosa nappe and, in the north, dips below the Mischabel fold, a large SE-closing antiform mostly affecting continental units of the St. Bernhard nappe system. The St. Bernhard nappe system is unanimously considered to be derived from the Briançonnais continental spur, an eastern prolongation of the Iberian plate located between the North- and South-Penninic oceanic basins (Schmid et al., 2004). The paleogeographic origin of the Monte Rosa nappe, however, is still controversial. According to some authors it represents Middle-Penninic continental crust (e.g. Escher et al., 1997; Keller and Schmid, 2001) whereas others attribute it to the European continental margin (e.g. Froitzheim, 2001; Pleuger et al., 2005). The geometry of the Paleogene nappe stack in the Swiss-Italian Western Alps has been largely modified by Oligocene - Miocene backfolding and formation of the Vanzone antiform after ca. 32 Ma (e.g. Pettke et al., 1999) as a result of collision between the European and Adriatic continental margins.

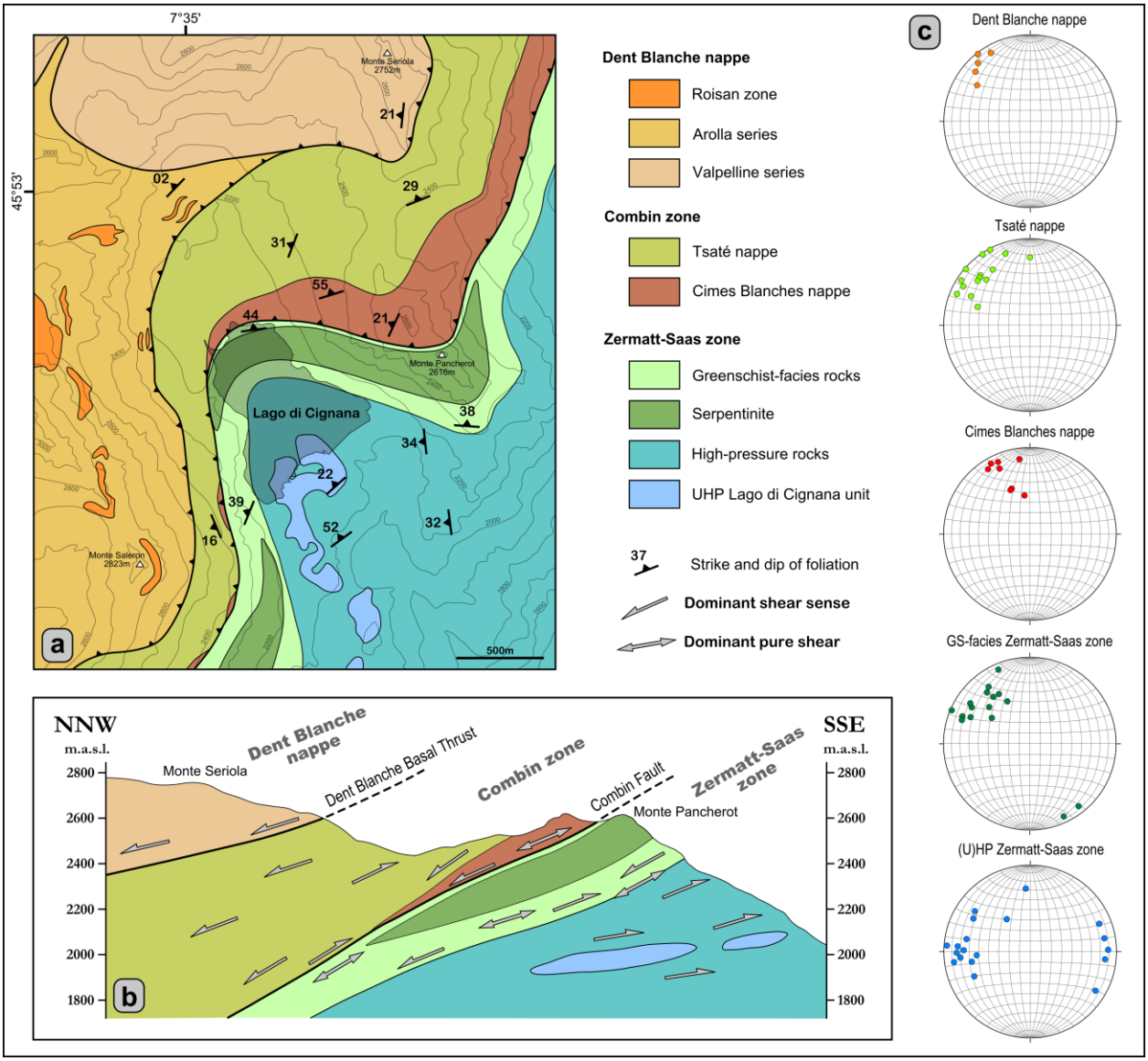

Figure 2.2: a) Geological sketch map of the Lago di Cignana area after Tamagno (2000), Forster et al. (2004), Groppo et al. (2009), Manzotti (2011), and own observations and interpretations. b) Cross-section with all units projected into the Monte Pancherot - Monte Seriola transect; shear senses are from this study. c) Stereoplots of stretching lineations as equal area projections in the lower hemisphere.

2.4 Field relations

The area around Lago di Cignana in the western Valtournenche of Italy displays a well-exposed cross-section through the three uppermost tectonic units of the Western Alps which are from top to bottom the Dent Blanche nappe, the Combin zone, and the Zermatt-Saas zone (Fig. 2.2). All units had an originally SE-dipping orientation during and after the main phase of nappe stacking but have been rotated into a NW-dipping orientation due to formation of the Vanzone antiform in the southeast. In the Lago di Cignana area, foliations dip to the west to north. Stretching lineations in all units mostly plunge to the NW, except for lineations in Zermatt-Saas (U)HP rocks which predominantly trend E-W (Fig. 2.2c). Ultrahigh-pressure rocks of the Zermatt-Saas zone occur south of Lago di Cignana as three dismembered

slivers less than 100m in thickness (Forster et al., 2004). They consist of eclogites and their former pelagic sedimentary cover, now mainly represented by quartzitic (mica)schists. The UHP unit is surrounded by metabasic and metasedimentary rocks equilibrated at eclogite-facies conditions during peak metamorphism. For detailed petrographic and petrological descriptions of UHP and HP lithologies, the reader is referred to Groppo et al. (2009) and references therein. Serpentinite especially occurs along zones of high strain and as large bodies in the uppermost part of the Zermatt-Saas zone. A large serpentinite body builds the peak of Monte Pancherot east of the lake and then wedges out towards the west, another large body occurs south of the lake. Garnet-bearing and garnet-free calcschists of the Zermatt-Saas zone especially occur in the hanging wall of the UHP unit towards the Combin Fault. Metabasite bodies at this structural level often exhibit typical greenschist-facies mineral assemblages suggesting a progressively increasing overprint in the uppermost part of the Zermatt-Saas zone (Figs. 2.2a and b). Despite their overall retrogressed nature, these rocks are attributed to the Zermatt-Saas zone because of abundant HP relics and their structural position in the footwall of the Cimes Blanches nappe (Pleuger et al., 2007; Groppo et al., 2009). The different tectonic affiliations of calcschists in the footwall and hanging wall of the Cimes Blanches nappe is further supported by a difference in peak temperatures obtained with Raman spectroscopy thermometry by. Rocks of the Zermatt-Saas zone in the footwall of Cimes Blanches metasediments record temperatures between 498° and 532° C whereas the overlying Combin zone records peak temperatures of 455° - 475° C (Negro et al., 2013). Metasedimentary rocks of the Cimes Blanches nappe occur at the base of the Combin zone in the direct hanging wall of the Combin Fault as a large sliver north of Monte Pancherot wedging out towards the west and north and as small dismembered fragments southwest of the lake. North of Monte Pancherot and from bottom to top, the Cimes Blanches nappe comprises a succession of quartzites, cellular dolomites (Rauhwacke), and marbles. The Tsaté nappe builds up the main part of the Combin zone and consists mainly of calcschists with minor metabasite bodies. Its thickness has been highly reduced in the Lago di Cignana area with a minimum of ca. 100m west of the lake. In the western Valtournenche area, the Tsaté nappe has a general thickness around 2 km and reaches several kilometres northwest of the Dent Blanche nappe. The Dent Blanche nappe at Lago di Cignana comprises basement rocks of the Arolla and Valpelline series as well as slivers of the metasedimentary Roisan zone. Rocks of the Valpelline series crop out in the northern part of the study area, mainly around Monte Seriola in the northeast and north of the plains to the north of the lake. To the west, they are interfolded with Arolla gneisses which crop out in the western part of the study area. Metasedimentary rocks of the Roisan zone are intimately folded into Arolla gneisses on the western side of the lake and occur as several dismembered slivers. Despite regional-scale folding of tectonic contacts during the Vanzone phase, the Combin Fault and DBBT at Lago di Cignana are not folded on a local scale but are planar structures (sub)parallel to the main foliation of mylonites in their direct footwall and hanging wall.

2.5 Deformation structures

In this section, I describe macroscopic (Fig. 2.3) and microscopic (Figs. 2.4 and 2.6) deformation structures as well as quartz textures (Fig. 2.5) from the area around Lago di Cignana (Fig. 2.7) to

determine the shear sense and to gain information on the prevailing geometry of deformation, i.e. the amount of rotational (simple shear) and coaxial (pure shear) deformation. Shear senses in outcrop and thin-section were determined from kinematic indicators, mainly c'-type shear bands and subordinately grain shape preferred orientation (GSPO) of quartz grains and asymmetric porphyroblasts and –clasts. All samples used for kinematic analyses show well-developed foliations and stretching lineations whereas the latter are considered true elongation lineations that track the finite strain ellipsoid. Therefore, all microstructural analyses were made on lineation-parallel, foliation-perpendicular cuts. Fabric asymmetry is assessed by the relative abundance of kinematic indicators. Samples with more or less equally abundant top-(N)W and top-(S)E shear senses are considered symmetric whereas samples with a clear predominance of one shear direction over the other are classified as asymmetric. Asymmetric fabrics are regarded the result of dominant simple shear (rotational) deformation whereas symmetric fabrics are regarded the result of dominant pure shear (coaxial) deformation. Accordingly, the occurrence of asymmetric and symmetric fabrics in one locality without any overprinting relations suggests general shear deformation. 2D finite strain geometries for the units are approximately estimated based on the relative abundance of deformation structures related to rotational or coaxial shear. The assumption that 2D kinematic and geometric analyses are able to sufficiently assess the structural evolution of tectonic units is justified by the prerequisite that most deformation in this area resulted from orogen-perpendicular, i.e. approximately NW-SE movement of tectonic units. Additional petrological observations are used to ascribe deformation structures to a metamorphic grade. The metamorphic conditions under which kinematic indicators formed have been estimated by the grade of the assemblage they are overprinting and by the presence or absence of diagnostic minerals within shear bands. A list of the samples used for thin-section analyses, the sample locations, and the approximate 2D strain geometries of the units are shown in figure 2.7.

2.5.1 Zermatt-Saas zone

Pristine and only weakly retrogressed (U)HP rocks occur at lower structural levels of the Zermatt-Saas zone at Lago di Cignana. Stretching lineations within these rocks dominantly trend E-W. The (U)HP assemblage in eclogites consists of garnet, glaucophane, and omphacite (for microprobe analyses see sample FD244 in appendix). Metasediments of the UHP slice are usually quartz-rich and consist mainly of garnet, white mica, and quartz. At higher structural levels, calcschists become more abundant and sometimes contain garnet. They consist of white mica, quartz, feldspar, calcite, and, in more strongly retrogressed rocks, chlorite and epidote. The uppermost part of the Zermatt-Saas zone shows a strong greenschist-facies overprint. Stretching lineations within strongly retrogressed calcschists and greenschists dominantly trend NW-SE. The greenschists mainly consist of epidote, chlorite, and albite. Thirty-two thin-sections from different structural levels of the Zermatt-Saas zone exposed around the lake have been analysed. Twenty thin-sections were identified as fresh or weakly-retrogressed (U)HP rocks and 12 as strongly overprinted by greenschist-facies metamorphism. Mineral compositions of phases stable in shear bands within eclogites were measured using the Jeol JXA-8200 superprobe at Steinmann-Institut, University of Bonn, to constrain conditions during shear band formation.

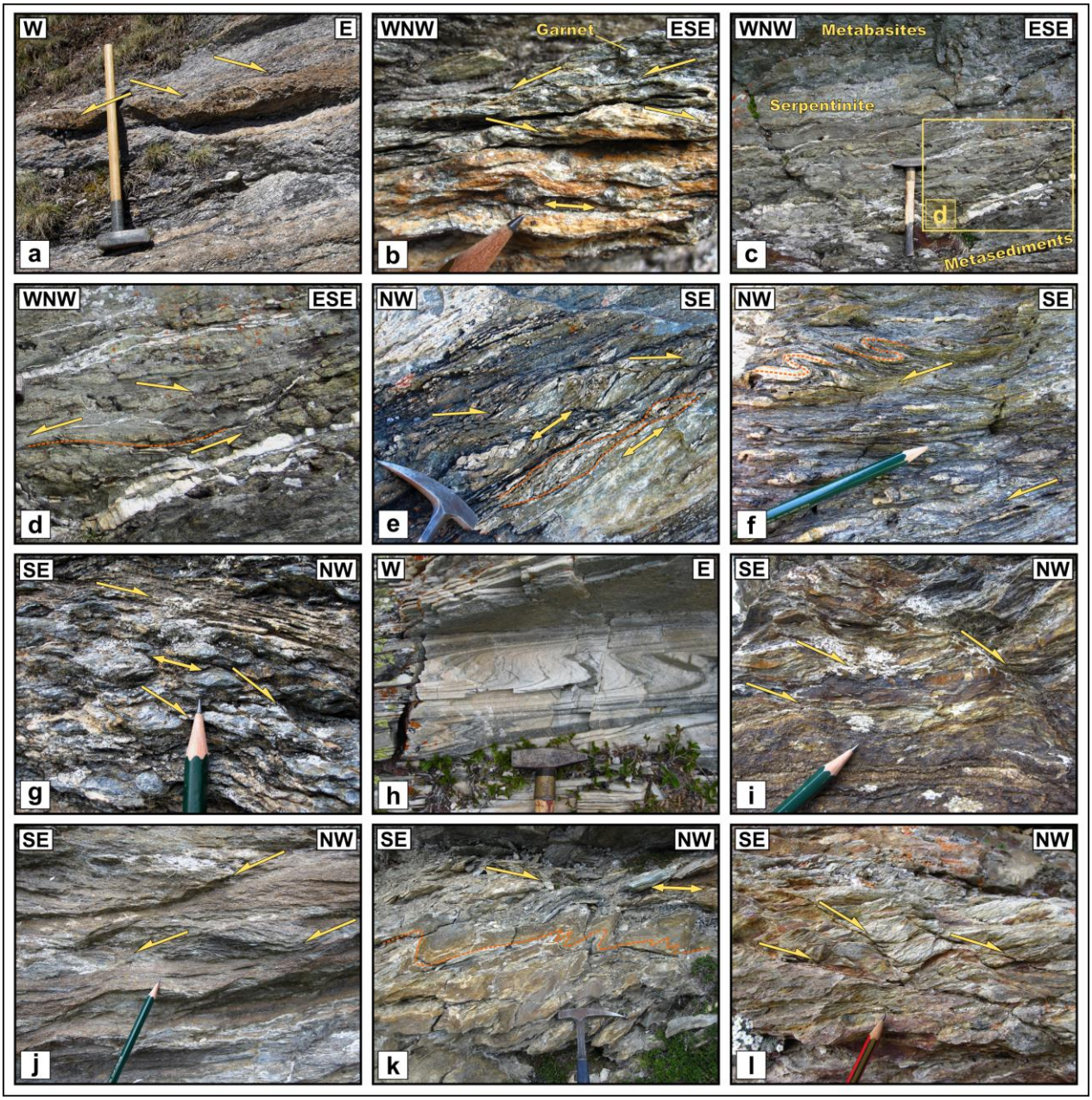

Figure 2.3: Macrostructures observed in outcrop. a) Quartz-rich metasediments of the UHP unit south of the lake showing top-E and subordinate top-W shear senses associated with asymmetric boudinage of a garnet-rich layer. b) Garnet-bearing metasediments of the Zermatt-Saas zone south of Monte Pancherot showing conjugate top-WNW and top-ESE shear senses. c) Serpentinite mélange zone of the Zermatt-Saas zone south of Monte Pancherot with metasediments in the footwall and metabasites in the hanging wall. d) Close-up of the serpentinite mélange showing boudinage of the layering and conjugate shear senses. e) Retrograde, garnet-free top-SE shear bands associated with NW-SE directed elongation and boudinage of the layering within metasediments of the Zermatt-Saas zone south of Monte Pancherot. f) Top-NW shear bands within garnet-free calcschists of the Zermatt-Saas zone south of Monte Pancherot associated with rootless tight to isoclinal, intrafolial folds within calcite layers. g) Calcschists of the Zermatt-Saas zone on the western side of the lake showing top-NW shear senses, small-scale boudinage of more competent layers, and a high-strain zone in the upper part. h) Folded quartzites of the Cimes Blanches nappe northeast of the lake with lineation-parallel, NNW-plunging fold axes. i) Top-NW shear bands within calcschists of the Combin zone west of the lake. j) Top-SE shear bands within calcschists at the base of the Combin zone on the eastern slope of Monte Saleron. k) Asymmetric, NW-vergent folds within Combin metasediments in the footwall of a top-NW shear band associated with boudinage of a competent layer. l) Semi-ductile top-NW shear bands within gneisses of the Arolla series at the base of the Dent Blanche nappe north of the lake.

Metabasites south of the lake display an eclogite-facies foliation mainly defined by omphacite and glaucophane which is often overprinted by top-E shear bands. Within shear bands, the eclogite-facies mineral assemblage is often preserved (Fig. 2.4a). In some cases, top-(S)E shear bands are associated with the growth of hornblende and albite indicating formation at lower amphibolite-facies to upper greenschist-facies conditions (Fig. 2.4b). Within metabasites, eclogite- to upper greenschist-facies shear senses are consistently top-(S)E (samples 1, 4, and 5). Metasediments of the UHP unit also display mostly top-E shear senses but subordinate top-W kinematic indicators can also be observed in outcrop and thin-section. In outcrop, more competent (e.g. garnet-rich) layers are often boudinaged and dismembered into lenses and nodules (Fig. 2.3a). Top-E shear senses are more abundant in surrounding host-rocks whereas top-W shear bands are more discrete and seem to be restricted to the observed boudinage. One sample from this domain shows top-W shear senses in thin-section (sample 3) whereas the other 3 samples display top-E shear senses (samples 3, 9, and 10). Most of these kinematic indicators formed under (U)HP conditions, only one formed under greenschist-facies conditions (sample 9). An eclogite sample further south outside the UHP slice shows the aforementioned lower amphibolite-facies to upper greenschist-facies top-E shear bands with hornblende and albite stable which cut the relatively fresh eclogite-facies assemblage (Fig. 2.4b; sample 1). Eclogite and metasediment samples to the west from within the UHP slice mainly show top-(S)E shear senses which partly formed under (U)HP (samples 4 and 6) and partly under greenschist-facies conditions (samples 5 and 7). Only one quartzitic sample shows greenschist-facies top-NW shear senses as indicated by a slight grain shape preferred orientation (sample 8). Six eclogite samples were collected east of the UHP slice but did not yield any shear sense criteria (samples 11 – 16). Metasediments become more abundant at higher structural levels within the Zermatt-Saas zone and can be well-observed south of Monte Pancherot in the footwall of the serpentinite body. Seven samples were collected in the transition zone between well-preserved HP rocks and pervasively retrogressed ones (samples 17 – 23). Three of these indicate top-(S)E shearing (samples 19, 21, and 23), 3 of them indicate top-(N)W shearing (samples 17, 18, and 20), and one sample shows ambiguous shear senses in thin-section (sample 22). Top-(S)E and top-(N)W shear senses can also be observed in outcrop south of Monte Pancherot. In some cases, these opposing shear senses are distributed into several meters thick dominant simple shear zones showing consistent shear sense criteria and sometimes they are equally distributed so that they form conjugate sets of shear bands within zones of dominant pure shear. The latter case can be well-observed in an outcrop of HP metasediments south of Monte Pancherot shown in figure 2.3b. Probable relics of the HP metamorphic stage in these rocks are large unaltered garnets visible in handspecimen. A bulk shear sense could not be unambiguously determined in outcrop. However, the two samples from this locality show bulk top-(N)W shear senses in thin-section formed under HP to greenschist-facies conditions (samples 17 and 18). Above these metasediments, a m-thick serpentinite mélange zone separates the metasediments in the footwall from a layer of metabasites in the hanging wall (Fig. 2.3c). Serpentinite layers are partly necked and boudinaged symmetrically. Shear bands and asymmetric flexure of the layering also indicate top-WNW and top-ESE shear senses (Fig. 2.3d). Further into the hanging wall, metasediments are cut by shallowly-dipping, garnet-free top-SE shear bands overprinting an earlier layer-parallel foliation (Fig. 2.3e). The compositional layering has been stretched

and boudinaged whereas no overprinting relations exist between shear bands and boudins. A sample taken close to this outcrop displays greenschist-facies top-S shear bands in thin-section (sample 21). Calcschists in the hanging wall show top-NW shear senses in outcrop (Fig. 2.3f). These metasediments are strongly retrogressed and do not contain any relic garnet. Rootless tight to isoclinal, intrafolial folds within calcite layers are sometimes associated with macroscopic top-NW shear bands. A garnet-free calcschist sample taken from an outcrop in the hanging wall, however, indicates retrograde top-SE shearing (sample 23). Pervasively retrogressed rocks of the uppermost Zermatt-Saas zone are also well-exposed on the western side of the lake where 9 samples were taken for thin-section analyses. All kinematic indicators observed in this area formed under greenschist-facies conditions based on the presence of synkinematic greenschist-facies mineral assemblages. Two samples show top-NW shear senses (samples 24 and 26) and 7 samples display strongly symmetric fabrics and conjugate sets of shear bands (samples 25, 27, and 28 – 32). Relic garnet often occurs within retrogressed metagabbroic rocks and calcschists along the greenschist-facies shear zone southwest of the lake suggesting that these rocks should be still attributed to the Zermatt-Saas and not to the overlying Combin zone. A garnet micaschist sample (sample 25) from this locality shows conjugate sets of shear bands indicating top-NW (Fig. 2.4c) as well as top-SE shearing (Fig. 2.4d). Chlorite replaces white mica in sheared parts documenting the greenschist-facies character of shear bands. Two samples from nearby outcrops, a garnet-bearing calcschist (sample 24) and a garnet-free greenschist (Fig. 2.4e; sample 26) show dominant top-NW shear senses in thin-section. In the greenschist, domains with conjugate shear senses can also be observed. Further to the north, calcschists become progressively more retrogressed so that garnet is not preserved anymore. In one calcschist sample, both shear senses can be observed in thin-section (Figs. 2.4f and g; sample 27). However, chlorite is not only stable in shear bands but is part of the mylonitic foliation which has later been overprinted by shear band formation. Fabric formation must have therefore already occurred under greenschist-facies conditions. Top-SE shear senses often dip very shallowly and are subparallel to the mylonitic foliation (Fig. 2.4f) whereas top-NW shear bands cut the foliation at a relatively high angle (Fig. 2.4g). This may indicate that top-SE shearing within these rocks was more pronounced during earlier stages and main fabric formation. In outcrop, calcschists southwest of the lake often display top-NW shear bands but also often show signs of a coaxial deformation component which is evident from boudinaged competent layers (Fig. 2.3g). Further to the north, greenschists just below the Combin Fault (samples 28 – 31) show strongly symmetric fabrics in thin-section with no signs of a rotational deformation component (Figs. 2.4h and i). Albite blasts are poikiloblastic and inclusions consist of the matrix phases. They are aligned with the main foliation suggesting that they grew synkinematically during the main phase of greenschist-facies retrogression. In outcrop, asymmetrically sheared and sigmoidal shaped quartz layers within these greenschists occasionally indicate top-NW shearing.

In summary, 2 samples of strongly retrogressed rocks show top-NW shear senses in thin-section (samples 24 and 26), 2 show top-SE shear senses (samples 21 and 23), and 8 ambiguous shear senses and rather symmetric fabrics (samples 22, 25, 27, and 28 – 32). Kinematic indicators that formed under (U)HP conditions gave top-(S)E shear senses in 4 thin-sections (samples 2, 4, 6, and 10) and top-(N)W shear senses in 3 thin-sections (samples 3, 18, 20). Kinematic indicators that formed under greenschist-facies

conditions gave top-(S)E shear senses in 6 thin-sections (samples 1, 5, 7, 9, 19, and 21) and top-(N)W shear senses in 2 thin-sections (samples 8 and 17). Six eclogite samples do not display any kinematic indicators (samples 11 – 16). The Zermatt-Saas zone at Lago di Cignana shows dominant top-(S)E shear senses at lower structural levels formed under (U)HP to greenschist-facies conditions. Top-(N)W shear senses occur subordinately within fresh or only weakly retrogressed (U)HP rocks. At higher structural levels, top-(S)E and top-(N)W shear senses become more equally distributed within more strongly retrogressed lithologies and, in the direct footwall of the Combin Fault, calcschists and greenschists display strongly symmetric fabrics.

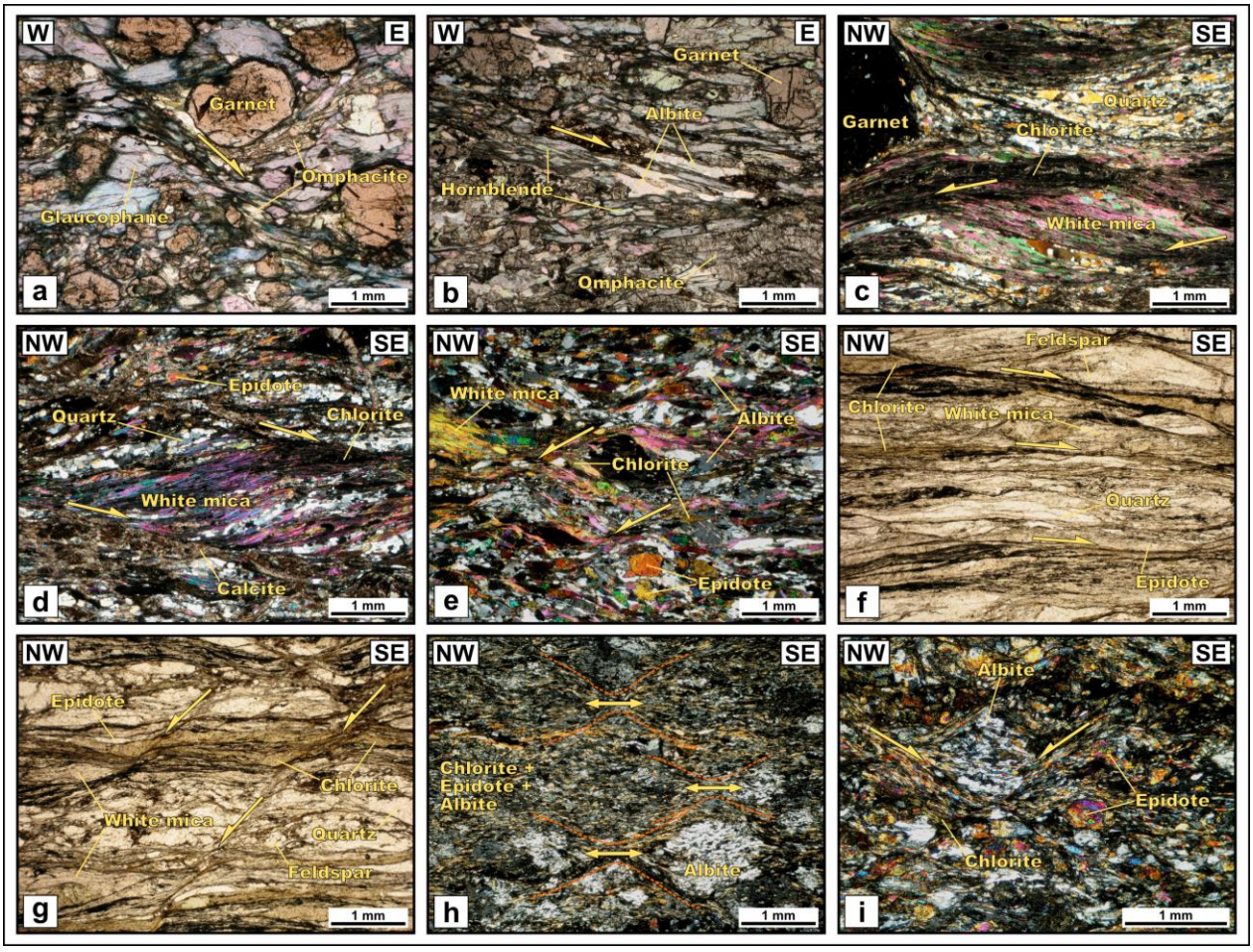

Figure 2.4: Photomicrographs of rocks from the Zermatt-Saas zone. All thin-sections were cut parallel to the xz-plane of the finite strain ellipsoid. Pictures a), b), f), and g) were taken with parallel polarizers, the others with crossed polarizers. a) Sample 4: eclogite from the UHP slice south of the lake showing top-E shear band with the UHP assemblage stable; for microprobe analyses of this sample see sample FD244 in appendix. b) Sample 1: partly retrogressed eclogite from an outcrop south of the lake with hornblende and albite stable in top-E shear band indicating formation at lower amphibolite-facies to upper greenschist-facies conditions. c) Sample 25: garnet calcschist from the western side of the lake showing retrograde top-NW shear sense with chlorite stable. d) Sample 25: garnet calcschist, same sample as before showing retrograde top-SE shear sense with chlorite stable. e) Sample 26: greenschist from southwest of the lake showing top-NW shear bands overprinting an earlier symmetric fabric. f) Sample 27: garnet-free metasediment from southwest of the lake with shallowly-dipping top-SE shear bands cutting through chlorite-bearing mylonitic foliation. g) Sample 27: garnet-free metasediment, same sample as before but with more steeply dipping top-NW shear bands cutting through chlorite-bearing foliation. h) Sample 29: fine-grained greenschist with poikiloblastic albite from the western side of the lake showing strongly symmetric fabric. i) Sample 30: greenschist with poikiloblastic albite from the western side of the lake showing strongly symmetric fabric.

2.5.2 Combin zone

2.5.2.1 Cimes Blanches nappe

Northeast of Monte Pancherot the Cimes Blanches nappe comprises quartzites, cellular dolomites (Rauhwacke), and marbles. Quartzites close to the base of the Cimes Blanches nappe were used for microstructural and textural analyses (Fig. 2.5) to gain information on the kinematics and geometry of deformation in the direct hanging wall of the Combin Fault. Stretching lineations within these strongly sheared rocks plunge to the NNW to N. Four samples (samples 35 – 38) were analysed in detail with sample 35 being the one closest to the Combin Fault and sample 38 the one farthest away. The quartzites are mylonitic and display a tabular foliation defined by cm- to dm-thick quartz layers of white to greyish colour. These layers are sometimes deformed into folds with NNW-plunging axes parallel to the stretching lineation (Fig. 2.3h). They may have formed contemporaneously with the main stretching lineation or may represent earlier folds that were transposed into parallelism with the stretching direction. The stretching lineation is defined by elongated quartz aggregates and aligned white mica. Samples 36 - 38 are mineralogically and texturally very similar. They consist of quartz with only minor amounts of white mica and feldspar and show only slight textural domains (Fig. 2.5). Sample 35 is relatively coarse-grained, contains more white mica, and locally shows textural domains which consist of larger quartz grains showing incipient subgrain formation. A slight GSPO can be observed in sample 35 indicating top-SSE as well as top-NNW transport in different domains. Rare shear bands and mica fish in samples 36 – 38 indicate top-NNW transport. Shear bands in sample 35 are conjugate and show top-NNW and top-SSE shear senses (Figs. 2.6a and b).

Textures of the four quartz mylonites were measured with the x-ray texture goniometer at Geowissenschaftliches Zentrum Universität Göttingen. Figure 2.5 depicts pole figures for [c]- and [a]-axes as equal area projections in the lower hemisphere with isolines being multiples of random distribution. The xy-plane in the pole figures corresponds to the foliation measured in the field. The x-direction is the stretching lineation measured in the field which plunges to the NNW in all quartz mylonites. All four samples show cross girdle type [c]-axis pole figures as a basis (e.g. Schmid and Casey, 1986). Rhomb <a> slip is dominant in all samples. Different contributions of basal <a> and prism <a> slip modify the basic cross girdles into partial cross girdles. The activity of these different slip systems and the absence of a single basal <a> maximum around the y-axis suggest texture formation at temperatures below 500° C (Stipp et al., 2002). C-axis opening angles in the pole figures are consistently around 50° suggesting temperatures of ca. 400 ± 50° C during texture formation (Kruhl, 1996; Law et al., 2004). [c]- and [a]-axes distributions have orthorhombic symmetries suggesting dominant coaxial deformation. [a]-axes form small circles about 25° away from the x-direction. The distribution of [a]-axes maxima in samples 36 and 38 suggests slight dominance of the sinistral, i.e. NNW-directed slip system. The dextral slip system is slightly better developed in sample 37 suggesting more pronounced top-SSE deformation. The different intensities of the textures are probably an effect of strain localization with sample 37 representing a high-strain zone and 35 a zone of relatively low strain during coaxial deformation. The higher content of white mica in sample 35 may also have contributed to the lower intensities of this sample.

In summary, microstructural and textural analyses on quartzites suggest that the base of the Cimes Blanches nappe at Lago di Cignana is characterized by dominant coaxial deformation. Orthorhombic textures indicate only a weak rotational component and conjugate top-SSE and top-NNW kinematic indicators in thin-section also suggest dominant pure shear deformation. Top-NNW shear senses are slightly dominant over top-SSE shear senses in thin-section and may represent a late top-NW overprint along the Combin Fault.

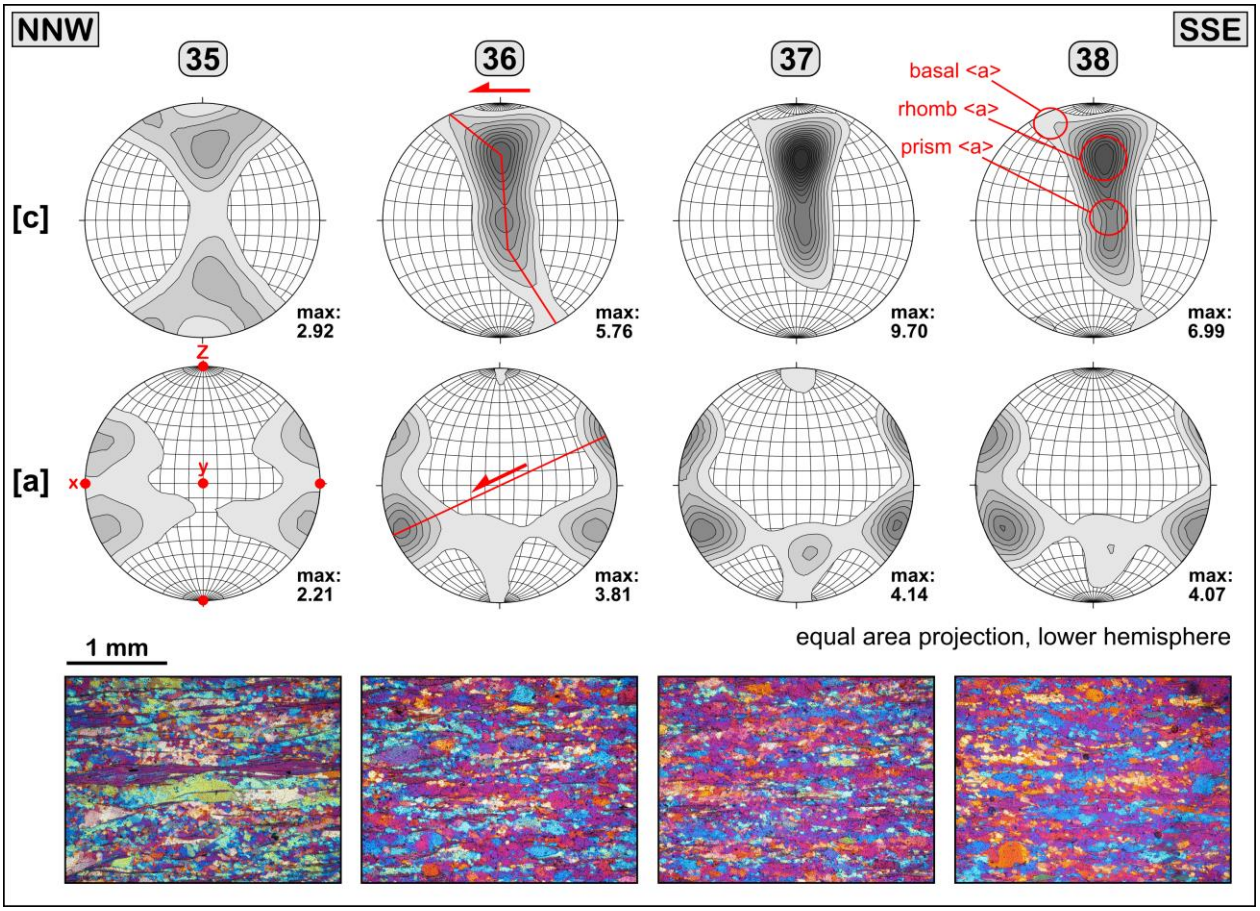

Figure 2.5: Pole figures of [c]- and [a]-axes distributions of quartzites from the Cimes Blanches nappe at the base of the Combin zone; equal are projections in the lower hemisphere; maxima of isolines being multiples of random distribution are indicated; the xy-plane in pole figures corresponds to the foliation and the x-direction to the stretching lineation measured in the field; pole figures are strongly orthorhombic and indicate dominant coaxial deformation under greenschist-facies conditions below 500° C (see text for further discussion); photomicrographs at the bottom correspond to the samples labeled above and were taken with gypsum plate inserted.

2.5.2.2 Tsaté nappe

The Tsaté nappe at Lago di Cignana comprises greenschist-facies calcschists and metabasites. No clear indicators of an earlier blueschist-facies imprint could be found. Calcschists are always garnet-free and consist of white mica, quartz, feldspar, calcite, chlorite, and epidote. They often show a strong metamorphic layering defined by ribbons of dominantly white mica and quartz, respectively. Chlorite often occurs as relatively large grains as part of the foliation indicating greenschist-facies conditions during formation. Metabasites display typical greenschist-facies assemblages consisting of epidote

(clinozoisite), actinolite, chlorite, and albite (for electron microprobe analyses see sample FD34 in appendix). Stretching lineations associated with penetrative fabrics mainly plunge to the NW. Thirteen samples were taken for thin-section analyses, most of them along the crest northeast of the lake between Monte Pancherot in the south and Monte Seriola in the north. 9 of them show top-NW shear senses (samples 33, 39 – 42, 44, 46 – 48), 2 show top-SE shear senses (samples 43 and 45), and 2 thin-sections display symmetric fabrics (samples 34 and 49).

In most calcschists, the greenschist-facies foliation has been overprinted by discrete top-NW shear bands (Fig. 2.6c). Greenschists also often show localization of strain into top-NW shear bands. In a fine-grained sample, poikilobastic albite has a slight sigmoidal shape (Fig. 2.6d) suggesting ductile deformation at temperatures exceeding ca. 450° C (e.g. Pryer, 1993). Inclusions are elongated and aligned parallel to the surrounding matrix fabric suggesting that albite grew synkinematically. Two samples from the central part of the Tsaté nappe along the crest display top-SE and top-S shear senses (samples 43 and 45). Macroscopic shear bands within calcschists show almost exclusively top-NW shear senses along the crest and on the western side of the lake (Fig. 2.3i). A few top-SE shear senses can be observed above the Combin Fault southwest of the lake (Fig. 2.3j). No overprinting relations could be found between these opposing shear senses. In a nearby outcrop within heterogeneous metasediments, NW-vergent, asymmetric tight folds in the lower part occur together with boudinage and top-NW shear bands in the upper part (Fig. 2.3k). Asymmetry of boudins and shallowly-dipping shear bands indicate bulk top-NW shearing. No clear overprinting relations exist between folding and boudinage. Antiforms seem to coincide with and sometimes intrude into boudin-necks whereas synforms rather correlate with boudins. This suggests contemporaneous folding and boudinage and simultaneous formation of shortening and extensional structures during bulk top-NW shearing within these anisotropic rocks. The two calcschist samples taken from nearby outcrops show top-NW (sample 33) and conjugate (sample 34) shear senses, respectively.

The Tsaté nappe at Lago di Cignana is characterized by dominant top-NW shearing which, however, often seems to postdate the pervasive greenschist-facies imprint observed in metasedimentary and metabasic rocks. These deformation structures suggest a significant rotational component during late greenschist-facies shearing. Deformation structures indicating a significant pure shear component or bulk top-SE shearing are subordinate within the Tsaté nappe.

2.5.3 Dent Blanche nappe

Rocks of the lower Dent Blanche nappe at Lago di Cignana often display greenschist-facies mylonitic fabrics with stretching lineations plunging to the NW. South of Monte Seriola, rocks of the Valpelline series are exposed in the hanging wall of Tsaté calcschists (samples 50 – 52). The mylonitic foliation consists of alternating layers of quartz + feldspar and white mica + epidote which are often overprinted by subsequent deformation. Small-scale, isoclinal, and recumbent folds affecting the original metamorphic layering are observed in one sample (Fig. 2.6e; sample 51). In the same sample, the metamorphic layering is cut by shallowly-dipping top-NW shear bands (Fig. 2.6f) which are interpreted to have formed during a relatively late stage and not contemporaneously with the mylonitic foliation. The metamorphic layering is

also cut by brittle, moderately- to steeply-dipping top-SE microfaults interpreted as late structures after cessation of ductile deformation within these rocks. In a quartzitic sample, quartz layers defined by different grain sizes have been folded into small-scale, asymmetric NW-facing folds. Quartz grains recrystallized dynamically during folding so that an axial surface foliation is defined by a GSPO which also indicates top-NW transport (Fig. 2.6g; sample 52). Dynamic recrystallization of quartz probably occurred mainly by sugrain rotation recrystallization (SGR) suggesting temperatures between ca. 400° and 500° C (Stipp et al., 2002). Epidote occurs along the boundaries of quartz layers.

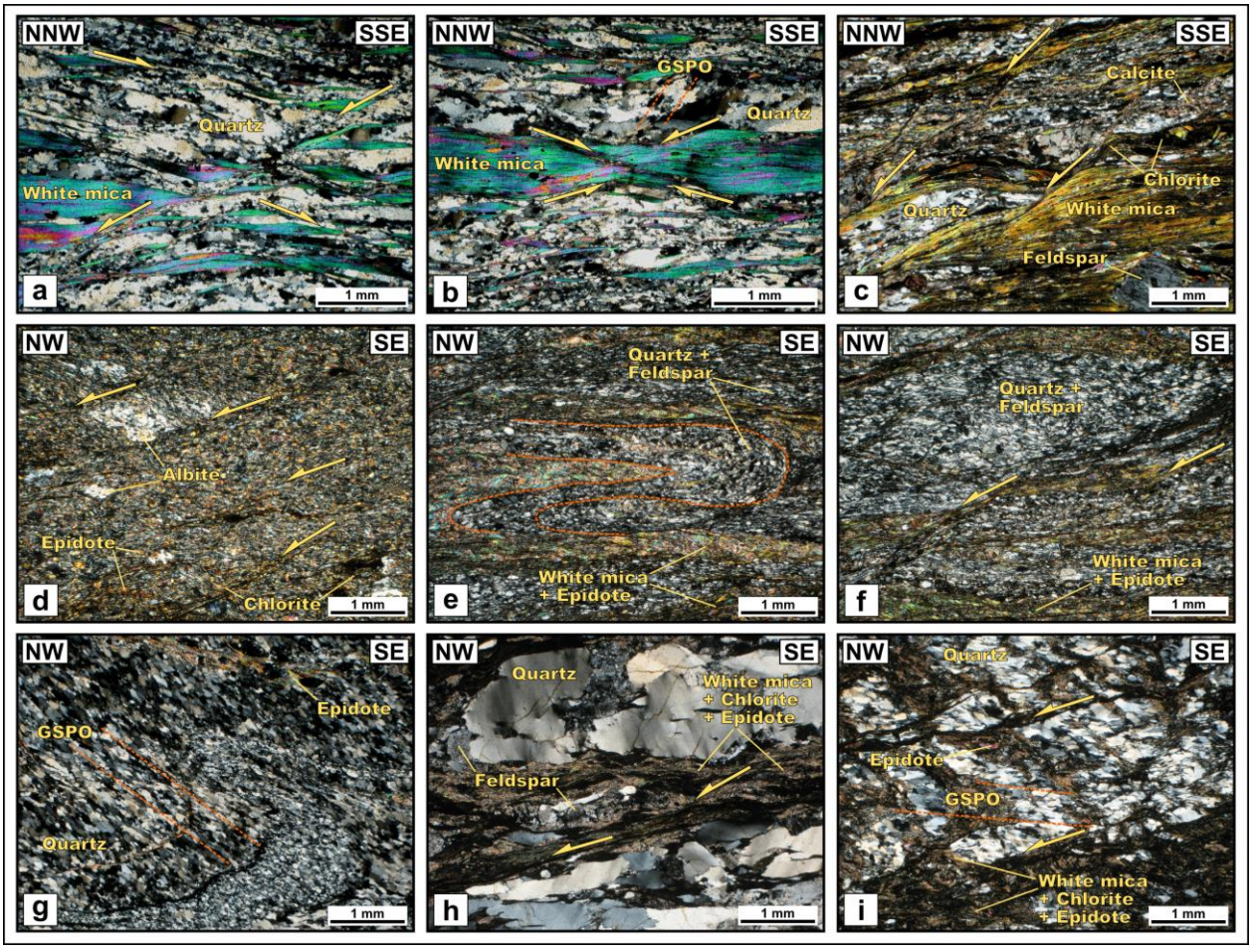

Figure 2.6: Photomicrographs of rocks from the Combin zone and Dent Blanche nappe. All thin-sections were cut parallel to the xz-plane of the finite strain ellipsoid. All pictures were taken with crossed polarizers. a) Sample 35: quartzite from the Cimes Blanches nappes indicating top-SSE as well as top-NNW shearing. b) Sample 35: quartzite from the Cimes Blanches nappe, same sample as before with necked muscovite indicating coaxial deformation; slight quartz GSPO indicates top-SSE shearing. c) Sample 40: calcschist from the Tsaté nappe displaying discrete top-NW shear bands; chlorite is stable as part of the mylonitic foliation and within shear bands. d) Sample 41: fine-grained greenschist from the Tsaté nappe with poikiloblastic albite; shear bands indicate top-NW shearing and ductiley deform albite. e) Sample 51: Valpelline series mylonite from the lowermost Dent Blanche nappe south of Monte Seriola; the greenschist-facies foliation has been folded into isoclinal recumbent folds. f) Sample 51: Valpelline series mylonite, same sample as before with top-NW shear band cutting through the mylonitic foliation. g) Sample 52: Valpelline series quartzitic mylonite from the lowermost Dent Blanche nappe south of Monte Seriola; quartz GSPO and vergence of asymmetric fold indicate top-NW transport. h) Sample 54: Arolla series gneiss from an outcrop northwest of the lake with top-NW shear band; associated patchy and undulose extinction of quartz indicate deformation around 300°C. i) Sample 53: Arolla series gneiss from the same outcrop as before with folded metamorphic layering which is cut by discrete top-NW shear bands; brittle offset of quartz layers indicates deformation below 300°C.

Mylonites of the Arolla series crop out along the plains north of the lake and also show deformation structures related to top-NW shearing. Macroscopic shear bands have a semi-ductile character suggesting that they formed during a relatively late stage of NW-directed shearing (Fig. 2.3l). In thin section, ductile top-NW shear bands are localized in domains of fine-grained intergrowths of white mica + epidote + chlorite (Fig. 2.6h; sample 54). They are associated with quartz grains showing a patchy and undulose extinction suggesting deformation between ca. 300° and 400° C (Stipp et al., 2002). In another sample, an older foliation defined by quartz ribbons in a matrix of white mica + epidote + chlorite has been folded into recumbent, open to tight folds (Fig. 2.6i; sample 53). Flattened and elongated quartz grains show a GSPO which again defines an axial surface cleavage. The folds have been cut by discrete top-NW shear bands that offset the folded quartz layers in a brittle manner and therefore indicate deformation below 300°C.

The lower Dent Blanche nappe at Lago di Cignana exhibits deformation structures that suggest several stages of top-NW shearing from highly ductile to low-grade and partly brittle greenschist-facies conditions. Some higher-grade top-NW structures probably predate pure shear-dominated deformation observed in other units whereas others most likely postdate this phase and therefore must be ascribed to a late stage of top-NW shearing. Deformation along the DBBT was strongly rotational without any signs of a pure shear component.

2.6 Discussion

2.6.1 Kinematics and geometry of deformation

In the area around Lago di Cignana, a continuous structural evolution of the exposed units related to progressive deformation under (U)HP to greenschist-facies conditions can be observed. 2D strain geometries for the different units have been estimated from the observed deformation structures and are depicted in figure 2.7c. Different structural levels can be observed which are characterized by different bulk shear senses and varying amounts of simple and pure shear deformation (Fig. 2.7c). Lower structural levels of the Zermatt-Saas zone at Lago di Cignana experienced bulk top-(S)E shearing and subordinate coaxial deformation whereas the uppermost part is characterized by large amounts of coaxial deformation. The Cimes Blanches nappe experienced dominant pure shear deformation with a minor top-NW overprint. The observed greenschist-facies deformation within the Tsaté nappe is characterized by bulk top-NW general shear. Deformation along the DBBT was related to strongly rotational top-NW shearing according to the observed deformation structures.

The majority of (U)HP rocks of the upper Zermatt-Saas zone shows top-E shear senses formed under eclogite- to upper greenschist-facies conditions. This suggests bulk top-E shear as dominant deformation mechanism in the upper Zermatt-Saas zone during main exhumation from (U)HP deths. Abundant conjugate top-W shear senses within (U)HP lithologies, however, suggest significant deviation from simple shear and significant amounts of coaxial deformation. This pure shear component is ascribed to internal deformation of the upper Zermatt-Saas zone possibly due to differential exhumation of distinct rock units and overall shortening perpendicular to tectonic boundaries during ascent. Greenschist-facies retrogression increases progressively into the hanging wall towards the Combin Fault. Some distinct

zones of dominant top-SE or top-NW shear can be observed in outcrop in the hanging wall of the UHP slice. In some outcrops and especially in thin-section, however, top-SE and top-NW shear bands are often closely associated without any overprinting relations. Opposing shear bands, however, often have different orientations with respect to the main fabric: While top-SE shear bands are sub-parallel to the foliation, top-NW shear bands cut it at high angles. This may indicate that the main stretching direction during coaxial deformation was not strictly parallel to an already existing fabric in these rocks. Both sets of shear bands are associated with partial replacement of white mica by chlorite along zones of high strain but they also affect pre-existing chlorite. I suggest that most of the observed conjugate top-SE and top-NW shear senses in the uppermost Zermatt-Saas zone formed during a stage of dominant pure shear deformation. However, top-(S)E shearing may have been dominant during early stages of greenschist-facies deformation based on geometric relations of top-SE shear bands with the main fabric and the occurrence of greenschist-facies shear bands within weakly retrogressed (U)HP rocks at lower structural levels. I interpret these observations to reflect bulk top-SE shearing during early greenschist-facies retrogression along the upper Zermatt-Saas zone most likely responsible for juxtaposition with the overlying Combin zone. Since top-SE structures are scarce within the Combin zone in the hanging wall of the Combin Fault, strain during exhumation of the Zermatt-Saas zone to mid-crustal levels is interpreted to have been localized along the uppermost Zermatt-Saas zone and to have been partly overprinted by subsequent deformation. The uppermost Zermatt-Saas zone in the direct footwall of the Combin Fault shows a pervasive greenschist-facies overprint mostly associated with symmetric fabrics in thin-section. This suggests dominant pure shear deformation during the main phase of low-pressure retrogression within these rocks. Close to the Combin Fault on the western side of the lake, macroscopic kinematic indicators in calcschists indicate top-NW shearing which overprints existing symmetric fabrics. My structural observations suggest that the Zermatt-Saas zone at Lago di Cignana experienced a progressive evolution from eclogite- to greenschist-facies bulk top-(S)E shearing to post-exhumational pure shear deformation with a minor top-NW overprint. Coaxial deformation can be traced across the Combin Fault into the lower Combin zone where it is preserved within quartzites of the Cimes Blanches nappe displaying orthorhombic textures and conjugate shear senses. Metasediments of the Tsaté nappe on the western side of the lake display abundant boudinage and top-NW structures and only subordinate top-SE shear senses close to the Combin Fault. The similar style and geometry of deformation in the immediate footwall and hanging wall of the Combin Fault suggests that the main phase of pure shear deformation postdates juxtaposition of the Zermatt-Saas and Combin zones. Considering the aforementioned structural evolution of the upper Zermatt-Saas zone and lowermost Combin zone, stacking of the two units most probably occurred along greenschist-facies bulk top-SE shear zones which are only scarcely preserved at Lago di Cignana due to subsequent coaxial deformation. Most of the observed large-scale boudinage of the UHP slice, serpentinites, and the Cimes Blanches nappe probably occurred under greenschist-facies conditions when strain became more localized into narrow shear zones during overall NW-SE directed crustal elongation. The Combin zone displays almost exclusively top-NW shear senses and only a few top-SE structures but may have experienced significant coaxial deformation after juxtaposition with the Zermatt-Saas zone as suggested by orthorhombic quartz textures and the strongly reduced thickness of the

Tsaté nappe in the Lago di Cignana area. Pure shear deformation occurred under medium-grade greenschist-facies conditions as suggested by temperature estimates from quartz textures and therefore most likely after retrograde peak temperatures. Temperatures further decreased when coaxial deformation evolved into bulk top-NW shearing as evident from low-grade top-NW shear senses along the DBBT. The Combin zone at Lago di Cignana mainly displays a progressive evolution from post-exhumational pure shear to subsequent top-NW general shear under decreasing greenschist-facies conditions. A progressive decrease in metamorphic grade from high- to low-grade greenschist-facies conditions can also be observed within Dent Blanche basal mylonites. Top-NW simple shear was the dominant deformation mechanism along the DBBT without any signs of pure shear or top-SE simple shear during ductile deformation. The decreasing metamorphic grade of kinematic indicators suggests that NW-vergent shearing occurred during several stages of the greenschist-facies evolution of the DBBT and underlying units. Late top-NW shearing along the Combin Fault and within the Tsaté nappe is attributed to renewed thrusting along the DBBT. The lowermost Dent Blanche nappe at Lago di Cignana shows a progressive evolution from upper to lower greenschist-facies conditions related to several stages of top-NW shearing.

2.6.2 Previously published structural works

Earlier structural works by different authors in the Lago di Cignana area are largely in agreement with my findings but also show some differences which should be discussed before further tectonic interpretation. Ballèvre and Merle (1993) reported equally top-E and top-W shear senses for Zermatt-Saas (U)HP rocks so that no bulk shear sense could be determined. Also Van der Klauw et al. (1997) reported rather conjugate sets of eclogite-facies shear bands and suggested that no appreciable deformation was localized into metabasites during exhumation from UHP depths. Although I confirm the existence of conjugate shear senses in (U)HP assemblages, I find a clear dominance of top-E shear criteria. My microstructural observations on (U)HP eclogites and metasediments, suggest that most of the deformation under eclogite-facies conditions can be related to bulk top-E shearing. Structures associated with this early deformation phase can be especially well-studied within eclogites and metasediments south of the lake. Since the UHP rocks at Lago di Cignana exhibit the youngest available ages related to peak-pressure metamorphism for the Zermatt-Saas zone, the UHP unit must have been exhumed at much higher rates than surrounding HP rocks. Differential exhumation must have led to deformation along the interface between UHP and HP rocks and therefore to conjugate shear senses which would correspond to the observations of Ballèvre and Merle (1993) and Van der Klauw et al. (1997). The strong greenschist-facies overprint in the uppermost Zermatt-Saas zone has already been recognized by Van der Klauw et al. (1997) who reported dominant top-NW kinematic indicators within these rocks in good agreement with my observations. However, this study also shows that top-NW structures have been preceded and accompanied by a considerable portion of coaxial deformation indicating a dominant pure shear regime after juxtaposition of the Zermatt-Saas and Combin zones at crustal levels.

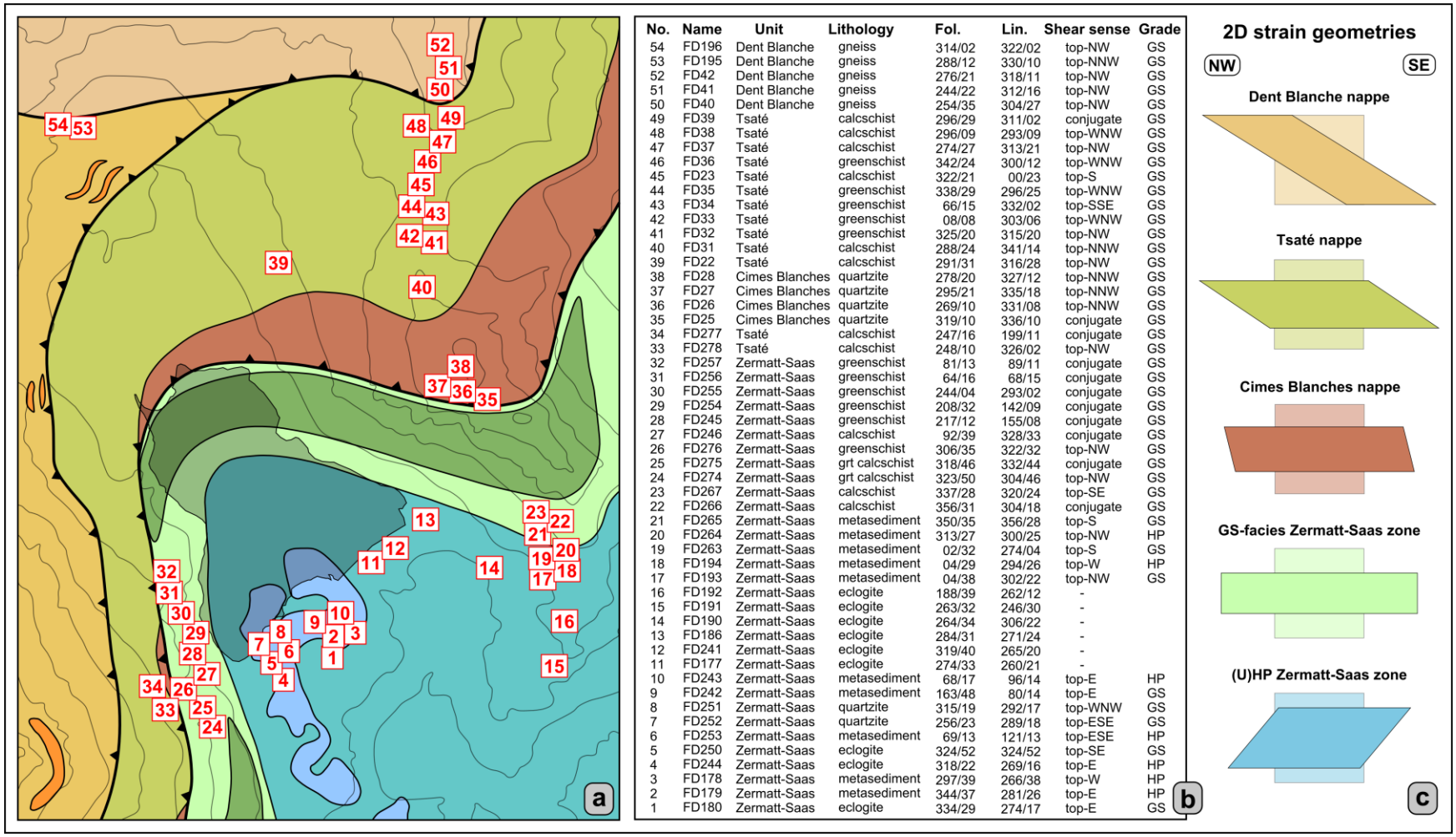

No.	Name	Unit	Lithology	Fol.	Lin.	Shear sense	Grade
54	FD196	Dent Blanche	gneiss	314/02	322/02	top-NW	GS
53	FD195	Dent Blanche	gneiss	288/12	330/10	top-NNW	GS
52	FD42	Dent Blanche	gneiss	276/21	318/11	top-NW	GS
51	FD41	Dent Blanche	gneiss	244/22	312/16	top-NW	GS
50	FD40	Dent Blanche	gneiss	254/35	304/27	top-NW	GS
49	FD39	Tsaté	calcschist	296/29	311/02	conjugate	GS
48	FD38	Tsaté	calcschist	296/09	293/09	top-WNW	GS
47	FD37	Tsaté	calcschist	274/27	313/21	top-NW	GS
46	FD36	Tsaté	greenschist	342/24	300/12	top-WNW	GS
45	FD23	Tsaté	calcschist	322/21	00/23	top-S	GS
44	FD35	Tsaté	greenschist	338/29	296/25	top-WNW	GS
43	FD34	Tsaté	greenschist	66/15	332/02	top-SSE	GS
42	FD33	Tsaté	greenschist	08/08	303/06	top-WNW	GS
41	FD32	Tsaté	greenschist	325/20	315/20	top-NW	GS
40	FD31	Tsaté	calcschist	288/24	341/14	top-NNW	GS
39	FD22	Tsaté	calcschist	291/31	316/28	top-NW	GS
38	FD28	Cimes Blanches	quartzite	278/20	327/12	top-NNW	GS
37	FD27	Cimes Blanches	quartzite	295/21	335/18	top-NNW	GS
36	FD26	Cimes Blanches	quartzite	269/10	331/08	top-NNW	GS
35	FD25	Cimes Blanches	quartzite	319/10	336/10	conjugate	GS
34	FD277	Tsaté	calcschist	247/16	199/11	conjugate	GS
33	FD278	Tsaté	calcschist	248/10	326/02	top-NW	GS
32	FD257	Zermatt-Saas	greenschist	81/13	89/11	conjugate	GS
31	FD256	Zermatt-Saas	greenschist	64/16	68/15	conjugate	GS
30	FD255	Zermatt-Saas	greenschist	244/04	293/02	conjugate	GS
29	FD254	Zermatt-Saas	greenschist	208/32	142/09	conjugate	GS
28	FD245	Zermatt-Saas	greenschist	217/12	155/08	conjugate	GS
27	FD246	Zermatt-Saas	calcschist	92/39	328/33	conjugate	GS
26	FD276	Zermatt-Saas	greenschist	306/35	322/32	top-NW	GS
25	FD275	Zermatt-Saas	grt calcschist	318/46	332/44	conjugate	GS
24	FD274	Zermatt-Saas	grt calcschist	323/50	304/46	top-NW	GS
23	FD267	Zermatt-Saas	calcschist	337/28	320/24	top-SE	GS
22	FD266	Zermatt-Saas	calcschist	356/31	304/18	conjugate	GS
21	FD265	Zermatt-Saas	metasediment	350/35	356/28	top-S	GS
20	FD264	Zermatt-Saas	metasediment	313/27	300/25	top-NW	HP
19	FD263	Zermatt-Saas	metasediment	02/32	274/04	top-S	GS
18	FD194	Zermatt-Saas	metasediment	04/29	294/26	top-W	HP
17	FD193	Zermatt-Saas	metasediment	04/38	302/22	top-NW	GS
16	FD192	Zermatt-Saas	eclogite	188/39	262/12	-	
15	FD191	Zermatt-Saas	eclogite	263/32	246/30	-	
14	FD190	Zermatt-Saas	eclogite	264/34	306/22	-	
13	FD186	Zermatt-Saas	eclogite	284/31	271/24	-	
12	FD241	Zermatt-Saas	eclogite	319/40	265/20	-	
11	FD177	Zermatt-Saas	eclogite	274/33	260/21	-	
10	FD243	Zermatt-Saas	metasediment	68/17	96/14	top-E	HP
9	FD242	Zermatt-Saas	metasediment	163/48	80/14	top-E	GS
8	FD251	Zermatt-Saas	quartzite	315/19	292/17	top-WNW	GS
7	FD252	Zermatt-Saas	quartzite	256/23	289/18	top-ESE	GS
6	FD253	Zermatt-Saas	metasediment	69/13	121/13	top-ESE	HP
5	FD250	Zermatt-Saas	eclogite	324/52	324/52	top-SE	GS
4	FD244	Zermatt-Saas	eclogite	318/22	269/16	top-E	HP
3	FD178	Zermatt-Saas	metasediment	297/39	266/38	top-W	HP
2	FD179	Zermatt-Saas	metasediment	344/37	281/26	top-E	HP
1	FD180	Zermatt-Saas	eclogite	334/29	274/17	top-E	GS

Figure 2.7: a) Simplified geological sketch map of the area around Lago di Cignana with sample locations. b) Table of samples taken for thin-section analyses with values for dip directions and angles of foliations, plunge directions and angles of stretching lineations, shear senses and metamorphic grade of kinematic indicators; HP: high-pressure conditions, GS: greenschist-facies conditions; names after sample numbers correspond to the original sample names given in the field. c) Approximate 2D strain geometries of units estimated from the observed deformation structures.

Groppo et al. (2009) also reported different metamorphic grades in the units above and below the UHP rocks which they attributed to the existence of three distinct tectonic elements, a lower and an upper HP unit with the UHP slice sandwiched in between. The described serpentinite mélange zone south of Monte Pancherot may indeed represent a contact between different tectonic elements. Also, calcschists only occur at higher structural levels in the uppermost Zermatt-Saas zone but are absent below the UHP unit which would support such an interpretation. In any case, the UHP unit was located at a structurally high position within the Zermatt-Saas zone during exhumation and subsequent retrogression and was therefore exposed to shearing along its upper boundary. My structural observations and interpretations are therefore not in conflict with the view that the Zermatt-Saas zone at Lago di Cignana comprises different tectonic elements. Reddy et al. (2003) reported abundant top-SE shear senses for the Cimes Blanches nappe at Lago di Cignana. This study revealed dominant orthorhombic quartz textures and microstructures that show top-SE as well as top-NW shear senses suggesting that the quartz mylonites recorded dominant pure shear deformation.

My findings are largely in agreement with existing work in the Lago di Cignana area but some new aspects of my structural observations will contribute to a better understanding of the structural evolution of the exposed units.

2.6.3 Structural and tectonic evolution

In this section, I embed my structural observations and interpretations into the tectonic framework of the Western Alps and propose a post-UHP peak evolution for the Penninic units at Lago di Cignana between ca. 43 and 35 Ma (Fig. 2.8). Initial exhumation of the Zermatt-Saas zone after 43 Ma was probably triggered by buoyancy resulting from large portions of hydrated rock material (serpentinite, lawsonite eclogite) (Angiboust and Agard, 2010). Buoyant ascent, most likely in the footwall of the upper plate lithospheric mantle wedge and, at later stages, the Sesia nappe, produced eclogite- and greenschist-facies top-E shear along the upper Zermatt-Saas zone (Fig. 2.8a). Buoyancy of low-density quartz-rich metasedimentary material of the UHP slice compared to surrounding mafic material may have led to differential exhumation of UHP rocks and internal deformation of the Zermatt-Saas zone (Fig. 2.8a).

The UHP unit reached greenschist-facies conditions around 38 Ma as suggested by Rb-Sr dating by Amato et al. (1999). This age has not been correlated with any kinematic data but may reflect the timing of retrograde top-SE shearing along the upper Zermatt-Saas zone (Fig. 2.8b) since greenschist-facies pure shear and top-NW deformation were localized at higher structural levels above the UHP unit. Constraints on the timing of top-SE shearing in the Zermatt-Saas zone are also given by the age of retrograde top-SE shear zones in the Täschalp area further to the northeast which formed between 42 – 37 Ma (Cartwright and Barnicoat, 2002). Formation of the Mischabel fold in the hanging wall of the northern Zermatt-Saas zone probably represents a late stage of SE-vergent shearing after juxtaposition of the Combin and Zermatt-Saas zones. Mischabel-phase folding may have occurred at ca. 37 Ma and is abundant in the Zermatt region (Sartori, 1987; Steck, 1989) but is scarce in the Valtournenche area.

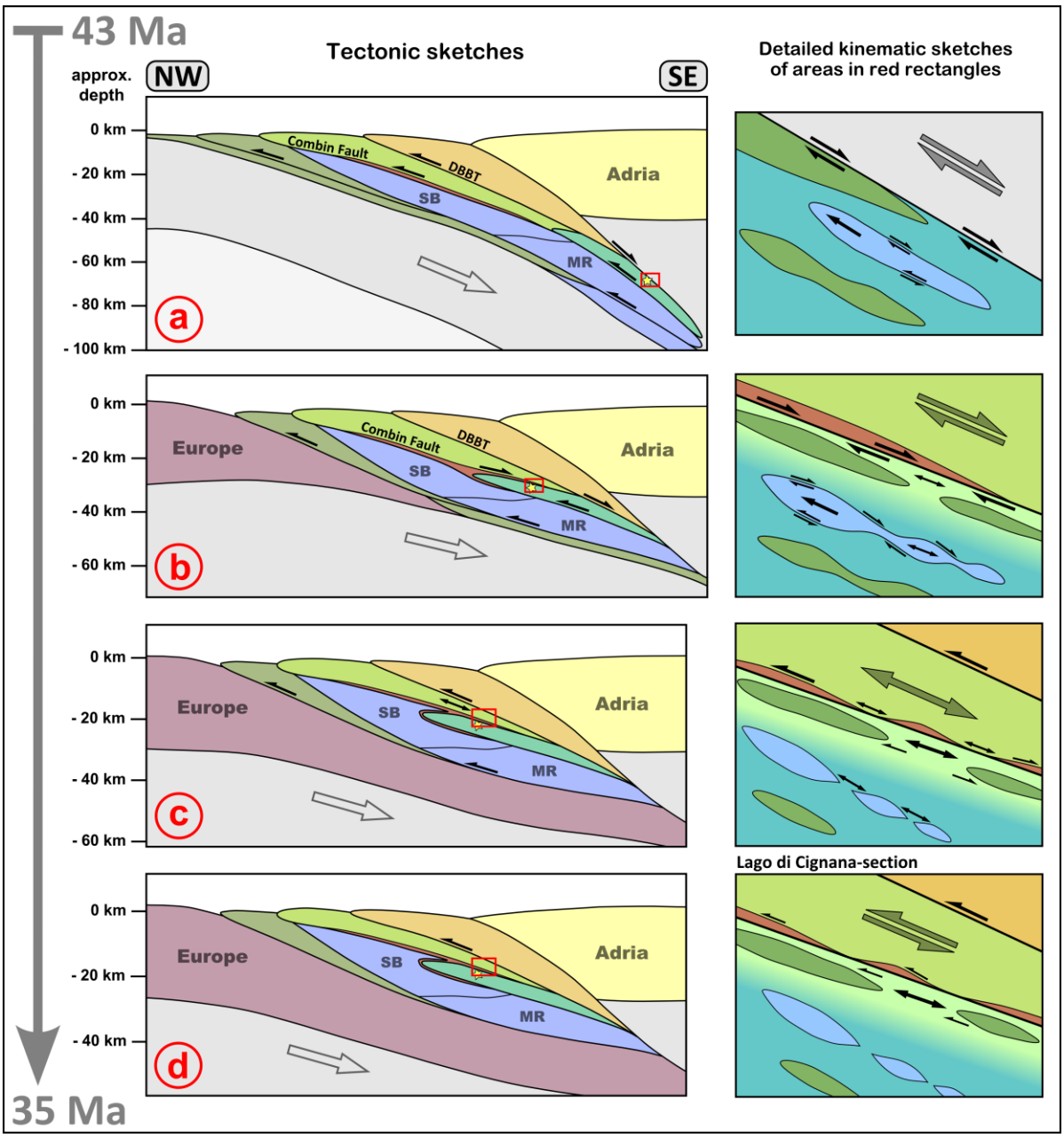

Figure 2.8: Tectonic evolution of the Western Alps with detail sketches of UHP rocks and adjacent units; colour coding of the tectonic sketches is the same as in figure 2.1, colours of the detail sketches correspond to the ones in figure 2.2; SB: St. Bernhard nappe system; MR: Monte Rosa nappe; yellow star indicates location of Lago di Cignana UHP unit; red rectangles indicate areas within detailed kinematic sketches on the right; sketches are not to scale; see further discussion in the text. a) First stages of exhumation of the Zermatt-Saas zone from (U)HP conditions following the peak at ca. 43 Ma during dominant top-(S)E shearing along the upper boundary. Subordinate top-(N)W shearing due to differential exhumation of rock slivers, especially the UHP unit, and internal deformation of the Zermatt-Saas zone. b) Exhumation of the Zermatt-Saas zone to mid-crustal levels, juxtaposition with the overlying Combin zone along greenschist-facies top-SE shear zones, and beginning boudinage due to localized deformation. c) Phase of dominant pure shear deformation under greenschist-facies conditions, strong retrogression of the uppermost Zermatt-Saas zone, and formation of symmetric deformation structures. d) Bulk top-NW shearing due to renewed thrusting along the Dent Blanche Basal Thrust (DBBT) partly overprinting earlier deformation structures and also partly affecting the Combin zone, Combin Fault, and uppermost Zermatt-Saas zone.

The Combin zone in the western Valtournenche area is dominated by top-NW shear senses (Ring, 1995; Pleuger et al., 2007) whereas top-SE kinematic indicators become more abundant towards the SE in the Val Gressoney area (Reddy et al., 1999; Pleuger et al., 2007, Gasco and Gattiglio, 2011). Since all these structures formed under greenschist-facies conditions, it is difficult to establish a relative chronology of deformation. This led to contradicting views regarding the significance and timing of top-SE shearing within the Combin zone. On the basis of structural and geochronological data, some authors proposed top-SE normal faulting along the Combin Fault accompanying exhumation of the Zermatt-Saas zone (Ballèvre and Merle, 1993; Reddy et al., 1999; Wheeler et al., 2001) whereas others suggested top-NW thrusting in the hanging wall of the Combin Fault during extraction faulting (Froitzheim et al., 2006; Pleuger et al., 2007; Weber et al., accepted). In the light of my structural observations, these different views do not necessarily contradict each other on a regional scale. Reddy et al. (2003) already proposed on the basis of their geochronological data that top-SE and top-NW shear zones overlapped in space and time due to a significant pure shear component. I support the hypothesis that deformation may have been distributed into conjugate shear zones and that top-SE and top-NW shear zones were partly active contemporaneously during overall NW-SE directed crustal elongation. However, a cluster of ages between 39 and 36 Ma, which are related to domains of dominant top-SE shear close to the Combin Fault, has been reported by Reddy et al. (1999). Therefore, juxtaposition of the Zermatt-Saas and Combin zones along the southeastern segment of the Combin Fault during this period most likely occurred during dominant normal-sense top-SE shearing (Fig. 2.8b). This phase was followed by pure shear deformation along the Combin/Zermatt-Saas boundary at ca. 36 Ma which was probably triggered by renewed overthrusting of the Dent Blanche nappe along the DBBT (Fig. 2.8c). The possible geometric relations between conjugate top-SE and top-NW shear zones during this phase of dominant coaxial deformation are depicted in figure 2.9. The circles mark areas of dominant pure shear deformation as observed for example in the Lago di Cignana area. Large amounts of shortening perpendicular to nappe boundaries during this major phase of NW-SE directed crustal elongation are probably responsible for tectonic thinning of the Combin zone. Large coaxial strain along the Combin Fault and within the Combin zone has already been reported by Ring (1995) based on finite strain analyses and by Pleuger et al. (2007) on the basis of quartz texture analysis. Coaxial deformation subsequently developed into top-NW general shear which can be attributed to renewed thrusting at higher structural levels along the DBBT (Fig. 2.8d). Top-NW shearing probably occurred at several stages along the DBBT as suggested by non-coaxial top-NW structures at Lago di Cignana and in the western Valtournenche (Mazurek, 1986; Ring, 1995). Post-exhumational NW-vergent shearing in this area has already been suggested by Ballèvre and Merle (1993) to explain the dominance of top-NW shear senses and has been proposed by Van der Klauw et al. (1997) to reflect underthrusting of European continental units and the onset of continental collision. Several reasons may be responsible for the scarcity of normal-sense top-SE shear senses in the hanging wall of the Combin Fault at Lago di Cignana. Strain during exhumation of the Zermatt-Saas zone may have been localized in the footwall of the Combin Fault along the uppermost Zermatt-Saas zone as suggested by abundant eclogite- to greenschist-facies top-(S)E shear senses. The Combin Fault may therefore have acted as a discrete decoupling horizon, i.e. as a fault in a strict sense, during ascent of the Zermatt-Saas

zone. Top-SE structures have also probably been obliterated by subsequent pure shear and top-NW deformation which were both related to renewed thrusting along the DBBT (Figs. 2.8c, 2.8d, and 2.9) before the onset of Vanzone-phase folding after ca. 32 Ma (Pettke et al., 1999). Late low-grade top-NW shearing was probably restricted to higher structural levels but also affected the Combin Fault and uppermost Zermatt-Saas zone at Lago di Cignana due to the strongly reduced thickness of the Combin zone in this area.

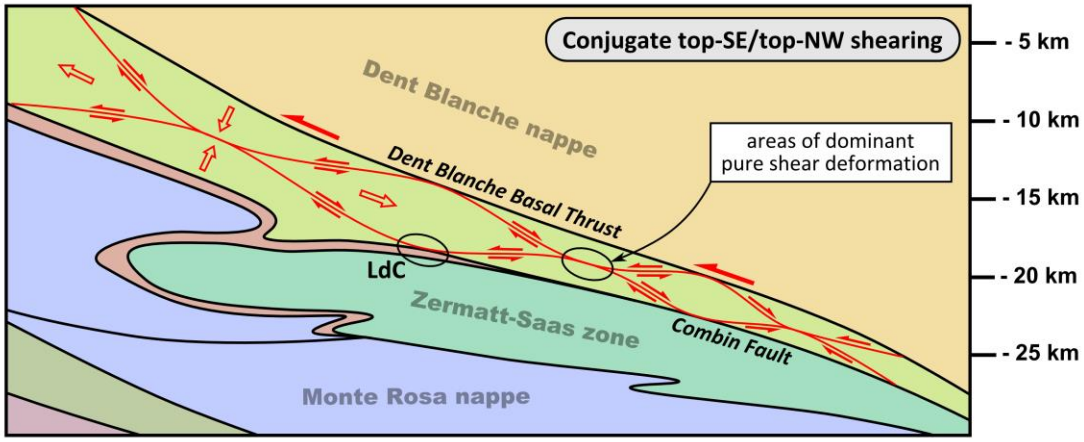

Figure 2.9: Possible geometric relations between conjugate top-SE and top-NW shear zones during dominant pure shear deformation which resulted in tectonic thinning of the Combin zone and was probably triggered by the onset of renewed overthrusting of the Dent Blanche nappe along the DBBT; circles mark areas of dominant pure shear deformation as observed in the Lago di Cignana (LdC) area.

My structural observations and interpretations from the Lago di Cignana area in conjunction with previously published data suggest that pure shear deformation and resulting conjugate shear zones may be of greater significance for the structural evolution of tectonic units in the Western Alps than previously estimated. The different views on the character of the Combin Fault and the overlying Combin zone, whether they represent thrust-related or normal-sense shear zones, may become compatible under the hypothesis that large amounts of pure shear led to the development of opposing top-SE and top-NW shear zones overlapping in space and time and leading to regional differences in the distribution of shear senses within the Combin zone, e.g. in the western Valtournenche and the areas to the southeast (eastern Valtournenche, Val Gressoney). The described structural evolution of the Penninic units at Lago di Cignana suggests that top-(S)E shearing was dominant during exhumation of the (U)HP Zermatt-Saas zone and was followed by pure shear and top-NW deformation due to renewed thrusting along the DBBT.

2.7 Conclusions

Kinematic and geometric analyses of the Penninic units at Lago di Cignana in the western Valtournenche of Italy revealed a continuous structural evolution from (U)HP to greenschist-facies conditions during Paleogene progressive syn- to post-exhumational orogenic deformation. The following sequence of deformation was deduced from structural observations and interpretations:

- Main exhumation of the Zermatt-Saas zone after the peak of UHP metamorphism at ca. 43 Ma occurred during dominant top-E shearing under eclogite- to upper greenschist-facies conditions. Subordinate conjugate high-pressure top-W shear senses suggest differential exhumation of UHP rocks and internal deformation of the Zermatt-Saas zone during the early stages of exhumation.
- Exhumation of the Zermatt-Saas zone to mid-crustal levels and juxtaposition with the Combin zone along the Combin Fault occurred during greenschist-facies normal-sense top-SE shearing. Strain was mainly localized along the uppermost Zermatt-Saas zone and top-SE structures along the Combin Fault have been partly obliterated by subsequent deformation.
- Top-SE shearing evolved into a phase of dominant pure shear deformation as indicated by symmetric fabrics, conjugate shear bands, boudinage, and orthorhombic quartz textures. Coaxial deformation affected units in the footwall and hanging wall of the Combin Fault and is most likely responsible for tectonic thinning of the Combin zone.
- Pure shear deformation was followed by top-NW shearing, especially at higher structural levels, due to renewed thrusting along the DBBT which continued until low-grade greenschist-facies conditions.

The geometry of deformation and the decreasing metamorphic grade of kinematic indicators within the Zermatt-Saas zone, Combin zone, and Dent Blanche nappe at Lago di Cignana suggest that the change from syn-exhumational top-SE shearing to post-exhumational top-NW shearing occurred progressively over a phase of dominant pure shear deformation. On a regional scale, a significant pure shear component throughout the deformation history of the Combin zone may have led to the development of conjugate top-SE and top-NW shear zones overlapping in space and time which offers an explanation for contradicting views regarding the nature of the Combin Fault and the Combin zone, i.e. whether they represent thrust-related or normal-sense shear zones.

- CHAPTER 3 -

Tectonometamorphic evolution of the Becca d'Aver continental sliver in the Western Alps (Valtournenche, Italy)

3.1 Abstract

The Becca d'Aver continental sliver (BACS) in the western Valtournenche of Italy represents a continental fragment from the former Piemont-Ligurian/Adriatic ocean-continent transition which experienced HP metamorphism during Paleogene Alpine subduction. It is now structurally located at the boundary between the continental Dent Blanche nappe in the hanging wall and the mainly oceanic Combin zone in the footwall. The BACS consists of gneissic and metasedimentary sequences and is underlain by a sole of serpentinite. Whereas the underlying Combin zone is characterized by a strong greenschist-facies overprint, prograde blueschist-facies assemblages are partly preserved within metasediments of the BACS. Petrological and mineralogical analyses of garnet-bearing metasedimentary sequences in conjunction with microstructural observations and thermodynamic modelling suggest that prograde metamorphism was linked to progressive breakdown of lawsonite, associated water release, fluid-mediated element transfer, and mineral growth. Spessartine-rich garnet often displays inclusion patterns and honeycomb- and cyclone-shaped intergrowths with quartz suggesting crystallization in the presence of a fluid phase. Garnet isopleth thermobarometry yields ca. 1.1 GPa and 390° C for core compositions and ca. 1.56 GPa and 450° C for the rims. Peak conditions were probably around 1.7 GPa and 500° C and are higher than previously reported PT-conditions for the Combin/Dent Blanche boundary. High-pressure shear bands and the sense of rotation in cyclone garnets indicate top-NW shearing on the prograde path which is consistent with deformation within a SE-dipping subduction zone. Perfect preservation of garnet growth zonations and absence of minerals like biotite and orthoclase suggest cold exhumation of the BACS. Deformation structures within the BACS and underlying Combin zone suggest a common structural evolution and complex kinematics on the retrograde path related to top-(W)NW and top-(E)SE shearing. Top-(E)SE shearing occurred below ca. 1.0 GPa and 450° C and was followed by another phase of top-NW shearing which evolved into semi-ductile to brittle orogen-perpendicular extension.

3.2 Introduction

Subduction zones and accretionary wedges are settings where units of continental and oceanic origin experience high- to ultrahigh-pressure ((U)HP) metamorphism. High-pressure metamorphism of deeply subducted units is closely related to dehydration of water-bearing minerals like chlorite, lawsonite, and amphibole and associated release of H_2O-rich fluids. Prograde growth of minerals may therefore be

linked to the presence and availability of reaction-enhancing fluids. Whereas hydration of the overlying mantle wedge, resulting melting and arc volcanism, and element-transfer across the subduction-interface are often-addressed topics (Schmidt and Poli, 1998; Manning, 2004; Malaspina et al., 2008), little is known about in-situ effects and consequences of fluid-release, fluid-rock interactions, and fluid-mediated metamorphism. Often observed vein networks cutting through HP rocks may be obvious witnesses of fluid-mediated mineral precipitation from internally- or externally-derived fluids (e.g. Zack and John, 2007; John et al., 2008; Spandler et al., 2011). On the other hand, host-rock "alteration" or autometasomatism by in-situ generated fluids due to prograde breakdown of hydrous minerals may be more subtle in influencing a rocks mineralogical and microstructural evolution (e.g. Konrad-Schmolke et al., 2008b).

I investigate the metamorphic evolution of a continental sliver at Becca d'Aver in the western Valtournenche of Italy which has been subducted and incorporated into the accretionary wedge at the Adriatic continental margin during Paleogene Alpine subduction. The Becca d'Aver continental sliver (BACS) is located close to the boundary between the continental Dent Blanche nappe in the hanging wall and the mainly ocean-derived Combin zone in the footwall. It most likely represents a continental fragment or extensional allochthon along the ocean-continent transition at the southeastern border of the Piemont-Ligurian ocean. I describe garnet-bearing metasedimentary lithologies from the BACS in terms of their petrography, mineralogy, and microstructures. One sample in particular displays mineral compositions, microstructures, and inclusion patterns which suggest fluid-mediated prograde metamorphism. Calculated prograde and peak blueschist-facies PT-conditions for the same sample are the highest so far reported for the boundary between the Combin zone and Dent Blanche nappe north of the Aosta valley. The BACS thus holds crucial information about metamorphic conditions and processes which have been erased in units in the footwall and hanging wall due to a pervasive greenschist-facies overprint. I also use structural observations from the BACS and the underlying Combin zone to link kinematic information to PT-conditions and to constrain their structural evolution. The aim of this study is to infer metamorphic conditions during HP metamorphism associated with subduction and accretion, to explore possible mineralogical and microstructural effects of fluid-mediated prograde metamorphism, and to constrain the tectonometamorphic evolution of a subducted ocean-continent transition.

3.3 Geological setting

3.3.1 Regional geology

In the Western Alps (Fig. 3.1a and b), a stack of continental and oceanic units is exposed which assembled during Late Cretaceous – Paleogene Alpine orogeny. Units derived from different paleogeographic domains were subducted in a SE-dipping subduction zone beneath the Adriatic continental margin, subsequently exhumed, and accreted to the growing orogen. In the Valtournenche area north of the Aosta valley in northern Italy, oceanic units derived from the Piemont-Ligurian ocean and continental units derived from the ocean-continent transition between the Piemont-Ligurian ocean in the northwest and the Adriatic continental margin in the southeast are exposed.

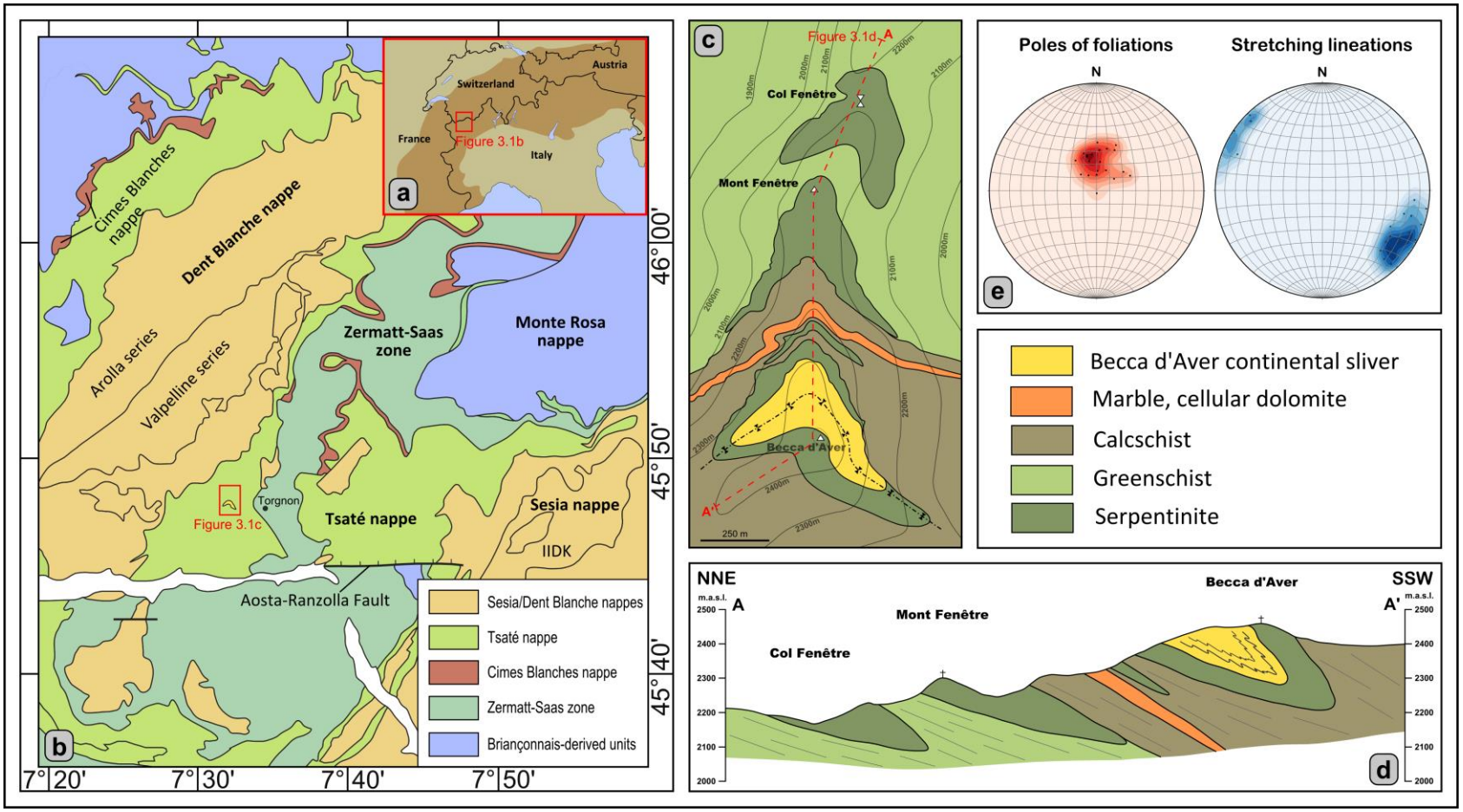

Figure 3.1: a) Sketch map of the European Alps with location of the tectonic map. b) Tectonic map of parts of the Swiss-Italian Western Alps; after Steck et al. (1999) and Pleuger et al. (2007); location of the geological map in figure 3.2c is indicated. c) Geological sketch map of the study area with trace of the cross-section in figure 3.2d. d) Schematic cross-section through the study area according to field observations. e) Stereoplots of poles of foliations and stretching lineations as equal area projections in the lower hemisphere.

Some parts of Piemont-Ligurian oceanic lithosphere experienced (ultra)high-pressure metamorphism during the Paleogene and are now exposed in the Zermatt-Saas zone. Other parts were only subducted to greenschist- to blueschist-facies conditions and formed an accretionary wedge whose remnants are represented by the Combin zone. These two oceanic units are overlain by the Dent Blanche/Sesia nappe system which represents the structurally highest unit of the Western Alpine nappe stack and is probably derived from one or more continental fragments along the southeastern ocean-continent transition zone within the Alpine paleogeographic realm. In the Valtournenche area and to the southeast, continental units have been largely eroded so that the Dent Blanche nappe in the northwest is separated from the Sesia nappe in the southeast. The Dent Blanche/Sesia nappe system probably represents an assemblage of several subnappes that are derived from continental fragments and extensional allochthons. These fragments stranded inside the Piemont-Ligurian oceanic domain during Jurassic rifting (Froitzheim et al., 1996; Dal Piaz et al., 2001; Babist et al., 2006) and experienced Late Cretaceous high-pressure metamorphism during early Alpine subduction. The metamorphic grade increases from northwest to southeast so that the Dent Blanche nappe reached Alpine greenschist- to blueschist-facies conditions up to 1.6 GPa and 520° C (Manzotti et al., 2014) whereas the Sesia nappe experienced eclogite-facies conditions around 2.0 GPa and 550° C (e.g. Lardeaux and Spalla, 1991; Regis et al., 2014). The Dent Blanche/Sesia nappe system consists of Paleozoic basement and remnants of its Permo-Mesozoic cover. The Dent Blanche nappe comprises two pre-Alpine basement units, the Arolla and Valpelline series. The Arolla series mainly consists of Permian granitoids and gabbros (Bussy et al., 1998; Monjoie et al., 2005) whereas the Valpelline series consists of pre-Alpine amphibolite- to granulite-facies metasediments (Gardien et al., 1994). The Dent Blanche nappe experienced a strong greenschist-facies overprint after the peak of Alpine metamorphism which can be especially observed along shear zones (Oberhänsli and Bucher, 1987; Manzotti et al., 2014). The timing of high-pressure metamorphism has not been determined for the Dent Blanche nappe yet but has been dated for the Sesia nappe at ca. 70 – 65 Ma (e.g. Inger et al., 1996; Rubatto et al., 1999). Rubatto et al. (2011) and Regis et al. (2014) proposed that HP metamorphism started as early as ca. 85 Ma and was characterized by several distinct pressure peaks. The basal tectonic contact of the Dent Blanche nappe is the Dent Blanche Basal Thrust (DBBT) which separates it from the underlying Combin zone. The Combin zone is a composite unit that mainly consists of an ophiolitic mélange, the Tsaté nappe, and thin metasedimentary sequences of continental affinity, the Cimes Blanches and Frilihorn nappes. The Tsaté nappe comprises Jurassic to Cretaceous calcschists, metabasites, and serpentinites (Sartori, 1987; Marthaler and Stampfli, 1989). The Cimes Blanches and Frilihorn nappes consist of successions of Permo-Mesozoic continental margin sediments comprising conglomerates, quartzites, marbles, and dolomites (Sartori, 1987; Vannay and Allemann, 1990). They occur as thin dismembered sheets along the base and structurally higher up in the Combin zone. The Combin zone reached greenschist- to blueschist-facies conditions (Kienast, 1973; Ballèvre and Merle, 1993; Reddy et al., 1999) with peak estimates around 1.2 GPa and 450° C (Bousquet, 2008) and experienced a pervasive greenschist-facies overprint (Ballèvre and Merle, 1993; Negro et al., 2013). Oceanic accretion along the active Adriatic margin mainly occurred between 60 and 48 Ma (Agard et al., 2002; Reddy et al., 2003). The Zermatt-Saas zone in the footwall of the Combin zone is separated from it

by the Combin Fault. The Zermatt-Saas zone consists of Jurassic to Cretaceous metabasalts, metagabbros, metaultramafics, and metasediments. Protolith ages for metagabbros have been determined at ca. 164 Ma by Rubatto et al. (1998) using U-Pb zircon geochronology. Ophiolitic units of the Zermatt-Saas zone experienced Paleocene – Eocene (ultra)high-pressure metamorphism whereas a large spread in available prograde and peak metamorphic ages between ca. 54 – 41 Ma (Bowtell et al., 1994; Rubatto et al., 1998; Amato et al., 1999; Lapen et al., 2003; Mahlen et al., 2005; De Meyer et al., 2014) suggests that the Zermatt-Saas zone consists of several slivers that were assembled in a subduction channel. The Zermatt-Saas zone generally reached eclogite-facies conditions of ca. 540° – 600° C and 2.3 – 3.0 GPa (Bucher et al., 2005; Angiboust et al., 2009) and peak conditions of ≥ 3.2 GPa and ≤ 600° C at the UHP locality at Lago di Cignana in the western Valtournenche (Reinecke, 1998; Groppo et al., 2009; Frezzotti et al., 2011). The Zermatt-Saas zone is overlain by a number of continental fragments which also experienced Alpine echlogite-facies metamorphism during the Paleocene – Eocene (Dal Piaz et al., 2001; Beltrando et al., 2010c; Faßmer, 2014; Weber et al., accepted). They probably represent continental outliers or extensional allochthons within the Piemont-Ligurian oceanic domain derived from the Adriatic continental margin.

3.3.2 Field relations

The study area with the Becca d'Aver continental sliver (BACS) is located around the peak Becca d'Aver west of the village Torgnon in the western Valtournenche of Italy (Fig. 3.1b). Most samples were taken along the crest between Becca d'Aver in the south and Col Fenêtre in the north (Fig. 3.2a). The sliver occurs in a structurally high position within or on top of the Combin zone. It differs lithologically from the underlying Combin zone in that it comprises continental gneissic and heterogeneous metasedimentary sequences. Metasediments are usually quartz- and phengite-rich lithologies which often contain garnet. The BACS is therefore regarded as a distinct unit. Its structure is that of a S-closing synform as suggested by folding of a metamorphic layering within gneissic lithologies in the core of the sliver (Fig. 3.2b and c). These rocks often display L>S fabrics with stretching lineations parallel to fold axes (Fig. 3.2d). In most parts, the sliver is structurally underlain by a sole of serpentinite which has been folded around it (Fig. 3.2e). The Combin zone in the footwall of the BACS consists of an association of greenschists, serpentinite (locally ophicalcite), and calcschists. Greenschists and large serpentinite bodies are predominant in the northern part of the study area whereas calcschists with minor lenses of greenschist and serpentinite (Fig. 3.2f) occur in the southern part. At Col Fenêtre in the northern part of the study area, serpentinites partly contain calcite veins and therefore can be characterized as ophicalcite (Fig. 3.2g). North of the BACS, a succession of sediments with continental affinity occurs. These are foliated marbles (Fig. 3.2h) and cellular dolomite ("Rauhwacke"; Fig. 3.2i) and are similar to the ones typical of the Cimes Blanches and Frilihorn nappes. Foliations within all lithologies, except for massive serpentinites, dip to the south and stretching lineations consistently trend (W)NW-(E)SE (Fig. 3.1e).

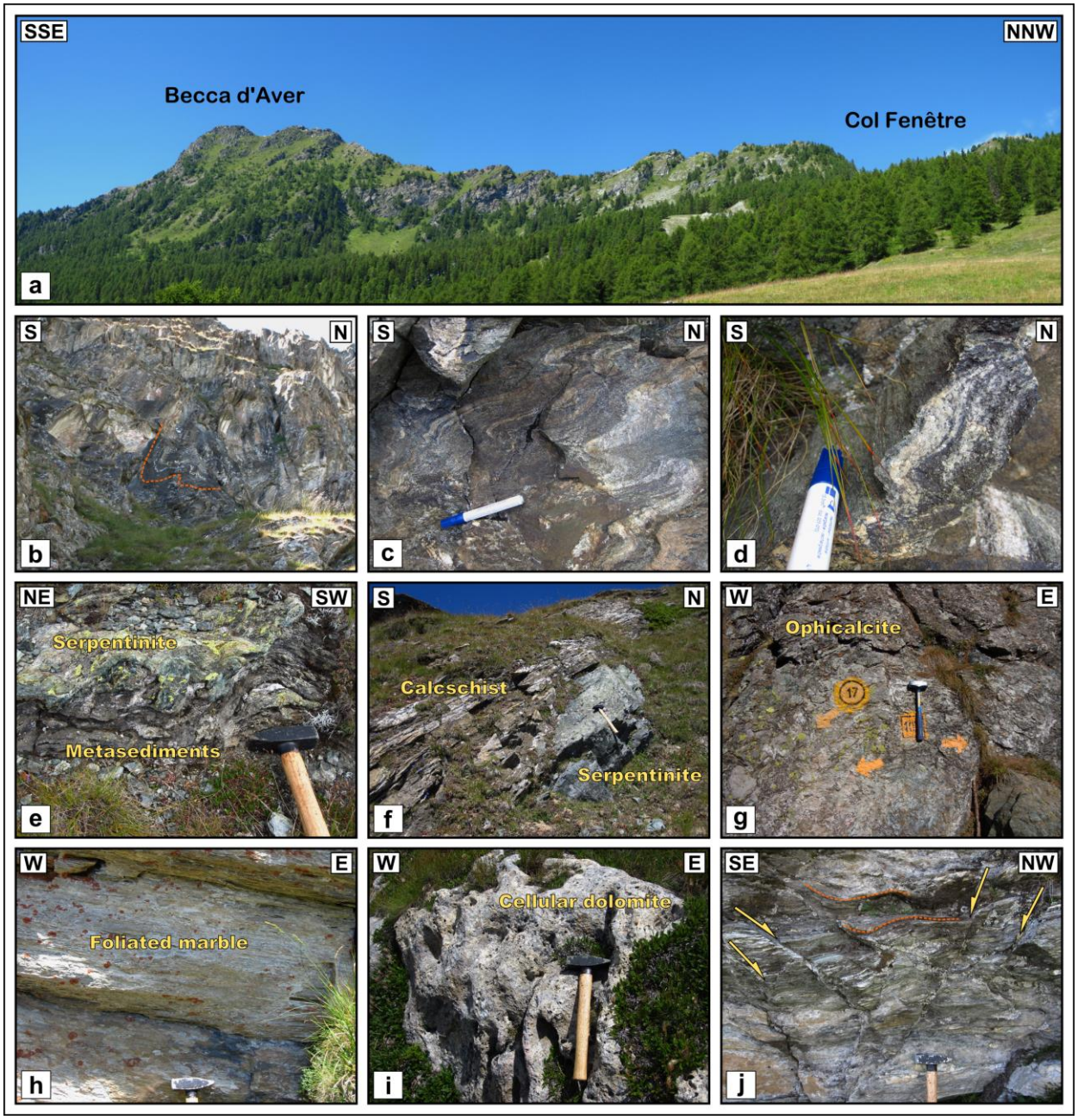

Figure 3.2: Outcrops and field relations in the Becca d'Aver area. a) Panorama view of the crest between Becca d'Aver in the south and Col de Fenêtre in the north. b) Folds within gneissic lithologies on the eastern slope of Becca d'Aver suggesting that the BACS has been folded into a S-closing synform. c) Folds within gneissic lithologies on the eastern slope of Becca d'Aver. d) L>S tectonites within folded gneissic lithologies on the eastern slope of Becca d'Aver; marker lies parallel to the stretching lineation which plunges to the ESE and is parallel to fold axes. e) Folded contact between metasediments of the BACS and structurally lower serpentinites just west of Becca d'Aver; metasediments are capped by serpentinites in this outcrop due to folding of the BACS and its serpentinite sole. f) Serpentinite lense within calcschists of the Combin zone south of Becca d'Aver. g) Ophicalcite of the Combin zone at Col de Fenêtre; picture courtesy of Gerrit Obermüller. h) Foliated marble within the Combin zone north of Becca d'Aver. i) Cellular dolomit (Rauhwacke) within the Combin zone north of Becca d'Aver suggesting a continental paleogeographic environment. j) Semi-ductile to brittle, conjugate shear planes in an outcrop of metasediments close to the base of the BACS northeast of Becca d'Aver indicating late-stage orogen-perpendicular (NW-SE) extension; note that the foliation is deflected next to top-NW shear planes whereas top-SE shear planes appear rather brittle suggesting that top-NW shearing was more pronounced at an earlier stage.

3.4 Sample description

In the following, samples from the BACS are described in terms of their petrography and microstructures. Four metasediment samples were chosen for petrological and microstructural analyses. These are samples FD356, FD370, FD372, and FD374. A more detailed description of sample FD370 is given which is a garnet-bearing quartz-rich sample displaying various inclusion patterns. Sample FD356 stems from an outcrop on the northeastern slope of Becca d'Aver. Samples FD370 and FD372 were taken from outcrops close to the base of the sliver north of Becca d'Aver. FD374 stems from an outcrop west of the peak. All samples contain garnet which could not be found in lithologies of the underlying Combin zone. Several samples from the Combin zone were also analysed in thin-section to gain further information on the kinematic evolution in the area.

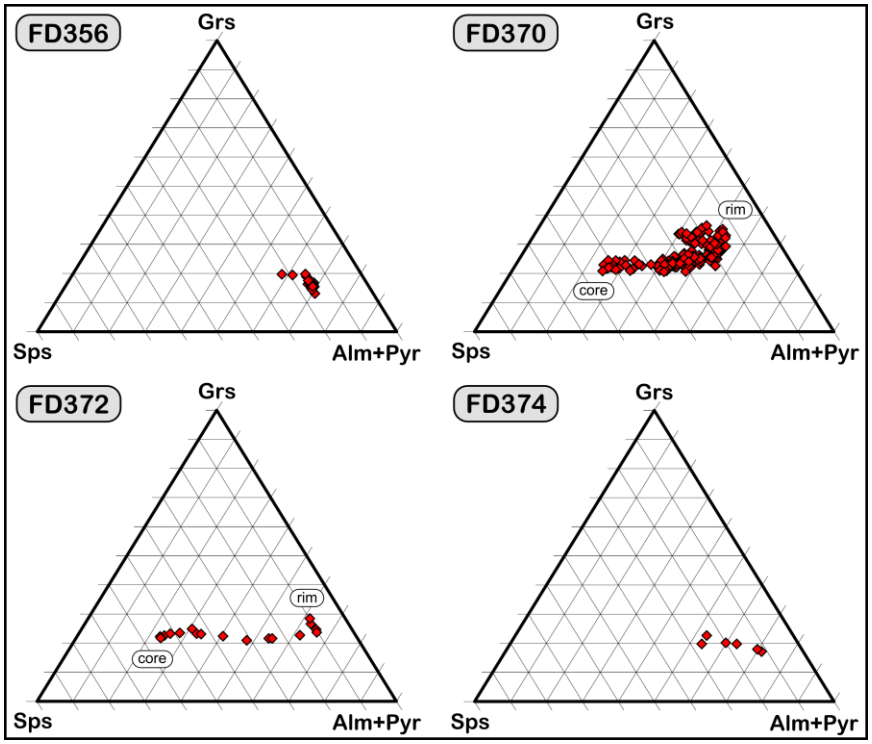

Figure 3.3: Endmember compositions of garnet in metasediment samples FD356, FD370, FD372, and FD374; Almandine and pyrope were summed up due to generally low pyrope contents.

3.4.1 Petrology and mineralogy

Mineral compositions of the 4 garnet-bearing metasediment samples from the BACS were measured with the Jeol JXA-8200 superprobe at Steinmann-Institut, University of Bonn. Representative microprobe analyses of mineral compositions are shown in table 3.1. The whole rock composition of sample FD370 was determined with XRF analysis also at Steinmann-Institut and is depicted in table 3.2. Garnet endmember compositions are shown in figure 3.3 and distribution maps of major bivalent cations are depicted in figure 3.4. Figure 3.5 shows two profiles across garnet in sample FD370.

	FD356				FD370						FD372				FD374			
	Grt	**Phg**	**Chl**	**Ab**	**Grt**	**Grt**	**Grt**	**Grt**	**Phg**	**Phg**	**Chl**	**Grt**	**Grt**	**Phg**	**Amp**	**Grt**	**Phg**	**Chl**
SiO2	37.35	53.09	24.64	68.45	37.13	36.91	37.66	37.86	54.01	52.36	27.18	36.74	36.74	53.99	54.19	37.10	53.39	24.04
TiO2	0.10	0.14	0.02	0.01	0.28	0.16	0.12	0.04	0.18	0.13	0.14	0.25	0.20	0.16	0.04	0.08	0.17	0.07
Al2O3	20.45	23.45	18.94	19.09	21.03	21.12	21.32	21.48	26.78	28.81	19.70	20.97	20.91	25.59	1.57	20.40	25.54	20.63
FeO	28.36	5.90	35.01	0.18	11.34	11.74	21.08	23.88	3.40	2.22	21.73	11.02	11.29	3.89	12.36	23.67	4.49	35.18
MnO	6.87	0.00	0.58	0.02	23.30	23.81	12.63	6.94	0.09	0.04	0.27	24.04	23.41	0.06	0.52	11.83	0.04	1.20
MgO	0.52	2.79	8.32	0.00	0.20	0.24	0.43	0.80	3.27	3.19	18.29	0.20	0.22	3.37	15.67	0.28	2.66	6.04
CaO	6.55	0.00	0.05	0.14	8.04	7.27	7.71	10.38	0.00	0.05	0.02	7.56	7.84	0.00	12.54	6.85	0.00	0.07
Na2O	0.03	0.07	0.07	12.00	0.04	0.02	0.04	0.02	0.16	0.29	0.03	0.00	0.03	0.08	0.31	0.00	0.10	0.00
K2O	0.00	10.69	0.04	0.06	0.00	0.00	0.01	0.01	9.81	9.99	0.01	0.01	0.02	9.92	0.05	0.01	10.62	0.35
Cr2O3	0.05	0.00	0.02	0.00	0.03	0.04	0.04	0.00	0.00	0.00	0.02	0.02	0.02	0.00	0.00	0.59	0.00	0.41
Sum	100.28	96.14	87.68	99.94	101.37	101.32	101.02	101.40	97.70	97.06	87.40	100.80	100.68	97.07	97.24	100.81	97.01	87.98
Si	6.04	7.13	5.51	3.00	5.94	5.92	6.01	5.98	7.00	6.81	5.63	5.92	5.93	7.06	7.83	5.99	7.04	5.39
Ti	0.01	0.01	0.00	0.00	0.03	0.02	0.01	0.01	0.02	0.01	0.02	0.03	0.02	0.02	0.00	0.01	0.02	0.01
Al	3.90	3.71	5.00	0.99	3.96	3.99	4.01	4.00	4.09	4.42	4.81	3.98	3.98	3.95	0.27	3.88	3.97	5.45
Fe	3.83	0.66	6.55	0.01	1.52	1.58	2.81	3.15	0.37	0.24	3.76	1.48	1.52	0.43	1.49	3.20	0.49	6.60
Mn	0.94	0.00	0.11	0.00	3.16	3.24	1.71	0.93	0.01	0.00	0.05	3.28	3.20	0.01	0.06	1.62	0.00	0.23
Mg	0.13	0.56	2.78	0.00	0.05	0.06	0.10	0.19	0.63	0.62	5.65	0.05	0.05	0.66	3.38	0.07	0.52	2.02
Ca	1.14	0.00	0.01	0.01	1.38	1.25	1.32	1.76	0.00	0.01	0.00	1.31	1.35	0.00	1.94	1.18	0.00	0.02
Na	0.01	0.02	0.03	1.02	0.01	0.01	0.01	0.01	0.04	0.07	0.01	0.00	0.01	0.02	0.09	0.00	0.03	0.00
K	0.00	1.83	0.01	0.00	0.00	0.00	0.00	0.00	1.62	1.66	0.00	0.00	0.00	1.65	0.01	0.00	1.79	0.10
Cr	0.01	0.00	0.00	0.00	0.00	0.01	0.00	0.00	0.00	0.00	0.00	0.00	0.00	0.00	0.00	0.08	0.00	0.07
Sum	16.00	13.93	20.00	5.02	16.05	16.06	15.98	16.02	13.77	13.84	19.95	16.06	16.07	13.79	15.08	16.02	13.86	19.89
O	24	22	28	16	24	24	24	24	22	22	28	24	24	22	23	24	22	28

Table 3.1: Representative electron microprobe analyses of major phases for the 4 investigated metasediment samples; all Fe was measured as ferrous iron.

3.4.1.1 Sample FD356

Sample FD356 consists of garnet + white mica + chlorite + albite + quartz + calcite. Hematite and pyrite occur as minor phases. Garnet is Fe-rich with ca. 65 mol% almandine component and contains up to 22 mol% spessartine component (Fig. 3.3). The sample contains abundant chlorite and also garnet has often been replaced by chlorite which is therefore interpreted to have grown during greenschist-facies retrogression (Fig. 3.6a). White mica is phengitic with 3.21 – 3.64 Si p.f.u. and feldspar is almost pure albite.

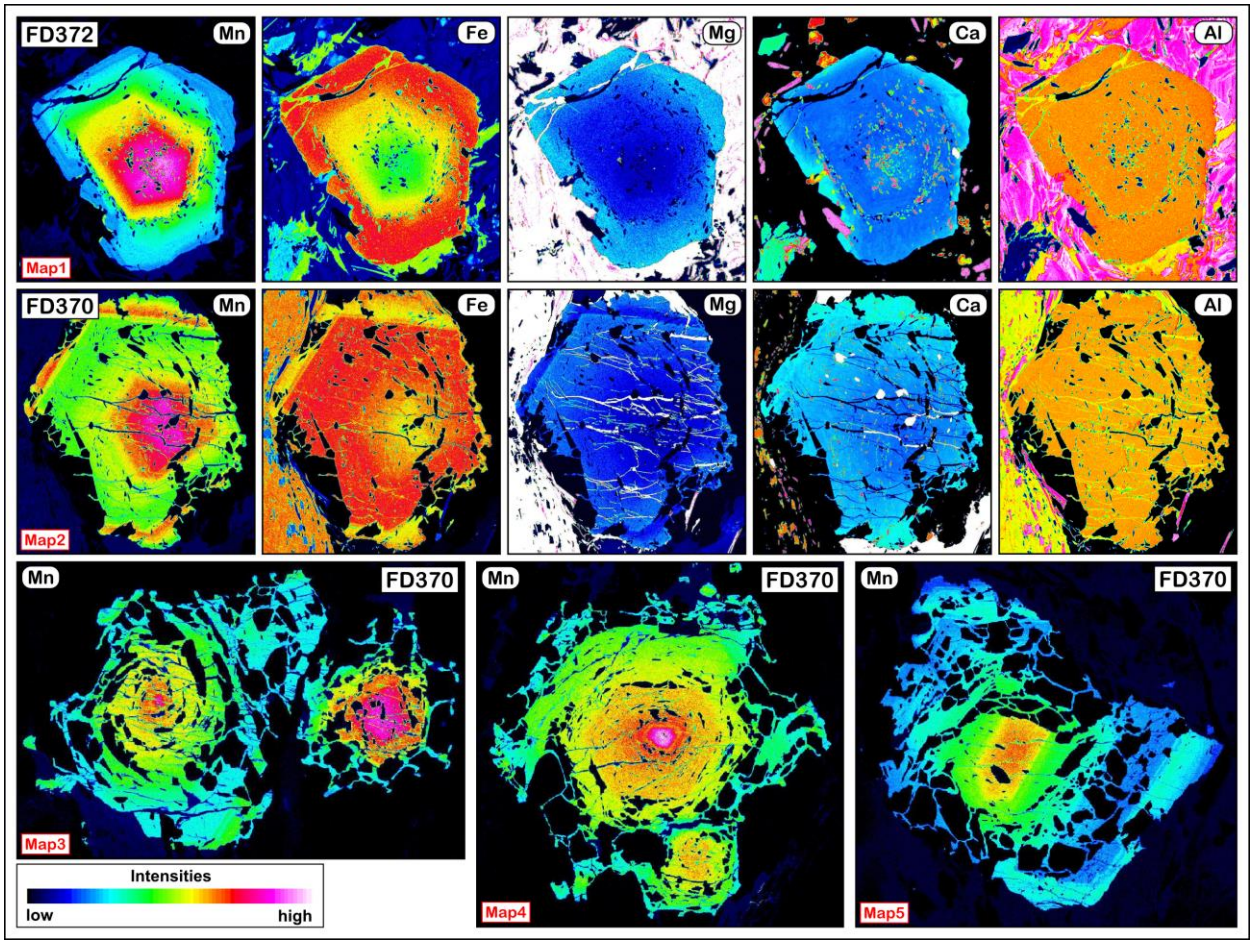

Figure 3.4: Distribution maps of major bivalent cations in garnet of samples FD370 and FD372 showing a prograde growth zonation with decreasing Mn and increasing Mg, Fe, and Ca from core to rim; garnet in sample FD370 usually displays a second growth generation close to the rims; note in map4 that the rims of quartz inclusions are parallel to the garnet growth zonation (see also figures 3.4a and b).

3.4.1.2 Sample FD370

Sample FD370 is a quartz- and calcite-rich metasediment consisting of garnet + phengite + epidote/allanite + quartz + calcite + chlorite + titanite. Garnet has a xenomorphic to hypidiomorphic shape and is Mn-rich with up to 54 mol% spessartine component in cores (Fig. 3.3). Distribution maps and profiles of major bivalent cations show a prograde growth zonation with decreasing Mn and increasing Mg, Fe, and Ca from core to rim (Figs. 3.4 and 3.5). Most garnet grains display a second

growth generation along the rims which is characterized by higher Mn- and Ca- values and lower Fe- and Mg-concentrations (Fig. 3.4). Aluminium-maps are homogeneous without any obvious zonation suggesting that no change in the amount of ferric iron incorporated into garnet and therefore the predominant oxidation state occurred during garnet growth. White mica is phengitic with 3.26 – 3.52 Si p.f.u. whereas most measurements give values around 3.5 Si p.f.u.. Most epidote grains have allanite-rich cores which show an oscillatory zonation. Chlorite occurs as retrograde phase in garnet cracks and partly replaces white mica. Calcite also occurs along cracks in fragmented garnet. According to XRF-analysis, the sample is rich in SiO_2 with 68.28 wt% and also contains abundant CaO (9.27 wt%), and Al_2O_3 (7.39 wt%). Smaller abundances of Fe_2O_3 (2.87 wt%), K_2O (1.76 wt%), and MgO (1.35 wt%) occur in the sample and MnO (0.42 wt%) and TiO2 (0.29 wt%) are only minor constituents. The sample does not contain any Na2O according to the bulk rock analysis explaining the absence of albite.

SiO2	TiO2	Al2O3	FeO	MnO	MgO	CaO	Na2O	K2O	LOI	Sum
68.28	0.29	7.39	2.87	0.42	1.35	9.27	0.00	1.76	7.53	99.16

Table 3.2: Whole rock composition of sample FD370 determined with XRF analysis.

3.4.1.3 Sample FD372

Sample FD372 consists mainly of garnet + white mica + actinolite + epidote with minor chlorite, quartz, calcite, and titanite. Garnet occurs as small hypidiomorphic to idiomorphic grains (Figs. 3.6c, d, and 3.8f) and is Mn-rich with up to 54.6 mol% spessartine component in cores (Fig. 3.3). Distribution maps again display a prograde growth zonation with decreasing Mn and increasing Mg, Fe, and Ca from core to rim (Fig. 3.4). A second growth zonation cannot be observed in this sample. Homogeneous Al-maps suggest constant amounts of ferric iron in garnet. Garnet occasionally contains circular inclusion trails of mostly epidote and allanite aligned parallel to the growth zonation (Figs. 3.6d and 3.4). Chlorite, quartz, calcite, titanite, and allanite occur as inclusions in garnet. White mica is phengitic with 3.42 – 3.54 Si p.f.u.. Allanite occurs in the cores of epidote grains. Epidote/allanite also occurs as inclusions in phengite. Chlorite is retrograde and occurs as intergrowths with white mica.

3.4.1.4 Sample FD374

Sample FD374 is a quartz-rich metasediment and consists mainly of garnet + white mica + quartz and minor chlorite and titanite. Garnet is Fe-rich with up to 69 mol% almandine component and contains up to 27 mol% spessartine component (Fig. 3.3). White mica is phengitic with 3.39 – 3.57 Si p.f.u. and is rich in chrome with up 1.27 wt%. Chlorite occurs together with quartz in cracks within garnet.

3.4.2 Inclusion patterns

Sample FD370 displays a variety of microstructural relations between garnet and other phases, especially quartz. Garnet is often highly poikiloblastic, contains large quartz inclusions, and often displays honeycomb-like intergrowths with quartz (Figs. 3.6f and g). Within "honeycomb garnets", the garnet/quartz ratio is very small so that garnet often only appears along quartz grain boundaries. All

garnet grains, however, display a typical prograde growth zonation (Fig. 3.4). Garnet grains often exhibit quartz inclusion-free garnet cores which are surrounded by inclusion-rich growth rims (Figs. 3.6f and g). Some garnet grains display circular "cyclone-shaped" inclusion patterns suggesting rotation during formation (Figs. 3.6h and i). The rims of quartz inclusions sometimes mimic the idiomorphic garnet crystal shape (Figs. 3.7a and b) which is traced by the growth zonation (Fig. 3.4). The same pattern and alignment along the garnet crystal shape can be observed with titanite inclusions in garnet (Fig. 3.7b). Oriented titanite inclusions often occur together with allanite within garnet (Fig. 3.7c). Allanite can also be observed as inclusions within quartz inclusions inside garnet (Fig. 3.7d). Allanite occurs in the cores of epidote grains (Fig. 3.7e) and often shows an oscillatory zonation (Fig. 3.7f). Occasionally, honeycomb-shaped intergrowths can also be observed between garnet and calcite (Fig. 3.7g). Besides the aforementioned phases, epidote and white mica occur as inclusions within garnet. Therefore, all matrix phases except for chlorite can be found as inclusions within garnet.

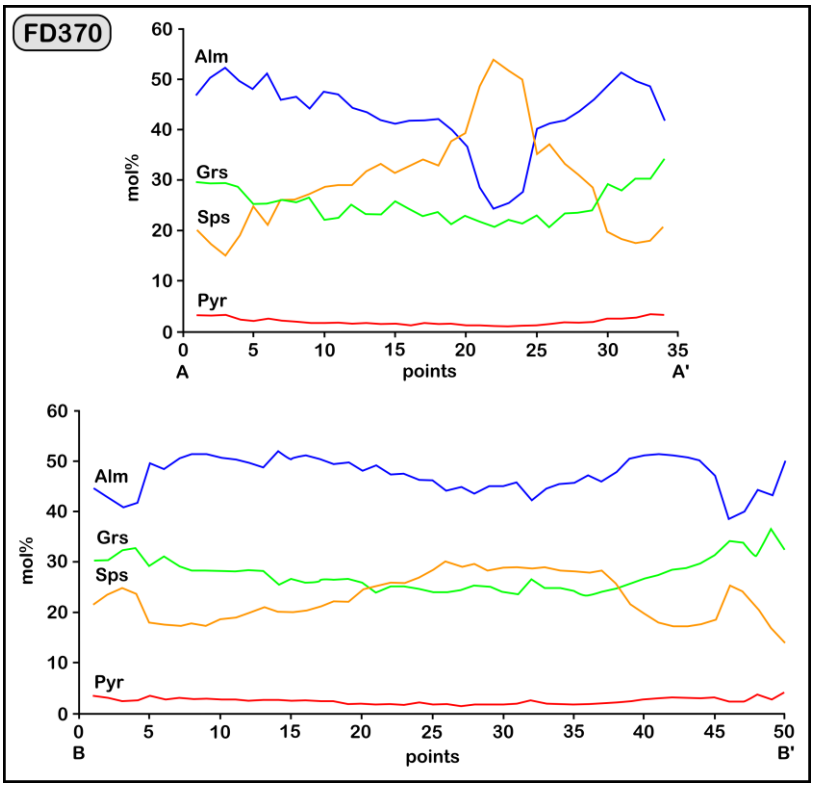

Figure 3.5: Profiles of garnet endmember compositions in sample FD370 characterized by decreasing Mn and increasing Mg, Fe, and Ca from core to rim; note the high spessartine content of up to 54 mol% in the core of profile AA'; relatively low spessartine contents in profile BB' suggest that it probably does not run through the actual core of the garnet grain.

3.4.3 Microstructures and kinematics

In this section, I describe microstructures within rocks from the BACS and the underlying Combin zone to determine the kinematics during different stages of their structural evolution.

Sample FD370 displays a foliation and contains foliation-parallel veins of quartz and calcite (Fig. 3.8a). Top-NW shear bands can be observed on a handspecimen-scale, in thin-section, and in BSE-images (Figs.

3.7h, i, and 3.8a). In some shear bands, phengite is stable and chlorite does not occur suggesting shear band formation at high-pressure conditions (Fig. 3.7h). Garnet often shows circular inclusion patterns with quartz (Figs. 3.6h and i). The sense of rotation in these "cyclone garnets" indicates top-NW movement during garnet growth and therefore on the prograde path. In BSE-images, top-NW shear senses cutting through and offsetting retrograde chlorite can also be identified (Fig. 3.7i). A sample (sample FD369) from the same outcrop as sample FD370, consisting of white mica, calcite, and quartz, shows similar top-NW shear bands which offset a pre-existing chlorite-bearing foliation (Fig. 3.8b and c).

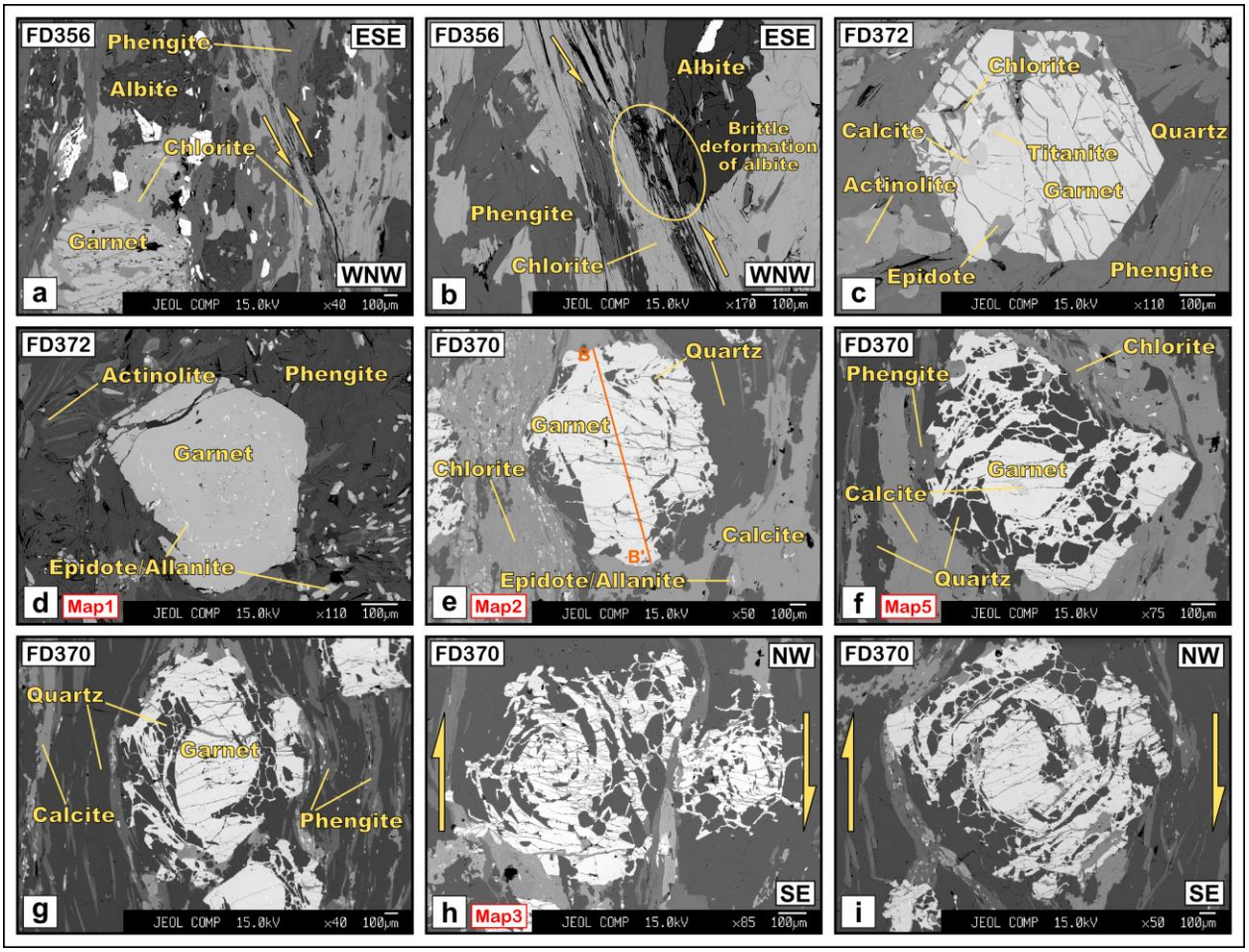

Figure 3.6: BSE images of metasediment samples FD356, FD370, and FD372. a) Sample FD356 showing greenschist-facies retrogression and top-ESE shear band; garnet and phengite have partly been replaced by chlorite. b) Sample FD356 with a close-up of the top-ESE shear band; phengite and chlorite have been deformed ductiley whereas albite has been fragmented in a brittle manner suggesting temperatures below ca. 450° C. c) Sample FD372 showing a euhedral garnet crystal in a phengite-rich matrix. d) Sample FD372 showing a hypidiomorphic to idiomorphic garnet crystal in a phengite-rich matrix; epidote and actinolite can also be found in the matrix; garnet contains a circular inclusion trail of epidote/allanite. e) Sample FD370 showing garnet in a phengite- and quartz-rich matrix; garnet and quartz are partly intergrown; trace of garnet profile in figure 3.8 is indicated. f) Sample FD370 with garnet showing honeycomb-shaped intergrowths with quartz; note quartz inclusion-free core; inclusions in the core are calcite. g) Sample FD370 with garnet showing honeycomb-shaped intergrowths with quartz; note quartz inclusion-free core; the trace of the foliation is visible and mainly marked by quartz and phengite. h) Sample FD370 with cyclone-shaped intergrowths of garnet and quartz; sense of rotation indicates top-NW transport. i) Sample FD370 with honeycomb- and cyclone-shaped intergrowths of garnet and quartz; sense of rotation indicates top-NW transport.

Both samples stem from an outcrop on the eastern slope close to the base of the BACS where macroscopic semi-ductile to brittle conjugate shear planes can be observed (Fig. 3.2j). Top-NW shear bands, however, seem to have formed slightly earlier as suggested by partly ductile deflection of the foliation whereas top-SE shear bands appear rather brittle. Large amounts of chlorite in sample FD356 and strongly chloritized garnet suggest a higher degree of retrogression in this sample. Ductile top-ESE shear bands can be observed in thin-section and BSE images (Figs. 3.6a, b, 3.8d, and e). Chlorite occurs as large grains in the matrix and has been partly deformed by shear bands suggesting pre- and synkinematic growth. The sample contains abundant albite which has been fragmented by brittle deformation within shear bands (Fig. 3.6b). This suggests that albite grew prekinematically and that temperatures during top-ESE deformation were most likely below ca. 450° C (e.g. Pryer, 1993).

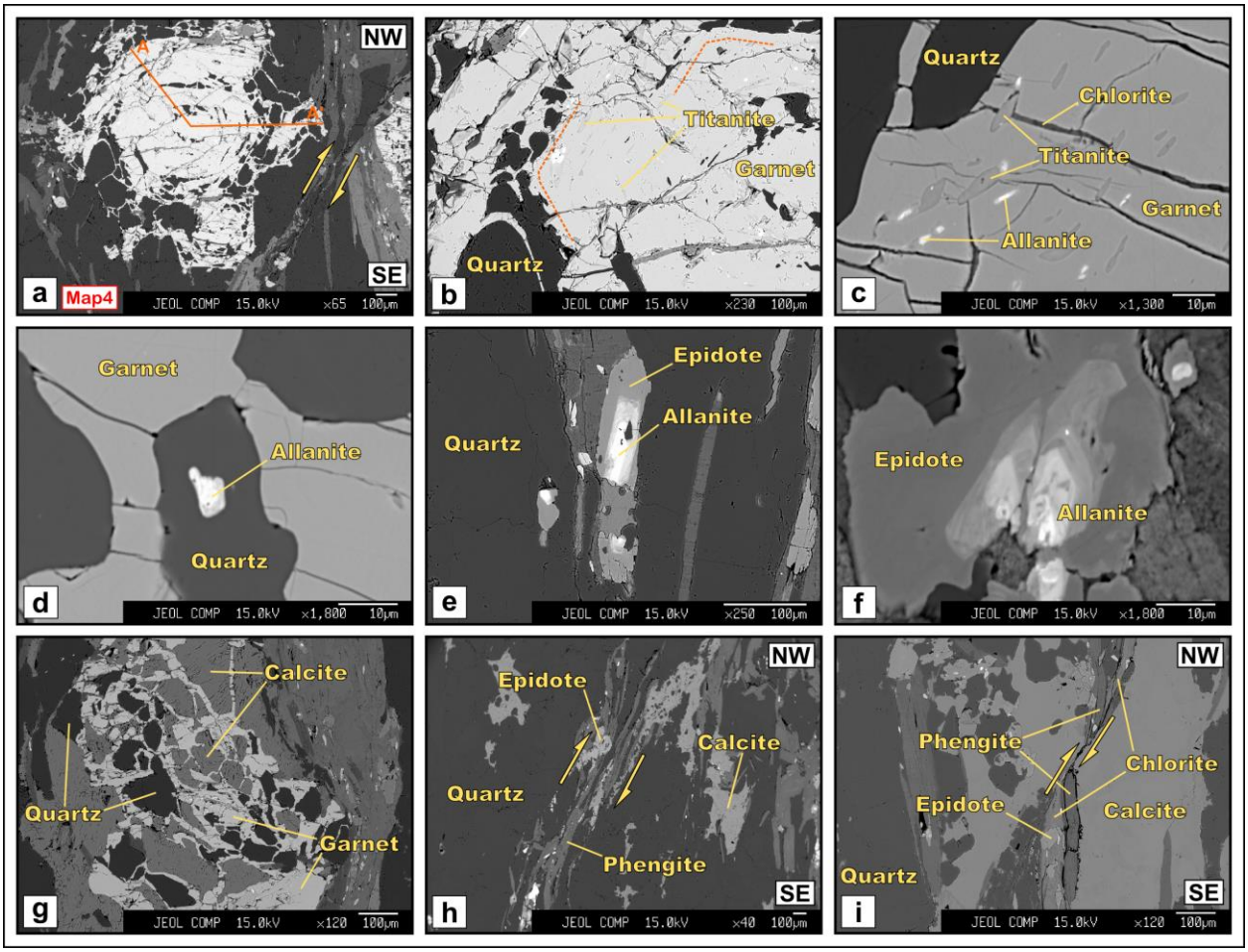

Figure 3.7: BSE images of metasediment sample FD370. a) Garnet partly intergrown with quartz; rims of quartz inclusions partly mimic the euhedral crystal shape; a top-NW shear band is visible on the right next to garnet; trace of garnet profile in figure 3.8 is indicated. b) Close-up view of the garnet in figure 3.4a; rims of quartz inclusions mimic the euhedral garnet shape; titanite inclusions are also aligned parallel to the crystal shape. c) Chlose-up view of a garnet with large quartz inclusions and smaller titanite and allanite inclusions; retrograde chlorite occurs in cracks. d) Close-up view of garnet with allanite inclusion within quartz inclusion. e) Epidote crystal with allanite in the core. f) Epidote with allanite in the core showing oscillatory zoning. g) Intergrowths of garnet, calcite, and quartz. h) Top-NW shear band with phengite stable indicating formation at high-pressure conditions. i) Top-NW shear band cutting through and offsetting chlorite indicating formation at low-pressure conditions on the retrograde path.

Sample FD372 does not show any microstructures that can be used to infer the vergence of shearing (Fig. 3.8f). In BSE-images, microfolding of phengite can be observed whereas no penetrative planar or linear fabric exists. In sample FD374, a NW-dipping compressional crenulation cleavage can be observed indicating NW-SE shortening (Figs. 3.8g and h). Garnet occasionally shows intergrowths with quartz defining an internal foliation which seems to have been slightly rotated (Fig. 3.8i).

Shear senses are scarce within the Combin zone so that only a few thin-sections yielded unambiguous kinematic indicators. A schist from the Combin zone south of Becca d'Aver (sample FD359) consists of white mica, chlorite, quartz, and calcite and shows top-WNW shear senses as suggested by deflection of white mica (Figs. 3.8j and k). Chlorite is aligned parallel to the main fabric, has partly been affected by top-WNW shearing, and partly replaces sheared white mica. Top-WNW shearing is therefore interpreted to have occurred on the retrograde path at greenschist-facies conditions. An impure foliated siliceous marble (sample FD353) from the slope east of the crest between Becca d'Aver and Mont Fenêtre shows top-SE shear bands in thin-section (Figs. 3.8l and m). The sample consists of calcite, quartz, and feldspar and the metamorphic grade of shear bands is difficult to determine due to the lack of diagnostic minerals. A sample from greenschists between Mont Fenêtre and Col Fenêtre (sample FD363) consists of chlorite, actinolite, epidote, and albite (Figs. 3.8n and o). The sample displays a mylonitic fabric and micro-scale shear zones which indicate dominant top-E shearing during synkinematic growth of greenschist-facies phases.

Microstructural observations suggest that an early top-NW shearing event on the prograde path was followed by penetrative top-WNW and top-ESE shearing on the retrograde path during greenschist-facies retrogression. A late phase of low-grade top-NW shearing was then followed by semi-ductile to brittle NW-SE extension.

3.5 Thermodynamic modelling and PT conditions

To constrain PT-conditions during the metamorphic history of sample FD370, thermodynamic modelling was performed with the THERIAK-DOMINO software package (De Capitani and Petrakakis, 2010) and the database JUN92.bs which is based on thermodynamic data by Berman (1988). Weight percent of oxides of the whole rock composition determined with XRF analysis were converted into mol% of elements and used as input for calculations. One equilibrium phase diagram (Fig. 3.9a) was calculated with additional oxygen to stabilize epidote at high-pressure conditions. Garnet isopleths (Fig. 3.9b) were calculated without additional oxygen. This is justified by the assumption that all ferric iron was incorporated into epidote and by the observation that no change in the ferrous/ferric iron content occurred during garnet growth as suggested by Al distribution maps. Additionally, pixelmaps of the total volume of lawsonite, free water, quartz, and the Si-content in white mica for the given bulk rock composition were calculated (Fig. 3.10) to gain further information on the 2D distribution of these contents. Garnet isopleths were calculated for specific core and rim compositions of Sps_{52} Alm_{25} Grs_{22} and Sps_{16} Alm_{52} Grs_{29}, respectively.

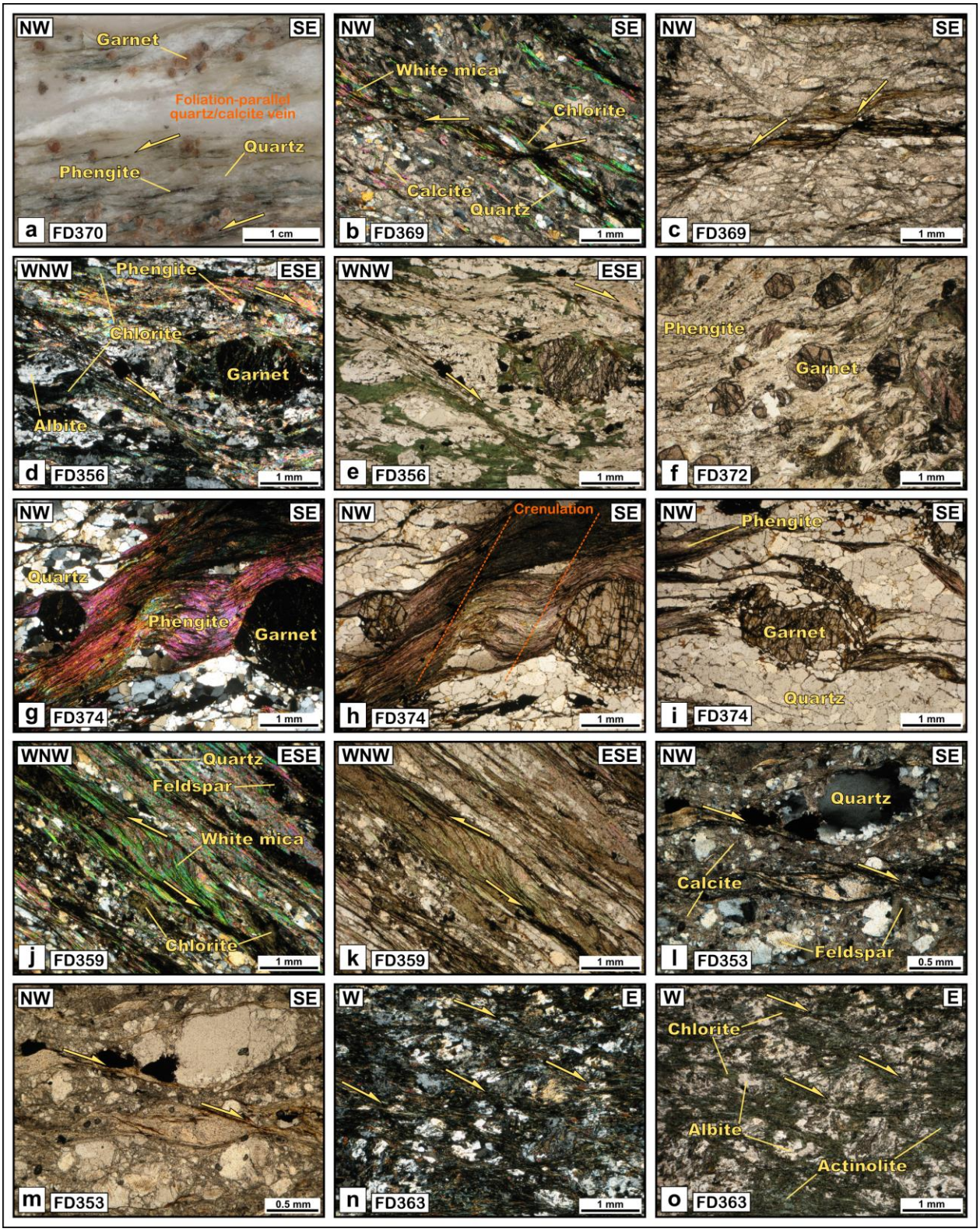

Figure 3.8: Photomicrographs of rocks from the BACS and the Combin zone; all thin-sections were cut parallel to the xz-plane of the finite strain ellipsoid; values of foliations (F) and stretching lineations (L) for each sample are given. a) Photograph of a thick-section of sample FD370; note foliation-parallel quartz/calcite vein and top-NW shear bands; F (356/02) L (304/01). b) Sample FD369 showing top-NW shear bands cutting through preexisting, chlorite-bearing foliation; crossed polarizers; F (203/38) L (138/15). c) Same section as 5b but with parallel polarizers. d) Partly retrogressed sample FD356 showing top-ESE

shear bands; crossed polarizers; F (187/22) L (118/07). e) Same section as 5d but with parallel polarizers. f) Sample FD372 with small hipidiomorphic to idiomorphic garnet in a phengite-rich matrix; parallel polarizers. g) Sample FD374 showing a NW-dipping crenulation; crossed polarizers; F (181/37) L (129/25). h) Same section as 5g but with parallel polarizers. i) Sample FD374 showing garnet/quartz intergrowths similar to the ones observed in sample FD370; parallel polarizers. j) Sample FD359 showing top-WNW shear senses as indicated by deflection of white mica; crossed polarizers; F (235/25) L (293/15). k) Same section as 5j but with parallel polarizers. l) Sample FD353 showing top-SE shear bands; crossed polarizers; F (183/15) L (137/07). m) Same section as 5l but with parallel polarizers. n) Sample FD363 showing asymmetric greenschist-facies fabric indicating top-E transport; crossed polarizers; F (184/31) L (100/02). o) Same section as 5o but with parallel polarizers.

Garnet isopleth thermobarometry yields ca. 1.1 GPa and 390° C for the core and ca. 1.56 GPa and 450° C for the rim. The calculated intersects are also marked in the main phase diagram for construction of the prograde path. The calculated equilibrium phase diagram suggests that all observed phases are stable under high-pressure conditions. Only chlorite becomes unstable above conditions of ca. 1.2 GPa and 400° C. The prograde path, as defined by garnet compositions, starts within the chlorite stability field and then runs approximately parallel to the epidote-in and lawsonite-out curves. Initial garnet growth is therefore interpreted to have been coupled to incipient breakdown of chlorite. The modelled maximum content of lawsonite in the rock is ca. 8.5 vol%. It decomposes within the narrow zone between the epidote-in and lawsonite-out curves (Fig. 3.10a) according to the following breakdown reaction (Newton and Kennedy, 1963):

Lawsonite = (clino)zoisite + kyanite + quartz + vapour

$$4\ CaAl_2Si_2O_8 \times 2\ H_2O = 2\ Ca_2Al_3Si_3O_{12}(OH) + Al_2SiO_5 + SiO_2 + 7\ H_2O$$

Kyanite cannot be observed in the sample so that Al_2O_3 and SiO_2 are interpreted to have been incorporated into garnet as peraluminous phase. Also, modelling suggests that no significant increase in the amount of free quartz occurs along the lawsonite breakdown curve (Fig. 3.10b) so that released SiO_2 must have been incorporated into other silicates. The 3.4 Si p.f.u. in white mica isopleth runs subparallel to the lawsonite breakdown curve (Figs. 3.9a and 3.10c) which correlates well with the high Si-contents observed in the sample suggesting that phengite grew mostly on the prograde path. Lawsonite breakdown releases water which may have coexisted as a free phase as suggested by modelled amounts of water in the sample (Fig. 3.10d). Peak pressure conditions were probably not much higher than those calculated for garnet rim compositions and therefore most likely did not exceed 1.7 GPa (Fig. 3.9). The perfect preservation of the prograde garnet growth zonation and the absence of retrograde biotite and amphibole suggest cold exhumation of the sample. Textural relations suggest that chlorite in the sample is retrograde and becomes stable below ca. 1.0 GPa on the retrograde path which is a realistic upper boundary for high-pressure greenschist-facies conditions.

Thermodynamic modelling suggests prograde blueschist-facies metamorphism of sample FD370 along the lawsonite breakdown curve. Growth of garnet, epidote, and muscovite are therefore interpreted to be closely related to the breakdown of lawsonite and associated element- and water-release. This relationship also suggests that prograde mineral growth was probably assisted by the presence of an H_2O-rich fluid phase.

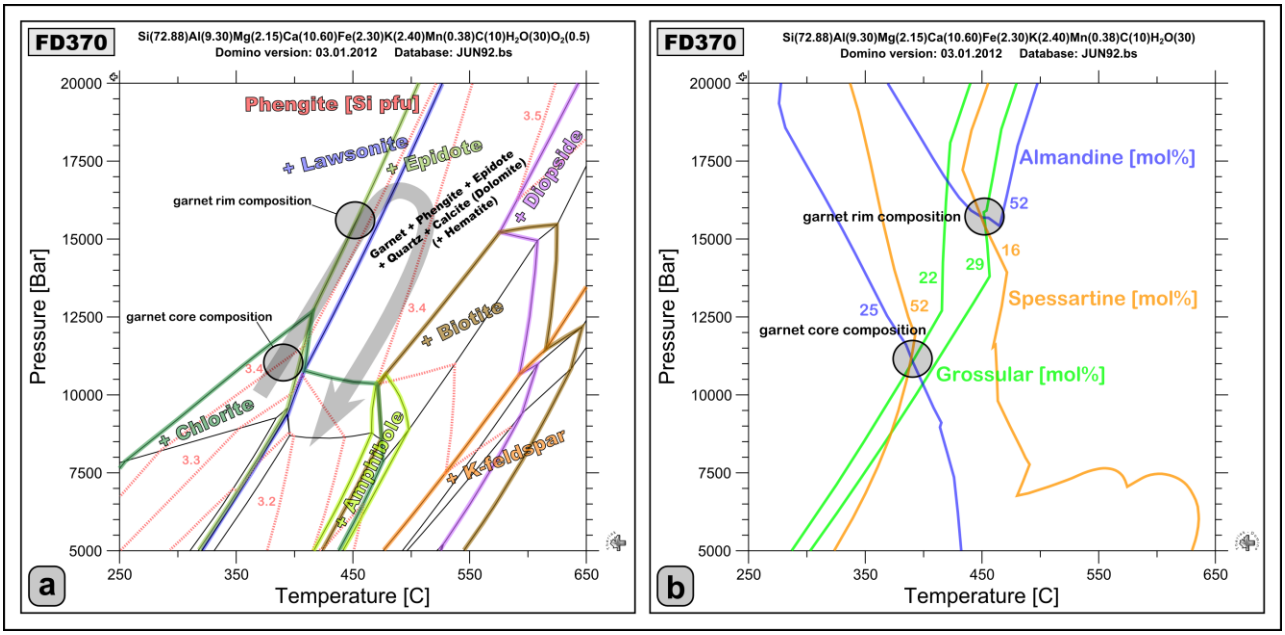

Figure 3.9: Thermodynamic modelling performed for sample FD370 with the THERIAK-DOMINO software package (De Capitani and Petrakakis, 2010) and the database JUN92.bs which is based on thermodynamic data by Berman (1988). a) Equilibrium phase diagram; note that the prograde path as determined from garnet isopleth thermobarometry runs subparallel to the lawsonite breakdown curve; see text for discussion. b) Garnet isopleth thermobarometry; core composition (Sps_{52} Alm_{25} Grs_{22}) indicates ca. 1.1 GPa 390° C, rim composition (Sps_{16} Alm_{52} Grs_{29}) indicates ca. 1.56 GPa and 450° C.

3.6 Discussion

The BACS at the Combin/Dent Blanche boundary partly consists of metasedimentary sequences which often display evidence of an Alpine HP imprint. A pre-Alpine formation of the observed assemblages seems very unlikely since prograde HP/LT growth zonations and (hyp)idiomorphic crystal shapes of garnet are well-preserved. Since the BACS is located at the boundary between continental units in the hanging wall and mainly ocean-derived lithologies in the footwall, the sliver is interpreted to represent a crustal fragment along the distal part of the ocean-continent transition between the Piemont-Ligurian ocean in the northwest and the Adriatic continental margin in the southeast (Fig. 3.11a). The timing of deposition of the metasediments is unknown. They may represent pre-rift sedimentary cover sequences of pre-Alpine continental crust or have been deposited during or after the main stage of passive margin formation. Larger fragments in a more proximal position with respect to the continent were represented by the later Dent Blanche/Sesia nappe system. The sole of serpentinite structurally underlying the BACS may represent its original post-rift substratum (Fig. 3.11a). This lithological association of rocks with continental affinity overlying serpentinized mantle is typical of extensional allochthons and also speaks for an ocean-continent transition origin (Mohn et al., 2011; Vitale Brovarone et al., 2011; Beltrando et al., 2014). The hypothesis is further supported by the occurrence of marble and dolomite with continental affinity within the Combin zone in the footwall of the sliver. The occurrence and formation of ophicalcite within the Combin zone may be attributed to rifting processes, most likely in a more distal position within the Piemont-Ligurian oceanic domain as suggested by large amounts of metamafics at lower structural levels in the study area.

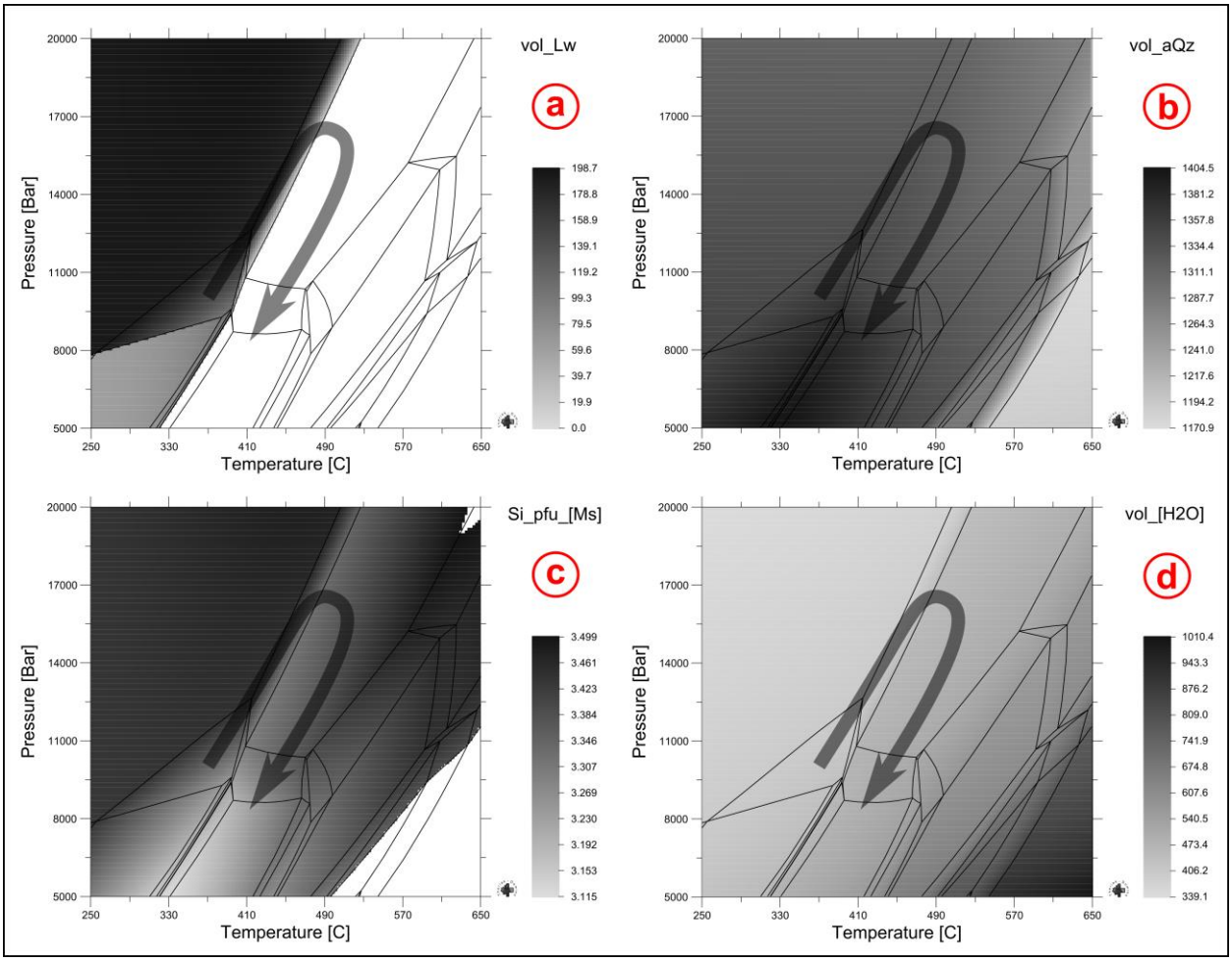

Figure 3.10: Pixelmaps calculated with the THERIAK-DOMINO software package showing the distribution of the volume of lawsonite (a), quartz (b), and water (d) and the amount of Si in white mica (c); see text for discussion.

Pseudosection modelling and garnet isopleth thermobarometry of sample FD370 suggest that the BACS experienced prograde blueschist-facies metamorphism during Alpine subduction and accretion. Peak conditions were most likely around 1.7 GPa and 500° C which are remarkably higher than the metamorphic grade observed in underlying lithologies of the Combin zone. This difference, however, may be mainly due to a pervasive greenschist-facies overprint which affected the Combin zone but partly spared the BACS. The prograde path, which can be well-constrained from garnet isopleth thermobarometry, runs subparallel and close to the lawsonite breakdown curve. This suggests that prograde metamorphism and formation of high-pressure phases like garnet, phengite, and epidote were coupled to progressive breakdown of lawsonite and associated fluid-assisted element transfer. Lawsonite is one of the major hydrous minerals in subduction zones with ca. 12 wt% H_2O bound in the crystal structure (Pawley, 1994; Schmidt and Poli, 1998; see Martin et al., 2014 for a review). It is rarely preserved as relic phase due to its water-dependent crystal structure which quickly becomes unstable during dehydration (Pawley, 1994). Pseudomorphs after lawsonite, however, are common features in mafic eclogites, also in the nearby Zermatt-Saas zone underlying the Combin zone, and often consist of fine-grained epidote and white mica (e.g. Angiboust and Agard, 2010) supporting the interpretation that

growth of these phases can be closely linked to lawsonite breakdown. A strong dependence of garnet growth and composition with breakdown of hydrous minerals, especially lawsonite at cooler geotherm tectonic settings, is suggested by several studies (e.g. Konrad-Schmolke et al., 2008a; 2008b; Baxter and Caddick, 2013). The lack of lawsonite pseudomorphs in sample FD370 can be explained by high element mobility due to the presence of a fluid phase. Fluid flow may have also been enhanced and partly channelized by deformation (Terry and Heidelbach, 2006; Konrad-Schmolke et al., 2011a) as suggested by foliation-parallel quartz/calcite veins. Lawsonite is a major carrier of light rare earth elements (LREE) (Hermann, 2000; Martin et al., 2014) which are mainly incorporated into allanite, and to a minor extent into titanite, during breakdown of lawsonite (e.g. Hickmott et al., 1992; Konrad-Schmolke et al., 2011a). Both phases occur abundantly as inclusions in the sample. Titanite occurs as oriented inclusions in garnet indicating contemporaneous crystallization of titanite and the garnet host. Allanite occurs as cores in epidote suggesting fluid-induced growth of epidote (Konrad-Schmolke et al., 2011b). The occurrence of allanite as inclusions within garnet and quartz suggests that crystallization and recrystallization, respectively, of these phases were also enhanced by the presence of a fluid. The consistently high Si-content in white mica of ca. 3.5 Si p.f.u. can be correlated with phengite growth on the prograde path since isopleths also run subparallel to the lawsonite breakdown curve. Sample FD370 contains almost no Na according to XRF and microprobe analyses which may be a primary feature or a leaching effect caused by fluid-rock interactions. The second garnet growth generation, which can be often observed in sample FD370, may either be related to final breakdown of lawsonite due to a temperature increase or influx of an externally-derived fluid. Garnet often displays honeycomb-like intergrowths with quartz which may also be related to fluid-mediated crystal growth. Inclusion patterns of poikiloblastic garnet and intergrowths of garnet with other phases have been described by several authors (e.g. Schoneveld, 1977; Hawkins et al., 2007; Robyr et al., 2007; 2009). Hawkins et al. (2007) described very similar honeycomb garnet within rocks of the Tauern Window in the Eastern Alps and interpreted garnet and quartz as products of contemporaneous precipitation from a highly polymerized fluid under HP conditions. The occurrence of allanite inclusions in quartz included within garnet indeed supports such an interpretation. However, the calculated distribution of the amount of free quartz suggests that no significant increase was caused by the breakdown of lawsonite so that garnet/quartz intergrowths are interpreted to result from garnet growth and contemporaneous mobilization of SiO_2 or recrystallization instead of newly formed quartz. Stöckhert et al. (1997) on the other hand explained similar poikiloblastic garnet within metapelites from the Tauern Window to result from garnet growth along grain boundaries of a preexisting quartz foam microstructure controlled by grain boundary free energy during low differential stress. Precipitation of garnet in quartz-rich domains may indeed have been favoured by fluid pathways along quartz grain boundaries (Kruhl et al., 2013). The occurrence of prograde top-NW shear bands and cyclone garnet, however, does not support the interpretation of a low-differential-stress environment during subduction. Observed cyclone garnets are interpreted as dynamic equivalents of honeycomb garnets formed during subduction-related shearing. The sense of rotation indicates top-NW transport during prograde garnet growth which is consistent with burial along a SE-dipping subduction zone.

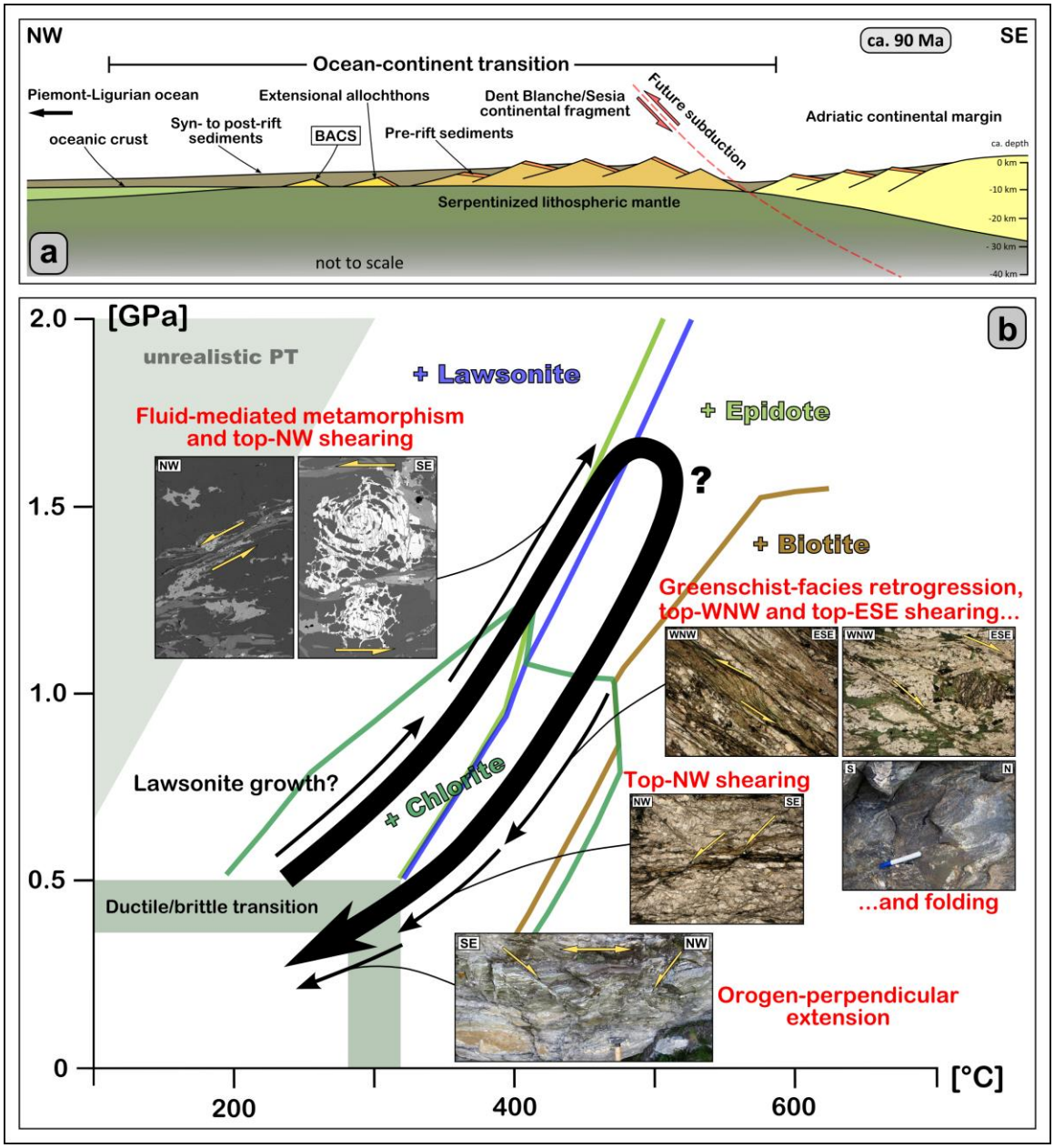

Figure 3.11: a) Late Cretaceous paleogeography of the rifted Adriatic continental margin and the Piemont-Ligurian/Adriatic continent transition; colour coding corresponds to the ones in figure 3.1; greenschists in the study area represent oceanic crust; calcschists are Jurassic to Cretaceous syn- to post-rift sediments; marbles and dolomites in the study area may represent Triassic pre-rift sediments sheared off continental basement during subduction; the BACS may correspond to a former extensional allochthon resting on exhumed and serpentinized subcontinental lithospheric mantle. b) Tectonometamorphic evolution of the BACS and possibly the underlying Combin zone along the PT-path constructed from petrological, mineralogical, and (micro)structural observations as well as thermodynamic modelling.

The presence or absence of rotated inclusion patterns can be explained by mechanical coupling/decoupling of garnet hosts from the local stress field due to the presence of a wetting fluid. The rims of quartz grains and titanite inclusions sometimes mimic the euhedral garnet crystal shape suggesting partly concomitant growth of inclusions and garnet hosts since it seems unlikely that quartz grains were arranged mechanically during garnet growth. In summary, I interpret garnet/quartz intergrowths to be the

result of precipitation of garnet and contemporaneous mobilization and recrystallization of SiO_2 due to the presence of a fluid phase which strongly enhanced element transfer. I propose fluid-mediated growth or precipitation of garnet rather than purely diffusion-controlled solid-state crystal growth. Abundant calcite as inclusions within garnet and along cracks and foliation-parallel veins suggests that calcite also behaved particularly mobile and crystallized during all stages of the metamorphic history. Perfect preservation of the prograde garnet growth zonation in samples FD370 and FD372 and the absence of orthoclase and biotite in all samples suggest cold exhumation and that the BACS did not experience any significant heating after peak conditions which were around 1.7 GPa and 500° C according to pseudosection modelling of sample FD370.

The tectonometamorphic evolution of the BACS and possibly the underlying Combin zone along the PT-path can be constructed from petrological, mineralogical, and (micro)structural observations as well as thermodynamic modelling (Fig. 3.11b). Kinematics on the prograde path can be well-constrained so that the observed blueschist-facies imprint can unambiguously be related to top-NW shearing during burial in a SE-dipping subduction zone. Deformation on the retrograde path, on the other hand, is not as easy to interpret since top-(W)NW and top-(E)SE shear senses can be observed within rocks from the BACS and the underlying Combin zone. Overprinting relations between these opposing shear senses could not be observed. Both, top-(W)NW and top-(E)SE shearing, occurred under greenschist-facies conditions as suggested by partly synkinematic chlorite. An upper pressure limit of ca. 1.0 GPa for the stability of chlorite is suggested by pseudosection modelling of sample FD370. Top-ESE shear bands in sample FD356 deform albite in a brittle manner which suggests temperatures below ca. 450° C (Pryer, 1993). The observed folding in the central part of the BACS probably occurred during the main stage of approximately orogen-perpendicular, greenschist-facies shearing since stretching lineations, especially within L>S tectonites, are strictly parallel to fold axes. It, however, cannot be attributed to mainly top-(W)NW or top-(E)SE shearing and may even represent a feature of strain accumulation. The overall synformal structure of the BACS and its serpentinite sole is probably also the result of the main stages of (W)NW-(E)SE elongation and associated orogen-parallel shortening. Folding and L>S tectonites cannot be observed within underlying calcschists of the Combin zone. These differences between the BACS and the Combin zone can be explained by rheology contrasts between more competent lithologies of the BACS and relatively incompetent calcschists of the Combin zone. The foliation within calcschists may in fact represent an axial surface foliation to the BACS synform which would support the assumption that folding and fabric formation occurred contemporaneously. The main stages of greenschist-facies deformation in the study area were followed by late top-NW shearing as suggested by low-grade shear bands in samples FD369 and FD370. This phase was followed by orogen-perpendicular extension as evident from macroscopic semi-ductile to brittle shear planes.

The BACS is interpreted to represent a continental fragment along the former Piemont-Ligurian/Adriatic ocean-continent transition which was subducted during the Paleogene and experienced blueschist-facies metamorphism. Prograde metamorphism was most likely related to progressive breakdown of lawsonite and associated fluid-mediated element transfer and mineral growth as suggested by mineralogical and

microstructural observations as well as thermodynamic modelling. Although the timing of HP metamorphism within the BACS is unknown, it most likely postdates HP metamorphism in the overlying Dent Blanche/Sesia nappe system which has been dated at ca. 70 – 65 Ma (e.g. Inger et al., 1996; Rubatto et al., 1999). Further geochronological analyses on the investigated garnet-bearing metasediments may help to determine the timing of HP metamorphism in the BACS and therefore the age of accretionary wedge formation.

3.7 Conclusions

I investigated the metamorphic and structural evolution of the BACS in the western Valtournenche of Italy. The continental sliver is structurally located at the boundary between the continental Dent Blanche/Sesia nappe system in the hanging wall and the mainly ocean-derived Combin zone in the footwall. Field relations suggest that it represents a continental fragment or extensional allochthon from the Piemont-Ligurian/Adriatic ocean-continent transition. It partly consists of monocyclic garnet-bearing metasedimentary sequences which record HP metamorphism related to Paleogene Alpine subduction. Detailed petrological and mineralogical analyses as well as thermodynamic modelling of a metasediment sample revealed prograde blueschist-facies metamorphism closely related to progressive breakdown of lawsonite, associated fluid-mediated element mobilization and transfer, and mineral growth of garnet, epidote/allanite, and phengite. Spessartine-rich garnet often displays microstructures and inclusion patterns suggesting crystallization or precipitation in the presence of a fluid phase. Poikiloblastic honeycomb and cyclone garnets are interpreted as the result of partly contemporaneous crystallization and recrystallization, respectively, of garnet and quartz. Garnet isopleth thermobarometry yielded ca. 1.1 GPa / 390° C and ca. 1.56 GPa / 450° C for core and rim compositions, respectively. Peak conditions were most likely around 1.7 GPa / 500° C and are higher than previously reported PT-conditions for the Combin/Dent Blanche boundary. Cold exhumation is suggested by perfect preservation of garnet growth zonations and absence of phases indicating higher temperatures, e.g. biotite and orthoclase. High-pressure shear bands and cyclone garnet indicate early top-NW shearing on the prograde path consistent with deformation in a SE-dipping subduction zone. Deformation on the retrograde path was more complex and related to top-(W)NW and top-(E)SE shearing as indicated by kinematic indicators within rocks from the BACS and the underlying Combin zone. Observed top-(E)SE shearing occurred below ca. 1.0 GPa and 450° C as suggested by sheared chlorite and brittle deformation of albite. It was followed by another phase of top-NW shearing which evolved into semi-ductile to brittle orogen-perpendicular extension.

- CHAPTER 4 -

Kinematics and geometry of shear zones along the Combin Fault and Dent Blanche Basal Thrust (Western Alps, Switzerland/Italy) during polyphase Alpine orogenic deformation

4.1 Abstract

The Combin Fault and Dent Blanche Basal Thrust (DBBT) in the Western Alps of Switzerland and Italy represent two major tectonic contacts which experienced polyphase deformation during Paleogene Alpine orogeny. Structural analyses of shear zones in the study area in the southern Valais and northern Aosta regions revealed a sequence of deformation that variably affected the northwestern and southeastern segments of the contacts. The main stage of nappe stacking and ductile top-(N)W shearing between ca. 48 and 44 Ma (D1) was related to thrusting of the continental Dent Blanche nappe over the underlying composite Combin zone and to thrusting of these units over continental Briançonnais units. This phase was associated with exhumation of the Dent Blanche nappe and Combin zone, formation of greenschist-facies mylonites along the DBBT, and a pervasive greenschist-facies overprint in the Combin zone. D1 top-(N)W shearing was followed by transpressional to orogen-parallel top-(S)W shearing between ca. 43 and 40 Ma (D2). Top-(S)W shearing especially affected the northwestern Combin Fault and occurred during ongoing exhumation of the Combin zone. The DBBT was probably characterized by continuing mylonitic top-W shearing during this phase. Top-SE normal-sense shearing between ca. 39 and 37 Ma (D3) affected the northwestern Combin zone along a NE-SW striking shear zone subparallel to nappe boundaries but only very locally the DBBT. Top-SE shear senses are subordinate in the southeastern realm and can locally be observed along the Combin Fault and at higher structural levels within the Combin zone. Top-SE shearing is held responsible for juxtaposition of the Combin zone and underlying (ultra)high-pressure rocks of the ophiolitic Zermatt-Saas zone at crustal levels. It was followed by renewed top-NW shearing and contemporaneous NW-SE shortening from ca. 35 Ma onwards (D4). This phase led to formation of folds and crenulation cleavages overprinting pre-existing greenschist-facies fabrics and to reactivation of the DBBT as an out-of-sequence thrust. It was followed by brittle NW-SE extension after ca. 30 Ma (D5) due to updoming of the Vanzone antiform southeast of the study area. Units in the southeastern realm of the study area were progressively rotated from a SE-dipping into a NW-dipping orientation which led to further exhumation and the synformal structure of the Dent Blanche nappe.

4.2 Introduction

Orogenic deformation in Alpine-type mountain belts is usually expressed as a sequence of consecutive deformation phases. Such deformation sequences are usually determined from overprinting and cross-cutting relations between deformation structures in combination with metamorphic and geochronological data. However, little attention is paid to regional or even local differences in the structural evolution of tectonic units. Especially post-nappe deformation after the main stage of juxtaposition of units derived from different paleogeographic domains may obliterate earlier deformation. Such deformation may also not be strictly parallel to first-order tectonic contacts and unequally distributed so that different contact segments may record different structural histories. Structural analyses of shear zones were performed along two major tectonic contacts, the Combin Fault and the Dent Blanche Basal Thrust (DBBT) in the southern Valais region of Switzerland and the northern Aosta region of Italy, to gain information on the dynamics and spatial and temporal variability of progressive orogenic deformation in the Swiss-Italian Western Alps. This area has been the site of extensive research and many controversies regarding the structural and tectonic evolution of units. The Western Alps exhibit a stack of tectonic units as the result of accretion of oceanic and continental units to the Adriatic continental margin during Late Cretaceous – Paleogene SE-directed subduction and subsequent continental collision between the European and Adriatic plates. The two uppermost tectonic units of this nappe pile are the continental Dent Blanche/Sesia nappe system in the hanging wall and the composite Combin zone in the footwall. The lower boundaries of these units are represented by the DBBT and the Combin Fault, respectively. The Combin Fault and overlying Combin zone have been the focus of several studies which reached contradictory conclusions regarding the contributions of orogen-perpendicular thrust-related top-NW and normal-sense top-SE shearing, i.e. whether the Combin Fault mainly represents a thrust or a normal fault (e.g. Ballèvre and Merle, 1993; Ring, 1995; Reddy et al., 1999; Froitzheim et al., 2006; Pleuger et al., 2007). Especially the role and importance of extensional top-SE shearing for the exhumation of (ultra)high-pressure rocks of the ophiolitic Zermatt-Saas zone in the footwall of the southeastern Combin Fault is still a matter of discussion. The nature of the DBBT is less controversial in that it represents a major Alpine thrust (Ballèvre et al., 1986; Mazurek, 1986; Oberhänsli and Bucher, 1987; Wust and Silverberg, 1989; Pleuger et al., 2007). Large displacement and strain accumulation along the DBBT led to formation of strongly sheared rocks at the base of the Dent Blanche nappe. However, no systematic analysis of these basal mylonites has been performed so far. In this chapter, I present structural data from the Combin Fault to the northwest and southeast of the Dent Blanche nappe and the DBBT to investigate the structural evolution of the units and their basal tectonic contacts. Shearing directions and overprinting relations were determined in outcrop and thin-section. Oriented samples were taken for further microstructural analyses from the base of the Dent Blanche nappe, from within the Tsaté nappe, especially its upper and lower parts, and from the Cimes Blanches and Frilihorn nappes (see appendix for table of samples and map with sample locations). Eleven subareas have been chosen where representative deformation structures and overprinting relations can be well observed. I establish correlations between the subareas to constrain the distribution of deformation and the relative chronology of shearing events. I propose a sequence of deformation along the Combin Fault and DBBT from the main stage of nappe

stacking to post-nappe deformation and collision-related deformation. Finally, I discuss the proposed structural evolution in the tectonic context of the Western Alps.

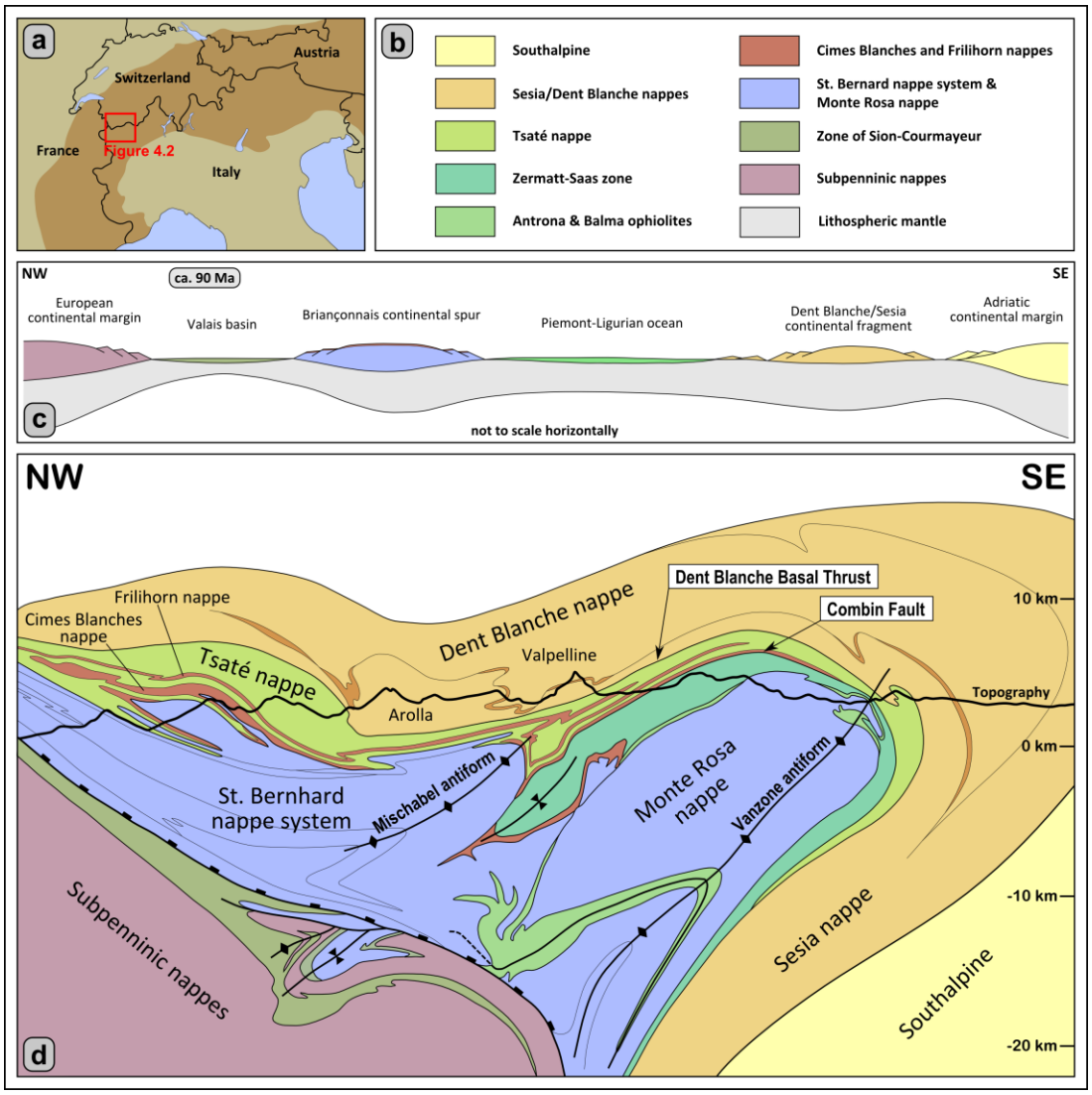

Figure 4.1: a) Sketch map of the European Alps with location of the tectonic map in figure 4.2. b) Key to the paleogeographic/tectonic configuration in c) and the cross-section in d). c) Sketch of the Late Cretaceous paleogeographic/tectonic configuration before the onset of Alpine subduction. d) Cross-section through the Western Alps; after Escher et al. (1993); trace of cross-section is indicated in figure 4.2.

4.3 Geological setting

In the Western Alps of Switzerland and Italy (Fig. 4.1a), continental and oceanic units with different paleogeographic origins are exposed (Fig. 4.1b). The Late Cretaceous paleogeographic configuration (e.g. Stampfli et al., 2002; Schmid et al., 2004; Handy et al., 2010) was characterized by the continental margins of Adria (Austroalpine domain) and Europe (Sub-Penninic domain) in the southeast and northwest, respectively, and two oceanic basins, the Piemont-Ligurian ocean (South-Penninic domain) in the southeast and the Valais ocean (North-Penninic domain) in the northwest. These in turn were

separated by the Briançonnais continental spur (Middle-Penninic domain), an eastern prolongation of the Iberian plate. Crustal slices from these different domains were progressively accreted to the Adriatic continental margin during SE-directed subduction from the Late Cretaceous onwards.

The study area is located in southern Switzerland (southern Valais region) and northern Italy (northern Aosta region) roughly between the Rhône valley in the north and the Aosta valley in the south (Fig. 4.1a and 2). Two major tectonic contacts are exposed in this area, the Combin Fault and the DBBT. The DBBT separates the continental Dent Blanche nappe in the hanging wall from the composite Combin zone in the footwall. The Combin Fault separates the Combin zone from the continental St. Bernhard nappe system in the northwest and the ophiolitic Zermatt-Saas zone in the southeast. The Dent Blanche nappe is the structurally highest unit in the Western Alps and is originally derived from the Adriatic continental margin. Its southeastern continuation is the Sesia nappe from which it is separated by erosion. The Dent Blanche/Sesia nappe system consists of several subnappes which probably originated from continental fragments stranded inside the Piemont-Ligurian oceanic domain during Jurassic rifting (Froitzheim et al., 1996; Dal Piaz et al., 2001; Babist et al., 2006). The Dent Blanche/Sesia nappes consist of Paleozoic basement units and Permo-Mesozoic cover sequences preferentially occuring along subnappe boundaries and shear zones (Babist et al., 2006; Manzotti, 2011). The Dent Blanche nappe comprises two pre-Alpine basement units, the Arolla and Valpelline series, which are different in terms of lithologies and their metamorphic evolutions. The Arolla series mainly comprises Permian granitoids and gabbros (Bussy et al., 1998; Monjoie et al., 2005) which experienced an Alpine metamorphic imprint. The Valpelline series consists of pre-Alpine amphibolite- to granulite-facies metasediments (Gardien et al., 1994) that also experienced an Alpine overprint. The Dent Blanche nappe reached blueschist-facies conditions of ca. 1.6 GPa and 520° C during Alpine subduction (Manzotti et al., 2014). It usually shows a strong pervasive greenschist-facies overprint, especially along shear zones (Oberhänsli and Bucher, 1987; Manzotti, 2014). On a regional scale, the Alpine overprint within the Dent Blanche/Sesia nappe system increases from northwest to southeast due to SE-directed subduction of the units so that the Sesia nappe records eclogite-facies conditions around 2.0 GPa and 550° C (e.g. Lardeaux and Spalla, 1991; Regis et al., 2014). The age of this high-pressure imprint has been dated at ca. 70 – 65 Ma (e.g. Inger et al., 1996; Rubatto et al., 1999) but has been proposed to have started at ca. 85 with several distinct pressure peaks (Rubatto et al., 2011; Regis et al., 2014; Fig. 4.3). According to structural and geochronological investigations by Babist et al. (2006) the Sesia nappe was mainly exhumed before 45 Ma during transpressional shearing and, subsequently, in the footwall of the Ometto Shear Zone (Fig. 4.3). The Combin zone below the Dent Blanche nappe is a composite unit comprising the ophiolitic Tsaté nappe and thin metasedimentary sequences of continental affinity, the Cimes Blanches and Frilihorn nappes. The Tsaté nappe consists of a mélange of Jurassic to Cretaceous calcschists, metabasites, and serpentinites derived from the Piemont-Ligurian oceanic domain and probably represent a former accretionary wedge at the Adriatic continental margin (Sartori, 1987; Marthaler and Stampfli, 1989). The Cimes Blanches and Frilihorn nappes occur as thin dismembered sheets along the base and structurally higher up in the Combin zone and consist of successions of Permo-Mesozoic sediments comprising conglomerates, quartzites, marbles, and dolomites (Sartori, 1987; Vannay and Allemann, 1990). They

may represent sheared-off cover sequences from the internal part of the Briançonnais continental spur but also an origin from more internal continental crust, e.g. the Dent Blanche/Sesia nappe system (Pleuger et al., 2007), has been discussed.

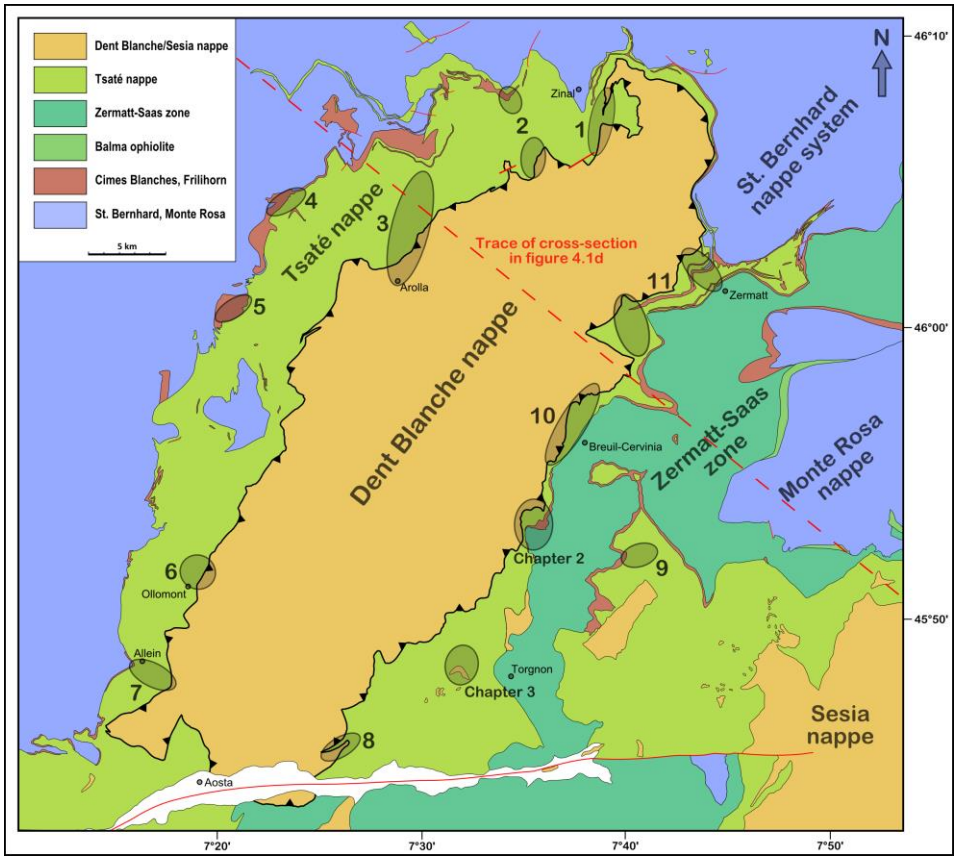

Figure 4.2: Tectonic map of the study area and adjacent areas; after Steck et al. (1999); the described subareas are indicated in grey ellipses and are numbered according to the order in the text; subareas "Becca d'Aver" and "Cignana" are described in detail in chapters 2 and 3, respectively.

The Combin zone reached greenschist- to blueschist-facies conditions during Alpine subduction and accretion (Kienast, 1973; Ballèvre and Merle, 1993; Reddy et al., 1999) with peak estimates around 1.2 GPa and 450° C (Bousquet, 2008) and experienced a pervasive greenschist-facies overprint (Ballèvre and Merle, 1993; Negro et al., 2013). Accretion at the southeastern Piemont-Ligurian active margin probably took place between 60 – 48 Ma as indicated by Ar/Ar white mica ages by Reddy et al. (2003) (Fig. 4.3). These are in agreement with ages between 62 – 55 Ma obtained by Agard et al. (2002) from in-situ Ar/Ar-dating of phengites within HP metasediments of the Schistes Lustrés complex south of the Aosta valley (Fig. 4.3). Rb-Sr ages between 45 – 36 Ma by Reddy et al. (1999) probably reflect greenschist-facies recrystallization and reworking of accretion-related structures within the Combin zone (Fig. 4.3). One locality within the northwestern lower Combin zone has been dated by Markley et al. (1998) with the Ar/Ar method on white mica. The obtained age of 44.5 ± 0.6 Ma probably represents late stages of fabric formation and ductile deformation along the northwestern Combin Fault (Fig. 4.3). Protolith ages for the Combin zone have not been determined so far. However, U-Pb zircon and Ar/Ar amphibole dating of

gabbros from the Gets nappe in the French Prealps further northwest yielded ages around 166 ± 1 Ma (Bill et al., 1997). The Gets nappe has been interpreted as a mélange from a shallow and internal part of an accretionary prism at the active SE-margin of the Piemont-Ligurian ocean and is located in a similar structural position as the Tsaté nappe (Escher et al., 1997). The Combin zone is underlain by the Zermatt-Saas zone in the southeast and the St. Bernhard nappe system in the northwest. The Zermatt-Saas zone is an ophiolitic unit consisting of metabasalts, metagabbros, metaultramafics, and metasediments which are derived from the Piemont-Ligurian oceanic domain. Protolith ages have been determined by Rubatto et al. (1998) using U-Pb geochronology on magmatic zircons from metagabbros and are around 164 Ma. The Zermatt-Saas zone experienced high- to ultrahigh-pressure metamorphism in the Paleocene – Eocene. A large spread in available prograde and peak metamorphic ages between ca. 54 – 41 Ma (Bowtell et al., 1994; Rubatto et al., 1998; Amato et al., 1999; Lapen et al., 2003; Mahlen et al., 2005; De Meyer et al., 2014; Fig. 4.3) suggests that the Zermatt-Saas zone experienced a prolonged history of HP metamorphism and possibly consists of several ophiolite slivers that were assembled in a subduction channel. Peak metamorphic conditions between ca. 540° – 600° C and 2.3 – 3.0 GPa have been reported for the Zermatt-Saas zone in general (Bucher et al., 2005; Angiboust et al., 2009) whereas peak conditions for coesite-bearing lithologies at the UHP locality at Lago di Cignana have been calculated at ≥ 3.2 GPa and ≤ 600° C (Reinecke, 1998; Groppo et al., 2009; Frezzotti et al., 2011). The timing of peak metamorphism within these rocks has been dated at ca. 44 – 43 Ma (Rubatto et al., 1998; Gouzu et al., 2006; Fig. 4.3). Dating of lower pressure retrogression within the Zermatt-Saas zone yielded ages between 42 – 38 Ma (Amato et al., 1999; Cartwright and Barnicoat, 2002; De Meyer et al., 2014; Fig. 4.3). At high structural levels and along the Combin Fault, several continental units occur within and on top of the Zermatt-Saas zone. The most prominent are the Monte Emilius klippe and Glacier Raffray slice south of the Aosta valley and the Etirol-Levaz slice in the western Valtournenche. These continental fragments also show an Alpine eclogite-facies imprint and probably represent continental outliers or extensional allochthons within the Piemont-Ligurian oceanic domain derived from the Adriatic continental margin (Dal Piaz et al., 2001; Beltrando et al., 2010c). Prograde metamorphism dated with Lu-Hf geochronology on eclogites from the Etirol-Levaz slice and another fragment near Zermatt yielded ages between 62 – 51 Ma confirming that these fragments are derived paleogeographically from a relatively internal position (Faßmer, 2014; Weber et al., accepted; Fig. 4.3). The peak of metamorphism in the Etirol-Levaz slice has been dated at ca. 47 – 45 Ma (Dal Piaz et al., 2001; Beltrando et al., 2010c; Fig. 4.3) which is only slightly older than peak ages determined for underlying ophiolitic units. In the northwest, the Combin zone is underlain by the continental St. Bernhard nappe system which is derived from Briançonnais continental crust. It consists of Paleozoic basement and Mesozoic cover rocks which experienced an Alpine greenschist- to blueschist-facies overprint (Bearth, 1963; Sartori, 1990). Ductile deformation has been dated by Markley et al. (1998) using Ar/Ar geochronology to have occurred between ca. 41 – 36 Ma (Fig. 4.3). Shear zones in the footwall limb of the Mischabel fold, a large southeast-closing antiform in the hanging wall of the northern Zermatt-Saas zone (e.g. Milnes et al., 1981), have been dated by Cartwright and Barnicoat (2002) with the Rb-Sr method at ca. 38 Ma (Fig. 4.3).

Unit	Age	Method	Event	Reference
Sesia nappe	85 - 60 Ma	U-Th-Pb	Eclogite-facies metamorphism	Regis et al. (2014)
	79 - 65 Ma	U-Pb	Eclogite-facies metamorphism	Rubatto et al. (2011)
	70 - 65 Ma	U-Pb	Eclogite-facies metamorphism	Rubatto et al. (1999)
	70 - 60 Ma	U-Pb, Rb-Sr	Eclogite-facies metamorphism	Inger et al. (1996)
	55 - 45 Ma	Rb-Sr	Exhumation	Babist et al. (2006)
Continental outliers	61.8 ± 2.3 Ma 51.3 ± 1.2 Ma	Lu-Hf	Prograde metamorphism ELS	Faßmer (2014)
	58 - 56 Ma	Lu-Hf	Prograde metamorphism TGU	Weber et al. (accepted)
	47 - 45 Ma	Rb-Sr	Eclogite-facies metamorphism ELS	Dal Piaz et al. (2001)
	47 - 45 Ma	U-Pb	Eclogite-facies metamorphism ELS	Beltrando et al. (2010)
Combin zone (Schistes Lustrés)	60 - 48 Ma	Ar/Ar	GS- to BS-facies deformation	Reddy et al. (2003)
	45 - 36 Ma	Rb-Sr	Greenschist-facies deformation	Reddy et al. (1999)
	44.5 ± 0.6 Ma	Ar/Ar	Ductile deformation	Markley et al. (1998)
	62 - 55 Ma		Blueschist-facies D1 deformation	
	51 - 45 Ma	Ar/Ar	Retrograde D2 deformation	Agard et al. (2002)
	38 - 35 Ma		Retrograde D3 deformation	
Zermatt-Saas zone	54.5 - 46.5 Ma	Lu-Hf	prograde metamorphism	Mahlen et al. (2005)
	52 ± 18 Ma	Sm-Nd	Eclogite-facies metamorphism	Bowtell et al. (1994)
	48.8 ± 2.1 Ma	Lu-Hf	Prograde metamorphism LdC	Lapen et al. (2003)
	45 - 43 Ma	Rb-Sr	prograde metamorphism	De Meyer et al. (2014)
	44 - 43 Ma	Ar/Ar	Prograde or peak LdC	Gouzu et al. (2006)
	44.1 ± 0.7 Ma	U-Pb	(U)HP-metamorphism LdC	Rubatto et al. (1998)
	40.6 ± 2.6 Ma	Sm-Nd	Peak or early exhumation LdC	Amato et al. (1999)
	38 ± 2 Ma	Rb-Sr	GS-facies overprint LdC	
	42 - 37 Ma	Rb-Sr	GS-facies retrogression	Cartwright & Barnicoat (2002)
	40 - 39 Ma	Rb-Sr	retrograde overprint	De Meyer et al. (2014)
Monte Rosa nappe	48 - 47 Ma	Ar/Ar	High-pressure deformation	Villa et al. (2014)
	42.6 ± 0.6 Ma	U-Pb	eclogite-facies metamorphism	Lapen et al. (2007)
St. Bernhard nappe system	41 - 36 Ma	Ar/Ar	Ductile deformation	Markley et al. (1998)
	38 Ma	Rb-Sr	GS-facies top-SE deformation	Cartwright & Barnicoat (2002)

Figure 4.3: Compilation of metamorphic ages of some major tectonic units in the Swiss-Italian Western Alps.

The paleogeographic origin of the Monte Rosa nappe below the Zermatt-Saas zone is still a matter of discussion. It may represent the eclogite-facies part of Briançonnais continental crust (e.g. Escher et al., 1997; Keller and Schmid, 2001) but has alternatively been attributed to the European continental margin (e.g. Froitzheim, 2001; Pleuger et al., 2005) or a distinct continental fragment (Beltrando et al., 2007b). Peak pressure conditions reached ca. 2.4 – 2.7 GPa and 550° – 570° C (Gasco et al., 2011) which are very similar to general peak metamorphic conditions reported for the Zermatt-Saas zone. The timing of eclogite-facies metamorphism has been dated by Lapen et al. (2007) at 42.6 ± 0.6 Ma using U-Pb geochronology on rutile (Fig. 4.3). An age of 48 – 47 Ma for an eclogite-facies shear zone overprinting basement gneisses has been reported by Villa et al. (2014) supporting the hypothesis of a Briançonnais origin (Fig. 4.3). Thin ophiolitic sheets on top of the Monte Rosa nappe, the Balma unit, show Cretaceous magmatic zircon ages of 93.4 ± 1.7 Ma which would speak for a Valais origin of these units and therefore a more external origin and European affinity of the underlying Monte Rosa nappe (Liati and Froitzheim, 2006; Herwartz et al., 2008). Cretaceous protolith ages are in conflict with Jurassic ages obtained for the

Antrona ophiolite between Monte Rosa and St. Bernhard continental units (Liati et al., 2005) so that the paleogeographic affiliations of these units and their relationship to the Zermatt-Saas zone remain questionable. Formation of the Vanzone antiform after ca. 32 Ma (Pettke et al., 1999) largely modified the geometry of the internal part of the Paleogene nappe stack in the Swiss-Italian Western Alps (Escher et al., 1993).

4.4 Deformation structures

In this section, I describe deformation structures in outcrop and thin-section from 11 exemplary and representative subareas along the Combin Fault and DBBT (Fig. 4.2). The areas around Lago di Cignana and Becca d'Aver have been described in detail in chapters 2 and 3, respectively. Most of the observed deformation in the 11 subareas occurred under greenschist-facies conditions so that the relative chronology of deformation is mainly deduced from overprinting relations and the degree of ductility of kinematic indicators. The study area has been subdivided into a northwestern and a southeastern realm which correspond to the areas to the northwest and southeast of the Dent Blanche nappe. All hand-specimens and thin-sections were cut parallel to the xz-plane of the finite strain ellipsoid. Lower hemisphere stereoplots of the orientation of poles of foliations and stretching lineations for the Combin zone and Dent Blanche nappe in the two realms are depicted in figure 4.4.

In the study area, the Combin zone comprises the ophiolitic Tsaté nappe and the Cimes Blanches and Frilihorn nappes which consist of successions of metasediments with continental affinity. The most common lithologies within the Tsaté nappe are calcschists and metabasites that experienced a strong greenschist-facies overprint. Calcschists in the studied areas consist of varying amounts of white mica, quartz, feldspar, calcite, chlorite, and epidote. They can be relatively undeformed but usually display a strong mylonitic foliation and metamorphic layering so that especially white mica and quartz occur as layers and ribbons. Metabasites usually occur as large bodies within calcschists and display typical greenschist-facies assemblages consisting of epidote, actinolite, chlorite, and albite. The Cimes Blanches and Frilihorn nappes mainly consist of continental margin sediments like marbles, dolomites, cellular dolomites (Rauhwacke), and quartzites. In the direct hanging wall of the DBBT, mostly rocks of the Arolla series are exposed. Valpelline series lithologies are exposed along the southeastern DBBT north of Lago di Cignana. Alpine deformation along the DBBT led to the development of strongly mylonitic fabrics formed under greenschist-facies conditions. Granitoid and gabbroic rocks of the Arolla series have often been altered along zones of high strain and as a result of increased deformation-induced fluid flow. Primary magmatic assemblages have been replaced by greenschist-facies phases and greater amounts of water-bearing minerals. Due to this strong alteration and a strong Alpine greenschist-facies overprint within Valpelline series rocks along the DBBT, mylonites of the two subunits have a similar appearance. Observed mylonitic foliations in Arolla and Valpelline series rocks often consist of alternating layers of quartz + feldspar and white mica + epidote + chlorite. These Alpine fabrics have often been overprinted by several stages of subsequent deformation along the DBBT.

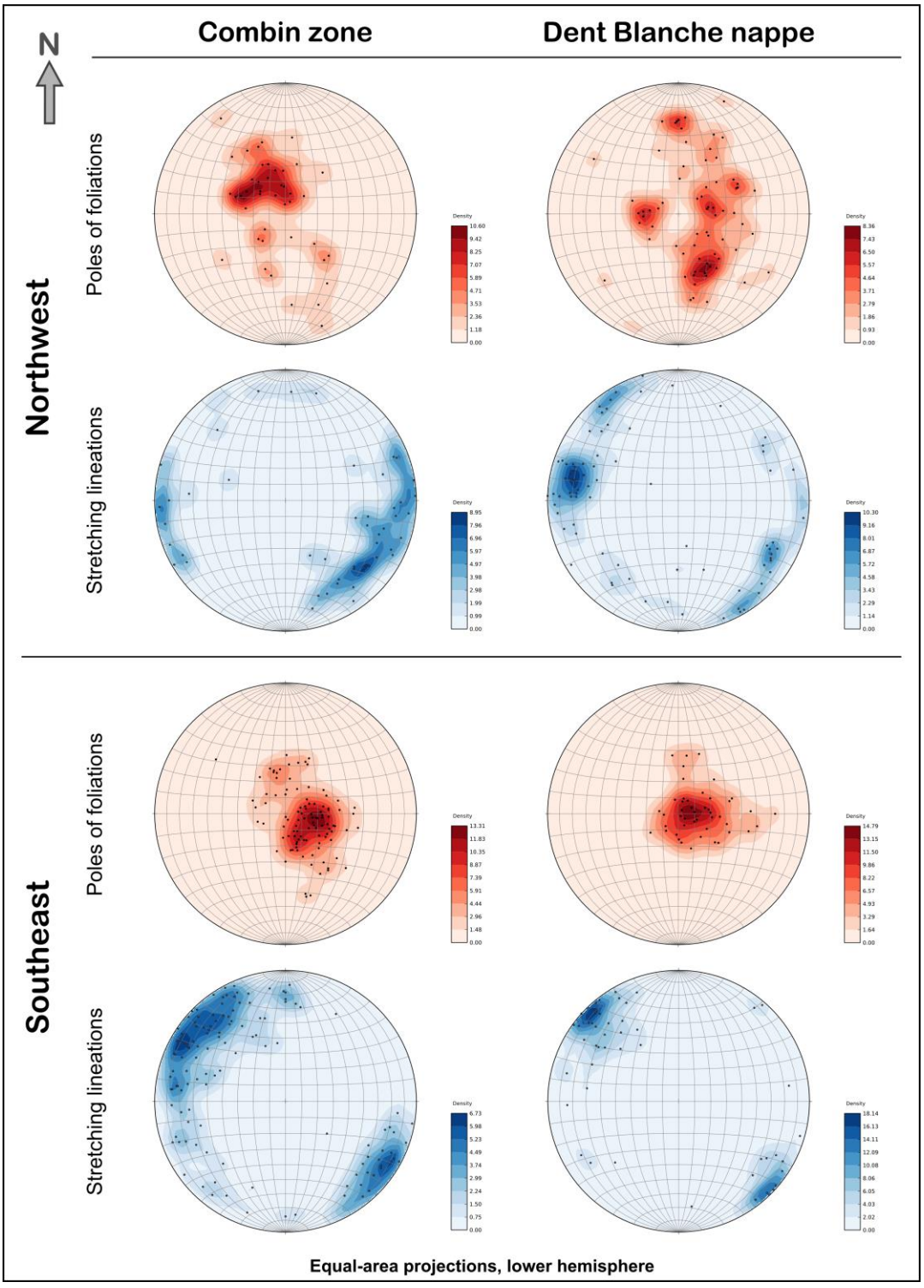

Figure 4.4: Stereoplots of stretching lineations and poles of foliations as equal area projections in the lower hemisphere for the northwestern and southeastern realms; measurements were plotted with the OpenStereo software (Grohmann and Campanha, 2010).

4.4.1 Northwestern realm

Foliations within rocks of the northwestern Combin zone mainly dip moderately to the southeast. Stretching lineations plunge very shallowly and show a maximum to the southeast but also partly strike E-W to WSW-ENE. Foliations within the northwestern lower Dent Blanche nappe show a more irregular distribution with a main maximum of moderately NNW-dipping foliations and three other maxima dipping shallowly to the east, shallowly to moderately to the southwest, and steeply to the south. Stretching lineations plunge very shallowly and show two distinct maxima of orientations, a main one that strikes WNW-ESE and a second minor one that strikes NW-SE.

4.4.1.1 Subarea 1 – Zinal

The north easternmost Dent Blanche nappe east of Val de Zinal (Fig. 4.2) has been folded into a large NE-facing recumbent fold. Folds with SE-plunging fold axes can be observed in outcrop within quartzitic gneisses of the lowermost Dent Blanche nappe. Fold axes plunge shallowly to the southeast and are parallel stretching lineations. Fold axial surfaces dip to the southeast and L-tectonites can be observed in some spots. Foliations within structurally lower calcschists of the Tsaté nappe also dip to the southeast and therefore probably represent an axial surface cleavage to Dent Blanche nappe folds. Locally, these folds have been overprinted by top-SE shearing along shallowly-dipping shear planes (Fig. 4.5a). White mica is concentrated along these shear planes, has been deformed ductiley and partly replaced by chlorite (Figs. 4.6a and b). Associated stretching lineations plunge to the southeast. Top-SE shearing led to refolding and elongation of previously folded layers depending on their orientation to shear planes. Shallowly-dipping top-SE shear planes have locally been overprinted by steeper top-NW shear bands that can be observed in thin-section (Fig. 4.6b). In an outcrop in the footwall of the observed folds, macroscopic shear bands within heterogeneous metasediments of the Tsaté nappe mainly show top-SE shear senses (Fig. 4.5b). These extensional top-SE structures are sometimes associated with NW-vergent folds with SE-plunging fold axes. Sheared layers have been folded with limbs following earlier extensional shear bands. Offset along the lower limb of a drag fold indicates top-NW shearing whereas offset along its upper limb shows the opposite transport direction (Fig. 4.5c). Top-NW shearing seems to have mainly reactivated and overprinted earlier top-SE structures but also may have been partly coeval with and developed progressively from top-SE shearing since no clear crosscutting relations can be observed. Steeply-dipping and brittle top-SE shear planes cut the layering in the same outcrop suggesting late normal faulting after cessation of ductile deformation (Fig. 4.5d). Macroscopic top-SE shear senses can also often be observed within the Tsaté nappe in the eastern Val de Zinal near Lac d'Arpitetta. Calcschists of the upper Tsaté nappe show abundant ductile top-SE shear bands (Fig. 4.5e).

In the upper Val de Zinal, the upper Tsaté nappe and lower Dent Blanche nappe show abundant top-SE shear senses overprinting the original basal thrust. Top-SE structures in turn seem to have been partly overprinted by a non-penetrative phase of top-NW shearing. Structures related to a brittle top-SE overprint can also be observed.

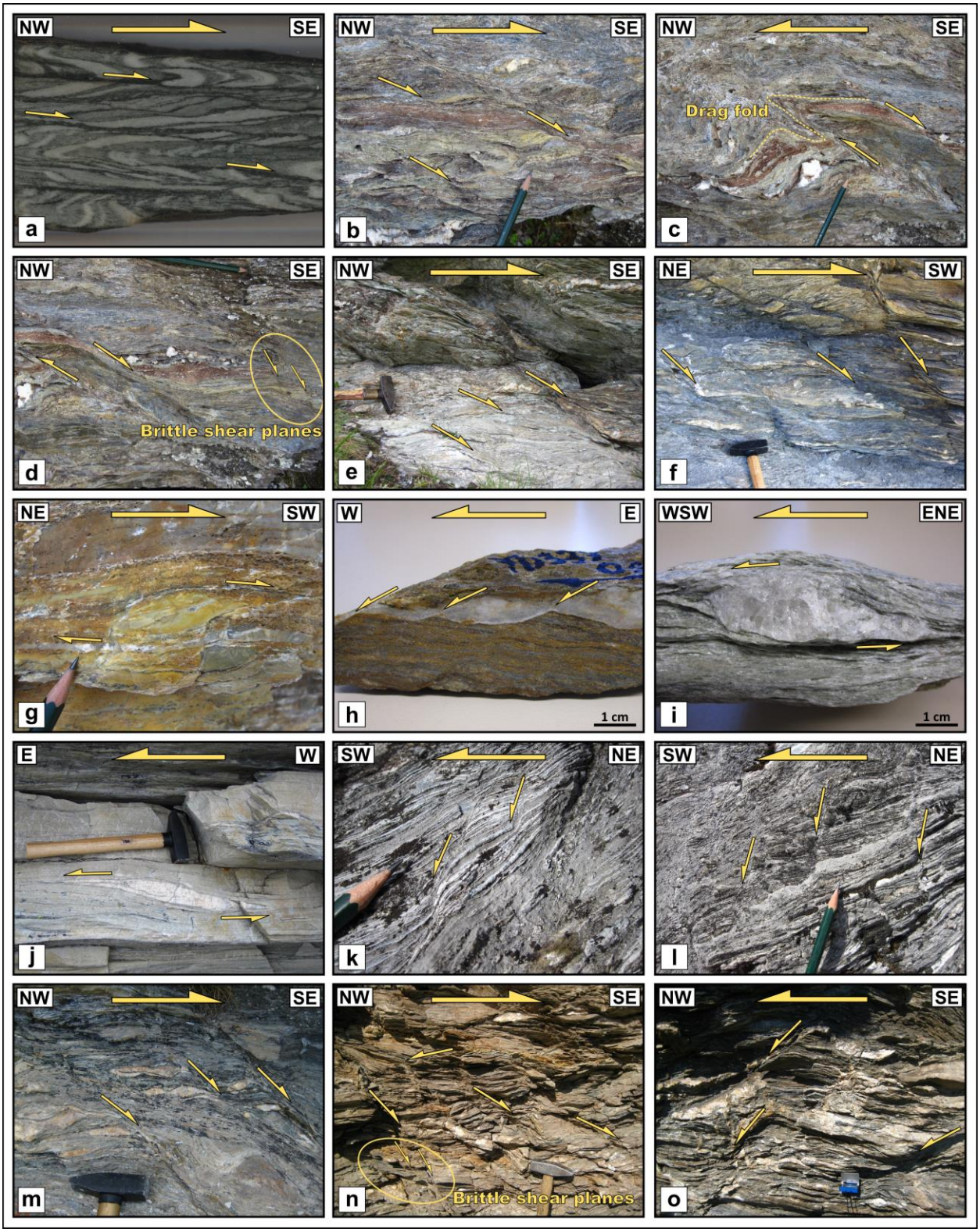

Figure 4.5: Deformation structures in outcrop in the northwestern realm. a) Sample FD311: hand-specimen of a quartz-rich gneiss from the lowermost Dent Blanche nappe east of Val de Zinal (subarea 1); preexisting folds with SE-plunging fold axes have been overprinted by top-SE shearing along shallowly-dipping shear planes; Fol (182/22) Lin (146/18). b) Heterogeneous metasediments of the upper Tsaté nappe east of Val de Zinal (subarea 1) showing ductile top-SE shear bands. c) Same outcrop as before (subarea 1) but the metasediments have additionally been affected by NW-vergent folding probably postdating the

aforementioned top-SE shearing; the lower limb of the drag fold indicates NW-directed shearing. d) Same outcrop as before (subarea 1); the metasediments are cut by more steeply dipping top-SE brittle shear planes indicating a late top-SE overprint. e) Calcschists of the upper Tsaté nappe in the eastern Val de Zinal near Lac d'Arpitetta (subarea 1) showing ductile top-SE shear bands. f) Calcschists of the lower Tsaté nappe on the eastern side of Lac de Moiry (subarea 2) showing moderately to steeply dipping top-SW shear bands. g) Sheared quartz layer within silicious marbles of the Cimes Blanches nappe east of Lac de Moiry (subarea 2) indicating ductile top-SW shearing. h) Sample FD337: hand-specimen from the base of the Tsaté nappe east of Lac de Moiry (subarea 2) showing discrete shear bands within a quartz layer and surrounding calcschists indicating low-grade greenschist-facies top-W deformation; Fol (177/27) Lin (259/07). i) Sample FD280: sheared quartz lense in white mica-rich schist from the Cimes Blanches nappe west of Lac des Dix (subarea 4) indicating ductile top-WSW shearing; Fol (342/79) Lin (69/10). j) Sheared white quartz layer in a greyish quartzitic matrix at Col des Roux west of Lac des Dix (subarea 4) indicating ductile top-E shearing. k) Ductile to brittle top-SW shear bands within laminated marbles north of Lac de Mauvoisin in the Val de Bagnes (subarea 5). l) Ductile to brittle top-SW shear bands within laminated marbles north of Lac de Mauvoisin in the Val de Bagnes (subarea 5). m) Calcschists of the upper Tsaté nappe near the village Ollomont in the Valpelline (Subarea 6) showing ductile top-SE shear bands. n) Calcschists of the Tsaté nappe near the village Allein (subarea 7) showing mainly ductile top-SE shear bands but also anastomosing shear zones and subordinate top-SE brittle shear planes. o) Calcschists of the Tsaté nappe near Allein (subarea 7) showing ductile top-NW shear bands.

4.4.1.2 Subarea 2 – Moiry

At Lac de Moiry in the Val de Moiry (Fig. 4.2), foliations within rocks of the lower Combin zone dip to the south to southeast and stretching lineations approximately trend E-W. Close to the Combin Fault, kinematic indicators in outcrop and thin-section mostly give top-(W)SW shear senses as indicated by abundant shear bands. Top-SW shear bands can often be observed within calcschists and show different inclinations from moderately to steeply dipping (Fig. 4.5f) and a range from ductile to semi-ductile characters. In an outcrop east of the lake, a sheared quartz layer within silicious marbles shows a sigmoidal shape indicating highly ductile deformation due to SW-vergent shearing (Fig. 4.5g). In a sample from an outcrop in the footwall, a sheared quartz layer and shear bands within surrounding calcschists indicate top-W shearing (Fig. 4.5h). Strain was localized into discrete shear bands within quartz suggesting relatively low-grade greenschist-facies deformation. The same sample shows ductile shear bands within the calcite/white mica matrix but brittle microfracturing of feldspar in thin-section (Fig. 4.6c) suggesting temperatures below ca. 450° C during deformation (Passchier and Trouw, 2005). Antithetic `bookshelf´ microfracturing can sometimes be observed and also indicates low-grade conditions below ca. 450° C (Pryer, 1993). Microfractures are often filled with calcite.

Along the eastern side moraine of the former Moiry glacier, a cross-section with calcschists in the footwall and metabasites in the hanging wall is exposed. Structurally lower calcschists often display steep top-SE shear zones cutting through the mylonitic foliation. Close to the DBBT, these calcschists are overlain by a nappe of folded greenschists. The northwestern exposure of these greenschists suggests a NW-closing sheath fold character of this subnappe, the formation of which was most likely related to NW-vergent shearing. Stretching lineations within the uppermost Tsaté nappe and lowermost Dent Blanche nappe trend NNW-SSE. No kinematic indicators could be found within gneisses of the Arolla series near the Cabane de Moiry.

The lower Combin zone at Lac de Moiry is characterized by top-W and top-SW shear senses which probably formed under decreasing metamorphic conditions as suggested by different degrees of ductility. At structurally higher levels, deformation structures related to top-SE shearing within calcschists and top-NW shearing within overlying metabasites can be observed.

4.4.1.3 Subarea 3 – Arolla

In the area around and north of Arolla in the southern Val d'Hérens (Fig. 4.2), foliations within rocks of the Dent Blanche and Tsaté nappes mostly dip to the south to southeast, stretching lineations dominantly trend WNW-ESE. Mylonites in the hanging wall of the DBBT often give top-W shear senses as indicated for example by a grain shape preferred orientation within quartz layers (Fig. 4.6d). The Dent Blanche nappe has been folded into open folds with mostly NE- to E-plunging axes deforming older foliations and stretching lineations. As a result of this late folding, the mylonitic foliation has an often steep and overturned orientation. A crenulation cleavage with dominantly E-W trending axes can often be observed to overprint greenschist-facies foliations. A similar style of deformation can be observed within heterogeneous metasediments of the underlying Tsaté nappe along the road to Arolla which have also been folded into mainly open folds with E-W trending axes. An approximately E-W striking crenulation cleavage can also be observed to have formed within these rocks. Within Tsaté calcschists further north along the road, two different orientations of SE-plunging stretching lineations with an angle of ca. 20° in between can be observed. These calcschists are often strongly mylonitic but a bulk shear sense could not unambiguously be determined since top-NW and top-SE shear senses can be observed. Calcschists have sometimes been folded into SE-vergent folds.

In the area around and north of Arolla, basal mylonites of the Dent Blanche nappe show top-W shear senses whereas calcschist mylonites of the Tsaté nappe show top-NW as well as top-SE shear senses. Both units have been folded and display crenulations due to late-stage compressional deformation.

4.4.1.4 Subarea 4 – Dix

West of Lac des Dix in the southern Val d'Héremence (Fig. 4.2), metasediments of the Cimes Blanches nappe are exposed. At the northern end of the lake, foliations dip moderately to steeply to the northwest. Exposed metasediments consist of quartz and white mica and have a schistose fabric. Stretching lineations approximately trend E-W whereas in some samples two distinct stretching lineations with an angle of ca. 25° in between can be distinguished. Kinematic indicators associated with these lineations indicate top-W (Fig. 4.6e) and top–WSW (Fig. 4.6f) shearing, respectively. Both shear directions show very similar microstructures. Quartz is usually very fine-grained within these schists indicating prolonged grain-size reduction during ongoing deformation and therefore large amounts of strain (Mitra, 1978). Shear bands in thin-section are sometimes associated with quartz ribbons showing bulging recrystallization, subgrain formation, and patchy undulose extinction (Fig. 4.6g) indicating temperatures of 300 – 400°C during ductile deformation (Stipp et al., 2002; Passchier and Trouw, 2005). Subordinate conjugate top-E shear bands suggest a minor pure shear component during bulk top-W shearing. On a hand-specimen scale, sheared quartz lenses within white mica-rich schists also indicate top-WSW shearing under ductile conditions (Fig. 4.5i). At Col des Roux further to the west, quartzitic rocks of the Cimes Blanches nappes are exposed. Foliations variably dip to the southeast to southwest and stretching lineations again trend E-W. In thin-section, a shear sense could not be determined. In outcrop, a sheared white quartz layer within a greyish quartzitic matrix indicates ductile top-E shearing (Fig. 4.5j).

Deformation structures within Cimes Blanches metasediments in the area west of Lac des Dix indicate ductile top-W and top-WSW shearing associated with two distinct stretching lineations. Subordinate, probably conjugate top-E shearing can also be observed.

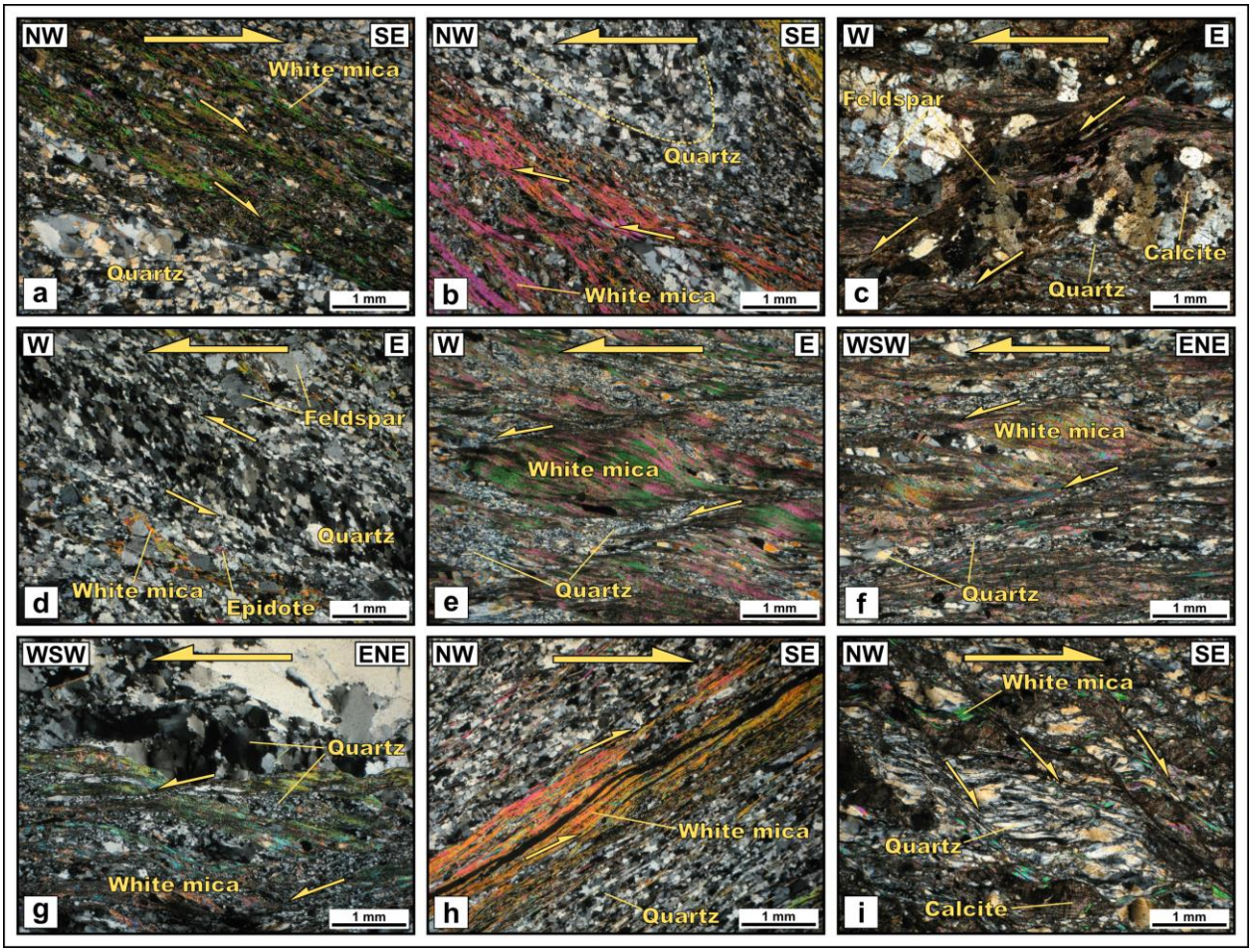

Figure 4.6: Photomicrographs of deformation structures from the northwestern realm; all thin-sections were cut parallel to the xz-plane of the finite strain ellipsoid; all pictures were taken with crossed polarizers; values for dip directions and angles of foliations as well as plunge directions and angles of stretching lineations are given. a) Sample FD311: quartz-rich gneiss from the lowermost Dent Blanche nappe east of Val de Zinal (subarea 1); same sample as in figure 4.5a; white mica is concentrated along shear planes between folded quartz-rich parts; asymmetry of larger white mica grains indicates top-SE shearing; Fol (182/22) Lin (146/18). b) Sample FD311: same sample as before (subarea 1) with folded quartz-rich layer in the upper part and white mica-rich layer in the lower part which corresponds to shear planes in figures 4.5a and 4.6a; shear bands within mica-rich part indicate top-NW shearing. c) Sample FD337: calcschist from the lower Tsaté nappe east of Lac de Moiry (subarea 2) showing ductile top-WSW shear bands within calcite and white mica-rich parts and brittle fracturing of feldspar clasts; Fol (177/27) Lin (259/07). d) FD118: orthogneiss from the base of the Dent Blanche nappe near Arolla (subarea 3); GSPO of quartz grains within quartz layer indicates top-W shearing; Fol (272/23) Lin (272/23). e) Sample FD281: metasediment from the Cimes Blanches nappe west of Lac des Dix (subarea 4) showing highly ductile top-W shear bands; quartz is very fine-grained indicating large amounts of strain; Fol (340/63) Lin (274/27). f) Sample FD280: metasediment from the same locality as the sample before (subarea 4) showing top-WSW shear bands; Fol (342/74) Lin (69/10). g) Sample FD280: same sample as before (subarea 4) showing top-WSW shear bands; the quartz ribbon in the upper part of the section shows bulging recrystallization, subgrain formation, and patchy undulose extinction indicating temperatures of ca. 300 – 400° C during ductile deformation (Stipp et al., 2002; Passchier and Trouw, 2005). h) Sample FD06: metasediment of the upper Tsaté nappe east of Ollomont in the Valpelline (subarea 6) showing a strong metamorphic layering and shallowly-dipping top-SE shear bands; Fol (128/20) Lin (128/20). i) Sample FD03: calcschist from the Tsaté nappe near Allein (subarea 7) showing ductile top-SE shear bands; associated quartz grains display undulose extinction, strong flattening, and rare bulging recrystallization indicating temperatures around or below 400° C during ductile deformation (Stipp et al., 2002); Fol (98/25) Lin (122/19).

4.4.1.5 Subarea 5 – Mauvoisin

The Cimes Blanches nappe north of Lac de Mauvoisin in the Val de Bagnes (Fig. 4.2) mainly consists of massive, laminated, or foliated marbles. Foliations dip moderately to steeply to the northwest and stretching lineations plunge to the (W)SW. In outcrop, kinematic indicators consistently show top-SW shear senses. Ductile to brittle shear bands and faults within finely-laminated marbles/dolomites indicate SW-directed shearing (Figs. 4.5k and l). The varying degree of ductility along shear planes is probably due to different viscosities of the (sub)mm- to cm-thick layers which are most likely the result of varying degrees of dolomitization. Sigma-shaped calcite clasts can sometimes be observed within marbles and also indicate top-SW shearing. White calcite layers within rather massive grey marbles have sometimes been deformed into upright, tight to isoclinal folds. A weak foliation within host marbles represents an axial surface cleavage.

North of Lac de Mauvoisin, the Cimes Blanches nappe is characterized by top-SW shearing within calcitic rocks.

4.4.1.6 Subarea 6 – Ollomont

Near the village Ollomont in the Valpelline (Fig. 4.2), strongly mylonitic rocks of the lowermost Dent Blanche nappe can be studied. Foliations within these rocks dip to the east. The Tsaté nappe in the footwall of the DBBT consists mainly of calcschists with minor greenschists and serpentinite. Foliations dip to the southeast. Stretching lineations in both units plunge shallowly to the (E)SE. SE-dipping shear bands can often be observed within Tsaté calcschists in outcrop. Quartz layers and ribbons within calcschists have occasionally been folded isoclinally and then overprinted by ductile top-SE shear bands (Fig. 4.5m). In some spots, SE-vergent folds and an associated crenulation cleavage with SW-plunging axes can be observed. In thin-section, schists of the Tsaté nappe often show a distinct metamorphic layering and exhibit top-SE shear senses as indicated by asymmetrically deformed white mica (Fig. 4.6h). In contrast, rocks of the Arolla series in the immediate hanging wall of the DBBT display top-WNW shear senses in thin-section (Fig. 4.7a). A crenulation cleavage with NE-plunging axes can often be observed to overprint the penetrative fabric in some parts.

<u>Ollomont mylonite</u>

In the following, I describe the structural and metamorphic evolution of one mylonite ("Ollomont mylonite") from the lowermost Dent Blanche nappe. Mineral compositions were measured with the Jeol JXA-8200 superprobe at Steinmann-Institut, University of Bonn (see appendix for electron microprobe analyses). The whole rock chemistry, which was used as input for pseudosection modelling, was determined with XRF analysis at the Steinmann-Institut and is shown in table 4.1.

The penetrative mylonitic foliation of the sample dips to the east. The stretching lineation is an aggregate lineation that plunges shallowly to the ESE. The mylonitic foliation has been overprinted in some parts by a SE-dipping crenulation cleavage with NE-plunging axes (Figs. 4.7b and d). The sample consists of quartz + albite + white mica + epidote + chlorite + titanite (+ rutile). The observed layering is due to different ratios of phases within layers whereas quartz has been completely segregated into

monomineralic layers and ribbons. Feldspar is almost pure albite (96.5 – 98.8 mol%). White mica is phengitic with 3.35 – 3.47 Si p.f.u.. Chlorite preferentially occurs as intergrowths with white mica. Most epidote grains display a distinct 4-phase zonation from core to rim with 1) allanite in the cores 2) Fe-rich, Al-poor epidote 3) Fe-poor, Al-rich epidote and 4) Fe-rich, Al-poor epidote (Fig. 4.7e). In some parts, a grain shape preferred orientation of quartz grains defines an oblique foliation indicating top-WNW shearing (Fig. 4.7a). Flattened quartz grains are also often parallel to crenulation planes and define an axial surface foliation to folds in microlithons. In one spot, the mylonitic foliation is cut by a shallow microthrust along a quartz layer slightly oblique to the main foliation (Fig. 4.7c). In the hanging wall of this microthrust, a crenulation cleavage formed due to shortening parallel to the transport direction whereas in the footwall, the primary foliation has been deformed into drag folds. The "drag" direction of folds indicates top-WNW movement along the thrust. The microthrust itself has partly been overprinted by the crenulation cleavage suggesting that thrust activity and formation of drag folds in the footwall partly predates formation of the compressional crenulation cleavage.

SiO_2	TiO_2	Al_2O_3	Fe_2O_3	MnO	MgO	CaO	Na_2O	K_2O	LOI	Sum
59.01	0.70	17.67	5.16	0.09	2.11	6.71	3.29	1.47	1.96	98.62

Table 4.1: Whole rock composition of the Ollomont mylonite determined with XRF analysis.

To constrain PT-conditions for the observed deformation structures and the metamorphic evolution of the Ollomont mylonite, equilibrium phase diagrams were calculated with the THERIAK-DOMINO software package (De Capitani and Petrakakis, 2010) and the JUN92 database which is based on thermodynamic data by Berman (1988). Oxygen was added to the bulk composition to stabilize epidote which occurs as a major phase in the sample. The observed mineral assemblage quartz + albite + phengite + epidote + chlorite is stable over a wide range of PT conditions according to thermodynamic modelling and is bounded by the stability of biotite towards higher temperatures (Fig. 4.7f). The Si content in phengite and the albite content in plagioclase both decrease with increasing temperatures which restricts the PT path for the modelled mylonite to rather cold exhumation (Fig. 4.7f). Along the retrograde path, paragonite and pargasitic amphibole are also stable according to the modelling but cannot be observed in the mylonite. Chlorite is stable below ca. 0.45 GPa and 330° C along the assumed PT path. The modelled stability of epidote is characterized by a decreasing epidote component in zoisite and therefore the Fe-content with increasing temperatures and then another increase. In the phase diagram, the epidote component in zoisite is indicated by shadings of green with lighter green indicating lower epidote (Fe) contents. The observed 4-stage zonation in epidote may be the result of progressive epidote growth along the retrograde path which runs through areas of higher and lower Fe contents (Fig. 4.7f). Allanite in cores also suggests that epidote growth was coupled to increased fluid mobility and/or fluid influx on the retrograde path (Konrad-Schmolke et al., 2011b). Partial replacement of white mica and the modelled low-grade stability suggest that chlorite grew relatively late on the retrograde path. However, there are no microstructural observations for post-kinematic growth of chlorite so that deformation, i.e. formation of the crenulation cleavage, is interpreted to have occurred under low-grade conditions.

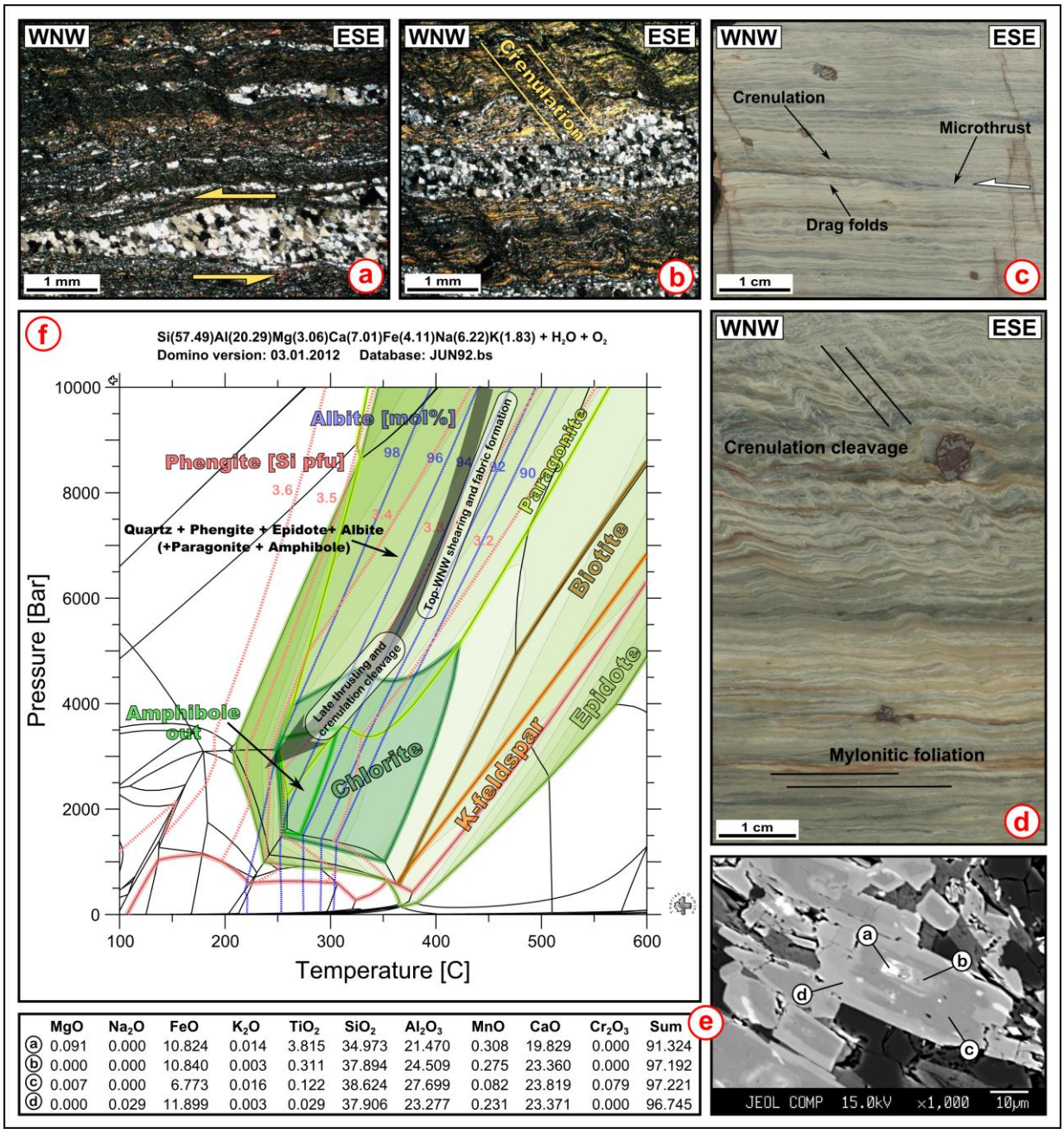

	MgO	Na_2O	FeO	K_2O	TiO_2	SiO_2	Al_2O_3	MnO	CaO	Cr_2O_3	Sum
ⓐ	0.091	0.000	10.824	0.014	3.815	34.973	21.470	0.308	19.829	0.000	91.324
ⓑ	0.000	0.000	10.840	0.003	0.311	37.894	24.509	0.275	23.360	0.000	97.192
ⓒ	0.007	0.000	6.773	0.016	0.122	38.624	27.699	0.082	23.819	0.079	97.221
ⓓ	0.000	0.029	11.899	0.003	0.029	37.906	23.277	0.231	23.371	0.000	96.745

e

Figure 4.7: Structures and metamorphism in a mylonite ("Ollomont mylonite": samples FD07, FD349 – FD351) from east of the village Ollomont in the Valpelline of Italy (subarea 6). a) Photomicrograph showing a slight crenulation cleavage and a sheared quartz layer; GSPO of quartz grains indicates top-WNW shearing. b) Photomicrograph showing a more pronounced crenulation cleavage. c) Hand-specimen showing a small-scale thrust in the middle, a crenulation cleavage in the upper part, and drag folds directly below the microthrust. Drag direction of the folds indicates top-WNW shearing along the thrust. The microthrust itself has partly been overprinted by the crenulation cleavage suggesting that thrust activity and formation of drag folds in the footwall partly predates formation of the compressional crenulation cleavage. d) Hand-specimen showing a pronounced crenulation cleavage in its upper part and the primary mylonitic foliation in its lower part due to strong strain partitioning. e) BSE-picture of zoned epidote and microprobe analysis of each of the 4 zones; an allanite-rich core is surrounded by distinct zones of relatively Fe-rich, Fe-poor, and another Fe-rich epidote. f) Equilibrium phase diagram calculated with the THERIAK-DOMINO software package (De Capitani and Petrakakis, 2010) with excess water and additional O_2; see text for discussion.

The observed quartz GSPO within monomineralic layers most likely formed contemporaneous with the greenschist-facies metamorphic layering and the penetrative mylonitic foliation and therefore on the retrograde path. Flattened quartz grains sometimes forming an axial surface cleavage to the crenulation indicate ductile quartz deformation during late-stage compression and therefore temperatures above ca. 300° C (e.g. Stipp et al., 2002). Chlorite and quartz deformation together indicate formation of the crenulation cleavage between ca. 300 – 330° C. Formation of the crenulation cleavage was probably owed to differential slip along layers as suggested by strong strain partitioning observed on a hand-specimen scale (Fig. 4.7d). Late-stage shortening was most likely related to renewed thrusting under low-grade greenschist-facies conditions as suggested by microthrust activity.

In the Ollomont mylonite, the observed deformation structures, mineral assemblage, and mineral compositions are the result of a structural and metamorphic evolution on the retrograde path, i.e. during exhumation of the Dent Blanche nappe. Exhumation along the DBBT occurred during thrusting and associated top-WNW shearing whereas mineral compositions suggest rather cold exhumation. A late stage of renewed thrusting and associated NW-SE shortening under low-grade greenschist-facies conditions affected the DBBT near Ollomont. Whereas basal mylonites show top-WNW shearing, the underlying Tsaté nappe is characterized by dominant top-SE shearing.

4.4.1.7 Subarea 7 – Allein

In the area around the village Allein northwest of Aosta (Fig. 4.2), a cross-section from the Cimes Blanches nappe into the Dent Blanche nappe is exposed. The dip of foliations ranges from east- to south-dipping whereas stretching lineations uniformly plunge to the southeast. The Cimes Blanches nappe near Allein mainly comprises marbles and metaconglomerates. Kinematic indicators within these rocks often indicate top-SE shearing in outcrop. Calcschists of the overlying Tsaté nappe also show dominantly top-SE shear senses in outcrop (Fig. 4.5n) and only subordinate top-NW shear bands (Fig. 4.5o). Shear bands in outcrop partly appear as anastomosing shear zones and, in more competent layers, have an already semi-ductile to brittle character (Fig. 4.5n). In thin-section, top-SE shear bands within calcschists are associated with quartz grains showing undulose extinction, strong flattening, and occasionally bulging recrystallization indicating temperatures around or below 400° C during ductile deformation (Fig. 4.6i; Stipp et al., 2002). SE-vergent folds can often be observed within calcschists deforming an older fabric and stretching lineation and partly forming a crenulation cleavage. Along the DBBT, mylonitic greenschist-facies metagranites of the Arolla series as well as calcschists and greenschists of the Tsaté nappe are exposed. A crenulation cleavage with ENE – WSW trending axes can sometimes be observed within rocks of the Arolla series. Kinematic indicators could not be found within rocks of the lowermost Dent Blanche nappe.

Rocks of the Combin zone near Allein show predominantly top-SE shear senses and subordinately top-NW shear senses.

4.4.2 Southeastern realm

Most foliations within rocks of the southeastern Combin zone dip shallowly to moderately to the southeast. Stretching lineations show a range of shallowly plunging orientations from southeast to north but most of them approximately trend NW-SE. Foliations within the southeastern lower Dent Blanche nappe mostly dip to the west at a shallow angle. Most stretching lineations trend NW-SE and plunge shallowly.

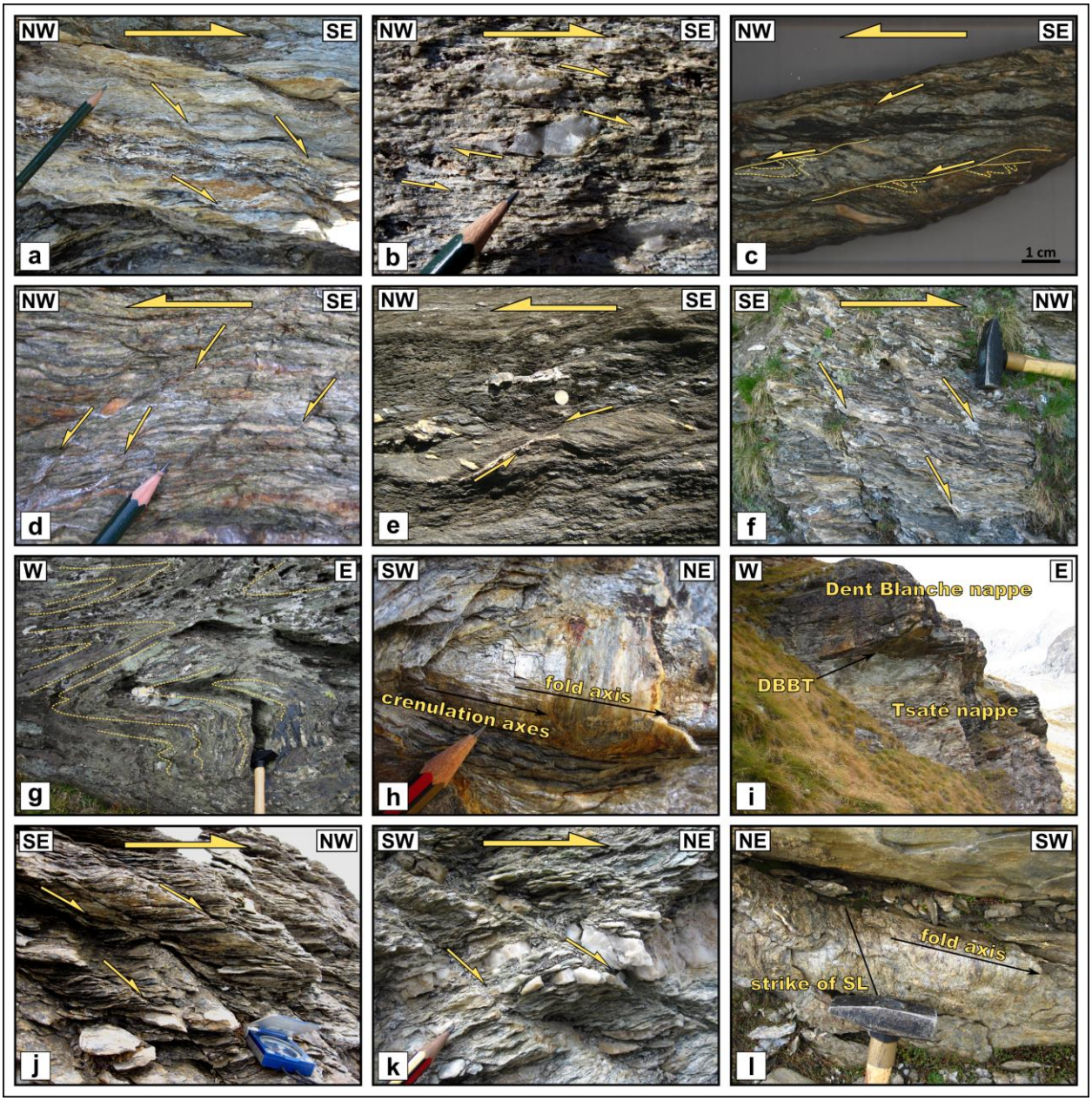

Figure 4.8: Deformation structures in outcrop in the southeastern realm. a) Quartzitic schists of the Cimes Blanches nappe west of Gran Tournalin in the eastern Valtournenche (subarea 9) showing ductile top-SE shear bands. b) Same locality as before (subarea 9); sheared quartz clast within impure quartzitic schists of the Cimes Blanches nappe indicating ductile top-SE shearing. c) Sample FD270: greenschist-facies mylonite from the base of the Dent Blanche nappe southwest of Breuil (subarea 10); the mylonitic foliation has been folded into NW-vergent folds which subsequently have been cut by discrete top-NW shear bands;

ductile deformation of quartz ribbons suggests temperatures above ca. 300°C during formation of late top-NW shear bands; Fol (270/63) Lin (326/47). d) Greenschist-facies mylonite from the base of the Dent Blanche nappe north of Breuil (subarea 10); discrete semi-ductile to brittle top-NW shear planes cut the mylonitic foliation indicating late top-NW shearing through the ductile/brittle transition along the DBBT. e) Highly ductile top-NW shear bands within calcschists of the lower Tsaté nappe north of Breuil (subarea 10). f) More discrete top-NW shear bands within calcschists of the Tsaté nappe just below the DBBT north of Breuil (subarea 10). g) Foliated metabasites of the upper Tsaté nappe north of Breuil (subarea 10) folded into open to isoclinal folds with NW-plunging axes parallel to stretching lineations. h) Folded metasediments of the Tsaté nappe on the northern side of the Zmutt valley west of Zermatt (subarea 11); folds with SW-NE trending fold axes deform a preexisting foliation and stretching lineation and are associated with formation of a SW-NE trending crenulation. i) Exposed DBBT on the northern side of the Zmutt valley west of Zermatt (subarea 11) with metasediments of the Tsaté nappe in the footwall and mylonites of the Dent Blanche nappe in the hanging wall; the contact is not folded but has a planar character. j) Top-NW shear bands within calcschists of the Tsaté nappe on the southern side of the Zmutt valley (subarea 11). k) Quartzitic schists of the Cimes Blanches nappe northwest of Zermatt (subarea 11) showing semi-ductile top-NE shear bands. l) Folds with (W)SW-plunging fold axes within metasediments of the uppermost Tsaté nappe in the direct footwall of the DBBT northwest of Zermatt (subarea 11) deforming a preexisting foliation and stretching lineation; folding cannot be traced into the overlying Dent Blanche nappe.

4.4.2.1 Subarea 8 – Trois Villes

In the area near the village Trois Villes northeast of Aosta (Fig. 4.2), the Dent Blanche/Combin contact has been deformed on the map-scale into a tight to isoclinal fold. Foliations within Arolla gneisses near Trois Villes are corrugated so that they variably dip to the S to WNW. Stretching lineations dominantly trend W-E and subordinately NW-SE. The exposed rocks consist of white mica, quartz, and minor feldspar, chlorite, and epidote. Most samples show top-W to –NW shear bands in thin-section. These shear bands deform quartz and white mica in a ductile manner (Fig. 4.9a). Grain sizes are often strongly reduced within strained areas. Quartz grains show undulose extinction, deformation lamellae, and subgrain formation (Fig. 4.9b). The dominant recrystallization mechanism is bulging recrystallization. These microstructures indicate ductile deformation at temperatures below 400° C (Stipp et al., 2002; Passchier and Trouw, 2005).

Mylonites from the base of the Dent Blanche nappe near Trois Villes record ductile top-(N)W deformation under low-grade greenschist-facies conditions.

4.4.2.2 Subarea 9 – Tournalin

In the area west of the peak Gran Tournalin in the eastern Valtournenche (Fig. 4.2), rocks of the Cimes Blanches and Tsaté nappes are exposed. The Cimes Blanches nappe mainly consists of marble and dolomite with quartzitic strata of several meters thickness. Quartzitic rocks contain varying amounts of white mica and display schistose to tabular fabrics. Foliations consistently dip to the east and stretching lineations plunge to the southeast. In outcrop, shear bands within foliated quartzitic rocks (Fig. 4.8a) and the sigmoidal shape of sheared quartz clasts within impure quartzites (Fig. 4.8b) indicate top-SE shearing. In thin-section, highly ductile top-SE shear bands within white mica-rich quartzites also indicate SE-vergent shearing (Fig. 4.9c). Quartz is relatively coarse-grained in areas between shear bands, very fine-grained in strained areas, and the dominant recrystallization mechanism is bulging recrystallization suggesting temperatures below ca. 400°C (Stipp et al., 2002).

The overlying Tsaté nappe mainly consists of greenschists and minor serpentinite and calcschists. Foliations variably dip to the W, SW, and SSE suggesting large-scale folding of the Combin zone in this area. Stretching lineations dominantly trend NW-SE. Macroscopic kinematic indicators could not be observed within the Tsaté nappe. In thin-section, rare shear bands in greenschists indicate bulk top-NW

shearing. A sample from a foliation-parallel quartz layer within greenschists close to the crest between Gran and Petit Tournalin exhibits the same orientation of stretching lineation as surrounding greenschists. In thin-section, textural domains can be observed and the dominant recrystallization mechanism is bulging recrystallization (Fig. 4.9d). In one domain, larger grains also show patchy undulose extinction and subgrain formation (Fig. 4.9d). A weakly developed GSPO in this domain suggests top-NW transport and may indicate that subgrain rotation recrystallization was also active during dynamic recrystallization. All these microstructures together suggest ductile deformation at temperatures around ca. 400° C (Stipp et al. 2002). According to these observations, top-NW shearing may have occurred at slightly higher-grade conditions than top-SE shearing. It is, however, not trivial to deduce a sequence of deformation from the inferred temperature conditions since thrusting can place hotter rocks on top of colder ones.

West of Gran Tournalin in the eastern Valtournenche, rocks of the Cimes Blanches nappes show ductile top-SE shear senses whereas rocks at higher structural levels within the Tsaté nappe dominantly show top-NW shear senses. Overprinting relations between these two opposing shear directions could not be observed. Quartz microstructures suggest that both, top-SE and top-NW shearing occurred at similar medium-grade greenschist-facies conditions.

4.4.2.3 Subarea 10 – Breuil

In the western upper Valtournenche near the town Breuil (Cervinia) (Fig. 4.2), the DBBT is well-exposed over a long-distance. In this area, rocks of the Arolla series crop out in the direct hanging wall of the contact.

In the area southwest of Breuil, foliations within rocks of the lowermost Dent Blanche nappe dip to the west to northwest. Stretching lineations plunge to the NW. Kinematic indicators within these basal mylonites consistently indicate top-NW shearing. In thin-section, quartz grains show undulose extinction and subordinate bulging recrystallization suggesting low-grade conditions well below 400° C during deformation (Fig. 4.9e; Stipp et al., 2002). On a hand-specimen and thin-section scale, the preexisting greenschist-facies foliation and metamorphic layering has sometimes been folded into NW-vergent folds (Figs. 4.8c and 4.9f). These folds in turn are cut and offset by discrete top-NW shear bands. Within these shear bands, the grain size is often strongly reduced indicating large strains (Fig. 4.8f). Quartz ribbons are often still ductiley deformed along these shear bands (Fig. 4.8c) suggesting activity at temperatures still above ca. 300° C (Stipp et al., 2002).

In the area north of Breuil, foliations within the Dent Blanche nappe dip to the northeast to east and, near Croce di Carrel, to the NW to N. Stretching lineations consistently trend NW-SE. Southwest of Croce di Carrel, semi-ductile to brittle shear planes cut through a greenschist-facies fabric and partly offset quartz layers in a brittle manner (Fig. 4.8d) indicating very low-grade conditions around and below ca. 300° C during NW-directed shearing. In thin-section, basal mylonites often show a metamorphic layering consisting of quartz + feldspar and white mica + epidote + chlorite. This fabric has often been overprinted by top-NW shear bands which often have a highly ductile character (Fig. 4.9g) but also offset more competent, e.g. epidote-rich layers in a rather semi-ductile manner (Fig. 4.9h). Conjugate top-NW and top-SE shear bands in one sample suggest a pure shear component during bulk top-NW shearing (Fig.

4.9i). Semi-ductile top-SE shear bands can be observed to cut through the greenschist-facies foliation in some samples. These structures suggest NW – SE directed crustal extension during a late stage of deformation along the DBBT. Top-NW shear senses can also be observed at all structural levels within the Combin zone north of Breuil in outcrop and thin-section. These have a ductile character at lower structural levels (Fig. 4.8e) but become more localized and discrete at higher structural levels (Fig. 4.8f). Foliated metabasites close to the DBBT near Croce di Carrel have been folded into open to isoclinal folds with NW-plunging axes parallel to stretching lineations (Fig. 4.8g).

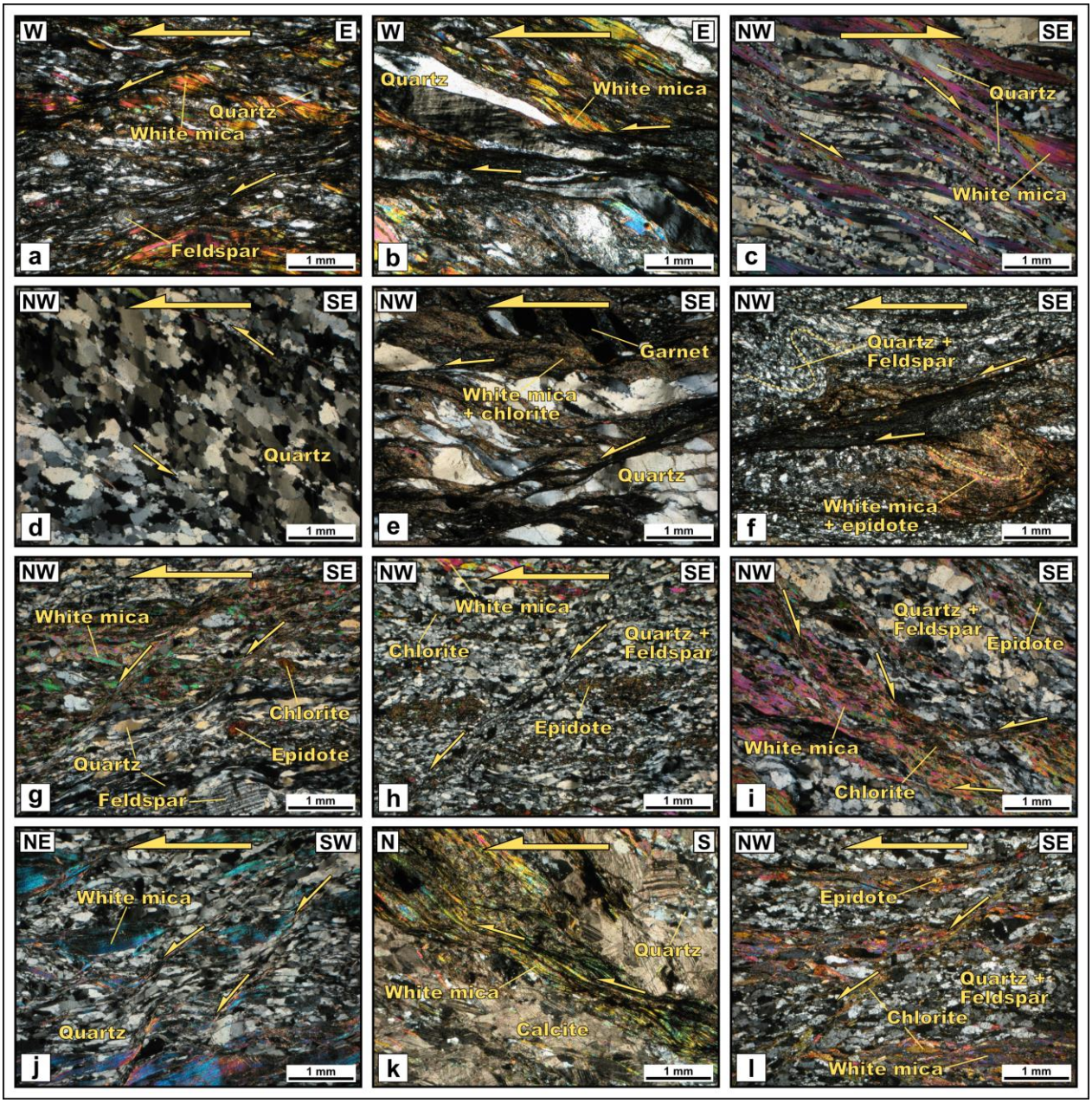

Figure 4.9: Photomicrographs of deformation structures from the southeastern realm; all thin-sections were cut parallel to the xz-plane of the finite strain ellipsoid; all pictures were taken with crossed polarizers; values for dip directions and angles of foliations as well as plunge directions and angles of stretching lineations are given. a) Sample FD21: mylonite from the base of

the Dent Blanche nappe near the village Trois Villes (subarea 8) showing top-W shear bands; grain sizes are strongly reduced within strained areas; Fol (229/20) Lin (268/16). b) Sample FD21: same sample as before; quartz shows undulose extinction, deformation lamellae, subgrain formation, and bulging recrystallization indicating temperatures below 400° C (Stipp et al., 2002; Passchier and Trouw, 2005). c) Sample FD233: metasediment from the Cimes Blanches nappe west of Gran Tournalin in the eastern Valtournenche (subarea 9) consisting of quartz and white mica and showing ductile top-SE shear bands; the grain size is strongly reduced along shear bands and the dominant recrystallization mechanism is bulging recrystallization suggesting temperatures below 400° C (Stipp et al., 2002); Fol (102/19) Lin (144/21). d) Sample FD229: foliation-parallel quartz layer within greenschists close to the crest between Gran and Petit Tournalin (subarea 9); textural domain in the middle of the picture shows patchy undulose extinction, subgrain formation, and a weakly developed GSPO indicating top-NW transport; bulging recrystallization and possibly subgrain rotation recrystallization suggest temperatures around 400° C (Stipp et al., 2002); Fol (261/08) Lin (299/06). e) Sample FD272: mylonite from the base of the Dent Blanche nappe southwest of Breuil (subarea 10) showing ductile top-NW shear bands; undulose extinction and subordinate bulging recrystallization of quartz suggest temperatures well below 400° C; Fol (284/46) Lin (312/40). f) Sample FD270: mylonite from the base of the Dent Blanche nappe southwest of Breuil (subarea 10); a preexisting greenschist-facies foliation has been folded into NW-vergent folds which subsequently have been cut by discrete top-NW shear bands; the grain size is strongly reduced within shear bands indicating large amounts of strains; Fol (270/63) Lin (326/47). g) Sample FD317: mylonite from the base of the Dent Blanche nappe north of Breuil (subarea 10) showing ductile top-NW shear bands; Fol (36/13) Lin (306/01). h) Sample FD46: mylonite from the base of the Dent Blanche nappe showing semi-ductile top-NW offset of a more competent epidote-rich layers; Fol (245/09) Lin (320/02). i) Sample FD317: mylonite from the base of the Dent Blanche nappe north of Breuil (subarea 10) showing conjugate ductile top-NW and top-SE shear bands; Fol (36/13) Lin (306/01). j) Sample FD64: metasediment from the Cimes Blanches nappe northwest of Zermatt (subarea 11) consisting of quartz and white mica and showing ductile top-NE shear bands; Fol (292/19) Lin (224/10). k) Sample FD71: calcschist from the Tsaté nappe in the Trift valley northwest of Zermatt (subarea 11) showing top-N shear bands within white mica-rich layer; Fol (238/28) Lin (180/13). l) Sample 139: mylonite from the base of the Dent Blanche nappe northwest of Zermatt (subarea 11) showing top-NW shear bands associated with growth of chlorite; Fol (199/40) Lin (135/21).

In the western upper Valtournenche, structures related to several stages of greenschist-facies deformation can be observed. Earlier foliations within Dent Blanche mylonites have been overprinted by NW-vergent folding and/or lower-grade top-NW shear bands through the ductile/brittle transition. Minor NW-SE extension within these rocks is evident from subordinate conjugate ductile shear bands, steep semi-ductile top-SE shear bands, and micro-scale necking. Top-NW shear bands within the Tsaté nappe also show an evolution from ductile to semi-ductile conditions. Folding of greenschist-facies foliations within Tsaté metabasites close to the DBBT with fold axes parallel to stretching lineations within surrounding Dent Blanche and Tsaté mylonitic rocks suggests formation of folds and stretching lineations in the course of a common progressive greenschist-facies deformation history.

4.4.2.4 Subarea 11 – Zermatt

West of Zermatt on the northern side of the Zmutt valley (Fig. 4.2), foliations within rocks of the upper Tsaté nappe and lower Dent Blanche nappe dip to the west to northwest. Stretching lineations mostly plunge to the northwest. The Tsaté nappe consists of successions of metasediments and metabasites. In an outcrop at Arben, these have been folded into open to tight, NW-vergent folds with SW-NE trending axes overprinting a preexisting foliation and stretching lineation (Fig. 4.8h). Folding also led to formation of a crenulation with SW-NE trending axes parallel to fold axes. Rocks in the immediate footwall and hanging wall of the DBBT and the contact itself, however, are not folded and foliations are strictly parallel to the contact (Fig. 4.8i). Kinematic indicators are not well developed within the exposed rocks so that a bulk shear sense could not be determined. However, abundant shear bands on the southern side of the Zmutt valley east of the Matterhorn consistently indicate top-NW shearing (Fig. 4.8j).

Northwest of Zermatt along the Trift valley (Fig. 4.2), a cross-section from the Cimes Blanches nappe into the Dent Blanche nappe is exposed. The Cimes Blanches nappe consists of heterogeneous successions of marbles, quartzites, quartzitic schists, and calcschists. Foliations dip to the west to northwest. Stretching lineations plunge to the southwest. In outcrop, semi-ductile shear bands within quartzitic schists indicate top-NE shearing (Fig. 4.8k). Top-NE shear bands can also be observed in thin-section to ductiley deform quartz and white mica (Fig. 4.9j). At higher structural levels within the Tsaté nappe, stretching lineations dominantly plunge to the west to northwest. In one locality, tight folds with W-plunging axes overprint an earlier layering whereas the dominant foliation within (calc)schists represents an axial surface cleavage. Stretching lineations are parallel fold axes and associated kinematic indicators show top-W shear senses. Therefore, these folds probably formed during the main stage of fabric formation which can be related to top-W shearing. In the same locality, garnet could be found within a thin layer which might be a relic of an earlier high-pressure imprint. It also suggests that the observed fabrics and folding indeed formed during an early stage in the evolution of the Combin zone. Further into the hanging wall, stretching lineations plunge to the northwest to north. Rare shear criteria, mostly within calcschists, indicate top-N(W) shearing (Fig. 4.9k). In the direct footwall of the DBBT, rocks of the Tsaté nappe have been folded into open to tight folds with (W)SW-plunging fold axes (Fig. 4.8l). Folding deforms preexisting foliations and stretching lineations and is associated with a crenulation cleavage with axes parallel to fold axes. This deformation cannot be observed in the overlying Dent Blanche nappe where the foliation is parallel to the contact. Basal mylonites from the lowermost Dent Blanche nappe show top-NW shear bands which overprint an earlier foliation and metamorphic layering and are associated with growth of chlorite (Fig. 4.9l).

In the area west and northwest of Zermatt, top-NE shear senses can be observed within the Cimes Blanches nappe whereas top-NW shear senses dominate within the Tsaté and Dent Blanche nappes. Top-W shear senses, possibly associated with an earlier deformation phase, could be observed in one locality. Late folding can often be observed within rocks of the Tsaté nappe but cannot be traced into the Dent Blanche nappe.

4.5 Overprinting relations and correlations

In this section, overprinting relations and correlations within and across subareas along the Combin Fault and DBBT are described. Based on structural observations and interpretations, a relative chronology of deformation is established.

The observed large-scale folding of the northwestern DBBT in the upper Val de Zinal (subarea 1) is probably a feature acquired during the main stage of thrusting of the Dent Blanche nappe over the underlying Combin zone. Shear criteria associated with this, probably W- to NW-directed shearing event, however, cannot be observed within the lowermost Dent Blanche nappe and uppermost Tsaté nappe. Instead, top-SE shear senses are widespread in this area. Top-SE shear bands overprint folded quartzitic gneisses of the Dent Blanche nappe and are also abundant within underlying Tsaté metasediments. Top-SE structures, in turn, have partly been reactivated and overprinted by a phase of non-penetrative top-NW shearing. Small-scale top-SE faults cutting through Tsaté metasediments are evidence of a late brittle

overprint. In the Val de Zinal area, an early, probably (N)W-directed thrust-related event was overprinted by penetrative top-SE shearing followed by minor top-NW shearing and a brittle top-SE overprint (Fig. 4.10).

Deformation structures in the Moiry area (subarea 2) suggest different structural evolutions of the Combin Fault and DBBT. The lower Combin zone is characterized by top-W to -SW shear senses which formed under decreasing metamorphic conditions as suggested by an observed decrease in the ductility of kinematic indicators. Towards the DBBT, top-SE shear bands can be observed within calcschists which are overlain by a NW-closing metabasite sheath fold nappe. It is difficult to establish a relative chronology between top-SE and top-NW structures. Since formation of the sheath fold calls for high strain, it may represent a feature of an early top-NW deformational event possibly associated with emplacement of the directly overlying Dent Blanche nappe. Since top-SE structures could not be found within the uppermost Tsaté nappe and overlying Dent Blanche nappe, top-SE shearing may have been partitioned into incompetent calcschists but may also have been postdated by renewed thrusting along the base of the metabasite nappe. The observed deformation structures in the Moiry area suggest that the Combin Fault experienced top-W to -SW shearing accompanying exhumation of the Combin zone whereas the upper Tsaté nappe experienced an early phase of NW-vergent shearing, subsequent top-SE shearing and possibly renewed top-NW shearing along preexisting thrust planes (Fig. 4.10).

Top-(S)W shear senses can be traced along the Combin Fault to the southwest. At Lac des Dix (subarea 4), two different stretching lineations within Cimes Blanches metasediments associated with top-WNW and top-WSW shear senses, respectively, suggest close spatial and temporal relations between thrust-related and transpressional to orogen-parallel shearing. Bulging recrystallization of quartz associated with top-WSW structures suggests low-temperature conditions below ca. 400° C during deformation (Stipp et al., 2002). The Cimes Blanche nappe north of Lac de Mauvoisin (subarea 5) is characterized by semi-ductile to brittle top-SW shearing within calcitic rocks. I therefore suggest that top-WNW shear senses represent remnants of an early thrusting event along the Combin Fault which was followed by transpressional to orogen-parallel top-(W)SW shearing under decreasing metamorphic conditions (Fig. 4.10). The importance of observed top-E shear senses at Lac des Dix could not be clarified. Their ductile character suggests that they formed before low-grade top-SW shearing and probably represent conjugate shear senses to ductile top-W structures.

Top-WNW to –WSW shear senses from the northwestern Combin Fault may be correlated with top-W shear senses within basal mylonites of the Dent Blanche nappe in the area around Arolla (subarea 3) (Fig. 4.10). Lower-grade top-SW structures, however, could not be observed. Instead, the DBBT and underlying Tsaté nappe in this area are characterized by late folding overprinting earlier foliations and stretching lineations. Often observed crenulations with axes parallel to fold axes can also be ascribed to late compressional deformation (Fig. 4.10). Rare top-SE and top-NW shear senses within calcschists of the Tsaté nappe most likely formed before this late-stage compression due to their association with mylonitic fabrics. Top-SE shear senses may also be correlated with SE-vergent folds within calcschists, therefore representing rather late top-SE shearing postdating mylonitic top-NW shearing (Fig. 4.10).

Mylonites from the base of the Dent Blanche nappe near Ollomont (subarea 6) show a retrograde evolution from upper greenschist-facies top-WNW shearing to lower greenschist-facies NW-SE shortening. The underlying Tsaté nappe, however, is characterized by abundant top-SE shear criteria. Direct crosscutting relations between these opposing shear senses in the footwall and hanging wall of the DBBT could not be observed. Top-SE shearing may either predate top-WNW shearing or may postdate thrusting and have mainly been partitioned into Tsaté schists. The observed close relationship between lower greenschist-facies thrust-activity and formation of a crenulation cleavage in the Ollomont mylonite suggests that the DBBT in this area has indeed been partly reactivated as a thrust and contemporaneously and subsequently overprinted by orogen-perpendicular shortening. The observed mylonitic fabric itself, however, is probably the result of an earlier higher greenschist-facies WNW-directed shearing event which was followed by top-SE shearing localized within Tsaté metasediments. Therefore, a similar sequence of deformation as observed along the DBBT in the upper Val de Zinal can be deduced: Early thrust-related top-WNW shearing was followed by top-SE shearing which in turn was postdated by thrust reactivation and compression (Fig. 4.10).

Top-SE structures within the Combin zone near Ollomont can be traced further southwest into the area around Allein (subarea 7). There, top-SE shearing has a ductile to partly brittle character and is therefore interpreted to postdate observed top-NW shearing (Fig. 4.10). However, anastomosing shear zones also suggest that top-SE and top-NW shear zones may have partly been active contemporaneously.

In the southeastern realm near Trois Villes (subarea 8), top-(N)W shear senses can be observed within Dent Blanche basal mylonites. Highly ductile shear bands are associated with lower greenschist-facies quartz microstructures suggesting an evolution from higher- to lower-grade conditions during ductile deformation. Their relationship to mylonites from the northwestern DBBT or to mylonites from the DBBT further northeast is difficult to determine. Trois Villes mylonites represent a high-strain zone during prolonged top-W to –NW shearing under decreasing metamorphic conditions but before the onset of semi-ductile to brittle top-NW shearing as observed along the upper western Valtournenche (Fig. 4.10).

West of Gran Tournalin on the eastern side of Valtournenche (subarea 9), highly ductile top-SE shear senses occur within Cimes Blanches metasediments in the hanging wall of the Combin Fault. These structures may represent the continuation of top-SE structures in the area around Allein (subarea 7) and therefore a deeper segment of an originally SE-dipping normal-sense shear zone. Top-NW shear senses at higher structural levels within the Tsaté nappe could not unambiguously be ascribed to an earlier or later deformation phase due to the absence of overprinting relations between these opposing shear directions. A comparison of quartz recrystallization mechanisms also suggests similar medium-grade greenschist-facies conditions which may have been slightly higher during top-NW shearing.

Mylonites from the base of the Dent Blanche nappe in the upper western Valtournenche near Breuil (subarea 10) show several stages of NW-directed shearing and a transition from ductile to brittle deformation. Folding of preexisting greenschist-facies mylonitic fabrics and a subsequent overprint by ductile to brittle shear bands suggest renewed top-NW shearing along the DBBT during exhumation of the Dent Blanche nappe through the ductile/brittle transition (Fig. 4.10). The observed penetrative fabrics most likely formed on the retrograde path similar to the ones observed within mylonites along the

northwestern DBBT near Ollomont. Subordinate conjugate shear bands, semi-ductile top-SE shear bands, and micro-scale necking of more competent layers within Dent Blanche mylonites suggest an evolution from purely thrust-related to extensional shearing during late stages of deformation along the DBBT. Prolonged top-NW shearing along the DBBT near Breuil led to folding of preexisting greenschist-facies foliations within Tsaté rocks near Croce di Carrel. A relationship between ductile top-NW deformation and the formation of folds is suggested by the parallel orientation of stretching lineations and fold axes (Fig. 4.10).

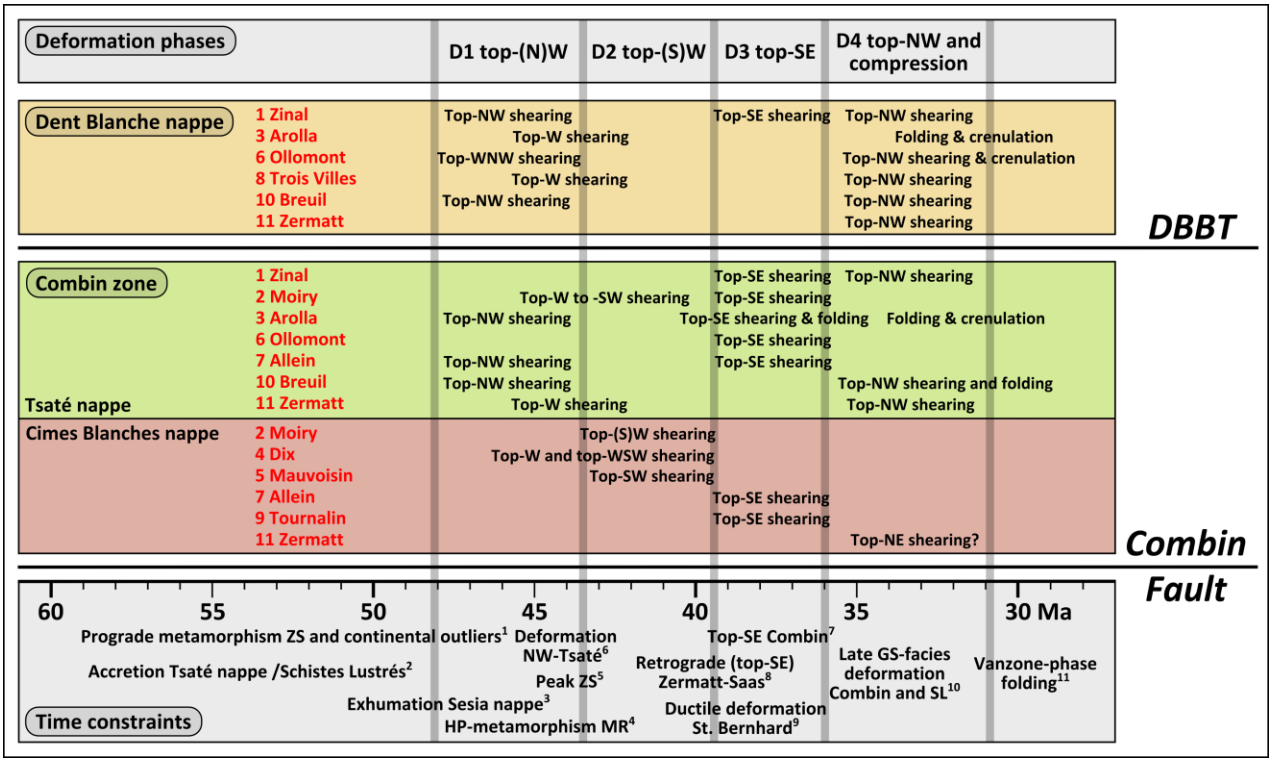

Figure 4.10: Diagram depicting the structural observations and resulting sequence of deformation without late brittle NW-SE extension; based on the "tectonic sequence diagrams" by Forster and Lister (2008); references for time constraints: 1) Lapen et al. (2003); Mahlen et al. (2005); De Meyer et al. (2014); Faßmer (2014); Weber et al. (accepted) 2) Agard et al. (2002); Reddy et al. (2003) 3) Babist et al. (2006) 4) Lapen et al. (2007); Villa et al. (2014) 5) Rubatto et al. (1998); Amato et al. (1999); Gouzu et al. (2006) 6) Markley et al. (1998) 7) Reddy et al. (1999) 8) Amato et al. (1999); Reddy et al. (1999); Cartwright and Barnicoat (2002); De Meyer et al. (2014) 9) Markley et al. (1998); Cartwright and Barnicoat (2002) 10) Reddy et al. (1999); Agard et al. (2002) 11) Pettke et al. (1999); ZS: Zermatt-Saas zone; MR: Monte Rosa nappe; SL: Schistes Lustrés; see text for discussion.

Folding of preexisting fabrics can also be observed in the areas to the west and northwest of Zermatt (subarea 11). This deformation cannot be traced into the overlying Dent Blanche nappe and the DBBT always appears as a planar surface. Kinematic indicators showing top-NW shear senses can be observed within the Tsaté nappe and along the DBBT and are associated with late growth of chlorite along the basal thrust suggesting late thrust reactivation (Fig. 4.10). In one locality in the Trift valley, folds with W-plunging fold axes parallel to surrounding stretching lineations represent intrafolial folds to the main foliation within metasediments. Rare garnet occurs in nearby metasediments suggesting that folds and fabrics may have formed during an early high-pressure stage of the Tsaté nappe (Fig. 4.10). Cimes

Blanches metasediments in the direct hanging wall of the Combin Fault northwest of Zermatt display top-NE shear senses. These cannot be correlated with other deformation structures in the southeastern realm and may represent a late stage of transpressional to orogen-parallel shearing along the Combin Fault in this area.

Overprinting relations and correlations within and across subareas suggest polyphase deformation along the Combin Fault and DBBT in the study area. A first phase of thrust-related, penetrative top-(N)W shearing (D1) affected all units and is well preserved along the DBBT and partly within the Combin zone (Fig. 4.11). Subsequent transpressional to orogen-parallel top-(S)W shearing (D2) can be observed along the northwestern Combin Fault (Fig. 4.11). This phase was followed by normal-sense top-SE shearing (D3) which variably affected the Combin zone and, only to a minor extent, the DBBT (Fig. 4.11). A late phase of top-NW shearing (D4) led to reactivation of earlier structures, formation of low-grade greenschist-facies top-NW shear senses, and folding of preexisting fabrics, especially along the southeastern DBBT but also within the underlying Combin zone and in the northwestern realm (Fig. 4.11). Brittle shear planes which sometimes overprint ductile deformation structures are attributed to a late phase of NW-SE directed extension (D5).

4.6 Regional distribution of deformation

The observed deformation structures, overprinting relations, and inferred correlations suggest that the northwestern and southeastern realms experienced structural evolutions which can be partly correlated but also show distinct differences.

The southeastern DBBT shows deformation structures related to penetrative greenschist-facies top-(N)W shearing as well as top-NW mylonites displaying a decreasing ductility through the ductile/brittle transition. For the northwestern DBBT, structural and petrological observations suggest an evolution from retrograde top-(N)W shearing to renewed thrusting and shortening under low-grade greenschist-facies conditions. Folding and formation of crenulation cleavages are abundant in the footwall and hanging wall of the DBBT and also the contact itself has been folded. In the southeastern realm, shortening structures are restricted to the Combin zone below the DBBT and cannot be traced into the Dent Blanche nappe. Top-W thrusting along the DBBT can be correlated with top-W shearing along the northwestern Combin Fault but can only rarely be observed within the Combin zone in the western Valtournenche/Zermatt area where stretching lineations predominantly dip to the northwest. Top-W shearing along the northwestern Combin Fault was followed by orogen-parallel top-SW shearing. No evidence of penetrative top-SW shearing could be found in the western Valtournenche/Zermatt area suggesting that this deformation phase was either restricted to the northwestern Combin zone or has been overprinted by subsequent deformation. In the northwestern realm, top-SE shearing can be observed in the footwall of and along the DBBT east of Val de Zinal, in the area north of Arolla and within the southwestern Combin zone. This distribution suggests that a NE-SW striking normal-sense shear zone developed subparallel to the nappe boundaries after the main stage of nappe-stacking. In the southeastern realm, top-SE shear senses can be observed in the immediate hanging wall of the Combin Fault in the eastern Valtournenche, along the

Combin Fault at Lago di Cignana (see chapter 2), and at a high structural level within the Combin zone at Becca d'Aver (see chapter 3). The uneven distribution of top-SE shear senses in the study area suggests that top-SE shearing was probably distributed into several high-strain zones. The connection between top-SE shear senses in the northwestern and southeastern realms is not clear due to insufficient exposure and obliteration by subsequent deformation. They may have been connected at depth as part of a larger normal-sense shear zone which was partly dismembered by subsequent deformation. A late phase of NW-vergent shearing affected the southeastern DBBT and underlying Combin zone and can also partly be observed along the northwestern DBBT. Folds and crenulations within the northwestern and southeastern Combin zone, which deform preexisting greenschist-facies fabrics, are attributed to renewed top-NW shearing along the DBBT.

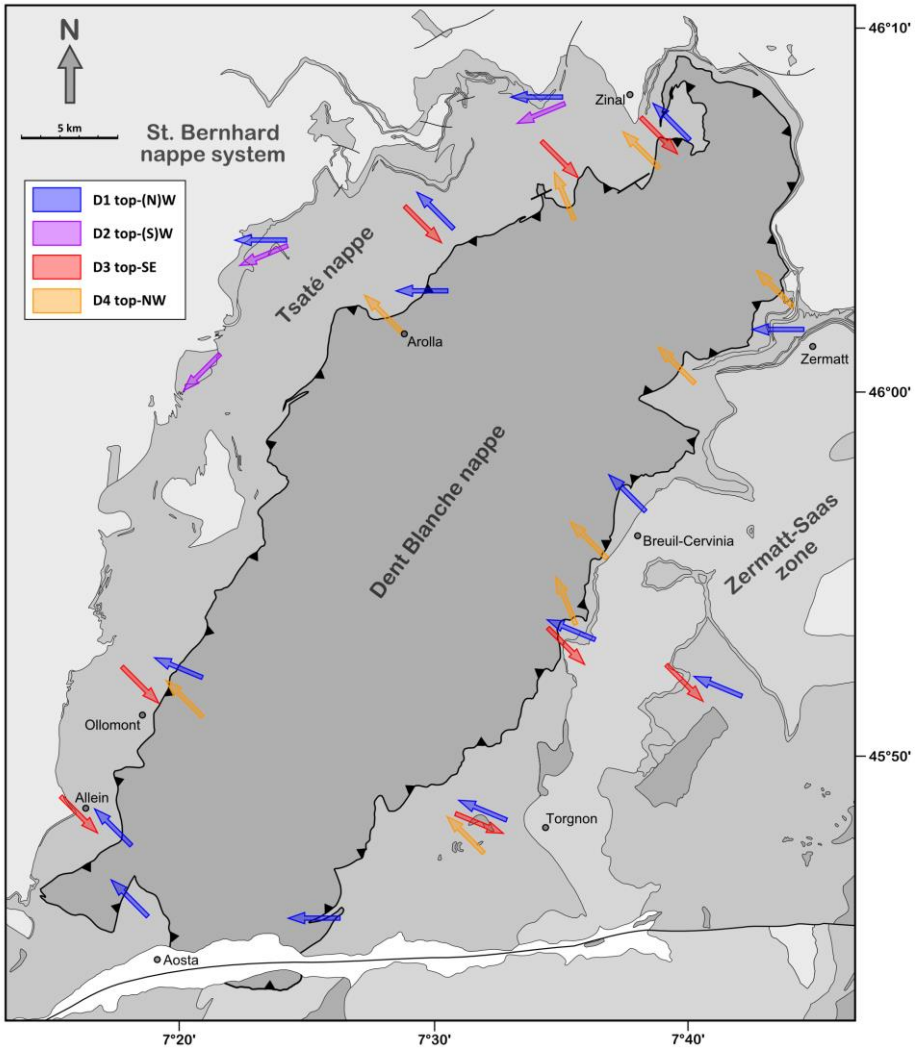

Figure 4.11: Schematic tectonic map of the study area with transport directions during D1 to D4 ductile shearing according to structural observations in the subareas; transport directions in the Lago di Cignana and Becca d'Aver areas are depicted as well but see chapters 2 and 3 for detailed descriptions and discussions on the observed deformation in these areas.

4.7 Structural evolution

In this section, I correlate the previously established relative chronology of deformation with available age data and propose a sequence of deformation and structural evolution for the Combin Fault and DBBT as well as associated tectonic units.

4.7.1 D1 top-(N)W shearing

D1 top-(N)W shearing represents the main stage of nappe-stacking and thrusting along the Combin Fault and DBBT and is preserved along northwestern and southeastern fault segments. It is held responsible for juxtaposition of the Dent Blanche nappe and the Combin zone and thrusting of these units over continental Briançonnais units in the northwest (Fig. 4.12a). Movement along basal thrusts probably started after subduction and accretion of the Dent Blanche nappe and Combin zone (Fig. 4.10). Subduction of continental Dent Blanche/Sesia units occurred in the Late Cretaceous (e.g. Inger et al., 1996; Rubatto et al., 2011) with subsequent subduction of the Piemont-Ligurian ocean as indicated by the age of prograde metamorphism (Agard et al., 2002; Mahlen et al., 2005; Faßmer, 2014; Weber et al., accepted). Retrograde D1 thrusting along the DBBT most likely occurred during exhumation of the Dent Blanche/Sesia nappe system before ca. 45 Ma as suggested by the activity of the Ometto Shear Zone along the top of the Sesia nappe (Babist et al., 2006; Figs. 4.10 and 4.12a). Accretion of the Tsaté nappe occurred until ca. 48 Ma (Agard et al., 2002; Reddy et al., 2003). Subduction of Briançonnais units below accreted Piemont-Ligurian oceanic units probably started around 50 Ma as suggested by HP ages reported for the Monte Rosa nappe (Lapen et al., 2007; Villa et al., 2014). Underthrusting of continental units led to accretion of cover sequences to the basal part of the Tsaté nappe to form the Cimes Blanches and Frilihorn nappes. Structurally lower parts of the northwestern Combin zone were folded into underlying Briançonnais units (Fig. 4.12a). Early stages of Piemont-Ligurian subduction and accretion after the peak of HP metamorphism in the Sesia nappe were responsible for a first HP imprint within the Tsaté nappe. Deformation structures and mineral assemblages related to prograde high-pressure top-(N)W shearing along a SE-dipping subduction channel can only rarely be observed within the Tsaté nappe. These have been largely obliterated by subsequent greenschist-facies retrogression and deformation. D1 top-(N)W shearing and associated exhumation from blueschist-facies conditions is most likely responsible for the pervasive greenschist-facies overprint observed in the Combin zone and the formation of penetrative greenschist-facies fabrics within the Combin zone and along the DBBT. An Ar/Ar age of 44.5 ± 0.6 Ma by Markley et al. (1998) for a locality at Lac de Moiry close to the northwestern Combin Fault may reflect the timing of fabric formation or ductile deformation in this area which is characterized by top-W and subsequent top-SW shearing. This age is therefore interpreted to reflect late stages of thrusting and W-vergent shearing along the Combin Fault which may have occurred until ca. 44 Ma. D1 top-(N)W shearing is also interpreted to predate exhumation of the Zermatt-Saas zone in the footwall of the southeastern Combin Fault as suggested by the above-mentioned constraints on the timing of D1 deformation along the Combin Fault and DBBT and the age of the peak of (U)HP metamorphism in the Zermatt-Saas zone at ca. 44 – 43 Ma (Rubatto et al., 1998; Gouzu et al., 2006). D1 top-(N)W shearing is therefore considered to have occurred between ca. 48 and 44 Ma as suggested by several time constraints.

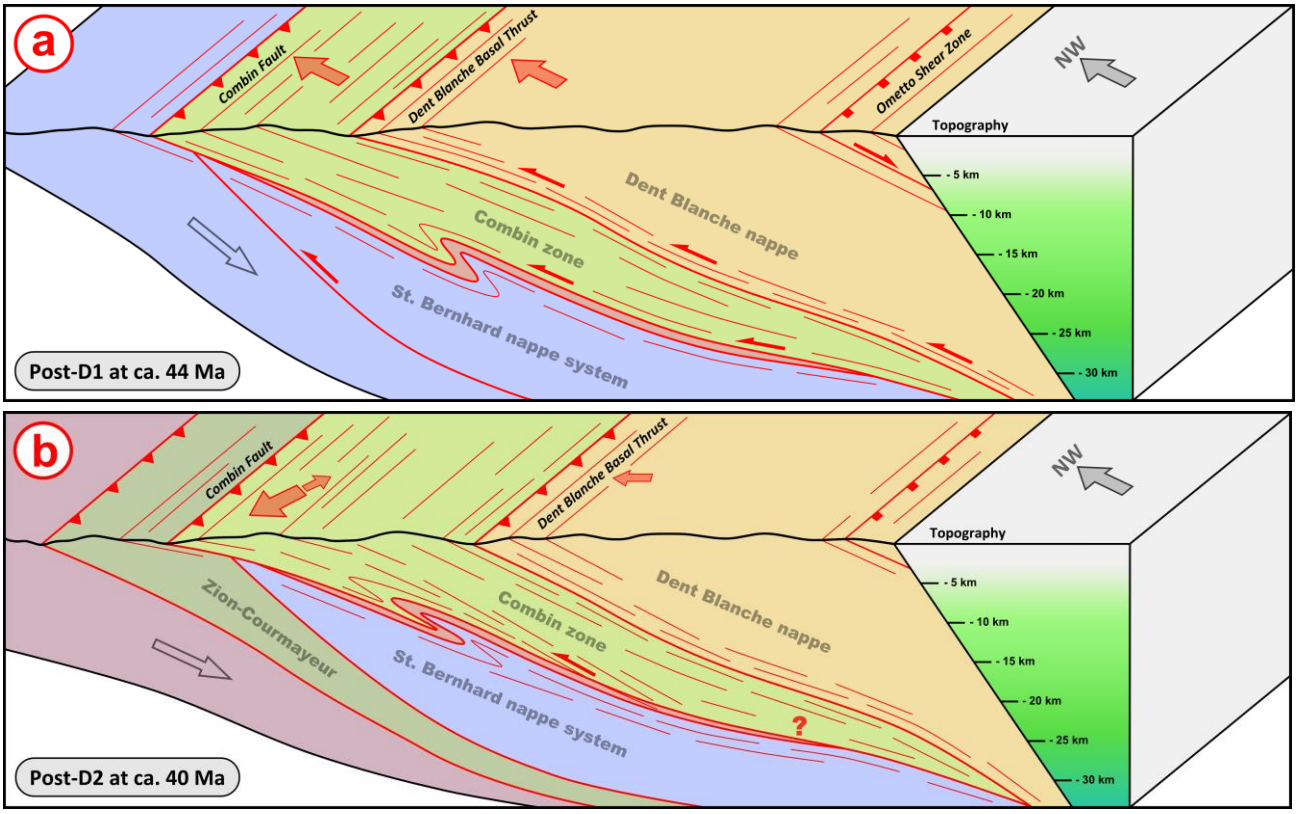

Figure 4.12: Schematic structural evolution as block diagrams according to the sequence of deformation described and discussed in the text; only accreted and underthrust crustal units are depicted; lithospheric mantle and Adriatic upper plate are not shown; shear zones in red are the ones that were active during the respective deformation phase; inactive shear zones are depicted in black; lines correspond to zones of high strain; sketches are not to scale; green and blue colours in depth profiles on the right indicate approximate depth of greenschist- and blueschist-facies conditions, respectively; note that depth profiles on the right change slightly throughout the structural evolution; colour coding of tectonic units is the same as in figure 4.1. a) Configuration at ca. 44 Ma after D1 top-(N)W shearing, the main stage of nappe stacking along the DBBT and Combin Fault; the Combin zone comprises the Tsaté nappe (green) and the Cimes Blanches nappe (red) at its base; top-(N)W led to exhumation of the Dent Blanche nappe and underlying Combin zone and to a pervasive greenschist-facies overprint along the DBBT and within the Combin zone; exhumation of the Dent Blanche/Sesia nappe system probably occurred in the footwall of the top-SE Ometto Shear Zone (see Babist et al., 2006). b) Configuration at ca. 41 Ma after D1 top-(S)W shearing which is well-preserved along the northwestern Combin Fault; the big arrow indicates the main shearing direction, the little arrow indicates the subordinate conjugate shearing direction.

4.7.2 D2 top-(S)W shearing

D2 top-(S)W shearing represents a phase of transpressional to orogen-parallel deformation which mainly affected or can be observed along the northwestern Combin Fault (Figs. 4.10 and 4.12b). Deformation structures associated with this deformation phase show a range of metamorphic conditions from highly ductile to semi-ductile and brittle conditions. This suggests ongoing exhumation of the Combin zone during transpressional deformation. SW-dipping shear planes are indeed often associated with E-W trending stretching lineations suggesting a thrust-component during early stages. Top-SW shear senses cannot be observed at higher structural levels within the Combin zone and are also absent along the DBBT. Top-W thrusting may, however, have continued along the DBBT during early stages of D2 as suggested by abundant top-W shear senses within Dent Blanche basal mylonites. Subordinate top-E shear senses observed along the northwestern Combin Fault in the Lac des Dix area may represent conjugate

shear zones during overall top-(S)W shearing (Fig. 4.12b). Since D2 top-(S)W shearing postdates D1 top-(N)W shearing, it is interpreted to have occurred from ca. 43 Ma onwards.

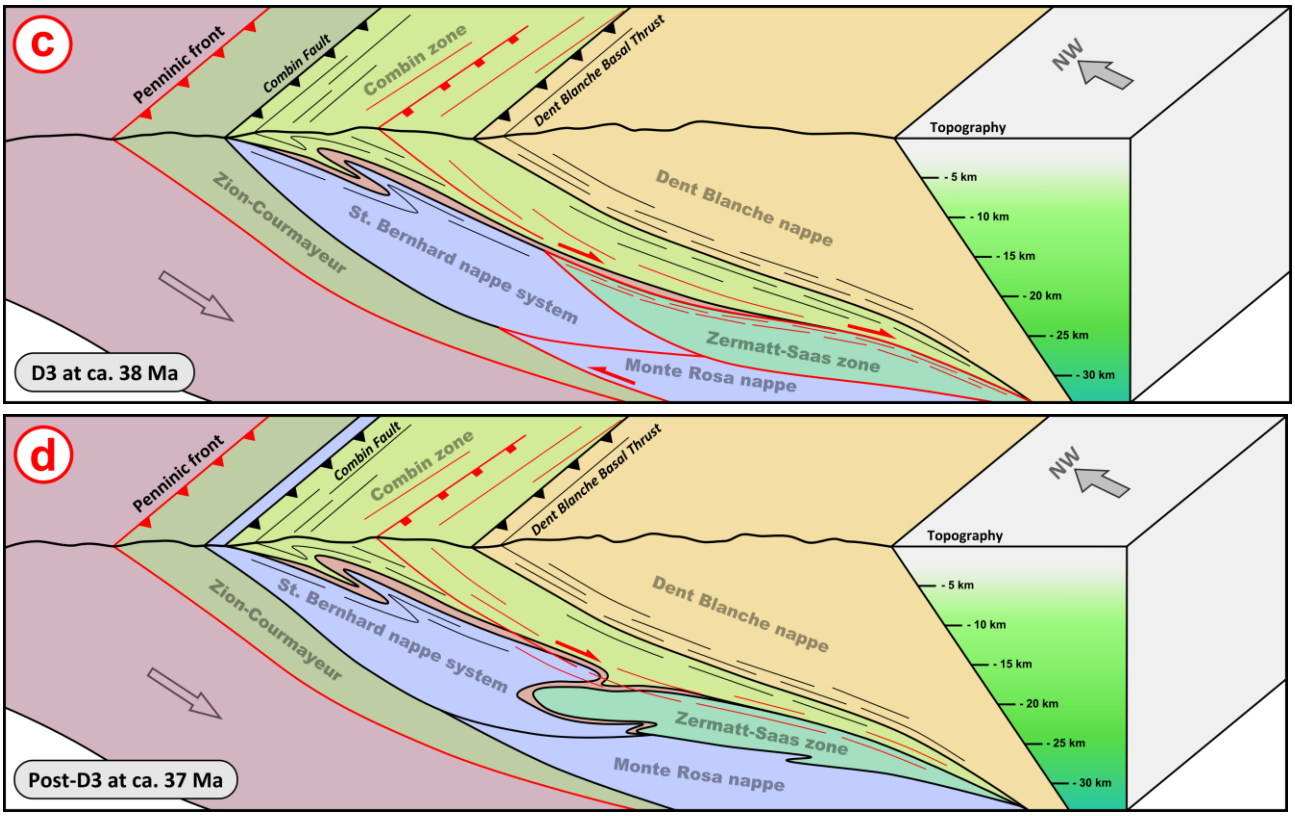

Figure 4.12 (continued): c) Configuration at ca. 38 Ma during D3 top-SE shearing which led to juxtaposition of the Combin and Zermatt-Saas zones at greenschist-facies conditions; strain was probably localized along the upper Zermatt-Saas zone as suggested by the scarcity of top-SE structures in the southeastern realm of the study area; top-SE shearing within the northern Combin zone was probably subparallel to nappe boundaries and only locally affected the DBBT. d) Configuration at ca. 37 Ma after D3 top-SE shearing and associated Mischabel-phase folding.

4.7.3 D3 top-SE shearing

D3 top-SE shearing represents a stage of normal-sense shearing which affected the northwestern Combin zone along a NE-SW striking shear zone subparallel to nappe boundaries (Fig. 4.12c). The DBBT largely escaped top-SE shearing and only locally shows top-SE shear senses along its northwestern segment but not its southeastern part (Fig. 4.10). Top-SE shear senses can also be observed in the Valtournenche area at low and high structural levels within the Combin zone. Retrograde greenschist-facies deformation in the Combin zone has been dated at ca. 45 – 36 Ma by Reddy et al. (1999) but cannot unambiguously be attributed to a kinematic event. A cluster of ages between 39 and 36 Ma, however, associated with domains of dominant top-SE shear close to the Combin Fault has been reported by these authors. High-pressure conditions within the Zermatt-Saas zone have been proposed to have lasted until ca. 41 Ma and greenschist-facies retrogression has been dated at ca. 40 – 38 Ma (Amato et al., 1999; De Meyer et al., 2014). Dating of retrograde top-SE shear zones within the Zermatt-Saas zone and St. Bernhard nappe system in the footwall of the Combin Fault by Cartwright and Barnicoat (2002) yielded ages between 42

– 37 Ma. Greenschist-facies top-SE shearing along the Combin Fault is therefore held responsible for juxtaposition of the Combin and Zermatt-Saas zones and is interpreted to have occurred between ca. 39 and 37 Ma (Fig. 4.12c). Formation of the Mischabel fold above the northern Zermatt-Saas zone probably represents a relatively late and non-penetrative stage of SE-vergent shearing (Fig. 4.12d; e.g. Sartori, 1987; Pleuger et al., 2007; Scheiber et al., 2013). Several circumstances may have contributed to the fact that ductile top-SE shear senses can only scarcely be observed in the western Valtournenche/Zermatt area. During exhumation of the Zermatt-Saas zone and juxtaposition with the Combin zone along the Combin Fault, strain may have been localized along the uppermost Zermatt-Saas zone and unevenly distributed in the hanging wall of the Combin Fault (Figs. 4.12c and d). Additionally, my structural observations suggest that top-SE shearing was postdated by renewed top-NW deformation which led to partial reworking and overprinting of earlier deformation structures.

4.7.4 D4 top-NW shearing and NW-SE shortening

D4 top-NW shearing affected the DBBT and partly the underlying Combin zone (Figs. 4.10 and 4.12e). This phase can be well-studied in the western Valtournenche/Zermatt area along the DBBT and at higher structural levels within the Combin zone but also partly along the northwestern segment of the DBBT. Renewed thrusting occurred under decreasing metamorphic conditions and is therefore interpreted to be related to further exhumation of the Dent Blanche nappe (Fig. 4.12e). Top-NW shearing probably led to folding within the underlying Combin zone which often cannot be traced into the overlying Dent Blanche nappe. Folds within the Combin zone, which deform a preexisting foliation and stretching lineation and are associated with formation of crenulation cleavages, are interpreted to have formed during late-stage top-NW shearing whereas folds with axes parallel to the main stretching lineation may already have formed during D1 top-(N)W shearing. The temporal relations between top-NW shearing and top-SE extensional shearing are often difficult to determine but overprinting relations at several localities and the often low metamorphic grade of top-NW structures strongly suggest that a distinct phase of top-NW shearing postdated top-SE shearing (Fig. 4.10). Renewed top-NW shearing is attributed to reactivation of the DBBT as an out-of-sequence thrust and probably started around ca. 35 Ma before the onset of Vanzone-phase folding. Folding of the northwestern DBBT is attributed to increased crustal shortening during a late stage of D4 and probably marks the cessation of thrust-related shearing (Fig. 4.12f).

4.7.5 D5 NW-SE extension

D5 NW-SE extension is interpreted to reflect upper-crustal brittle deformation in response to updoming of the Vanzone antiform from ca. 32 Ma onwards (Fig. 4.12g). The large-scale synformal structure of the Dent Blanche nappe is owed to this phase which also led to a brittle overprint of ductile structures in a graben-like manner, i.e. with mainly SE-dipping faults in the northwest and NW-dipping ones in the southeast (Fig. 4.12g) whereas also conjugate shear planes can be observed (see chapter 3). The transition from D4 top-NW thrusting to D5 top-NW normal faulting along the southeastern segment of the DBBT probably occurred progressively during rotation of the units in the southeastern realm into their current NW-dipping orientation. Early stages of Vanzone-phase updoming were probably still accompanied by

semi-ductile top-NW thrusting along the DBBT (Fig. 4.12f) so that orogen-perpendicular brittle extension is interpreted to have started around ca. 30 Ma after substantial uplift and exhumation of units on the northwestern limb of the Vanzone antiform (Fig. 4.12g).

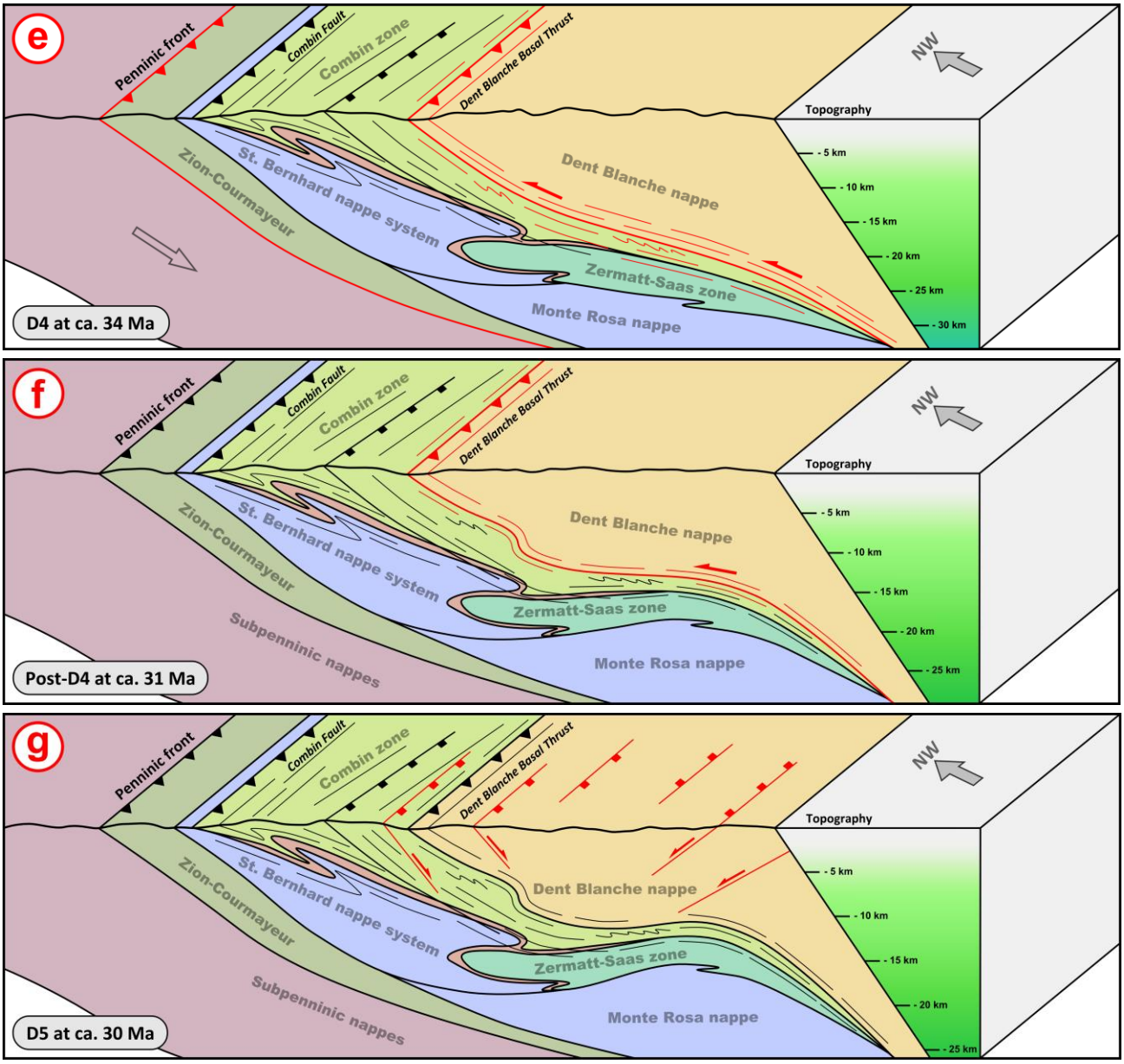

Figure 4.12 (continued): e) Configuration at ca. 34 Ma during D4 top-NW shearing; reactivation of the DBBT as an out-of-sequence thrust led to formation of low-grade greenschist-facies top-NW shear senses along the DBBT and folding within the Combin zone in the footwall of the DBBT; note that the Combin zone has been tectonically thinned due to the activity of conjugate shear zones at ca. 36 Ma (see chapter 2). f) Configuration at ca. 32 Ma after D4 top-NW shearing; compression led to folding of the northwestern DBBT and formation of crenulation cleavages; transition from ductile to brittle top-NW shearing along the southeastern DBBT; note that the depth scale changed. g) Configuration at ca. 30 Ma during brittle NW-SE extension; upper-crustal, orogen-perpendicular extension in the study area was probably the result of an increased uplift of units due to updoming of the Monte Rosa nappe in a more internal position; units in the southeastern realm were progressively rotated into a NW-dipping orientation.

4.8 Discussion and tectonic evolution

In the following, the tectonic evolution of the Western Alps is discussed on the basis of my own observations and interpretations as well as previously published data and models.

4.8.1 Early accretion, thrusting, and orogen-parallel shearing

The generally accepted Late Cretaceous paleogeographical configuration for the Western Alpine realm is based on geochronological constraints for subduction-related metamorphic events (Berger and Bousquet, 2008 and references therein) and oceanic spreading (e.g. Rubatto et al., 1999; Liati et al., 2005) as well as geophysical data, retrodeformations, and stratigraphic evidence (e.g. Froitzheim et al., 1996; Stampfli et al., 2002; Schmid et al., 2004; Rosenbaum and Lister, 2005; Handy et al., 2010). The Piemont-Ligurian (South-Penninic) ocean in the southeast and the Valais (North-Penninic) basin in the northwest were separated by an eastern prolongation of the Iberian plate, the Briançonnais (Middle-Penninic) continental spur. Several more continental fragments and extensional allochthons may have existed along ocean-continent transition zones that were later incorporated into the Alpine orogenic wedge (e.g. Beltrando et al., 2014). The Dent Blanche/Sesia nappe system, for example, may have originated from several continental fragments which were separated from the Adriatic continental margin during Jurassic rifting and stranded inside a domain characterized by extensive extension along the ocean-continent transition (e.g. Froitzheim and Manatschal, 1996; Beltrando et al., 2014). This configuration before the onset of Alpine subduction may have been a prerequisite for subduction of these units to eclogite-facies depths in that subduction was able to originate in a more internal position. In other interpretations, the Dent Blanche/Sesia system is viewed as a true microcontinent separated from the Adriatic continental margin by another oceanic spreading center (Froitzheim et al., 2006; Pleuger et al., 2007). Remnants of lithological associations reminiscent of oceanic crust have been reported from along the Canavese Line in a structural position above the Sesia nappe (Elter et al., 1966; Pleuger et al., 2007). These slivers were taken as possible evidence for the existence of an oceanic suture between the Sesia nappe and Southalpine units (e.g. Pleuger et al., 2007). However, there are no geochronological data so far, neither protolith nor metamorphic ages, which support the hypothesis of another spreading center to the southeast of the Dent Blanche/Sesia system. Subduction of continental units beneath the Adriatic margin may have started as early as 90 Ma as suggested by a HP age of 85 Ma reported by Regis et al. (2014) for the Sesia nappe. This age comes close to the timing of eclogite-facies metamorphism at ca. 90 Ma within Austroalpine units of the Eastern Alps (e.g. Thöni, 2006). (Ultra)high-pressure metamorphism in the Eastern Alps has been proposed to be the result of intracontinental subduction (e.g. Janák et al., 2004; Stüwe and Schuster, 2010) which may therefore also account for the first stages of subduction along the Adriatic continental margin. Subduction and accretion of Piemont-Ligurian oceanic units in the course of one continuous lithospheric subduction is interpreted to have followed accretion of the Dent Blanche/Sesia nappe system at approximately 65 Ma as suggested by the age of peak metamorphism in the Sesia nappe and prograde metamorphism in continental outliers and the Zermatt-Saas zone (e.g. Inger et al., 1996; Faßmer, 2014). I interpret the Tsaté nappe to represent the lower-pressure equivalent of the Zermatt-Saas zone instead of attributing these units to distinctly different paleogeographic domains or even separate oceanic basins.

This interpretion is supported by overlapping ages for prograde metamorphism in the two units and almost identical protolith ages in high-pressure (Zermatt-Saas zone) and low-pressure (Gets nappe) ophiolitic units. Parts of the downgoing Piemont-Ligurian slab were therefore only subducted to blueschist-facies conditions, exhumed, and accreted (Tsaté nappe) whereas other parts reached eclogite-facies conditions and only then were detached and exhumed (Zermatt-Saas zone). A complex paleogeographic configuration with continental fragments and extensional allochthons along the Piemont-Ligurian/Adriatic ocean-continent transition may be responsible for the observed associations of ocean- and continent-derived units which were also partly subducted to blueschist-facies (e.g. Becca d'Aver continental sliver; see chapter 3) and partly to eclogite-facies conditions (e.g. Etirol-Levaz slice; e.g. see Dal Piaz et al., 2001). The Briançonnais continental spur followed the Piemont-Ligurian slab into the subduction zone from ca. 50 Ma onwards (Villa et al., 2014). According to the proposed structural evolution, detachment of parts of its sedimentary cover and accretion to the base of the overlying Tsaté nappe led to formation of the Cimes Blanches and Frilihorn nappes. At the time of Briançonnais subduction, exhumation of the Dent Blanche/Sesia nappe system already occurred as an extruding crustal wedge between the normal-sense Ometto Shear Zone in the hanging wall (Babist et al., 2006) and the DBBT in the footwall. This stage of (N)W-directed thrusting is interpreted to be responsible for most of the observed retrograde shearing along the DBBT and also for exhumation of more deeply subducted parts of the Combin zone from blueschist- to greenschist-facies conditions. The timing of thrusting of the Gets nappe, a possible low-pressure equivalent of the Tsaté nappe, over underlying units in the French Prealps from ca. 50 Ma onwards (Bill et al., 2001) also correlates well with the assumed main period of overthrusting of the Dent Blanche nappe and Combin zone between ca. 50 - 45 Ma, suggesting a link between foreland-directed thrusting within continental and underlying oceanic units. This stage of early thrusting was followed by transpressional to orogen-parallel top-(S)W shearing along the northwestern Combin Fault between ca. 43 and 40 Ma. The often close association of top-W and top-SW shear senses as well as SW-dipping shear bands and E-W trending stretching lineations suggest that top-W shearing progressively evolved into orogen-parallel top-SW shearing during later stages of this deformation phase. Top-W shearing along the DBBT may therefore also have partly continued during early stages of this phase. A dextral strike-slip component along the northwestern Combin Fault may have been related to eastward movement of the Briançonnais spur (Babist et al., 2006) and resulting oblique subduction. It is not clear whether the observed orogen-parallel top-SW shearing had a higher-grade equivalent at depth or was restricted to the northwestern Combin zone. Only a few SW-NE trending stretching lineations associated with top-NE shear senses were found near Zermatt which may therefore represent a late phase of orogen-parallel shearing. More penetrative top-SW shearing has been reported for the Monte Rosa nappe (Pleuger et al., 2008) and for the Sesia nappe (Babist et al., 2006) suggesting that orogen-parallel ductile shearing was active at different times during the structural evolution of the Western Alps. Top-SW shearing has also been reported by Scheiber et al. (2013) as part of the structural record within the St. Bernhard nappe system but has not been attributed to a distinct deformation phase but to an effect of strain-superposition between an early top-NW and a late top-SE shearing event. My structural observations, however, strongly suggest that transpressional to orogen-parallel shearing was penetrative

along the northwestern Combin Fault with formation of a stretching lineation that can be distinguished from D1 top-(N)W and D3 top-SE stretching lineations and therefore should be regarded as a distinct deformation phase.

4.8.2 Exhumation and the role and importance of top-SE shearing

In the study area, top-(S)W shearing was followed by top-SE shearing between ca. 39 and 37 Ma. The timing, distribution, and importance of top-SE shearing in the Western Alps are still a matter of discussion (Sartori, 1987; Ring, 1995; Reddy et al., 1999; Ganne et al., 2006; Pleuger et al., 2007; Gasco and Gattiglio, 2011). Especially its role for the exhumation of Zermatt-Saas (U)HP rocks in the footwall of the southeastern segment of the Combin Fault has been discussed by several authors (e.g. Reddy et al., 1999; Wheeler et al., 2001; Froitzheim et al., 2006; Pleuger et al., 2007). Due to the large difference in peak pressures across the Combin Fault, it has often been interpreted as a major normal-sense shear zone accompanying juxtaposition of the Zermatt-Saas and Combin zones (e.g. Ballèvre and Merle, 1993). Such a scenario was also favoured by Reddy et al. (1999; 2003) and Wheeler et al. (2001) who proposed, based on structural and geochronological data, that exhumation of the Zermatt-Saas zone occurred in the footwall of a regional-scale top-SE shear zone, the Gressoney Shear Zone, comprising the entire Combin zone and lowermost Dent Blanche/Sesia nappes. In many places, however, the application of this model is complicated and seems inappropriate due to the scarcity of top-SE shear senses, which is the case for the western Valtournenche area. Ballèvre and Merle (1993) proposed a subsequent overprint due to renewed top-NW thrusting along the Combin Fault which was followed by another phase of top-SE backshearing and backfolding. The view that top-SE shearing represents the last deformation before Vanzone-phase folding and is related to late backshearing and –folding is shared by many authors (e.g. Mazurek, 1986; Sartori, 1987; Ring, 1995; Lebit et al., 2002; Pleuger et al., 2007; Scheiber et al., 2013). This may be true for many areas but, as suggested by the structural data presented in this study, regional differences should be taken into account. Froitzheim et al. (2006) and Pleuger et al. (2007) proposed a scenario in which the Combin Fault represents an extraction fault and the Dent Blanche/Sesia nappes were extracted from between the Combin and Zermatt-Saas zone and subsequently thrust out-of-sequence over the Combin zone to explain the structural record. In this model, top-SE exhumation of the Zermatt-Saas zone occured in the footwall of the extracting block whereas the Combin zone in the hanging wall of the Dent Blanche/Sesia nappes experienced top-NW shearing. This model has far-reaching consequences for the paleogeographical configuration and the structural and metamorphic evolution of these units. According to this scenario, the Tsaté nappe originated from an oceanic basin to the southeast of the Dent Blanche/Sesia continental fragment and the Cimes Blanches and Frilihorn nappes represent the sheared-off sedimentary cover of the continental fragment (see Pleuger et al., 2007). Also, the Tsaté nappe would have experienced its blueschist-facies imprint before HP metamorphism in the Sesia nappe. Froitzheim et al. (2006) and Pleuger et al. (2007) argue that top-SE shearing postdates greenschist-facies top-NW shearing and therefore cannot be responsible for exhumation of (U)HP rocks in the footwall. The structural evolution envisaged in this thesis, however, suggests that the Combin zone was exhumed from blueschist- to greenschist-facies conditions and experienced its pervasive overprint before juxtaposition

with the Zermatt-Saas zone. According to this proposed sequence of deformation and exhumation, no other than greenschist-facies top-SE shear senses postdating greenschist-facies top-(N)W shearing would be expected. Weber et al. (accepted) proposed a refined version of the original extraction fault model in which the Dent Blanche/Sesia mantle wedge represents the extracting block. This model envisages 3 SE-dipping subduction zones for the Western Alpine realm, one that subducts the Tsaté and Dent Blanche/Sesia units, one for the Zermatt-Saas and Briançonnais units, and one for the Valais basin and European units, with the Monte Rosa nappe representing European basement. The geometry of the northwestern subduction zone would be according to the slab extraction model proposed by Froitzheim et al. (2003) for the Central Alps in which exhumation of European continental units occurred by extraction of the overlying Briançonnais slab between ca. 37 and 35 Ma after HP metamorphism within continental units at ca. 38 – 37 Ma (Herwartz et al., 2011; Sandmann et al., subm.). Extraction of the Dent Blanche/Sesia mantle wedge could have only occurred after exhumation of the Zermatt-Saas zone to greenschist-facies conditions at ca. 38 Ma to prevent the overlying Combin zone from any exhumation-related top-SE shearing. The model presented in Weber et al. (accepted) therefore calls for simultaneous extraction of two mantle slabs, the Dent Blanche/Sesia and Briançonnais slabs, after ca. 38 Ma. It is also questionable why the Dent Blanche/Sesia mantle wedge remained in its position for at least 27 Ma (ca. 65 – 38 Ma) until after exhumation of the Zermatt-Saas zone but was extracted immediately afterwards whereas the Briançonnais slab was extracted only a few Ma after formation of the third subduction zone. Syn-exhumational top-SE shearing would be expected at the top of the Monte Rosa nappe for the period after ca. 38 – 37 Ma due to extraction of the overlying mantle slab. This contradicts the chronology presented by Pleuger et al. (2005; 2007; 2008) who proposed greenschist-facies top-NW shearing and a common structural evolution of the Zermatt-Saas zone and Monte Rosa nappe after ca. 40 Ma. So far, no geochronological data exist to support the hypothesis of two separate Zermatt-Saas and Tsaté oceanic basins or exhumation of the Dent Blanche/Sesia nappes only after 38 Ma. Also, available Ar/Ar-ages for phengites in metasediments from the Combin zone and Schistes Lustrés complex suggest HP metamorphism in these units to be largely contemporaneous with prograde metamorphism in the Zermatt-Saas zone and continental outliers and not significantly older (Agard et al., 2002; Reddy et al., 2003; Lapen et al., 2003; Mahlen et al., 2005; Faßmer, 2014; Weber et al., accepted). Despite the aforementioned reasons which speak against extraction of the Dent Blanche/Sesia nappes, extraction faulting along the Combin Fault remains kinematically feasible. It may be possible that continental outliers at high structural levels of the Zermatt-Saas zone and along the Combin Fault represent remnants of an originally larger fragment that was partly extracted from between the Combin and Zermatt-Saas zone. A similar geometry and scenario in which the Combin and Zermatt-Saas zones were separated by continental units at depth has been proposed by Ring (1995) who interpreted the Combin Fault as an out-of-sequence thrust responsible for stacking of the Combin zone on top of lower Austroalpine units (later being part of the Sesia nappe) and the Zermatt-Saas zone. Wheeler et al. (2001) proposed a model in which top-SE shearing in the Western Alps occurred in response to ascending and exhuming crustal wedges bounded by top-SE normal faults at the top and foreland-directed thrusts at the bottom (`pip geometry´). Rosenbaum and Lister (2005) and Groppo et al. (2009) suggested models in which periods of

major upper-plate extension were induced by lower-plate slab rollback and slab steepening, respectively, and therefore led to exhumation of rocks from (U)HP depths.

The model presented in this study suggests that early stages of top-SE shearing along the Combin Fault accompanied juxtaposition of the Combin and Zermatt-Saas zones at crustal levels whereas late stages are responsible for the formation of SE-vergent folds within units and along contacts. The most prominent of these are the Mischabel fold deforming the St. Bernhard nappe system and the folded Zermatt-Saas/Monte Rosa contact zone (e.g. Sartori, 1987; Pleuger et al., 2005). Whereas greenschist-facies top-SE shear senses are scarce in the hanging wall of the southeastern Combin Fault in the study area, structural analyses in the Lago di Cignana area (see chapter 2) unambiguously showed that exhumation of the Zermatt-Saas zone from (U)HP to greenschist-facies conditions occurred during top-(S)E shearing along its upper boundary. Strain may therefore have been mainly localized along the top of the Zermatt-Saas zone, i.e. in the footwall of the Combin Fault. Structural observations and the proposed sequence of deformation also suggest that greenschist-facies top-SE shearing was followed by a phase of dominant pure shear deformation at ca. 36 Ma and subsequently by renewed top-NW shearing after ca. 35 Ma which may have obliterated earlier top-SE structures. Even though the importance of top-SE shearing for juxtaposition of the Piemont-Ligurian units along the Combin Fault has been questioned by several authors (Sartori, 1987; Ring, 1995; Froitzheim et al., 2003; Pleuger et al., 2007), there is no conclusive evidence that speaks against juxtaposition of the Combin and Zermatt-Saas zones along greenschist-facies top-SE shear zones. My study, however, also suggests that the importance and regional extent of top-SE shearing may have been overestimated by some studies which suggest a regional top-SE shear zone comprising the entire Combin zone and the base of the Dent Blanche nappe (e.g. Reddy et al., 1999; Wheeler et al., 2001). The DBBT for example can only be interpreted as a major thrust which escaped any significant top-SE deformation. The structural evolution envisaged in this chapter probably comes closest to the kinematic and geometric model proposed by Wheeler et al. (2001) in which normal-sense shear zones form along the upper boundaries of ascending individual crustal units, in this case the Zermatt-Saas zone and probably also the St. Bernhard nappe system in the footwall of the Combin zone.

4.8.3 Conjugate top-SE and top-NW shear zones?

The temporal and spatial relations between greenschist-facies ductile top-NW and top-SE shear senses in the study area are often difficult to determine, for example in the areas around Becca d'Aver (see chapter 3), Allein, and Gran Tournalin. Both shear directions show highly ductile to semi-ductile and sometimes brittle deformation structures suggesting either episodicity due to deformation mode switches (e.g. Beltrando et al., 2007a; Lister and Forster, 2009) or an overlap of top-NW and top-SE shear zones in space and time due to a large pure shear component during progressive orogenic deformation. Local and regional variations in the predominance of thrust-related or normal-sense deformation structures may therefore partly be explained by the existence of conjugate shear zones. Structural analyses in the Lago di Cignana area suggest that the transition from normal-sense top-SE shearing to renewed top-NW thrusting probably occurred over a period of dominant pure shear deformation (see chapter 2). This phase is therefore interpreted to have occurred around 36 Ma after the main stage of top-SE shearing. Coaxial

deformation may have been triggered by incipient overthrusting of the Dent Blanche nappe and most likely resulted in tectonic thinning of the Combin zone. Especially in the western Valtournenche area, the thickness of the Combin zone has been strongly reduced suggesting large amounts of shortening perpendicular to nappe boundaries. The western and eastern Valtournenche areas are characterized by different distributions of shear senses. In the western Valtournenche, top-NW shear senses are predominant (subareas 10 and 11) whereas top-SE shear senses can only be observed at high structural levels (see chapter 3). In the eastern Valtournenche, top-SE shear senses can be observed in the direct hanging wall of the Combin Fault whereas top-NW shear senses dominate at higher structural levels (subarea 9). Such a distribution of shear zones and strain can be explained by up-section and down-section cutting conjugate shear zones (see fig. 2.9). Partly coeval activity of orogen-perpendicular shear zones in the period between ca. 45 and 36 Ma has been suggested by Reddy et al. (2003) based on overlapping Ar/Ar-ages between domains of dominant top-NW and top-SE shear. Significant deviation from simple shear during greenschist-facies deformation in this area is also suggested by other studies (Ring, 1995; Pleuger et al., 2007). Conjugate shear zones during late stages of ductile orogenic deformation in the Western Alps have been attributed to updoming of the Internal Crystalline Massifs, i.e. the Monte Rosa, Gran Paradiso, and Dora Maira Massifs, by Ganne et al. (2006) and Gasco et al. (2013). My structural observations, however, suggest late ductile to semi-ductile thrust-reactivation along the DBBT after ductile top-SE shearing and before the onset of orogen-perpendicular brittle extension. Ductile pure shear deformation is therefore interpreted to have linked these phases of normal-sense and thrust-related shearing and to have occurred before any significant updoming of the Monte Rosa nappe. During this phase, the Combin zone may have acted as ductile coupling between more competent, mostly continental units in the footwall and hanging wall (e.g. Escher and Beaumont, 1997).

4.8.4 Out-of-sequence thrusting and orogen-perpendicular extension

Out-of-sequence thrusting along the DBBT, shearing and folding within the Combin zone, as well as folding of the northwestern DBBT occurred from ca. 35 Ma onwards and can most likely be ascribed to increased collision-related deformation. In the Western Alps, continental collision ultimately led to formation of the Vanzone antiform which largely modified the geometry of the internal part of the nappe stack. Since late stages of greenschist-facies ductile deformation within the Combin zone have been proposed to have occurred around ca. 35 Ma (Reddy et al., 1999; Agard et al., 2002), renewed top-NW shearing is interpreted to have commenced at ca. 35 Ma. Late top-NW shearing in the study area is related to out-of-sequence reactivation of the DBBT and can therefore be well-observed along the Combin/Dent Banche contact and at high structural levels within the Combin zone but becomes less pronounced into the footwall. Low-grade greenschist-facies top-NW shear senses are often closely associated with shortening structures like folds and crenulation cleavages suggesting increasing amounts of orogen-perpendicular shortening. The decreasing ductility of top-NW kinematic indicators along the DBBT suggests that late top-NW shearing was associated with exhumation of the Dent Blanche nappe through the ductile/brittle transition. Incipient updoming of the Monte Rosa nappe most likely supported exhumation of units in its hanging wall from mid- to upper-crustal levels. The transition from out-of-

sequence thrusting and associated shortening to Vanzone-phase folding from ca. 32 Ma onwards may in fact have occurred gradually so that units in the southeastern realm of the study area were progressively rotated from a SE- into a NW-dipping orientation which led to the current synformal structure of the Dent Blanche nappe. A similar geometry and relationship between updoming of deep-crustal continental units and continuing thrusting along the DBBT at higher structural levels has been described by Le Bayon and Ballèvre (2006) for the Gran Paradiso transect south of the Aosta valley. Thrust-related top-NW shearing may have progressively evolved into normal-sense top-NW movements during continuing updoming southeast of the study area. Further uplift of the units due to increasing updoming of the Monte Rosa nappe subsequently led to upper-crustal, orogen-perpendicular extension (e.g. Gasco et al., 2013) and a brittle overprint in the southeastern and northwestern realms. A similar evolution has already been proposed by Manzotti et al. (2014) who reported low-angle and low-grade top-NW shearing followed by high-angle brittle faulting within the southeastern Dent Blanche nappe.

4.9 Conclusions

Structural analysis of shear zones along the Combin Fault and DBBT in the Swiss-Italian Western Alps (southern Valais and northern Aosta regions) revealed a polyphase structural evolution of these major tectonic contacts during Paleogene Alpine orogenic deformation. The following sequence of deformation has been deduced from deformation structures in outcrop and thin-section, overprinting relations, and correlations:

- **D1 top-(N)W shearing between ca. 48 and 44 Ma** can be ascribed to the main stage of nappe stacking and thrusting along the DBBT and Combin Fault. Top-(N)W shearing occurred during exhumation of the Dent Blanche nappe and underlying Combin zone and is held responsible for pervasive greenschist-facies retrogression within the Combin zone and the formation of greenschist-facies mylonites along the DBBT. Underthrusting of continental Briançonnais units led to accretion of the Cimes Blanches and Frilihorn nappes to the base of the Tsaté nappe.
- Transpressional to orogen-parallel **D2 top-(S)W shearing between ca. 43 and 40 Ma** affected the northwestern realm, especially the northwestern segment of the Combin Fault, and occurred under still decreasing metamorphic conditions during ongoing exhumation of the Combin zone. The DBBT was probably characterized by continuing W-vergent shearing during early stages of this phase.
- **D3 top-SE normal-sense shearing between ca. 39 and 37 Ma** affected the northwestern realm along a NE-SW striking shear zone subparallel to nappe boundaries. The DBBT largely escaped extensional top-SE shearing. In the southeastern realm, top-SE structures are subordinate but can be observed along the Combin Fault and at higher structural levels within the Combin zone. Greenschist-facies top-SE shearing accompanied the late stages of exhumation of the (U)HP Zermatt-Saas zone to crustal levels and is therefore held responsible for juxtaposition of the Combin and Zermatt-Saas zones.
- **D4 top-NW shearing and NW-SE shortening after ca. 35 Ma** resulted from reactivation of the DBBT as an out-of-sequence thrust and especially affected the southeastern realm and partly the northwestern DBBT. Renewed thrusting also led to the formation of folds and crenulation cleavages

and occurred during ongoing exhumation of the Dent Blanche nappe. The close association of top-NW shear senses with folds and crenulation cleavages suggests increasing influence of orogen-perpendicular shortening before the onset of Vanzone-phase folding from ca. 32 Ma onwards.

- Late top-NW shearing and shortening was followed by brittle **D5 NW-SE extension after ca. 30 Ma** due to updoming of the Vanzone antiform southeast of the study area. Units in the southeastern realm were progressively rotated from a SE-dipping into a NW-dipping orientation leading to further exhumation and the synformal structure of the Dent Blanche nappe.

My structural observations and interpretations from shear zones along the Combin Fault and DBBT suggest that the northwestern and southeastern segments of these major tectonic contacts record different stages of a polyphase structural evolution during progressive orogenic deformation. The described shearing events variably affected the northwestern and southeastern realms hindering assessment of the regional extent of deformation phases but also enabling reconstruction of a continuous sequence of deformation from the main stage of nappe stacking to post-nappe deformation.

- CHAPTER 5 -

Conclusions

The aim of this study was to reconstruct the structural evolution of the tectonic units in the study area and to deduce the sequence of deformation along two major Alpine tectonic contacts, the Combin Fault and the Dent Blanche Basal Thrust. For this purpose, structural and petrological investigations were performed in the study area in the southern Valais and northern Aosta regions of Switzerland and Italy, respectively. Most deformation observed in the field and in thin-section occurred under greenschist-facies conditions. Deformation under (U)HP conditions can be observed and studied in the two areas around Lago di Cignana and Becca d'Aver in the western Valtournenche of Italy. The observations and models presented for these areas and the whole study area are compatible and in good agreement with each other. They allow reconstruction of a comprehensive evolution and sequence of deformation in conjunction with published age constraints for the timing of deformation. The following general evolution can be deduced from the observations and interpretations presented in this thesis.

- **Before ca. 48 Ma:** HP metamorphism of the Dent Blanche nappe and Combin zone during subduction and accretion and associated top-NW shearing.
- **Ca. 48 – 44 Ma:** Top-(N)W shearing associated with the main stage of nappe stacking, exhumation, and greenschist-facies retrogression of the Dent Blanche nappe and Combin zone.
- **Ca. 43 – 40 Ma:** Transpressional to orogen-parallel top-(S)W shearing in the northwestern realm of the study area, especially along the northwestern Combin Fault during continuing exhumation of the Combin zone, and incipient exhumation of the Zermatt-Saas zone from (U)HP depths during normal-sense top-(S)E shearing along its upper boundary.
- **Ca. 39 – 37 Ma:** Top-SE shearing within the Combin zone and along the Combin Fault and juxtaposition of the Combin and Zermatt-Saas zones at crustal depths.
- **At ca. 36 Ma:** Phase of dominant pure shear deformation along the Combin Fault and within the Combin zone during the transition from normal-sense top-SE to thrust-related top-NW shearing.
- **After ca. 35 Ma:** Renewed top-NW shearing and associated NW-SE shortening as a result of reactivation of the DBBT as out-of-sequence thrust.
- **After ca. 30 Ma:** Brittle NW-SE extension due to updoming of the Vanzone antiform southeast of the study area.

The proposed evolution and sequence of deformation suggests that the Dent Blanche nappe and Combin zone experienced a common retrograde evolution and greenschist-facies overprint during top-(N)W shearing between ca. 48 and 44 Ma. Abundant mylonitic rocks along the base of the Dent Blanche nappe suggest that the DBBT represented a high-strain zone during this main stage of exhumation from blueschist-facies conditions. Evidence of early subduction- and accretion-related deformation and metamorphism is scarce within the Combin zone and along the Combin/Dent Blanche boundary. This "gap" could be filled by observations from the Becca d'Aver area where HP

deformation structures and mineral assemblages are partly preserved within metasediments of the Becca d'Aver continental sliver (BACS). Petrological and microstructural investigations on these rocks revealed prograde blueschist-facies metamorphism associated with fluid-mediated mineral growth and element transfer during top-NW shearing. Peak metamorphic conditions reached ca. 1.7 GPa and 500° C and are higher than previously reported PT conditions for the Combin/Dent Blanche boundary. The age of the HP imprint within the Dent Blanche nappe and Combin zone is not well constrained but is interpreted to have occurred after peak metamorphism in the Sesia nappe at ca. 70 – 65 Ma (Inger et al., 1996; Rubatto et al., 1999) but before the peak in the Zermatt-Saas zone at ca. 44 - 43 Ma (Rubatto et al., 1998; Gouzu et al., 2006). Dating the prograde metamorphism observed within BACS metasediments, e.g. with Lu-Hf garnet geochronology, might contribute significantly to constraining the timing of HP metamorphism along the Combin/Dent Blanche boundary and is therefore considered for future studies. There are also no reliable ages for the timing of retrograde shearing along the DBBT which is interpreted to have occurred after accretion of the Combin zone until ca. 48 Ma (Reddy et al., 2003) and mainly before the onset of exhumation of the (U)HP Zermatt-Saas zone after ca. 43 Ma but may have continued until ca. 40 Ma during transpressional deformation. Dating of synkinematic phases within basal mylonites, e.g. white mica with Ar/Ar geochronology, might therefore be an important step to constrain the timing of greenschist-facies mylonitic top-(N)W shearing. According to the model presented in this thesis, the early retrograde evolution of the Combin zone was closely related to the overlying Dent Blanche nappe in that the two units were exhumed and overprinted together. After the main stage of greenschist-facies top-(N)W shearing and overthrusting of the Combin zone and Dent Blanche nappe over continental Briançonnais units, the Combin zone experienced greenschist-facies post-nappe deformation which only locally affected the DBBT and variably affected the northwestern and southeastern realms of the study area. Top-(N)W shearing was followed by transpressional to orogen-parallel top-(S)W shearing between ca. 43 and 40 Ma which especially affected the northwestern Combin Fault and occurred during ongoing exhumation of the Combin zone. Especially the extent of orogen-parallel shearing and its role in deeper crustal deformation needs further clarification. Top-(S)W shearing has been reported from adjacent areas (e.g. Mancktelow, 1985; Pleuger et al., 2007; Scheiber et al., 2013) but has been ascribed to different periods and events. According to the proposed model, transpressional to orogen-parallel shearing may have been the result of a dextral strike-slip component along the Briançonnais/Combin boundary due to oblique subduction. Top-(S)W shearing was followed by a phase of normal-sense top-SE shearing within the Combin zone and along the Combin Fault between ca. 39 and 37 Ma. Structural analyses in the Lago di Cignana area showed that exhumation of the Zermatt-Saas zone from (U)HP to crustal levels after ca. 43 Ma also occurred during top-(S)E shearing along its upper boundary. Top-SE normal-sense shearing is therefore interpreted to be responsible for juxtaposition of the Combin and Zermatt-Saas zones at greenschist-facies conditions. Top-SE structures are, however, scarce in the hanging wall of the southeastern Combin Fault in the study area which may be due to several reasons: (1) Strain may have been mainly localized along the top of the Zermatt-Saas zone and in the footwall of the Combin Fault. (2) The sequence of deformation presented in this thesis also envisages that top-SE shearing was followed by a phase of dominant pure shear deformation at ca. 36 Ma and subsequently by renewed top-NW shearing after ca. 35 Ma which may have obliterated earlier top-SE structures. Structural observations in the Lago di Cignana area showed that pure shear deformation affected units in the footwall and hanging wall of the Combin Fault after juxtaposition of the Combin

and Zermatt-Saas zones. On a regional scale, a large pure shear component during post-exhumational, greenschist-facies deformation may have led to partly contemporaneous activity of top-SE and top-NW shear zones and tectonic thinning of the Combin zone. Whereas the relative chronology between greenschist-facies top-NW and top-SE shear senses is often difficult to determine, structural observations from the Lago di Cignana and Becca d'Aver areas as well as many other localities in the study area strongly suggest that tectonic units were affected by a late phase of top-NW shearing before the onset of brittle deformation. This phase of renewed top-NW shearing and associated NW-SE shortening is ascribed to reactivation of the DBBT as out-of-sequence thrust which also affected the underlying Combin zone. This late top-NW shearing event can be inferred from overprinting relations, late folding, and the decreasing and often low-grade metamorphic grade of top-NW structures along the DBBT which unambiguously often postdate observed ductile top-SE shear senses at lower structural levels. The last distinguishable deformation phase was orogen-perpendicular brittle extension after ca. 30 Ma which can be observed as brittle top-SE and top-NW shear planes overprinting earlier ductile structures. This phase is attributed to updoming of the Vanzone antiform southeast of the study area which led to increased exhumation and modification of overall nappe geometries.

The DBBT in the Swiss-Italian Western Alps represents an important Alpine greenschist-facies shear zone which was active during several stages of top-(N)W shearing under generally decreasing metamorphic conditions. The early retrograde evolution of the Combin Fault and overlying Combin zone was closely related to the overlying Dent Blanche nappe but shows a more complex structural evolution during subsequent shearing events. Post-nappe deformation variably affected the northwestern and southeastern realms of the study area and was, in most cases, not strictly parallel to previously established nappe boundaries. Whereas exhumation of the Combin zone and Dent Blanche nappe and the main stage of nappe-stacking can be attributed to thrust-related top-(N)W shearing, exhumation of the Zermatt-Saas zone from (U)HP depths and juxtaposition with the overlying Combin zone at greenschist-facies conditions occurred during normal-sense top-(S)E shearing. Renewed top-NW shearing and NW-SE shortening due to out-of-sequence thrusting along the DBBT was the last ductile deformation in the study area before the onset of orogen-perpendicular brittle extension.

References

Agard, P., Monié, P., Jolivet, L., and Goffé, B. (2002): Exhumation of the Schistes Lustrés complex: in situ laser probe 40Ar/39Ar constraints and implications for the Western Alps. J. Met. Geol. 20, 599-618.

Agard, P., Yamato, P., Jolivet, L., and Burov, E. (2009): Exhumation of oceanic blueschists and eclogites in subduction zones: Timing and mechanisms. Earth-Sci. Rev. 92, 53-79.

Amato, J.M., Johnson, C.M., Baumgartner, L.P., and Beard, B.L. (1999): Rapid exhumation of the Zermatt-Saas ophiolite deduced from high-precision Sm-Nd and Rb-Sr geochronology. Earth Planet. Sci. Lett. 171, 425-438.

Angiboust, S., Agard, P., Jolivet, L., and Beyssac, O. (2009): The Zermatt-Saas ophiolite: the largest (60-km wide) and deepest (c. 70-80 km) continuous slice of oceanic lithosphere detached from a subduction zone?. Terra Nova 21, 171-180.

Angiboust, S. and Agard, P. (2010): Initial water budget: The key to detaching large volumes of eclogitized oceanic crust along a subduction channel?. Lithos 120, 453-474.

Argand, É. (1916): Sur l'arc des Alpes Occidentales. Eclogae Geol. Helv. 14, 145-204.

Babist, J., Handy, M.R., Konrad-Schmolke, M., and Hammerschmidt, K. (2006): Precollisional, multistage exhumation of subducted continental crust: The Sesia Zone, western Alps. Tectonics 25, TC6008.

Ballèvre, M., Kienast, J.R., and Vuichard, J.P. (1986): La "nappe de la Dent-Blanche" (Alpes occidentals); deux unites austroalpines independantes. Eclogae Geol. Helv. 79, 57-74.

Ballèvre, M. and Kienast, J.R. (1987): Découverte et signification de paragenèses a grenat-amphibole bleu dans la couverture mésozoique de la nappe de la Dent-Blanche (Alpes Occidentales). Comptes Rendus de l'Académie des Sciences Paris 305, 43-46.

Ballèvre, M. and Merle, O. (1993): The Combin fault: compressional reactivation of a Late Cretaceous–Early Tertiary detachment fault in the Western Alps. Schweiz. Mineral. Petrogr. Mitt. 73, 205-227.

Baxter, E.F. and Caddick, M.J. (2013): Garnet growth as a proxy for progressive subduction zone dehydration. Geology 41, 643-646.

Bearth, P. (1963): Contribution à la subdivision tectonique et stratigraphique du cristallin de la nappe du Grand Saint-Bernard dans le Valais (Suisse). In: Durand Delga, M. (ed.): Livre à la mémoire du Professeur Fallot. 2. Mémoire de la Société géologique de France, Paris, 407-418.

Beltrando, M., Hermann, J., Lister, G., and Compagnoni, R. (2007a): On the evolution of orogens: Pressure cycles and deformation mode switches. Earth Planet. Sci. Lett. 256, 372-388.

Beltrando, M., Rubatto, D., Compagnoni, R., and Lister, G. (2007b): Was the Valaisan basin floored by oceanic crust? Evidence of Permian magmatism in the Versoyen unit (Valaisan domain, NW Alps). Ofioliti 32, 85-99.

Beltrando, M., Lister, G.S., Rosenbaum, G., Richards, S., and Forster, M.A. (2010a): Recognizing episodic lithospheric thinning along a convergent plate margin: The example of the Early Oligocene Alps. Earth Sci. Rev. 103, 81-98.

Beltrando, M., Compagnoni, R., and Lombardo, B. (2010b): (Ultra-) High-pressure metamorphism and orogenesis: An Alpine perspective. Gondwana Research 18, 147-166.

Beltrando, M., Rubatto, D., and Manatschal, G. (2010c): From passive margins to orogens: The link between ocean-continent transition zones and (ultra)high-pressure metamorphism. Geology 38, 559-562.

Beltrando, M., Manatschal, G., Mohn, G., Dal Piaz, G.V., Vitale Brovarone, A., and Masini, E. (2014): Recognizing remnants of magma-poor rifted margins in high-pressure orogenic belts. Earth Sci. Rev. 131, 88-115.

Berger, A. and Bousquet, R. (2008): Subduction-related metamorphism in the Alps: review of isotopic ages based on petrology and their geodynamic consequences. In: Siegesmund, S., Fügenschuh, B., and Froitzheim, N. (eds.): Tectonic aspects of the Alpine-Dinaride-Carpathian System. Geological Society, London, Special Publications 298, 117-144.

Berman, R.G. (1988): Internally-consistent thermodynamic data for minerals in the system Na2O-K2O-CaO-MgO-FeO-Fe2O3-Al2O3-SiO2-TiO2-H2O-CO2. J. Petrol. 29, 445-522.

Bill, M., Bussy, F., Cosca, M., Masson, H., and Hunziker, J.C. (1997): High-precision U-Pb and 40Ar/39Ar dating of an Alpine ophiolite (Gets nappe, French Alps). Eclogae Geol. Helv. 90, 43-54.

Bill, M., Masson, H., and Thélin, P. (2001): Low-grade metamorphism of the Gets nappe (Western Alps). Schweiz. Mineral. Petrogr. Mitt. 81, 229-237.

Bousquet, R., Engi, M., Gosso, G., Oberhänsli, R., Berger, A., Spalla, M.I., Zucali, M. & Goffé, B. (2004): Explanatory notes to the map: metamorphic structure of the Alps transition from the Western to the Central Alps. Mitt. Österr. Miner. Ges., 149, 145-156.

Bousquet, R. (2008): Metamorphic heterogeneities within a single HP unit: Overprint effect or metamorphic mix?. Lithos 103, 46-69.

Bousquet, R., Oberhänsli, R., Goffé, B., Wiederkehr, M., Koller, F., Schmid, S.M., Schuster, R., Engi, M., Berger, A., and Martinotti, G. (2008): Metamorphism of metasediments at the scale of an orogen: a key to the Tertiary geodynamic evolution of the Alps. In: Siegesmund, S., Fügenschuh, B., and Froitzheim, N. (eds.): Tectonic aspects of the Alpine-Dinaride-Carpathian System. Geological Society, London, Special Publications 298, 393-411.

Bowtell, S.A., Cliff, R.A., and Barnicoat, A.C. (1994): Sm-Nd isotopic evidence on the age of eclogitization in the Zermatt-Saas ophiolite. J. Met. Geol. 12, 187-196.

Bucher, K., Fazis, Y., de Capitani, C., and Grapes, R. (2005): Blueschists, eclogites, and decompression assemblages of the Zermatt-Saas ophiolite: high-pressure metamorphism of subducted Tethys lithosphere. Am. Mineral. 90, 821-835.

Bussy, F., Venturini, G., Hunziker, J.C., and Martinotti, G. (1998): U-Pb ages of magmatic rocks of the Western Austroalpine Dent-Blanche-Sesia unit. Schweiz. Mineral. Petrogr. Mitt. 78, 163-168.

Cartwright, I. and Barnicoat, A.C. (2002): Petrology, geochronology, and tectonics of shear zones in the Zermatt-Saas and Combin zones of the Western Alps. J. Met. Geol. 20, 263-281.

Dal Piaz, G.V. (1999): The Austroalpine-Piedmont nappe stack and the puzzle of Alpine Tethys. Mem. Sci. Geol. 51, 155-176.

Dal Piaz, G.V., Cortiana, G., Del Moro, A., Martin, S., Pennacchioni, G., and Tartarotti, P. (2001): Tertiary age and paleostructural inferences of the eclogitic imprint in the Austroalpine outliers and Zermatt-Saas ophiolite, western Alps. Int. J. Earth Sci. 90, 668-684.

De Capitani, C. and Petrakakis, K. (2010): The computation of equilibrium assemblage diagrams with Theriak/Domino software. Am. Mineral. 95, 1006-1016.

De Meyer, C.M.C, Baumgartner, L.P., Beard, B.L., and Johnson, C.M. (2014): Rb-Sr ages from phengite inclusions in garnets from high pressure rocks of the Swiss Western Alps. Earth Planet. Sci. Lett. 395, 205-216.

Elter, G., Elter, P., Sturani, C., and Weidmann, M. (1966): Sur la prolongation du domaine ligure de l'Appennin dans la Montferrat et les Alpes et sur l'origine de la Nappe de Simme s.l. des Préalpes romandes et chablaisiennes. Arch. Sci. 19, 279-377.

Escher, A., Masson, H., and Steck, A. (1993): Nappe geometry in the Western Alps. J. Struct. Geol. 15, 501-509.

Escher, A. and Beaumont, C. (1997): Formation, burial and exhumation of basement nappes at crustal scale: a geometric model based on the Western Swiss-Italian Alps. J. Struct. Geol. 19, 955-974.

Escher, A., Hunziker, J.C., Marthaler, M., Masson, H., Sartori, M., and Steck, A. (1997): Geologic framework and structural evolution of the western Swiss-Italian Alps. In: Pfiffner, O.A., Lehner, P., Heitzmann, P., Müller, S., Steck, A. (Eds.), Deep structure of the Swiss Alps – Results from NRP 20: Basel, Switzerland, Birkhäuser, 205-221.

Faßmer, K. (2014): Das Alter und die Petrologie eklogitfazieller Gesteine in der Etirol-Levaz-Schuppe (Valtournenche, Italien). Unpublished Master thesis, University of Bonn.

Forster, M., Lister, G., Compagnoni, R., Giles, D., Hills, Q., Betts, P., Beltrando, M., and Tamagno, E. (2004): Mapping of oceanic crust with „HP" to „UHP" metamorphism: The Lago di Cignana Unit (Western Alps). In: Pasquarè, G., Venturini, C., Groppelli, G. (Eds.), Mapping Geology in Italy, APAT – Dip. Difesa del Suolo, Servizio Geologico d'Italia, Roma 2004, Map 33, 279-286.

Forster, M.A. and Lister, G.S. (2008): Tectonic sequence diagrams and the structural evolution of schists and gneisses in multiply deformed terranes. J. Geol. Soc. 165, 923-939.

Fossen, H. (2010): Structural Geology. 480 pp, Cambridge University Press.

Frezzotti, M.L., Selverstone, J., Sharp, Z.D., and Compagnoni, R. (2011): Carbonate dissolution during subduction revealed by diamond-bearing rocks from the Alps. Nature Geoscience 4, 703-706.

Froitzheim, N. and Manatschal, G. (1996): Kinematics of Jurassic rifting, mantle exhumation, and passive-margin formation in the Austroalpine and Penninic nappes (eastern Switzerland). GSA Bulletin 108, 1120-1133.

Froitzheim, N., Schmid, S.M., and Frey, M. (1996): Mesozoic paleogeography and the timing of eclogite-facies metamorphism in the Alps: A working hypothesis. Eclogae Geol. Helv. 89/1, 81-110.

Froitzheim, N. (2001): Origin of the Monte Rosa nappe in the Pennine Alps – A new working hypothesis. GSA Bulletin 113, 604-614.

Froitzheim, N., Pleuger, J., Roller, S., and Nagel, T. (2003): Exhumation of high- and ultrahigh-pressure metamorphic rocks by slab extraction. Geology 31, 925-928.

Froitzheim, N., Pleuger, J., and Nagel, T.J. (2006): Extraction faults. J. Struct. Geol. 28, 1388-1395.

Ganne, J., Marquer, D., Rosenbaum, G., Bertrand, J.M., and Fudral, S. (2006): Partitioning of deformation within a subduction channel during exhumation of high-pressure rocks: a case study from the Western Alps. J. Struct. Geol. 28, 1193-1207.

Gardien, V., Reusser, E., and Marquer, D. (1994): Pre-Alpine metamorphic evolution of the gneisses from Valpelline series (Western Alps, Italy). Schweiz. Mineral. Petrogr. Mitt. 74, 489-502.

Gasco, I. and Gattiglio, M. (2011): Geological map of the upper Gressoney Valley, Western Italian Alps. Journal of Maps, 82-102.

Gasco, I., Borghi, A., and Gattiglio, M. (2011): P-T Alpine metamorphic evolution of the Monte Rosa nappe along the Piedmont Zone boundary (Gressoney Valley, NW Italy). Lithos 127, 336-353.

Gasco, I., Gattiglio, M., and Borghi, A. (2013): Review of metamorphic and kinematic data from Internal Crystalline Massifs (Western Alps): PTt paths and exhumation history. J. Geod. 63, 1-19.

Gouzu, C., Itaya, T., Hyodo, H., and Matsuda, T. (2006): Excess 40Ar-free phengite in ultrahigh-pressure metamorphic rocks from the Lago di Cignana area, Western Alps. Lithos 92, 418-430.

Grohmann, C.H. and Campanha, G.A.C. (2010): OpenStereo: open source, cross-platform software for structural geology analysis. AGU Fall Meeting, San Francisco, CA.

Groppo, C., Beltrando, M., and Compagnoni, R. (2009): The P-T path of the ultra-high pressure Lago di Cignana and adjoining meta-ophiolitic units: insights into the evolution of the subducting Tethyan slab. J. Met. Geol. 27, 207-231.

Handy, M.R., Schmid, S.M., Bousquet, R., Kissling, E., and Bernoulli, D. (2010): Reconciling plate-tectonic reconstructions of Alpine Tethys with the geological-geophysical record of spreading and subduction in the Alps. Earth Sci. Rev. 102, 121-158.

Hawkins, A.T., Selverstone, J., Brearley, A.J., Beane, R.J., Ketcham, R.A., and Carlson, W.D. (2007): Origin and mechanical significance of honeycomb garnet in high-pressure metasedimentary rocks from the Tauern Window, Eastern Alps. – J. Metam. Geol. 25, 565-583.

Hermann, J. (2002): Allanite: thorium and light rare earth element carrier in subducted crust. Chem. Geol. 192, 289-306.

Herwartz, D., Nagel, T.J., Münker, C., Scherer, E.E., and Froitzheim, N. (2011): Tracing two orogenic cycles in one eclogite sample by Lu-Hf garnet chronometry. Nat. Geosci. 4, 178-183.

Hickmott, D.D., Sorensen, S.S., and Rogers, P.S.Z. (1992): Metasomatism in a subduction complex: Constraints from microanalysis of trace elements in minerals from garnet amphibolite from the Catalina Schist. Geology 20, 347-350.

Husson, L., Brun, J.-P., Yamato, P., and Faccenna, C. (2009): Episodic slab rollback fosters exhumation of HP-UHP rocks. Geophys. J. Int. 179, 1292-1300.

Inger, S., Ramsbotham, W., Cliff, R.A., and Rex, D.C. (1996): Metamorphic evolution of the Sesia-Lanzo Zone, Western Alps: time constraints from multi-system geochronology. Contrib. Mineral. Petrol. 126, 152-168.

Janák, M., Froitzheim, N., Lupták, B., Vrabec, M., and Krogh Ravna, E.J. (2004): First evidence for ultrahigh-pressure metamorphism of eclogites in Pohorje, Slovenia: Tracing deep continental subduction in the Eastern Alps. Tectonics 23, TC5014, DOI: 10.1029/2004TC001641.

John, T., Klemd, R., Gao, J., and Garbe-Schönberg, C.D. (2008): Trace-element mobilization in slabs due to non steady-state fluid-rock interaction: Constraints from an echlogite-facies vein in blueschist (Tianshan, China). Lithos 103, 1-24.

Keller, L.M. and Schmid, S.M. (2001): On the kinematics of shearing near the top of the Monte Rosa nappe and the nature of the Furgg zone in Val Loranco (Antrona valley, N.Italy): tectonometamorphic and paleogeographic consequences. Schweiz. Mineral. Petrogr. Mitt. 81, 347-367.

Keller, L.M., Hess, M., Fügenschuh, B., and Schmid, S.M. (2005): Structural and metamorphic evolution of the Camughera – Moncucco, Antrona and Monte Rosa units southwest of the Simplon line, Western Alps. Eclogae Geol. Helv. 98, 19-49.

Kienast, J.R. (1973): Sur l'existence de deux series différentes au sein de l'ensemble "schistes lustrés-ophiolites" du Val d'Aoste: quelques arguments fondés sur l'étude des roches métamorphiques. C. R. Acad. Sc. Paris (Sér. D) 276, 2621-2624.

Konrad-Schmolke, M., O'Brien, P.J., De Capitani, C., and Carswell, D.A. (2008a): Garnet growth at high- and ultra-high pressure conditions and the effect of element fractionation on mineral modes and composition. Lithos 103, 309-332.

Konrad-Schmolke, M., Zack, T., O'Brien, P.J., and Jacob, D.E. (2008b): Combined thermodynamic and rare earth element modelling of garnet growth during subduction: Examples from ultrahigh-pressure eclogite of the Western Gneiss Region, Norway. Earth Planet. Sci. Lett. 272, 488-498.

Konrad-Schmolke, M., O'Brien, P.J., and Zack, T. (2011a): Fluid migration above a subducted slab – constraints on amount, pathways and major element mobility from partially overprinted eclogite-facies rocks (Sesia Zone, Western Alps). J. Petrol. 52, 457-486.

Konrad-Schmolke, M., Zack, T., O'Brien, P.J., and Barth, M. (2011b): Fluid migration above a subducted slab – Thermodynamic and trace element modelling of fluid-rock interaction in partially overprinted eclogite-facies rocks (Sesia Zone, Western Alps). Earth Planet. Sci. Lett. 311, 287-298.

Kruhl, J.H. (1996): Prism- and basal-plane parallel subgrain boundaries in quartz: a microstructural geothermobarometer. J. Met. Geol. 14, 581-589.

Kruhl, J.H., Wirth, R., and Morales, L.F.G. (2013): Quartz grain boundaries as fluid pathways in metamorphic rocks. J. Geophys. Res. 118, 1957-1967.

Kylander-Clark, A.R.C., Hacker, B.R., and Mattinson, C.G. (2012): Size and exhumation rate of ultrahigh-pressure terranes linked to orogenic stage. Earth Planet. Sci. Lett. 321, 115-120.

Lapen, T.J., Johnson, C.M., Baumgartner, L.P., Mahlen, N.J., Beard, B.L., and Amato, J.M. (2003): Burial rates during prograde metamorphism of an ultrahigh-pressure terrane: an example from Lago di Cignana, Western Alps, Italy. Earth Planet. Sci. Lett. 215, 57-72.

Lapen, T.J., Johnson, C.M., Baumgartner, L.P., Dal Piaz, G.V., Skora, S., and Beard, B.L. (2007): Coupling of oceanic and continental crust during Eocene eclogite-facies metamorphism: evidence from the Monte Rosa nappe, western Alps. Contrib. Mineral. Petrol. 153, 139-157.

Lardeaux, J.M. and Spalla, M.I. (1991): From granulites to eclogites in the Sesia Zone (Italian Western Alps), a record of opening and closure of the Piedmont ocean. J. Met. Geol. 9, 35-59.

Law, R.D., Searle, M.P., and Simpson, R.L. (2004): Strain, deformation temperatures and vorticity of flow at the top of the Greater Himalayan Slab, Everest Massif, Tibet. J. Geol. Soc. London. 161, 305-320.

Le Bayon, B. and Ballèvre, M. (2006): Deformation history of a subducted continental crust (Gran Paradiso, Western Alps): continuing crustal shortening during exhumation. J. Struct. Geol. 28, 793-815.

Lebit, H. Klaper, E.M., and Lüneburg, C.M. (2002): Fold-controlled quartz textures in the Pennine Mischabel backfold near Zermatt, Switzerland. Tectonophysics 359, 1-28.

Leiss, B., Ullemeyer, K., Weber, K., Brokmeier, H.G., Bunge, H.J., Drury, M., Faul, U., Fueten, F., Frischbutter, A., Klein, H., Kuhs, W., Launeau, P., Lloyd, G.E., Prior, D.J., Scheffzüg, C., Weiss, T., Walther, K., and Wenk, H.R. (2000): Recent developments and goals in texture research of geological materials. J. Struct. Geol. 22, 1531-1540.

Liati, A., Froitzheim, N., and Fanning, C.M. (2005): Jurassic ophiolites within the Valais domain of the Western and Central Alps: geochronological evidence for re-rifting of oceanic crust. Contrib. Mineral. Petrol. 149, 446-461.

Liati, A. and Froitzheim, N. (2006): Assessing the Valais ocean, Western Alps: U-Pb SHRIMP zircon geochronology of eclogite in the Balma unit, on top of the Monte Rosa nappe. Eur. J. Mineral. 18, 299-308.

Lister, G.S. and Williams, P.F. (1979): Fabric development in shear zones: theoretical controls and observed phenomena. J. Struct. Geol. 1, 283-297.

Lister, G.S. and Snoke, A.W. (1984): S-C mylonites. J. Struct. Geol. 6, 617-638.

Lister, G., Forster, M.A., and Rawling, T.J. (2001): Episodicity during orogenesis. Geol. Soc. London, Spec. Publ. 184, 89-113.

Lister, G. and Forster, M. (2009): Tectonic mode switches and the nature of orogenesis. Lithos 113, 274-291.

Lloyd, G.E., Law, R.D., Mainprice, D., and Wheeler, J. (1992): Microstructural and crystal fabric evolution during shear zone formation. J. Struct. Geol. 14, 1079-1100.

Mahlen, N.J., Skora, S., Johnson, C.M., Baumgartner, L.P., Lapen, T.J., Skora, S., Beard, B.L., and Pilet, S. (2005): Lu-Hf geochronology of eclogites from Pfulwe, Zermatt-Saas Ophiolite, western Alps, Switzerland. Geochimica et Cosmochimica Acta 69, A305.

Malaspina, N., Hermann, J., Scambelluri, M. (2009): Fluid/mineral interaction in UHP garnet peridotite. Lithos 107, 38-52.

Mancktelow, N.S. (1985): The Simplon Line: a major displacement zone in the western Lepontine Alps. Eclogae Geol. Helv. 78, 73-96.

Manning, C.E. (2004): The chemistry of subduction-zone fluids. Earth Planet. Sci. Lett. 223, 1-16.

Manzotti, P. (2011): Petro-structural map of the Dent Blanche tectonic system between Valpelline and Valtournenche valleys, Western Italian Alps. Journal of Maps, 340-352.

Manzotti, P., Zucali, M., Ballèvre, M., Robyr, M., and Engi, M. (2014): Geometry and kinematics of the Roisan-Cignana Shear Zone, and the orogenic evolution of the Dent Blanche Tectonic System (Western Alps). Swiss J. Geosci., DOI: 10.1007/s00015-014-0157-9.

Markley, M.J., Teyssier, C., Cosca, M.A., Caby, R., Hunziker, J.C., and Sartori, M. (1998): Alpine deformation and 40Ar/39Ar geochronology of synkinematic white mica in the Siviez-Mischabel Nappe, western Pennine Alps, Switzerland. Tectonics 17, 407-425.

Marthaler, M. and Stampfli, G.M. (1989): Les Schistes lustrés à ophiolites de la nappe du Tsaté: un ancien prisme d'accrétion issu de la marge active apulienne?. Schweiz. Mineral. Petrogr. Mitt. 69, 211-216.

Martin, L.A.J., Hermann, J., Gauthiez-Putallaz, L., Whitney, D.L., Vitale Brovarone, A., Fornash, K.F., and Evans, N.J. (2014): Lawsonite geochemistry and stability – implications for trace element and water cycles in subduction zones. J. Met. Geol. 32, 455-478.

Mazurek, M. (1986): Structural evolution and metamorphism of the Dent Blanche nappe and the Combin zone west of Zermatt (Switzerland). Eclogae Geol. Helv. 79, 41-56.

Milnes, A.G., Greller, M., and Müller, M. (1981): Sequence and style of major post-nappe structures, Simplon-Pennine Alps. J. Struct. Geol. 3, 411-420.

Mitra, G. (1978): Ductile deformation zones and mylonites: the mechanical processes involved in the deformation of crystalline basement rocks. Am. J. Sci. 278, 1057-1084.

Mohn, G., Manatschal, G., Masini, E., and Müntener, O. (2011): Rift-related inheritance in orogens: a case study from the Austroalpine nappes in Central Alps (SE-Switzerland and N-Italy). Int. J. Earth. Sci. 100, 937-961.

Monjoie, P., Bussy, F., Lapierre, H., and Pfeifer, H.R. (2005): Modeling of in-situ crystallization processes in the Permian mafic layered intrusion of Mont Collon (Dent Blanche nappe, western Alps). Lithos 83, 317-346.

Negro, F., Bousquet, R., Vils, F., Pellet, C.-M., and Hänggi-Schaub, J. (2013): Thermal structure and metamorphic evolution of the Piemont-Ligurian metasediments in the northern Western Alps. Swiss J. Geosci. 106, 63-78.

Newton, R.C. and Kennedy, G.C. (1963): Some equilibrium reactions in the join CaAl2Si2O8-H2O. J. Geophys. Res. 68, 2967-2983.

Oberhänsli, R. and Bucher, K. (1987): Tectonometamorphic evolution of the Dent Blanche nappe. Terra Cognita 7/2-3, 95.

Passchier, C.W. and Trouw, R.A.J. (2005): Microtectonics. 366 pp, Springer, Berlin.

Pawley, A.R. (1994): The pressure and temperature stability limits of lawsonite: implications for H2O recycling in subduction zones. Contrib. Mineral. Petrol. 118, 99-108.

Pettke, T., Diamond, L.W., and Villa, I.M. (1999): Mesothermal gold veins and metamorphic devolatilization in the northwestern Alps: the temporal link. Geology 27, 641-644.

Platt, J.P. and Vissers, R.L.M. (1980): Extensional structures in anisotropic rocks. J. Struct. Geol. 2, 397-410.

Pleuger, J., Froitzheim, N., and Jansen, E. (2005): Folded continental and oceanic nappes on the southern side of Monte Rosa (western Alps, Italy): Anatomy of a double collision suture. Tectonics 24, TC4013.

Pleuger, J., Roller, S., Walter, J.M., Jansen, E., and Froitzheim, N. (2007): Structural evolution of the contact between two Penninic nappes (Zermatt-Saas zone and Combin zone, Western Alps) and implications for the exhumation mechanism and paleogeography. Int. J. Earth Sci. 96, 229-252.

Pleuger, J., Froitzheim, N., Derks, J.F., Kurz, W., Albus, J., Walter, J.M., and Jansen, E. (2009): The contribution of neutron texture goniometry to the study of complex tectonics in the Alps. In: Liang et al. (eds.): Neutron Applications in Earth, Energy and Environmental Sciences, Neutron Scattering Applications and Techniques. Springer Science+Business Media, LLC.

Pryer, L.L. (1993): Microstructures in feldspars from a major crustal thrust zone: the Grenville Front, Ontario, Canada. J. Struct. Geol. 15, 21-36.

Reddy, S.M., Wheeler, J., and Cliff, R.A. (1999): The geometry and timing of orogenic extension: an example from the Western Italian Alps. J. Met. Geol. 17, 573-589.

Reddy, S.M., Wheeler, J., Butler, R.W.H., Cliff, R.A., Freeman, S., Inger, S., Pickles, C., and Kelley, S.P. (2003): Kinematic reworking and exhumation within the convergent Alpine Orogen. Tectonophysics 365, 77-102.

Regis, D., Rubatto, D., Darling, J., Cenki-Tok, B., Zucali, M., and Engi, M. (2014): Multiple metamorphic stages within an eclogite-facies terrane (Sesia Zone, Western Alps) revealed by Th-U-Pb petrochronology. J. Petrol. 55, 1429-1456.

Reinecke, T. (1991): Very-high-pressure metamorphism and uplift of coesite-bearing metasediments from the Zermatt-Saas zone, Western Alps. Eur. J. Mineral. 3, 7-17

Reinecke, T. (1998): Prograde high- to ultrahigh-pressure metamorphism and exhumation of oceanic sediments at Lago di Cignana, Zermatt-Saas Zone, western Alps. Lithos 42, 147-189.

Ring, U. (1995): Horizontal contraction or horizontal extension? Heterogeneous Late Eocene and Early Oligocene general shearing during blueschist and greenschist facies metamorphism at the Pennine-Austroalpine boundary zone of the Western Alps. Geol. Rundsch. 84, 843-859.

Robyr, M., Vonlanthen, P., Baumgartner, L.P., and Grobety, B. (2007): Growth mechanism of snowball garnets from the Lukmanier Pass area (Central Alps, Switzerland): a combined CT/EPMA/EBSD study. Terra Nova 19, 240-244.

Robyr, M., Carlson, W.D., Passchier, C., and Vonlanthen, P. (2009): Microstructural, chemical and textural records during growth of snowball garnet. J. Met. Geol. 27, 423-237.

Rosenbaum, G. and Lister, G.S. (2005): The Western Alps from the Jurassic to Oligocene: spatio-temporal constraints and evolutionary reconstructions. Earth Sci. Rev. 69, 281-306.

Rubatto, D., Gebauer, D., and Fanning, M. (1998): Jurassic formation and Eocene subduction of the Zermatt-Saas-Fee ophiolites: implications for the geodynamic evolution of the Central and Western Alps. Contrib. Mineral. Petrol. 132, 269-287.

Rubatto, D., Gebauer, D., and Compagnoni, R. (1999): Dating of eclogite-facies zircons: the age of Alpine metamorphism in the Sesia-Lanzo zone (western Alps). Earth Planet. Sci. Lett. 167, 141-158.

Rubatto, D., Regis, D., Hermann, J., Boston, K., Engi, M., Beltrando, M., and McAlpine, S.R.B. (2011): Yo-yo subduction recorded by accessory minerals in the Italian Western Alps. Nature Geoscience 4, 338-342.

Sandmann, S., Nagel, T.J., Herwartz, D., Fonseca, R.O.C., Kurzawski, R.M., Münker, C., and Froitzheim, N. (subm.): Lu-Hf garnet systematics of a polymetamorphic basement unit: New evidence for coherent exhumation of the Adula Nappe (Central Alps) from eclogite-facies conditions. Contrib. Mineral. Petrol..

Sartori, M. (1987): Structure de la zone du Combin entre les Diablos et Zermatt (Valais). Eclogae Geol. Helv. 80, 789-814.

Sartori, M. (1990): L'unité du Barrhorn (zone pennique, Valais, Suisse). Mémoires de Géologie, 6. Lausanne, 156 pp.

Scheiber, T., Pfiffner, O.A., and Schreurs, G. (2013): Upper crustal deformation in continent-continent collision: A case study from the Bernard nappe complex (Valais, Switzerland). Tectonics 32, 1320-1342.

Schmid, S.M. and Casey, M. (1986): Complete fabric analysis of some commonly observed quartz [c]-axis patterns. In: Hobbs, B.E., Heard, H.C. (Eds.), Mineral and Rock Deformation: Laboratory Studies. Geophysical Monograph 36, 263-286.

Schmid, S.M., Pfiffner, O.A., Froitzheim, N., Schönborn, G., and Kissling, E. (1996): Geophysical-geological transect and tectonic evolution of the Swiss-Italian Alps. Tectonics 15, 1036-1064.

Schmid, S.M. and Kissling, E. (2000): The arc of the western Alps in the light of geophysical data on deep crustal structure. Tectonics 19, 62-85.

Schmid, S.M., Fügenschuh, B., Kissling, E., and Schuster, R. (2004): Tectonic map and overall architecture of the Alpine orogen. Eclogae geol. Helv. 97, 93-117.

Schmidt, M.W. and Poli, S. (1998): Experimentally based water budgets for dehydrating slabs and consequences for arc magma generation. Earth Planet. Sci. Lett. 163, 361-379.

Schoneveld, C. (1977): A study of some typical inclusion patterns in strongly paracrystalline-rotated garnets. Tectonophysics 39, 453-471.

Spandler, C., Pettke, T., and Rubatto, D. (2011): Internal and external fluid sources for eclogite-facies veins in the Monviso Meta-ophiolite, Western Alps: Implications for fluid flow in subduction zones. J. Petrol. 52, 1207-1236.

Stampfli, G.M., Borel, G.D., Marchant, R., and Mosar, J. (2002): Western Alps geological constraints on western Tethyan reconstructions. J. Virt. Expl. 8, 77-106.

Steck, A. (1989): Structures des déformations alpines dans la région de Zermatt. Schweiz. Min.. Petr. Mitt 69, 205-210.

Steck, A. Bigioggero, B., Dal Piaz, G.V., Escher, A., Martinotti, G., and Masson, H. (1999): Carte tectonique des Alpes de Suisse occidentale et des régions avoisinantes 1:100.000, Carte spèc. n. 123 (4 maps). Serv. Hydrol. Géol. Nat., Bern.

Stipp, M., Stünitz, H., Heilbronner, R., and Schmid, S.M. (2002): The eastern Tonale fault zone: a "natural laboratory" for crystal plastic deformation of quartz over a temperature range from 250 to 700° C. J. Struct. Geol. 24, 1861-1884.

Stöckhert, B., Massonne, H.J., and Nowlan, E.U. (1997): Low differential stress during high-pressure metamorphism: The microstructural record of a metapelite from the Eclogite Zone, Tauern Window, Eastern Alps. Lithos 41, 103-118.

Stüwe, K. and Schuster, R. (2010): Initiation of subduction in the Alps: Continent or ocean?. Geology 38, 175-178.

Tamagno, E. (2000): L'unitá meta-ofiolitica di pressione molto alta del Lago di Cignana (Valtournenche – Aosta) e le sue relazioni con le unitá tettoniche vicine. Unpubl. M.Sc. thesis, University of Torino (Italy), 188 pp.

Terry, M.P. and Heidelbach, F. (2006): Deformation-enhanced metamorphic reactions and the rheology of high-pressure shear zones, Western Gneiss Region, Norway. J. Met. Geol. 24, 3-18.

Thöni, M. (2006): Dating eclogite-facies metamorphism in the Eastern Alps – approaches, results, interpretations: a review. Mineral. Petrol. 88, 123-148.

Vannay, J.C. and Allemann, R. (1990): La Zone Piémontaise dans le Haut-Valtournanche (Val d'Aoste, Italie). Eclogae Geol. Helv. 83/1, 21-39.

Vitale Brovarone, A., Beltrando, M., Malavieille, J., Giuntoli, F., Tondella, E., Groppo, C., Beyssac, O., and Compagnoni, R. (2011): Inherited Ocean-Continent Transition zones in deeply subducted terranes: Insights from Alpine Corsica. Lithos 124, 273-290.

Warren, C.J., Beaumont, C., and Jamieson, R.A. (2008): Modelling tectonic styles and ultra-high pressure (UHP) rock exhumation during the transition from oceanic subduction to continental collision. Earth Planet. Sci. Lett. 267, 129-145.

Weber, S., Sandmann, S., Fonseca, R.O.C., Froitzheim, N., Münker, C., and Bucher, K. (accepted): Dating the beginning of Piemonte-Liguria Ocean subduction: Lu-Hf garnet chronometry of eclogites from the Theodul Glacier Unit (Zermatt-Saas Zone, Switzerland). Swiss J. Geosci..

Wheeler, J. and Butler, R.W.H. (1993): Evidence for extension in the western Alpine orogen: the contact between the oceanic Piemonte and overlying continental Sesia units. Earth Planet. Sci. Lett. 117, 457-474.

Wheeler, J., Reddy, S. M., and Cliff, R.A. (2001): Kinematic linkage between internal zone extension and shortening in more external units in the NW Alps. J. Geol. Soc. 158, 439-443.

Wust, G.S. and Silverberg, D.S. (1989): Northern Combin zone complex – Dent Blanche nappe contact: extension within the convergent Alpine belt. Schweiz. Mineral. Petrograph. Mitt. 69, 251-259.

Yamato, P., Burov, E., Agard, P., Le Pourhiet, L., and Jolivet, L. (2008): HP-UHP exhumation during slow continental subduction: Self-consistent thermodynamically and thermomechanically coupled model with application to the Western Alps. Earth Planet. Sci. Lett. 271, 63-74.

Zack, T. and John, T. (2007): An evaluation of reactive fluid flow and trace element mobility in subducting slabs. Chem. Geol. 239, 199-216.

Acknowledgements

Many people contributed to this project and thesis with their personal, scientific, technical, and financial support. I hope to have included most of them in these acknowledgements.

Before all others, I thank Ashlea Wainwright for her endless love, her constant encouragement, and her guidance through darkest moments. Without her, I would not have been able to finish this thesis. She also proofread large parts of this thesis for which I am very grateful.

I thank my parents for their encouragement, financial support, and lending me their car for field work on several occasions. I also thank the rest of my family for their support and encouragement.

I especially thank my supervisor Thorsten Nagel for his support, scientific advice, and discussions on many different topics.

I owe special thanks to Reiner Kleinschrodt from Cologne University for spontaneously stepping in as reviewer.

I also and especially thank …

… Niko Froitzheim for giving me the opportunity to start this PhD project.
… Bernd Leiss for the opportunity to use the x-ray texture goniometer at Geowissenschaftliches Zentrum, University of Göttingen.
… Rebecca Kühn for handling the texture goniometer and managing measurements.
… Sebastian Weber for help in the field and numerous discussions on Alpine geology.
… Sascha Sandmann for practically sharing an office with me and many fruitful discussions.
… Jacek Kossak for his company in the institute and discussions on (micro)structural topics.
… Irena Miladinova for her company in the institute and discussions on geochronological topics.
… Kathrin Faßmer and Gerrit Obermüller for their participation in the project and for providing very interesting age data and mapping results.
… Roman Giesbrecht for cutting and preparing samples and thin-sections as well as looking for zircons in vain.
… Derya Gürer for her company in the institute and elsewhere, for making talk arrangements, and for dissecting a metagabbro sample in search of zircons.
… Nils Jung for the preparation of ca. 400 thin-sections.
… Radegund Hoffbauer for performing XRF analyses and Doro Pahsmann for preparing tablets for XRF analyses.
… Thorsten Geisler-Wierwille and Frank Tomaschek for letting us check “zircons“ with the Raman spectrometer.
… Raúl Fonseca and Alex Heuser for managing LA-ICPMS measurements.
… Daniela Bungartz, Dagmar Hambach, and Elke Haque for handling bureaucratic matters.
… Thorsten Geisler-Wierwille and Chris Ballhaus for their encouragement and interest in my project.

… Alessandro Bragagni for his selfless effort in communicating with Italians on the phone.
… Jan Pleuger for interesting discussions and getting me started on the literature about my study area and the Swiss-Italian Western Alps
… Hemin Koyi for the offer to perform analogue modelling at the Geological Institute of Uppsala university and discussions on faults and shear zones with opposing shear senses.

This project and my thesis were financially supported by scholarships from the Rheinische Friedrich-Wilhelms-Universität Bonn (2 years) and the Deutscher Akademischer Austauschdienst (1 month) as well as funding from DFG-grant FR 700/15-1 (13 months), Niko Froitzheim, Thorsten Nagel, and my family which are all greatly acknowledged.

Appendix

- List of conference abstracts
- Electron microprobe analyses
- Table of samples
- Map with sample locations

List of conference abstracts

- Kirst, F., Froitzheim, N., Nagel, T.J., and Pleuger, J. (2011): Deformation along the Combin Fault and the Dent Blanche Basal Thrust. CorseAlp 2011, St. Florent, Corsica.

- Kirst, F., Froitzheim, N., Nagel, T.J., Leiss, B., and Pleuger, J. (2012): The role of extraction and out-of-sequence thrusting of nappes for the exhumation of (ultra)high-pressure rocks – A case study from Lago di Cignana (Western Alps, Italy). TSK14, Kiel, Germany.

- Kirst, F., Froitzheim, N., Nagel, T.J., Leiss, B., and Pleuger, J. (2012): Extraction faulting and out-of-sequence thrusting in collisional orogeny – An example from the Swiss-Italian Western Alps. Geophysical Research Abstracts, Vol. 14, EGU2012-2846, EGU General Assembly 2012, Vienna, Austria.

- Kirst, F., Froitzheim, N., and Nagel, T.J. (2013): The structure and evolution of the Becca d'Aver continental sliver in the Western Alps (Valtournenche, Italy): A first ascent. Geophysical Research Abstracts, Vol. 15, EGU2013-7833-1, EGU General Assembly 2013, Vienna, Austria.

- Kirst, F., Froitzheim, N., and Nagel, T.J. (2013): Progressive orogenic deformation recorded in a mylonite sample from the Dent Blanche Basal Thrust (Pennine Alps). Geophysical Research Abstracts, Vol. 15, EGU2013-7717, EGU General Assembly 2013, Vienna, Austria.

- Kirst, F., Nagel, T.J., Froitzheim, N., Faßmer, K., and Sandmann, S. (2013): Alpine metamorphism in the continental Etirol-Levaz slice (Western Alps, Italy) – Insights from petrological, thermodynamic and geochronological investigations. Alpine Workshop 2013, Schladming, Austria.

- Kirst, F., Nagel, T.J., and Froitzheim, N. (2013): Metamorphism and fluid-rock interactions during subduction and accretion – an example from the Western Alps (Valtournenche, Italy). Geofluids 2013, Tübingen, Germany.

- Kirst, F., Nagel, T.J., and Leiss, B. (2014): Progressive orogenic deformation of the Penninic units at Lago di Cignana (Western Alps, Italy). GeoFrankfurt 2014, Frankfurt, Germany.

Electron microprobe analyses

Sample FD34

Measurement	SiO_2	Al_2O_3	MgO	FeO	CaO	MnO	TiO_2	Na_2O	K_2O	Cr_2O_3	Sum
FD34_m1	39.54	32.17	0.00	1.19	25.09	0.09	0.14	0.01	0.00	0.03	98.26
FD34_m2	68.90	19.71	0.00	0.02	0.06	0.00	0.00	11.51	0.06	0.00	100.26
FD34_m3	56.14	1.51	20.44	5.22	12.54	0.15	0.00	0.60	0.07	0.02	96.69
FD34_m4	50.95	30.07	3.63	1.56	0.03	0.02	0.19	0.20	10.86	0.04	97.55
FD34_m5	39.70	32.17	0.04	1.77	25.13	0.07	0.05	0.01	0.00	0.00	98.95
FD34_m6	27.84	21.79	25.75	10.06	0.03	0.23	0.00	0.00	0.02	0.16	85.87
FD34_m7	39.74	32.09	0.01	1.58	25.00	0.06	0.11	0.04	0.00	0.06	98.66
FD34_m8	56.13	1.34	20.21	5.66	12.20	0.25	0.01	0.66	0.08	0.00	96.53
FD34_m9	68.38	19.62	0.00	0.04	0.03	0.00	0.02	11.63	0.09	0.00	99.82
FD34_m10	28.75	21.92	25.85	9.84	0.11	0.19	0.01	0.02	0.02	0.07	86.77
FD34_m11	53.00	28.36	3.66	1.09	0.02	0.00	0.15	0.37	10.38	0.21	97.23
FD34_m12	53.02	26.71	4.15	1.29	0.00	0.07	0.10	0.15	10.70	0.76	96.93
FD34_m13	56.07	0.61	22.11	3.79	13.27	0.10	0.04	0.22	0.04	0.00	96.25
FD34_m14	28.74	19.94	26.87	9.97	0.00	0.19	0.04	0.02	0.00	0.15	85.93
FD34_m15	39.47	32.36	0.00	0.88	25.31	0.00	0.06	0.00	0.01	0.19	98.28
FD34_m16	67.33	19.74	0.00	0.02	0.12	0.03	0.03	11.53	0.08	0.03	98.91
FD34_m17	68.44	19.79	0.00	0.03	0.04	0.01	0.00	11.72	0.06	0.02	100.10
FD34_m18	52.50	27.48	3.94	1.07	0.04	0.00	0.14	0.17	11.11	0.94	97.38
FD34_m19	38.64	32.49	0.00	0.96	25.12	0.01	0.07	0.02	0.00	0.23	97.53
FD34_m20	52.17	27.79	3.80	1.08	0.07	0.02	0.12	0.25	10.58	0.45	96.32
FD34_m21	56.34	0.72	20.68	5.10	13.06	0.09	0.01	0.27	0.00	0.08	96.35
FD34_m22	38.78	32.53	0.01	1.15	25.19	0.00	0.05	0.02	0.00	0.04	97.76
FD34_m23	55.96	1.46	20.28	5.05	12.68	0.21	0.00	0.55	0.04	0.04	96.27
FD34_m24	56.02	0.84	21.68	4.58	13.61	0.15	0.00	0.11	0.00	0.06	97.04
FD34_m25	28.07	21.57	26.06	9.78	0.04	0.19	0.02	0.02	0.00	0.04	85.79
FD34_m26	54.98	2.09	20.74	4.86	13.34	0.13	0.04	0.28	0.05	0.00	96.52
FD34_m27	28.40	21.20	25.95	9.46	0.13	0.13	0.00	0.00	0.00	0.06	85.34
FD34_m28	39.25	33.17	0.00	0.57	24.97	0.08	0.14	0.02	0.01	0.05	98.26
FD34_m29	38.96	32.10	0.05	1.83	24.83	0.06	0.09	0.00	0.01	0.04	97.98
FD34_m30	56.51	0.92	20.78	5.01	12.87	0.18	0.02	0.40	0.03	0.04	96.77
FD34_m31	56.21	0.74	21.14	4.89	13.11	0.11	0.00	0.25	0.02	0.00	96.48
FD34_m32	53.51	27.10	3.99	1.33	0.00	0.07	0.13	0.19	10.13	1.21	97.66
FD34_m33	28.08	21.81	26.33	9.49	0.04	0.18	0.02	0.00	0.01	0.00	85.96
FD34_m34	38.75	32.35	0.02	1.14	25.09	0.08	0.02	0.00	0.00	0.09	97.54
FD34_m35	39.00	31.78	0.00	2.12	24.87	0.07	0.01	0.00	0.01	0.03	97.89
FD34_m36	51.92	27.87	3.52	1.20	0.01	0.00	0.15	0.42	9.80	0.89	95.77
FD34_m37	57.17	0.88	21.17	4.25	13.08	0.13	0.00	0.29	0.03	0.06	97.06

Sample FD244

Measurement	SiO_2	Al_2O_3	MgO	FeO	CaO	MnO	TiO_2	Na_2O	K_2O	Cr_2O_3	Sum
FD244_m1	38.86	30.11	0.08	3.95	24.45	0.07	0.07	0.04	0.00	0.04	97.67
FD244_m2	38.16	28.37	0.06	6.15	24.23	0.03	0.07	0.00	0.03	0.01	97.10
FD244_m3	47.55	40.53	0.09	0.33	0.17	0.02	0.06	7.10	0.54	0.02	96.39
FD244_m4	46.85	39.30	0.11	0.35	0.21	0.05	0.04	6.48	0.65	0.05	94.09
FD244_m5	57.88	11.67	11.98	7.07	0.89	0.06	0.00	7.10	0.04	0.02	96.71
FD244_m6	51.40	28.76	3.12	1.70	0.04	0.03	0.22	0.69	9.72	0.00	95.68
FD244_m7	51.56	7.98	14.12	9.88	8.59	0.18	0.11	3.21	0.18	0.03	95.84

FD244_m8	57.53	11.33	12.24	7.57	1.04	0.04	0.01	6.96	0.01	0.00	96.71
FD244_m9	48.40	10.41	12.34	12.83	8.64	0.14	0.21	3.61	0.26	0.03	96.85
FD244_m10	37.90	21.66	5.00	27.49	7.86	0.44	0.07	0.10	0.01	0.00	100.54
FD244_m11	37.67	21.73	4.35	27.30	8.51	0.45	0.09	0.14	0.02	0.02	100.25
FD244_m12	51.41	7.63	13.67	11.67	8.44	0.14	0.04	3.32	0.14	0.01	96.46
FD244_m13	57.26	11.01	12.55	7.17	1.13	0.00	0.00	6.91	0.03	0.03	96.09
FD244_m14	0.00	0.02	17.48	6.76	28.27	0.33	0.00	0.04	0.01	0.00	52.91
FD244_m15	67.68	20.21	0.12	0.28	0.59	0.07	0.04	11.01	0.06	0.00	100.06
FD244_m16	38.52	29.70	0.06	4.62	24.39	0.10	0.09	0.00	0.00	0.04	97.50
FD244_m17	38.17	28.38	0.06	6.38	24.01	0.08	0.10	0.00	0.00	0.04	97.22
FD244_m18	49.98	29.07	2.95	2.28	0.16	0.00	0.17	0.72	10.01	0.05	95.40
FD244_m19	39.03	32.13	0.05	1.79	24.52	0.00	0.07	0.04	0.00	0.04	97.66
FD244_m20	46.49	39.22	0.13	0.29	0.18	0.05	0.10	6.84	0.71	0.04	94.05
FD244_m21	94.82	0.00	0.00	0.03	0.01	0.00	0.01	0.02	0.00	0.01	94.89
FD244_m22	58.29	11.64	11.99	7.36	0.64	0.00	0.02	7.09	0.03	0.06	97.11
FD244_m23	56.56	11.82	10.27	9.52	1.34	0.11	0.06	7.12	0.01	0.00	96.80
FD244_m24	47.24	11.48	12.10	13.32	8.88	0.28	0.07	3.56	0.31	0.00	97.23
FD244_m25	58.11	11.35	12.46	6.76	0.89	0.04	0.00	6.99	0.01	0.11	96.72
FD244_m26	57.00	11.13	12.23	7.33	0.83	0.05	0.00	6.87	0.00	0.06	95.48
FD244_m27	67.99	19.52	0.02	0.32	0.27	0.00	0.00	11.26	0.02	0.02	99.42
Line 1	39.33	22.51	9.42	24.26	4.75	0.67	0.00	0.00	0.01	0.02	100.97
Line 2	39.34	22.54	8.41	25.28	4.89	0.20	0.03	0.00	0.00	0.01	100.70
Line 3	38.74	19.47	8.42	25.44	4.99	0.33	0.03	0.04	0.04	0.04	97.53
Line 4	39.40	22.11	7.98	25.89	5.28	0.30	0.02	0.03	0.01	0.01	101.02
Line 5	39.13	22.37	7.79	26.13	5.28	0.30	0.05	0.00	0.00	0.02	101.07
Line 6	38.48	22.97	7.39	26.73	5.21	0.27	0.01	0.04	0.00	0.00	101.08
Line 7	39.13	22.37	7.13	26.99	5.60	0.30	0.00	0.03	0.00	0.03	101.58
Line 8	39.18	22.03	6.55	28.04	5.61	0.32	0.05	0.00	0.01	0.00	101.78
Line 9	39.02	21.88	6.27	27.65	6.00	0.24	0.00	0.03	0.01	0.03	101.12
Line 10	38.66	22.17	5.74	27.77	6.20	0.32	0.04	0.06	0.00	0.00	100.96
Line 11	38.83	21.79	5.53	28.23	6.23	0.32	0.01	0.03	0.00	0.02	100.97
Line 12	38.80	21.96	5.14	29.44	6.48	0.26	0.00	0.03	0.00	0.04	102.14
Line 13	38.59	21.53	4.50	28.79	6.86	0.38	0.04	0.02	0.01	0.05	100.77
Line 14	38.27	21.64	4.03	29.79	7.24	0.51	0.07	0.01	0.00	0.03	101.58
Line 15	38.27	21.69	3.98	29.76	7.32	0.69	0.02	0.04	0.00	0.04	101.81
Line 16	38.25	21.63	3.72	29.39	7.80	0.71	0.06	0.05	0.01	0.00	101.62
Line 17	38.37	21.52	3.72	29.26	8.06	0.75	0.19	0.01	0.01	0.03	101.92
Line 18	38.16	21.83	3.34	28.89	8.01	0.79	0.20	0.00	0.01	0.05	101.28
Line 19	38.17	21.41	2.92	28.69	9.02	0.79	0.09	0.05	0.02	0.00	101.17
Line 20	27.08	24.91	1.68	27.68	8.62	0.82	0.05	0.00	0.00	0.04	90.88
Line 21	37.89	21.67	2.72	28.85	8.96	0.84	0.07	0.04	0.00	0.00	101.03
Line 22	38.12	21.57	2.68	28.67	9.20	0.88	0.13	0.02	0.00	0.01	101.27
Line 23	38.26	21.54	2.91	28.60	8.65	0.92	0.08	0.03	0.00	0.02	101.02
Line 24	91.30	0.82	0.05	1.05	0.37	0.09	0.04	0.00	0.00	0.01	93.73
Line 25	38.45	21.15	2.65	27.48	10.14	0.71	0.25	0.05	0.00	0.06	100.93
Line 26	38.43	21.45	3.05	27.61	9.49	0.74	0.08	0.05	0.00	0.02	100.91
Line 27	60.60	8.95	6.75	7.00	10.84	0.08	0.03	6.02	0.02	0.02	100.30
Line 28	37.90	21.44	2.61	27.54	9.83	0.82	0.12	0.00	0.00	0.00	100.27
Line 29	37.91	21.33	2.88	28.51	8.95	0.78	0.10	0.00	0.00	0.02	100.49
Line 30	37.92	21.14	3.00	28.60	9.00	0.69	0.08	0.03	0.00	0.05	100.51
Line 31	38.71	21.51	3.66	28.50	8.45	0.71	0.03	0.13	0.01	0.02	101.71
Line 32	46.49	12.30	6.32	16.37	11.24	0.11	0.20	5.76	0.34	0.03	99.17
Line 33	38.18	21.32	3.60	29.31	7.87	0.80	0.11	0.05	0.00	0.06	101.30
Line 34	54.91	8.20	8.15	8.10	13.20	0.04	0.03	6.85	0.02	0.03	99.53
Line 35	38.11	21.72	3.77	29.13	7.64	0.72	0.05	0.02	0.00	0.01	101.17

Line 36	38.06	21.78	4.22	28.66	7.49	0.59	0.03	0.03	0.00	0.01	100.86
Line 37	38.08	22.27	4.45	29.29	7.01	0.41	0.06	0.01	0.00	0.02	101.60
Line 38	38.69	22.01	5.62	28.16	6.59	0.29	0.05	0.00	0.00	0.04	101.45
Line 39	38.77	22.19	6.66	27.78	5.87	0.31	0.00	0.04	0.02	0.07	101.70
Line 40	39.04	22.35	7.49	27.43	5.38	0.27	0.04	0.01	0.01	0.03	102.04
FD244_m28	38.42	21.71	4.38	29.18	6.94	0.54	0.01	0.03	0.02	0.04	101.26

Sample FD306

Measurement	SiO_2	Al_2O_3	MgO	FeO	CaO	MnO	TiO_2	Na_2O	K_2O	Cr_2O_3	Sum
FD306_m1	51.31	2.98	14.20	7.61	22.08	0.26	0.90	0.47	0.00	0.09	99.91
FD306_m2	49.91	6.15	14.84	12.38	12.06	0.20	0.65	1.76	0.06	0.04	98.03
FD306_m3	38.59	25.40	0.00	9.78	23.62	0.09	0.13	0.00	0.01	0.00	97.63
FD306_m4	38.70	27.70	0.01	7.40	24.27	0.02	0.08	0.04	0.00	0.02	98.23
FD306_m5	38.28	26.27	3.33	2.74	22.28	0.20	0.03	0.14	0.02	0.04	93.33
FD306_m6	56.91	0.59	18.91	8.33	13.07	0.09	0.02	0.28	0.02	0.00	98.23
FD306_m7	56.16	0.89	19.04	7.87	13.20	0.20	0.01	0.29	0.04	0.01	97.71
FD306_m8	38.02	25.97	3.40	2.68	22.44	0.31	0.11	0.16	0.00	0.06	93.15
FD306_m9	56.32	0.69	18.47	9.04	12.92	0.03	0.00	0.38	0.01	0.02	97.87
FD306_m10	27.84	20.17	20.77	16.59	0.27	0.23	0.09	0.00	0.03	0.21	86.20
FD306_m11	69.35	20.47	0.01	0.05	0.07	0.07	0.00	11.42	0.02	0.00	101.45
FD306_m12	69.72	20.04	0.02	0.09	0.10	0.00	0.02	12.77	0.03	0.00	102.77
FD306_m13	69.45	19.91	0.00	0.09	0.03	0.04	0.05	11.88	0.02	0.00	101.47
FD306_m14	38.47	25.64	0.03	9.86	24.01	0.06	0.03	0.00	0.00	0.00	98.09
FD306_m15	38.27	25.70	3.26	3.18	22.28	0.21	0.17	0.14	0.01	0.03	93.25
FD306_m16	39.16	28.27	0.03	6.56	24.35	0.00	0.11	0.03	0.00	0.00	98.50
FD306_m17	38.22	25.25	0.00	10.86	23.65	0.03	0.03	0.03	0.01	0.02	98.10
FD306_m18	38.48	26.94	0.01	8.12	23.95	0.10	0.05	0.02	0.00	0.00	97.67
FD306_m19	38.06	26.08	3.34	2.90	22.49	0.20	0.12	0.14	0.01	0.00	93.34
FD306_m20	68.54	19.95	0.02	0.11	0.04	0.00	0.03	11.60	0.02	0.03	100.33
FD306_m21	27.49	19.91	20.92	16.16	0.12	0.19	0.01	0.04	0.01	0.02	84.87
FD306_m22	68.28	20.18	0.01	0.10	0.07	0.00	0.02	11.88	0.04	0.00	100.57
FD306_m23	38.29	25.81	0.00	9.45	23.83	0.05	0.12	0.02	0.01	0.00	97.59
FD306_m24	38.70	26.18	3.73	1.60	21.90	0.19	0.08	0.16	0.01	0.03	92.58
FD306_m25	37.96	26.00	3.42	2.63	22.26	0.18	0.05	0.10	0.00	0.00	92.61
FD306_m26	68.76	19.95	0.00	0.29	0.18	0.00	0.01	11.73	0.04	0.00	100.95
FD306_m27	38.39	25.84	0.01	9.67	23.89	0.08	0.04	0.00	0.01	0.01	97.95
FD306_m28	40.63	27.50	0.02	5.66	23.66	0.10	0.06	0.44	0.00	0.00	98.06
FD306_m29	27.87	20.14	20.74	18.31	0.08	0.19	0.02	0.01	0.01	0.00	87.35
FD306_m30	51.47	2.72	13.94	9.28	20.93	0.29	0.94	0.59	0.03	0.01	100.20
FD306_m31	51.04	2.80	14.08	8.59	21.28	0.25	0.85	0.49	0.01	0.06	99.46
FD306_m32	28.11	19.62	20.51	18.97	0.03	0.15	0.00	0.01	0.02	0.00	87.41
FD306_m33	52.71	3.10	18.00	9.06	12.71	0.17	0.30	0.93	0.03	0.05	97.05
FD306_m34	51.84	1.88	14.77	8.47	21.61	0.28	0.52	0.44	0.01	0.01	99.82
FD306_m35	56.18	0.51	18.41	9.22	12.83	0.13	0.00	0.22	0.03	0.00	97.52
FD306_m36	28.02	20.34	21.49	17.68	0.09	0.22	0.05	0.03	0.01	0.03	87.97
FD306_m37	42.66	11.96	13.07	13.16	11.04	0.11	3.70	3.10	0.16	0.07	99.03
FD306_m38	28.40	19.94	21.56	17.89	0.02	0.16	0.01	0.02	0.02	0.04	88.04
FD306_m39	69.31	20.15	0.00	0.23	0.05	0.02	0.02	11.88	0.04	0.02	101.71
FD306_m40	38.19	25.06	0.00	10.35	23.54	0.03	0.00	0.00	0.01	0.01	97.19
FD306_m41	55.75	0.73	18.66	9.07	12.88	0.16	0.00	0.34	0.01	0.00	97.60
FD306_m42	68.17	20.33	0.05	0.07	0.54	0.04	0.00	11.41	0.04	0.00	100.65
FD306_m43	37.85	26.04	3.52	2.41	22.46	0.09	0.01	0.11	0.01	0.00	92.51
FD306_m44	29.03	20.71	24.64	13.13	0.07	0.25	0.01	0.02	0.01	0.04	87.89

Sample FD351

Measurement	SiO_2	Al_2O_3	MgO	FeO	CaO	MnO	TiO_2	Na_2O	K_2O	Cr_2O_3	Sum
FD351_m1	52.80	27.31	3.28	3.83	0.04	0.00	0.14	0.19	9.61	0.00	97.21
FD351_m2	45.11	25.50	6.58	5.73	0.04	0.09	0.24	0.10	8.68	0.03	92.10
FD351_m3	52.24	29.41	2.70	3.13	0.02	0.04	0.12	0.12	10.24	0.00	98.01
FD351_m4	38.11	24.76	0.01	10.55	23.46	0.15	0.05	0.00	0.04	0.05	97.17
FD351_m5	69.40	19.91	0.02	0.26	0.32	0.02	0.54	11.65	0.06	0.00	102.18
FD351_m6	68.36	19.51	0.00	0.40	0.08	0.02	0.06	12.15	0.04	0.00	100.62
FD351_m7	38.16	23.66	13.54	11.08	0.03	0.19	0.06	0.09	3.95	0.00	90.75
FD351_m8	50.85	28.95	2.55	2.65	0.05	0.09	0.11	0.08	10.28	0.04	95.66
FD351_m9	27.20	21.58	20.23	17.05	0.16	0.49	0.15	0.00	0.01	0.05	86.91
FD351_m10	51.13	28.80	2.76	2.47	0.06	0.00	0.16	0.18	9.83	0.00	95.39
FD351_m11	53.55	26.84	3.04	3.92	0.06	0.02	0.22	0.17	10.43	0.00	98.24
FD351_m12	51.73	28.48	2.70	3.13	0.03	0.00	0.14	0.15	10.32	0.01	96.70
FD351_m13	38.78	28.34	0.00	6.24	24.02	0.09	0.18	0.00	0.01	0.00	97.66
FD351_m14	38.43	27.07	0.28	7.88	23.66	0.22	0.09	0.03	0.01	0.08	97.75
FD351_m15	27.39	20.85	20.48	16.78	0.10	0.41	0.03	0.00	0.01	0.04	86.10
FD351_m16	69.74	19.80	0.00	0.08	0.10	0.03	0.02	11.79	0.04	0.02	101.63
FD351_m17	68.54	19.88	0.01	0.18	0.06	0.00	0.00	11.74	0.05	0.05	100.52
FD351_m18	27.49	21.06	20.28	17.27	0.12	0.42	0.10	0.00	0.03	0.02	86.77
FD351_m19	52.50	27.07	3.07	3.24	0.02	0.05	0.16	0.54	10.44	0.04	97.14
FD351_m20	69.39	19.77	0.00	0.16	0.14	0.03	0.09	11.68	0.03	0.01	101.30
FD351_m21	37.44	23.15	0.00	12.55	23.47	0.20	0.07	0.03	0.01	0.00	96.91
FD351_m22	3.21	0.87	0.00	0.34	52.73	0.06	0.09	0.19	0.00	0.00	57.49
FD351_m23	30.50	1.35	0.03	0.48	28.19	0.02	76.81	0.02	0.01	0.06	137.46
FD351_m24	26.87	21.40	20.42	17.11	0.19	0.37	0.46	0.00	0.04	0.00	86.86
FD351_m25	27.40	21.01	20.18	16.95	0.11	0.40	0.14	0.04	0.06	0.00	86.29
FD351_m26	38.07	24.89	0.00	10.40	23.70	0.33	0.13	0.01	0.00	0.01	97.53
FD351_m27	97.58	0.00	0.00	0.15	0.05	0.00	0.22	0.02	0.00	0.06	98.07
FD351_m28	27.34	21.27	20.22	16.65	0.18	0.43	0.65	0.00	0.01	0.00	86.75
FD351_m29	96.23	0.00	0.00	0.03	0.06	0.05	0.07	0.01	0.00	0.00	96.44
FD351_m30	27.81	20.57	20.88	16.85	0.17	0.42	0.11	0.00	0.02	0.03	86.85
FD351_m31	26.97	21.54	20.16	17.42	0.12	0.40	0.16	0.03	0.04	0.00	86.83
FD351_m32	27.13	21.49	20.35	17.15	0.08	0.30	0.01	0.02	0.01	0.00	86.54
FD351_m33	34.97	21.47	0.09	10.82	19.83	0.31	3.82	0.00	0.01	0.00	91.32
FD351_m34	37.89	24.51	0.00	10.84	23.36	0.28	0.31	0.00	0.00	0.00	97.19
FD351_m35	38.62	27.70	0.01	6.77	23.82	0.08	0.12	0.00	0.02	0.08	97.22
FD351_m36	37.91	23.28	0.00	11.90	23.37	0.23	0.03	0.03	0.00	0.00	96.75
FD351_m37	27.56	21.07	20.89	15.76	0.14	0.31	0.19	0.03	0.02	0.02	85.98
FD351_m38	96.66	0.00	0.00	0.23	0.04	0.00	0.06	0.00	0.01	0.02	97.02
FD351_m39	26.91	21.49	19.90	17.64	0.10	0.33	0.08	0.01	0.01	0.00	86.48
FD351_m40	27.40	20.84	21.21	16.24	0.10	0.45	0.07	0.04	0.00	0.07	86.43
FD351_m41	51.73	27.18	3.07	3.52	0.09	0.08	0.14	0.19	10.01	0.02	96.02
FD351_m42	27.26	21.03	21.07	16.57	0.02	0.49	0.06	0.01	0.02	0.01	86.53
FD351_m43	52.06	27.77	3.29	3.11	0.05	0.00	0.15	0.16	10.24	0.04	96.87
FD351_m44	68.90	19.88	0.00	0.18	0.06	0.00	0.09	11.87	0.07	0.01	101.06
FD351_m45	47.46	26.49	5.13	4.49	0.03	0.00	0.16	0.12	8.81	0.03	92.72
FD351_m46	52.68	27.85	2.89	2.73	0.03	0.08	0.12	0.13	10.71	0.00	97.20
FD351_m47	96.68	0.00	0.00	0.06	0.00	0.03	0.00	0.02	0.02	0.00	96.81
FD351_m48	27.55	20.78	20.07	17.77	0.01	0.37	0.12	0.02	0.00	0.01	86.69
FD351_m49	34.21	20.15	0.25	10.91	18.92	0.33	0.19	0.00	0.00	0.00	84.96
FD351_m50	30.57	1.85	0.00	0.67	28.38	0.00	70.46	0.01	0.01	0.03	131.96

FD351_m51	30.31	1.55	0.07	0.62	28.65	0.07	37.62	0.00	0.01	0.11	99.00
FD351_m52	35.09	23.42	16.36	13.87	0.08	0.30	0.04	0.12	2.39	0.00	91.65
FD351_m53	46.28	26.44	6.60	5.01	0.05	0.02	0.04	0.12	7.45	0.01	92.02
FD351_m54	31.62	23.31	18.65	15.00	0.07	0.26	0.07	0.07	1.49	0.02	90.54
FD351_m55	29.51	22.73	20.61	16.02	0.06	0.39	0.00	0.02	0.55	0.00	89.90
FD351_m56	39.03	27.86	0.02	7.07	23.97	0.19	0.12	0.01	0.02	0.00	98.30
FD351_m57	38.82	27.89	0.01	7.22	24.07	0.16	0.05	0.00	0.04	0.00	98.25
FD351_m58	51.91	29.87	3.06	2.75	0.02	0.06	0.09	0.09	10.34	0.02	98.20
FD351_m59	38.21	26.48	0.03	8.80	23.70	0.29	0.05	0.00	0.12	0.01	97.68
FD351_m60	37.66	23.86	0.01	12.18	23.10	0.31	0.04	0.01	0.09	0.00	97.26
FD351_m61	51.88	28.52	3.12	3.39	0.12	0.00	0.10	0.29	9.56	0.02	96.98
FD351_m62	70.01	20.50	0.00	0.06	0.04	0.04	0.07	11.85	0.02	0.01	102.61
FD351_m63	29.83	0.69	0.00	0.10	28.72	0.01	41.70	0.04	0.01	0.00	101.10
FD351_m64	69.37	20.18	0.00	0.15	0.05	0.00	0.02	11.95	0.04	0.00	101.76
FD351_m65	97.09	0.01	0.00	0.13	0.01	0.00	0.07	0.01	0.01	0.00	97.33
FD351_m66	51.98	29.24	3.10	3.23	0.05	0.09	0.10	0.16	10.20	0.02	98.16
FD351_m67	52.41	27.38	3.30	3.43	0.10	0.07	0.09	0.24	10.14	0.03	97.17
FD351_m68	52.30	30.25	2.65	2.78	0.08	0.06	0.07	0.08	10.37	0.02	98.66
FD351_m69	70.09	20.52	0.00	0.20	0.09	0.00	0.00	11.50	0.05	0.03	102.47
FD351_m70	95.83	0.01	0.00	0.14	0.04	0.00	0.00	0.00	0.02	0.00	96.03
FD351_m71	95.33	0.00	0.00	0.00	0.02	0.00	0.02	0.00	0.00	0.00	95.37
FD351_m72	27.17	21.70	19.59	19.11	0.00	0.47	0.06	0.00	0.01	0.00	88.11
FD351_m73	27.01	21.16	19.03	20.61	0.00	0.46	0.07	0.00	0.01	0.00	88.34
FD351_m74	47.11	21.68	0.09	10.70	21.09	0.20	0.05	0.01	0.01	0.00	100.94
FD351_m75	96.19	0.08	0.02	0.25	0.01	0.01	0.02	0.03	0.00	0.00	96.61
FD351_m76	27.58	21.53	21.11	16.99	0.05	0.35	0.00	0.04	0.02	0.01	87.67
FD351_m77	39.13	28.39	0.00	6.10	24.03	0.09	0.10	0.03	0.00	0.00	97.87
FD351_m78	38.49	27.13	0.04	7.78	23.85	0.17	0.05	0.01	0.00	0.00	97.51
FD351_m79	37.93	23.77	0.03	11.72	23.28	0.21	0.02	0.02	0.00	0.00	96.99
FD351_m80	27.71	22.26	21.22	16.64	0.01	0.44	0.04	0.01	0.00	0.00	88.33
FD351_m81	27.26	22.13	19.83	17.72	0.00	0.49	0.02	0.02	0.02	0.01	87.50

Sample FD356

Measurement	SiO_2	Al_2O_3	MgO	FeO	CaO	MnO	TiO_2	Na_2O	K_2O	Cr_2O_3	Sum
FD356_m1	23.20	20.81	7.84	35.02	0.00	0.67	0.03	0.03	0.00	0.03	87.63
FD356_m2	24.64	18.94	8.32	35.01	0.05	0.58	0.02	0.07	0.04	0.02	87.68
FD356_m3	52.36	25.89	2.38	6.41	0.00	0.00	0.14	0.09	10.83	0.05	98.15
FD356_m4	48.18	31.72	1.00	4.64	0.00	0.00	0.06	0.46	10.23	0.06	96.34
FD356_m5	51.80	24.74	2.71	5.74	0.00	0.02	0.16	0.08	10.52	0.00	95.76
FD356_m6	51.81	24.86	2.67	5.98	0.00	0.02	0.19	0.03	10.82	0.02	96.39
FD356_m7	52.22	24.84	2.61	6.37	0.00	0.08	0.19	0.05	10.62	0.04	97.03
FD356_m8	51.49	25.78	2.38	6.65	0.00	0.03	0.16	0.12	10.62	0.05	97.30
FD356_m9	48.69	28.63	1.27	5.93	0.00	0.05	0.09	0.53	9.55	0.03	94.76
FD356_m10	67.70	19.37	0.00	0.01	0.03	0.00	0.01	12.34	0.03	0.00	99.49
FD356_m11	69.76	19.98	0.00	0.02	0.06	0.01	0.06	11.42	0.03	0.00	101.34
FD356_m12	67.85	19.79	0.00	0.02	0.11	0.00	0.02	12.18	0.03	0.06	100.06
FD356_m13	47.56	30.93	1.03	4.68	0.00	0.02	0.00	0.57	9.88	0.03	94.70
FD356_m14	49.25	30.37	1.26	5.48	0.00	0.03	0.14	0.27	10.69	0.03	97.52
FD356_m15	37.00	20.53	0.49	25.02	6.79	9.63	0.14	0.01	0.00	0.00	99.60
FD356_m16	37.13	20.58	0.53	27.00	6.74	8.46	0.15	0.00	0.00	0.00	100.58
FD356_m17	0.04	0.07	0.00	92.55	0.02	0.06	0.08	0.00	0.00	0.02	92.84
FD356_m18	50.28	23.71	2.36	6.88	0.00	0.00	0.16	0.07	10.72	0.01	94.19
FD356_m19	51.14	24.13	2.23	6.95	0.00	0.01	0.20	0.11	10.34	0.10	95.19

FD356_m20	36.20	32.93	7.83	4.60	0.39	0.00	0.36	2.02	0.06	0.07	84.46
FD356_m21	34.79	28.03	4.29	13.73	0.06	0.05	1.18	2.99	0.09	0.07	85.26
FD356_m22	0.02	0.00	0.01	0.06	54.31	0.09	0.05	0.01	0.01	0.00	54.56
FD356_m23	51.19	23.45	2.62	6.44	0.01	0.07	0.12	0.06	10.28	0.00	94.23
FD356_m24	52.32	24.42	2.54	6.22	0.00	0.01	0.20	0.07	10.44	0.02	96.23
FD356_m25	23.68	20.04	6.98	35.42	0.03	0.64	0.04	0.05	0.07	0.00	86.94
FD356_m26	23.74	19.44	7.05	35.50	0.03	0.67	0.12	0.00	0.00	0.00	86.55
FD356_m27	37.35	20.45	0.52	28.36	6.55	6.87	0.10	0.03	0.00	0.05	100.28
FD356_m28	37.53	20.76	0.55	30.09	5.23	7.20	0.05	0.00	0.00	0.00	101.41
FD356_m29	37.74	20.70	0.55	29.57	5.71	7.35	0.06	0.03	0.02	0.01	101.72
FD356_m30	23.86	20.70	7.11	35.64	0.01	0.79	0.07	0.00	0.04	0.00	88.21
FD356_m31	0.22	0.15	0.01	92.11	0.01	0.08	0.03	0.01	0.00	0.22	92.83
FD356_m32	51.29	26.33	2.00	5.57	0.02	0.04	0.18	0.14	10.21	0.02	95.80
FD356_m33	68.89	19.52	0.00	0.05	0.07	0.00	0.00	12.34	0.04	0.04	100.95
FD356_m34	23.89	20.75	7.20	35.31	0.01	0.69	0.04	0.00	0.01	0.02	87.92
FD356_m35	48.12	28.55	1.37	5.33	0.02	0.03	0.23	0.28	10.41	0.05	94.38
FD356_m36	23.90	20.22	7.51	35.39	0.01	0.78	0.06	0.00	0.03	0.00	87.90
FD356_m37	68.55	19.39	0.00	0.18	0.03	0.00	0.00	12.35	0.05	0.01	100.57
FD356_m38	24.72	21.60	6.50	33.32	0.01	0.66	0.05	0.05	0.50	0.01	87.41
FD356_m39	97.48	0.03	0.00	0.31	0.00	0.00	0.01	0.00	0.00	0.00	97.82
FD356_m40	23.63	21.06	7.03	34.99	0.00	0.67	0.09	0.01	0.02	0.03	87.52
FD356_m41	50.82	25.84	2.25	5.86	0.00	0.00	0.22	0.18	10.78	0.04	95.98
FD356_m42	50.86	25.03	2.42	6.22	0.00	0.00	0.24	0.12	10.82	0.04	95.73
FD356_m43	23.36	20.45	7.11	35.24	0.03	0.67	0.09	0.07	0.03	0.01	87.04
FD356_m44	51.84	23.96	2.29	6.81	0.00	0.04	0.16	0.10	10.94	0.00	96.14
FD356_m45	23.67	20.27	7.30	35.07	0.00	0.71	0.07	0.00	0.02	0.02	87.13
FD356_m46	48.74	29.11	1.33	5.37	0.01	0.05	0.00	0.42	10.13	0.00	95.16
FD356_m47	48.24	29.84	1.00	5.31	0.00	0.00	0.09	0.41	10.46	0.05	95.39
FD356_m48	23.74	20.22	7.15	35.31	0.00	0.64	0.07	0.00	0.03	0.04	87.19
FD356_m49	47.71	29.91	1.02	5.57	0.02	0.01	0.20	0.32	10.79	0.03	95.56
FD356_m50	23.90	20.09	7.48	35.44	0.01	0.66	0.05	0.00	0.02	0.00	87.66
FD356_m51	23.58	20.24	7.15	35.97	0.01	0.70	0.10	0.00	0.03	0.00	87.78
FD356_m52	23.91	20.73	7.31	35.25	0.03	0.75	0.08	0.01	0.03	0.04	88.13
FD356_m53	23.49	20.82	7.18	35.94	0.00	0.60	0.04	0.03	0.01	0.01	88.12
FD356_m54	23.71	20.58	7.14	34.92	0.01	0.63	0.12	0.06	0.06	0.01	87.23
FD356_m55	24.93	19.47	7.37	35.22	0.05	0.48	0.09	0.02	0.12	0.00	87.75
FD356_m56	24.83	18.83	7.40	35.96	0.03	0.67	0.01	0.00	0.05	0.00	87.77
FD356_m57	23.70	20.52	7.19	35.62	0.03	0.68	0.09	0.03	0.03	0.00	87.89
FD356_m58	23.87	20.45	7.38	34.82	0.03	0.48	0.07	0.06	0.05	0.00	87.20
FD356_m59	97.25	0.06	0.03	0.42	0.00	0.08	0.03	0.02	0.03	0.04	97.95
FD356_m60	48.02	29.31	1.08	5.86	0.01	0.02	0.31	0.25	10.92	0.05	95.83
FD356_m61	47.93	28.25	1.31	6.05	0.00	0.08	0.24	0.25	10.90	0.02	95.02
FD356_m62	47.44	29.12	1.22	6.07	0.01	0.00	0.26	0.22	10.92	0.01	95.27
FD356_m63	24.12	20.35	7.29	35.32	0.03	0.74	0.02	0.03	0.05	0.00	87.95
FD356_m64	68.45	19.09	0.00	0.18	0.14	0.02	0.01	12.00	0.06	0.00	99.94
FD356_m65	23.54	20.82	7.39	35.56	0.04	0.59	0.10	0.00	0.04	0.02	88.10
FD356_m66	23.43	20.76	7.19	35.29	0.02	0.65	0.10	0.00	0.04	0.02	87.50
FD356_m67	50.16	25.74	2.24	5.85	0.01	0.08	0.23	0.08	10.21	0.03	94.62
FD356_m68	51.67	23.77	2.48	6.82	0.01	0.00	0.13	0.06	10.59	0.04	95.56
FD356_m69	51.91	24.13	2.61	6.47	0.02	0.03	0.18	0.09	10.34	0.06	95.84
FD356_m70	47.77	29.46	1.10	6.20	0.01	0.00	0.21	0.75	9.94	0.00	95.44
FD356_m71	97.21	0.05	0.01	0.43	0.00	0.00	0.01	0.00	0.01	0.00	97.71
FD356_m72	49.00	25.91	2.30	5.74	0.13	0.12	0.14	0.06	8.66	0.02	92.08
FD356_m73	23.55	21.04	7.02	35.39	0.02	0.75	0.09	0.07	0.04	0.02	87.98
FD356_m74	23.53	20.20	7.15	35.40	0.01	0.54	0.11	0.02	0.05	0.01	87.02

FD356_m75	23.58	20.25	7.06	35.74	0.00	0.60	0.03	0.00	0.01	0.01	87.28
FD356_m76	37.86	20.14	0.54	28.75	6.90	6.87	0.15	0.04	0.01	0.00	101.25
FD356_m77	24.08	20.54	6.85	35.91	0.04	0.81	0.05	0.00	0.23	0.01	88.51
FD356_m78	23.77	21.23	6.78	36.02	0.03	0.74	0.04	0.00	0.10	0.05	88.76
FD356_m79	37.49	20.89	0.57	29.88	5.86	6.47	0.13	0.00	0.01	0.00	101.29
FD356_m80	37.41	20.62	0.53	30.82	4.54	7.14	0.05	0.04	0.02	0.03	101.20
FD356_m81	24.21	20.90	7.55	35.53	0.01	0.63	0.06	0.00	0.02	0.08	88.99
FD356_m82	37.66	20.48	0.54	30.02	5.50	7.03	0.07	0.00	0.00	0.01	101.30
FD356_m83	24.33	19.55	7.67	35.66	0.04	0.82	0.09	0.00	0.04	0.01	88.20
FD356_m84	37.39	20.61	0.50	29.24	5.85	6.97	0.06	0.04	0.01	0.07	100.74
FD356_m85	24.21	19.75	7.09	35.33	0.07	0.78	0.03	0.04	0.14	0.00	87.44
FD356_m86	37.32	20.53	0.50	29.55	5.90	6.98	0.11	0.03	0.01	0.02	100.93
FD356_m87	23.71	20.74	7.32	35.50	0.01	0.94	0.05	0.04	0.03	0.02	88.34
FD356_m88	37.28	20.86	0.60	29.53	5.76	6.83	0.12	0.01	0.01	0.03	101.01
FD356_m89	24.15	20.40	6.88	35.28	0.03	0.79	0.06	0.02	0.22	0.02	87.85
FD356_m90	37.62	20.84	0.54	29.50	5.61	6.60	0.05	0.03	0.01	0.07	100.87
FD356_m91	24.38	20.79	7.13	36.17	0.04	0.79	0.14	0.03	0.12	0.01	89.61
FD356_m92	23.82	19.90	7.07	35.12	0.11	0.88	0.02	0.01	0.03	0.01	86.97
FD356_m93	37.74	21.00	0.56	29.99	5.38	6.70	0.04	0.05	0.01	0.00	101.46
FD356_m94	23.95	20.72	6.87	36.24	0.01	0.92	0.00	0.00	0.09	0.01	88.82
FD356_m95	37.71	20.89	0.56	30.14	5.21	7.19	0.00	0.00	0.02	0.03	101.75
FD356_m96	24.35	38.33	1.35	26.34	0.02	0.78	0.00	0.00	0.00	0.04	91.22
FD356_m97	24.46	37.87	1.19	27.22	0.02	0.79	0.02	0.00	0.02	0.02	91.61
FD356_m98	36.32	29.65	5.00	12.18	0.05	0.26	0.07	2.84	0.01	0.02	86.40
FD356_m99	24.39	38.43	1.32	27.23	0.02	0.77	0.00	0.00	0.00	0.06	92.23
FD356_m100	37.67	20.84	0.55	29.52	5.17	7.13	0.00	0.02	0.00	0.05	100.96
FD356_m101	37.87	20.67	0.54	29.02	6.20	6.75	0.09	0.04	0.03	0.00	101.19
FD356_m102	24.28	38.68	1.19	27.43	0.03	0.75	0.00	0.04	0.01	0.10	92.50
FD356_m103	37.90	20.98	0.61	30.20	5.04	7.27	0.10	0.02	0.00	0.06	102.16
FD356_m104	24.29	38.67	1.27	26.46	0.03	1.10	0.05	0.03	0.00	0.02	91.93
FD356_m105	37.51	20.66	0.59	29.80	5.39	6.89	0.07	0.00	0.00	0.03	100.95
FD356_m106	48.02	33.79	0.75	3.29	0.00	0.05	0.04	0.24	10.88	0.01	97.07
FD356_m107	69.03	19.32	0.00	0.05	0.09	0.00	0.00	12.41	0.05	0.03	100.99
FD356_m108	23.75	20.47	7.32	35.62	0.03	0.74	0.04	0.01	0.04	0.00	88.02
FD356_m109	37.65	20.57	0.54	28.87	6.12	6.99	0.16	0.02	0.02	0.04	100.96
FD356_m110	24.41	38.96	1.46	25.92	0.00	0.95	0.00	0.00	0.00	0.05	91.74
FD356_m111	23.82	20.74	7.05	35.56	0.01	0.64	0.10	0.02	0.03	0.04	88.01
FD356_m112	49.12	28.08	1.55	5.61	0.00	0.07	0.23	0.55	10.15	0.04	95.40
FD356_m113	53.09	23.45	2.79	5.90	0.00	0.00	0.14	0.07	10.69	0.06	96.20
FD356_m114	23.38	19.54	7.28	34.12	0.01	0.58	0.05	0.04	0.02	0.00	85.02
FD356_m115	5.50	5.57	1.80	77.49	0.00	0.22	0.16	0.00	0.01	0.00	90.75
FD356_m116	97.00	0.01	0.00	0.09	0.00	0.00	0.00	0.00	0.00	0.04	97.14
FD356_m117	69.23	19.44	0.00	0.02	0.11	0.00	0.00	12.16	0.04	0.02	101.01

Sample FD370

Measurement	SiO_2	Al_2O_3	MgO	FeO	CaO	MnO	TiO_2	Na_2O	K_2O	Cr_2O_3	Sum
FD370_m1	37.08	21.79	0.44	19.99	8.36	14.49	0.24	0.02	0.01	0.08	102.49
FD370_m2	37.94	29.97	0.03	4.93	23.63	0.31	0.23	0.02	0.01	0.02	97.08
FD370_m3	52.35	29.35	3.30	2.25	0.01	0.03	0.18	0.14	10.57	0.02	98.20
FD370_m4	37.25	21.54	0.71	23.20	10.07	8.00	0.10	0.03	0.01	0.03	100.93
FD370_m5	51.95	29.51	2.99	2.16	0.00	0.08	0.06	0.41	10.05	0.00	97.21
FD370_m6	0.02	0.02	0.33	0.56	53.71	0.36	0.00	0.00	0.00	0.05	55.05
FD370_m7	95.97	0.00	0.00	0.03	0.01	0.06	0.07	0.01	0.00	0.00	96.14

FD370_m8	52.81	28.66	3.53	2.26	0.00	0.03	0.07	0.15	10.49	0.02	98.02
FD370_m9	52.73	29.15	3.18	1.90	0.00	0.00	0.12	0.19	10.56	0.00	97.82
FD370_m10	37.26	21.07	0.42	20.08	8.02	14.62	0.06	0.00	0.01	0.00	101.54
FD370_m11	37.54	21.28	0.40	21.12	8.52	12.87	0.11	0.00	0.00	0.08	101.93
Line 1	37.63	21.46	0.73	19.64	12.01	8.91	0.19	0.05	0.01	0.02	100.62
Line 2	37.47	21.08	0.60	18.60	11.51	10.85	0.24	0.02	0.00	0.06	100.43
Line 3	37.77	21.36	0.81	20.62	10.82	9.60	0.14	0.03	0.00	0.00	101.16
Line 4	51.36	16.95	0.64	18.44	7.38	5.77	0.09	0.12	0.02	0.01	100.77
Line 5	37.39	21.06	0.68	23.07	9.97	8.14	0.14	0.00	0.03	0.00	100.47
Line 6	89.17	0.86	0.00	1.08	0.46	0.44	0.02	0.05	0.00	0.07	92.15
Line 7	37.28	21.57	0.58	23.03	9.26	9.16	0.01	0.05	0.00	0.00	100.93
Line 8	29.10	14.89	0.66	19.89	14.09	8.04	0.13	0.09	0.02	0.04	86.93
Line 9	35.48	18.26	0.43	19.49	12.62	8.69	6.05	0.02	0.00	0.01	101.04
Line 10	29.01	16.35	9.94	23.85	3.38	4.98	0.10	0.11	0.03	0.00	87.75
Line 11	37.23	21.19	0.40	21.27	8.53	11.53	0.18	0.03	0.00	0.00	100.36
Line 12	37.29	21.19	0.43	20.45	9.02	12.21	0.18	0.01	0.00	0.07	100.83
Line 13	36.56	20.75	0.37	19.58	8.50	14.10	0.16	0.00	0.00	0.00	100.02
Line 14	12.77	7.55	0.16	7.10	38.44	5.54	0.00	0.00	0.00	0.00	71.57
Line 15	37.40	21.12	0.34	18.77	8.55	15.07	0.18	0.04	0.01	0.05	101.54
Line 16	37.13	20.86	0.33	17.52	8.76	15.56	0.88	0.02	0.01	0.01	101.06
Line 17	36.93	21.17	0.29	18.11	7.63	16.58	0.06	0.06	0.01	0.00	100.85
Line 18	37.17	21.21	0.35	18.03	7.59	16.42	0.07	0.02	0.00	0.10	100.96
Line 19	35.86	20.56	0.30	18.06	8.33	15.44	0.34	0.06	0.01	0.00	98.97
Line 20	37.29	21.19	0.36	18.81	7.84	14.73	0.16	0.05	0.00	0.00	100.42
Line 21	37.48	21.28	0.38	19.02	8.00	14.49	0.13	0.00	0.00	0.00	100.79
Line 22	37.28	20.78	0.32	19.02	8.71	13.72	0.18	0.05	0.02	0.00	100.09
Line 23	37.24	21.40	0.42	19.49	8.67	13.56	0.13	0.01	0.01	0.09	101.02
Line 24	97.09	0.01	0.01	0.35	0.02	0.13	0.00	0.01	0.00	0.01	97.64
Line 25	37.88	21.28	0.50	22.19	8.86	11.04	0.27	0.06	0.00	0.06	102.14
Line 26	37.80	21.45	0.59	22.63	9.22	9.29	0.16	0.01	0.00	0.00	101.15
Line 27	38.02	21.21	0.60	23.28	9.45	9.25	0.16	0.02	0.02	0.10	102.10
Line 28	37.70	21.23	0.70	22.81	9.49	8.51	0.13	0.02	0.01	0.03	100.62
Line 29	37.81	21.11	0.63	22.93	10.20	8.05	0.18	0.03	0.00	0.00	100.94
Line 30	37.95	21.31	0.77	23.39	9.72	7.88	0.06	0.00	0.00	0.00	101.10
FD370_m12	96.69	0.00	0.00	0.05	0.02	0.00	0.00	0.01	0.00	0.00	96.78
FD370_m13	36.61	27.59	0.05	4.29	20.79	0.21	0.16	0.04	0.04	0.09	89.86
FD370_m14	0.02	0.01	0.20	0.53	57.59	0.14	0.00	0.04	0.02	0.05	58.60
FD370_m15	54.23	26.54	3.43	3.25	0.03	0.01	0.15	0.17	10.31	0.02	98.14
FD370_m16	54.01	26.78	3.27	3.40	0.00	0.09	0.18	0.16	9.81	0.06	97.76
FD370_m17	96.23	0.00	0.00	0.00	0.01	0.00	0.01	0.00	0.01	0.00	96.26
FD370_m18	26.78	21.16	16.35	22.56	0.07	0.90	0.08	0.05	0.02	0.00	87.96
FD370_m19	26.65	20.74	16.61	22.95	0.04	0.40	0.00	0.00	0.00	0.00	87.38
FD370_m20	52.53	29.63	2.95	2.39	0.00	0.02	0.17	0.15	10.30	0.00	98.14
FD370_m21	0.02	0.03	0.25	0.87	55.04	1.18	0.05	0.04	0.00	0.00	57.47
FD370_m22	0.01	0.00	0.00	0.25	55.12	0.18	0.00	0.05	0.00	0.02	55.64
FD370_m23	36.07	20.76	0.29	17.82	9.62	11.34	0.08	0.06	0.01	0.03	96.08
FD370_m24	0.00	0.00	0.15	0.29	56.87	0.78	0.08	0.01	0.00	0.03	58.22
FD370_m25	38.14	28.40	0.04	6.45	23.91	0.21	0.16	0.00	0.00	0.03	97.34
FD370_m26	51.45	28.91	3.10	2.11	0.10	0.01	0.13	0.26	10.02	0.00	96.08
FD370_m27	96.23	0.00	0.00	0.04	0.01	0.01	0.00	0.00	0.01	0.00	96.30
FD370_m28	37.63	21.32	0.62	19.60	11.00	11.05	0.28	0.00	0.01	0.02	101.52
FD370_m29	0.02	0.00	0.01	0.29	54.77	0.11	0.00	0.00	0.01	0.00	55.20
FD370_m30	37.45	21.35	0.50	22.84	9.10	9.73	0.22	0.00	0.00	0.07	101.26
FD370_m31	37.61	21.71	0.59	24.11	9.49	8.73	0.19	0.00	0.00	0.00	102.44
FD370_m32	37.54	21.06	0.61	18.69	11.30	10.97	0.23	0.00	0.00	0.02	100.41

FD370_m33	0.04	0.03	0.07	0.64	56.87	0.96	0.00	0.00	0.02	0.03	58.66
FD370_m34	26.37	21.11	17.50	21.80	0.01	0.46	0.06	0.01	0.01	0.04	87.37
FD370_m35	27.18	19.70	18.29	21.73	0.02	0.27	0.14	0.03	0.01	0.02	87.40
FD370_m36	96.26	0.00	0.00	0.31	0.03	0.02	0.04	0.00	0.01	0.00	96.67
FD370_m37	30.64	2.42	0.03	0.57	28.77	0.00	38.05	0.06	0.16	0.00	100.69
FD370_m38	38.50	28.55	0.02	6.52	23.94	0.20	0.13	0.00	0.02	0.10	97.97
FD370_test	36.67	21.59	0.24	13.18	7.57	21.34	0.25	0.05	0.00	0.00	100.90
FD370_test	37.70	21.62	0.89	22.60	10.96	6.54	0.00	0.03	0.00	0.03	100.37
FD370_test	53.81	26.36	3.48	3.36	0.00	0.00	0.19	0.15	10.48	0.00	97.81
Line 1 WM	50.21	31.15	2.57	2.73	0.03	0.17	0.18	0.23	10.81	0.00	98.07
Line 2 WM	50.44	31.15	2.72	2.57	0.00	0.03	0.20	0.19	10.87	0.02	98.16
Line 3 WM	51.61	29.85	2.99	2.70	0.00	0.06	0.22	0.25	10.83	0.02	98.52
Line 4 WM	51.97	29.51	3.16	2.66	0.01	0.04	0.14	0.26	10.66	0.04	98.44
Line 5 WM	52.36	28.81	3.19	2.22	0.05	0.04	0.13	0.29	9.99	0.04	97.11
Line 6 WM	51.84	28.95	3.28	2.51	0.00	0.06	0.19	0.29	10.78	0.01	97.90
Line 7 WM	51.92	28.75	3.25	2.42	0.02	0.00	0.19	0.26	10.61	0.04	97.47
Line 8 WM	52.65	28.28	3.23	2.28	0.00	0.01	0.10	0.22	10.76	0.01	97.53
Line 9 WM	52.34	28.55	3.33	2.51	0.02	0.04	0.12	0.23	10.38	0.06	97.57
Line 10 WM	52.62	28.64	3.29	2.24	0.00	0.04	0.16	0.24	10.61	0.08	97.91
Line 11 WM	52.61	28.60	3.39	2.08	0.00	0.00	0.09	0.20	10.65	0.02	97.64
Line 12 WM	53.51	28.09	3.44	2.14	0.00	0.10	0.09	0.19	10.77	0.00	98.32
Line 13 WM	53.06	28.37	3.40	2.08	0.00	0.05	0.14	0.12	10.92	0.02	98.15
Line 14 WM	52.83	28.81	3.31	2.27	0.01	0.00	0.16	0.19	10.70	0.04	98.33
Line 15 WM	53.05	27.80	3.35	2.54	0.00	0.03	0.22	0.20	10.54	0.04	97.76
Line 16 WM	53.41	26.55	3.75	2.73	0.00	0.01	0.18	0.14	10.69	0.07	97.52
Line 17 WM	53.81	26.43	3.54	3.18	0.00	0.03	0.19	0.11	10.79	0.03	98.12
Line 18 WM	53.70	26.48	3.40	3.12	0.00	0.00	0.16	0.20	10.87	0.06	97.99
Line 19 WM	53.81	26.32	3.44	3.21	0.00	0.06	0.15	0.13	10.89	0.02	98.03
Line 20 WM	53.61	26.45	3.46	3.24	0.02	0.09	0.16	0.16	10.72	0.06	97.96
Line 21 WM	53.52	26.17	3.43	3.33	0.00	0.00	0.16	0.14	10.82	0.06	97.62
Line 22 WM	53.95	26.60	3.48	3.27	0.00	0.04	0.14	0.17	10.67	0.00	98.32
Line 23 WM	54.20	26.34	3.46	3.32	0.00	0.00	0.14	0.19	10.81	0.03	98.49
Line 24 WM	53.33	26.94	3.32	3.27	0.00	0.04	0.08	0.14	10.93	0.03	98.08
Line 25 WM	53.83	26.93	3.34	3.30	0.00	0.03	0.20	0.14	10.87	0.03	98.67
Line 26 WM	53.14	26.48	3.26	3.13	0.01	0.04	0.12	0.14	10.78	0.02	97.12
Line 27 WM	52.93	26.58	3.27	3.04	0.02	0.00	0.19	0.22	10.46	0.00	96.71
Line 28 WM	53.40	26.76	3.40	3.24	0.00	0.00	0.19	0.15	10.88	0.00	98.03
Line 29 WM	53.93	26.78	3.45	3.36	0.00	0.05	0.17	0.22	10.68	0.03	98.65
Line 30 WM	54.26	25.35	3.43	2.87	0.05	0.00	0.14	0.26	10.20	0.02	96.59
FD370_m39	37.12	21.55	0.30	17.05	7.85	16.85	0.17	0.03	0.00	0.03	100.94
FD370_m40	37.34	21.39	0.28	18.28	7.56	16.17	0.13	0.05	0.01	0.04	101.24
FD370_m41	37.25	21.25	0.38	18.44	8.03	15.36	0.17	0.06	0.00	0.05	101.00
FD370_m42	37.25	21.39	0.36	19.37	7.91	14.93	0.14	0.00	0.00	0.05	101.40
FD370_m43	37.05	21.49	0.42	20.52	8.85	12.57	0.14	0.00	0.00	0.05	101.09
FD370_m44	37.08	21.45	0.41	19.54	7.74	14.67	0.13	0.01	0.00	0.03	101.07
FD370_m45	36.81	21.56	0.39	21.11	7.89	12.57	0.06	0.00	0.00	0.01	100.40
FD370_m46	37.08	21.66	0.49	21.87	8.72	11.14	0.16	0.00	0.00	0.00	101.11
FD370_m47	37.10	21.64	0.60	23.45	9.31	8.71	0.15	0.04	0.00	0.02	101.00
FD370_m48	37.35	21.51	0.77	23.33	10.43	7.49	0.16	0.03	0.00	0.00	101.06
FD370_m49	37.37	21.37	0.58	19.55	11.33	10.34	0.21	0.03	0.00	0.03	100.82
FD370_m50	37.44	21.54	0.70	23.94	8.79	8.92	0.03	0.04	0.00	0.03	101.45
FD370_m51	37.45	21.67	0.73	23.47	10.27	7.31	0.08	0.02	0.00	0.01	100.99
FD370_m52	37.41	21.36	0.71	22.86	10.89	7.28	0.12	0.05	0.00	0.03	100.72
FD370_m53	36.89	21.39	0.21	12.60	7.70	22.32	0.18	0.03	0.00	0.02	101.34
FD370_m54	36.88	21.19	0.26	13.44	8.16	21.18	0.23	0.04	0.01	0.02	101.39

FD370_m55	36.74	21.67	0.26	13.24	7.94	21.12	0.17	0.07	0.00	0.05	101.26
FD370_m56	36.90	21.32	0.30	14.24	7.59	20.29	0.15	0.02	0.00	0.04	100.84
FD370_m57	37.16	21.50	0.25	15.14	7.58	20.12	0.28	0.01	0.01	0.00	102.05
FD370_m58	37.19	21.33	0.29	17.29	7.85	16.63	0.26	0.01	0.01	0.06	100.90
FD370_m59	37.29	21.30	0.31	17.77	7.32	16.73	0.08	0.07	0.00	0.05	100.93
FD370_m60	36.87	21.32	0.34	17.92	7.48	16.22	0.16	0.02	0.00	0.02	100.35
FD370_m61	36.97	21.40	0.53	20.18	7.69	13.39	0.13	0.04	0.00	0.00	100.33
FD370_m62	37.55	21.49	0.53	22.20	8.12	11.55	0.08	0.08	0.02	0.00	101.60
FD370_m63	37.54	21.36	0.65	23.88	7.92	9.63	0.01	0.00	0.01	0.00	101.00
FD370_m64	37.34	21.53	0.71	23.37	10.14	7.21	0.20	0.01	0.03	0.03	100.56
FD370_m65	37.27	21.31	0.44	20.95	8.74	12.42	0.22	0.01	0.01	0.02	101.38
FD370_m66	37.44	21.36	0.36	19.12	9.02	13.95	0.14	0.00	0.00	0.01	101.40
FD370_m67	37.21	21.64	0.22	11.50	7.72	23.15	0.17	0.00	0.01	0.01	101.62
FD370_m68	37.34	21.16	0.23	11.78	7.88	22.59	0.35	0.00	0.02	0.05	101.38
FD370_m69	37.09	21.38	0.49	22.83	8.88	10.28	0.17	0.00	0.00	0.00	101.13
FD370_m70	32.20	19.12	0.01	11.07	15.54	0.68	0.04	0.00	0.01	0.00	78.67
FD370_m71	35.43	24.14	0.12	8.83	20.25	0.24	0.03	0.00	0.00	0.01	89.03
FD370_m72	38.49	28.39	0.03	6.11	23.62	0.28	0.16	0.03	0.02	0.02	97.14
FD370_m73	37.25	21.18	0.44	20.57	8.29	12.19	0.11	0.00	0.02	0.01	100.05
FD370_m74	37.51	21.17	0.66	23.19	9.67	9.02	0.08	0.02	0.01	0.00	101.34
FD370_m75	37.03	21.42	0.26	11.69	7.85	23.00	0.18	0.03	0.01	0.00	101.46
FD370_m76	0.05	0.01	0.01	0.22	53.82	0.28	0.00	0.00	0.01	0.00	54.39
FD370_m77	0.06	0.01	0.02	0.41	53.88	0.63	0.00	0.00	0.00	0.01	55.02
FD370_m78	0.02	0.02	0.03	0.20	56.15	0.30	0.02	0.02	0.00	0.00	56.77
FD370_m79	33.12	20.83	0.10	10.81	16.98	1.14	0.12	0.01	0.00	0.04	83.14
FD370_m80	37.56	21.37	0.92	21.90	12.21	6.45	0.05	0.00	0.01	0.04	100.50
FD370_m81	37.87	21.50	0.83	22.06	12.49	6.00	0.09	0.02	0.00	0.08	100.93
FD370_m82	37.63	21.57	0.85	22.62	11.70	6.15	0.11	0.08	0.00	0.00	100.70
FD370_m83	37.83	21.59	0.92	22.32	11.77	6.62	0.08	0.03	0.01	0.00	101.17
FD370_m84	37.48	21.64	0.89	21.57	11.57	7.08	0.08	0.01	0.02	0.03	100.37
FD370_m85	37.69	21.53	0.72	19.50	12.15	9.52	0.15	0.00	0.00	0.02	101.27
FD370_m86	37.62	21.44	0.85	20.04	10.76	10.65	0.10	0.00	0.01	0.02	101.49
FD370_m87	37.66	21.27	0.68	19.94	9.76	11.47	0.13	0.04	0.00	0.02	100.97
FD370_m88	37.21	21.35	0.70	20.86	8.56	11.74	0.10	0.04	0.00	0.02	100.58
FD370_m89	37.15	21.10	0.60	19.35	9.42	12.46	0.24	0.04	0.00	0.02	100.38
FD370_m90	37.48	21.18	0.73	19.67	12.23	8.49	0.12	0.00	0.01	0.04	99.95
FD370_m91	37.76	21.62	0.83	19.12	11.27	9.93	0.13	0.00	0.00	0.04	100.69
FD370_m92	37.66	21.46	0.82	22.67	9.44	8.39	0.05	0.04	0.00	0.00	100.53
FD370_m93	37.59	21.25	0.72	22.91	9.74	7.98	0.08	0.00	0.00	0.04	100.30
FD370_m94	37.71	21.25	0.73	23.34	9.48	8.37	0.09	0.03	0.00	0.02	101.03
FD370_m95	37.37	21.41	0.66	22.94	9.16	8.62	0.02	0.02	0.00	0.00	100.21
FD370_m96	37.47	21.37	0.59	21.73	10.01	8.55	0.09	0.03	0.01	0.00	99.85
FD370_m97	37.46	21.16	0.61	22.04	9.96	8.57	0.15	0.00	0.01	0.01	99.95
FD370_m98	37.57	21.05	0.57	22.23	9.93	9.09	0.17	0.02	0.00	0.00	100.62
FD370_m99	37.52	21.34	0.58	22.58	9.48	9.50	0.10	0.00	0.00	0.01	101.10
FD370_m100	37.06	21.35	0.56	22.72	8.43	9.81	0.06	0.00	0.00	0.00	99.99
FD370_m101	37.38	21.15	0.48	21.81	8.77	10.73	0.14	0.00	0.00	0.00	100.46
FD370_m102	36.99	21.25	0.46	20.94	8.81	11.12	0.11	0.03	0.00	0.03	99.72
FD370_m103	37.02	21.16	0.48	20.58	8.78	11.25	0.15	0.02	0.00	0.03	99.48
FD370_m104	37.44	21.13	0.52	20.97	8.78	10.72	0.14	0.02	0.00	0.00	99.70
FD370_m105	37.16	21.34	0.41	20.58	8.46	12.71	0.11	0.07	0.00	0.00	100.83
FD370_m106	37.23	21.19	0.38	19.98	8.65	13.20	0.18	0.07	0.00	0.03	100.89
FD370_m107	36.99	21.38	0.40	20.36	8.53	12.37	0.15	0.03	0.01	0.00	100.22
FD370_m108	37.00	21.40	0.45	20.76	8.54	12.67	0.11	0.02	0.01	0.03	100.99
FD370_m109	37.26	21.43	0.46	20.83	8.86	11.80	0.11	0.00	0.00	0.03	100.78

FD370_m110	94.06	0.07	0.01	0.39	0.04	0.30	0.00	0.01	0.01	0.02	94.90
FD370_m111	36.91	21.40	0.39	20.29	8.25	13.79	0.17	0.06	0.01	0.02	101.27
FD370_m112	37.26	21.29	0.39	20.01	8.56	13.24	0.13	0.07	0.00	0.02	100.97
FD370_m113	37.31	21.33	0.41	20.69	8.98	13.04	0.15	0.00	0.02	0.00	101.91
FD370_m114	37.25	21.21	0.40	19.20	8.19	14.62	0.13	0.01	0.00	0.02	101.03
FD370_m115	37.19	21.49	0.47	19.42	7.77	14.44	0.09	0.05	0.00	0.00	100.92
FD370_m116	37.77	21.26	0.50	19.27	8.13	14.09	0.12	0.02	0.01	0.01	101.17
FD370_m117	37.23	21.22	0.34	18.77	7.85	15.97	0.11	0.04	0.01	0.02	101.55
FD370_m118	37.22	21.52	0.35	18.31	7.19	15.73	0.09	0.03	0.00	0.00	100.45
FD370_m119	37.59	21.35	0.41	18.08	7.67	15.55	0.12	0.00	0.00	0.00	100.76
FD370_m120	37.37	21.29	0.35	17.63	7.55	16.36	0.19	0.02	0.01	0.04	100.81
FD370_m121	36.95	21.10	0.32	17.41	7.53	16.54	0.16	0.00	0.01	0.01	100.04
FD370_m122	37.49	21.52	0.30	15.34	7.92	18.69	0.15	0.00	0.01	0.02	101.44
FD370_m123	37.32	21.06	0.24	13.73	8.61	20.40	0.22	0.02	0.00	0.00	101.59
FD370_m124	37.34	21.34	0.30	14.48	8.60	19.23	0.20	0.04	0.00	0.02	101.55
FD370_m125	37.30	21.39	0.29	13.14	8.40	21.31	0.23	0.00	0.00	0.00	102.05
FD370_m126	37.30	21.51	0.28	13.76	8.08	20.77	0.23	0.07	0.00	0.02	102.01
FD370_m127	37.13	21.28	0.23	12.45	8.39	21.03	0.22	0.00	0.01	0.00	100.73
FD370_m128	37.22	21.25	0.24	12.20	8.58	21.51	0.19	0.04	0.00	0.06	101.26
FD370_m129	37.33	21.16	0.21	11.74	8.44	22.60	0.16	0.02	0.00	0.05	101.71
FD370_m130	37.23	21.30	0.23	11.28	7.93	23.21	0.17	0.03	0.00	0.03	101.40
FD370_m131	37.06	21.19	0.21	11.68	7.77	22.78	0.22	0.01	0.00	0.05	100.96
FD370_m132	37.69	21.19	0.23	11.61	8.15	22.27	0.20	0.05	0.02	0.02	101.42
FD370_m133	37.20	21.02	0.23	11.79	8.07	22.13	0.29	0.02	0.00	0.01	100.77
FD370_m134	0.00	0.01	0.30	0.58	56.87	0.71	0.00	0.00	0.04	0.01	58.54
FD370_m135	52.29	27.16	3.36	2.71	0.10	0.00	0.12	0.18	9.74	0.07	95.73
FD370_m136	38.29	27.94	0.01	6.31	23.83	0.15	0.11	0.01	0.03	0.03	96.72
FD370_m137	37.10	25.57	0.06	7.60	21.95	0.35	0.12	0.00	0.00	0.01	92.74
FD370_m138	32.11	19.35	0.09	10.96	15.35	0.93	0.01	0.04	0.02	0.02	78.90
FD370_m139	35.38	23.58	0.07	9.38	20.51	0.35	0.13	0.00	0.02	0.00	89.42
FD370_m140	36.45	25.54	0.08	7.86	21.95	0.20	0.07	0.04	0.03	0.09	92.31
FD370_m141	64.54	0.08	0.03	0.16	0.12	0.11	0.01	0.00	0.05	0.00	65.09
FD370_m142	0.00	0.00	0.30	0.51	54.92	0.88	0.02	0.00	0.00	0.03	56.64
FD370_m143	38.34	28.12	0.02	6.19	24.00	0.14	0.12	0.00	0.01	0.04	96.98
FD370_m144	25.66	22.01	16.37	21.67	0.12	0.67	0.02	0.04	0.00	0.01	86.57
FD370_m145	53.91	27.03	3.52	2.60	0.19	0.10	0.12	0.25	9.80	0.01	97.52
FD370_m146	0.00	0.00	0.24	0.50	55.79	0.80	0.00	0.00	0.01	0.00	57.33
FD370_m147	95.83	0.00	0.01	0.10	0.04	0.00	0.01	0.00	0.00	0.02	96.00
FD370_m148	26.89	20.27	18.13	21.13	0.07	0.45	0.09	0.08	0.01	0.05	87.15
FD370_m149	37.65	17.72	0.07	11.32	14.02	0.99	0.00	0.07	0.00	0.00	81.83
FD370_m150	32.13	19.31	0.07	11.46	15.02	1.62	0.02	0.01	0.00	0.00	79.66
FD370_m151	31.22	17.94	0.15	12.13	11.87	1.89	0.07	0.09	0.00	0.00	75.36
FD370_m152	30.19	4.05	0.00	0.94	27.78	0.27	30.48	0.06	0.00	0.00	93.78
FD370_m153	26.19	20.62	13.13	22.78	1.43	1.68	0.05	0.08	0.01	0.03	85.98
FD370_m154	0.11	0.03	0.00	0.67	54.86	0.31	0.01	0.00	0.00	0.00	55.98
FD370_m155	33.86	19.58	0.19	14.01	13.37	4.60	0.07	0.04	0.02	0.00	85.73
FD370_m156	0.00	0.00	0.29	0.46	55.81	0.68	0.02	0.01	0.00	0.00	57.26
FD370_m157	0.01	0.00	0.30	0.09	57.08	0.03	0.03	0.01	0.00	0.00	57.54
Line 1 Grt2	38.04	21.41	0.97	22.15	11.53	6.01	0.06	0.01	0.03	0.07	100.27
Line 2 Grt2	37.74	21.38	0.78	20.29	12.14	7.88	0.17	0.01	0.00	0.01	100.40
Line 3 Grt2	38.08	21.21	0.74	19.53	12.07	9.03	0.16	0.03	0.01	0.01	100.88
Line 4 Grt2	38.04	21.35	0.62	18.84	11.44	10.63	0.26	0.05	0.00	0.01	101.26
Line 5 Grt2	38.12	21.18	0.53	17.70	11.94	11.90	0.20	0.02	0.01	0.07	101.67
Line 6 Grt2	38.08	20.76	0.54	18.41	12.00	11.53	0.18	0.02	0.00	0.00	101.52
Line 7 Grt2	38.01	21.18	0.79	19.24	12.59	8.48	0.15	0.02	0.00	0.00	100.45

Line 8 Grt2	37.92	21.10	0.73	22.06	10.25	8.23	0.08	0.02	0.00	0.00	100.38
Line 9 Grt2	38.03	21.14	0.76	22.24	10.73	7.92	0.09	0.00	0.00	0.00	100.90
Line 10 Grt2	92.66	1.07	0.04	1.57	0.50	0.38	0.00	0.01	0.01	0.01	96.24
Line 11 Grt2	59.27	11.46	8.25	13.91	0.63	0.99	0.04	0.06	0.00	0.00	94.61
Line 12 Grt2	37.80	21.29	0.73	23.31	9.88	8.05	0.05	0.00	0.02	0.00	101.14
Line 13 Grt2	97.82	0.16	0.00	0.49	0.10	0.19	0.01	0.00	0.00	0.00	98.77
Line 14 Grt2	72.28	9.71	0.26	11.55	4.72	4.61	0.02	0.07	0.00	0.00	103.22
Line 15 Grt2	98.34	0.00	0.00	0.35	0.03	0.21	0.02	0.00	0.01	0.00	98.96
Line 16 Grt2	37.69	21.08	0.64	22.08	9.98	9.06	0.10	0.01	0.00	0.00	100.64
Line 17 Grt2	30.53	16.26	0.50	18.25	18.44	7.28	0.06	0.00	0.01	0.00	91.32
Line 18 Grt2	36.74	21.30	0.47	21.12	10.93	7.80	0.14	0.03	0.01	0.00	98.55
Line 19 Grt2	37.59	21.33	0.56	22.66	9.45	9.36	0.16	0.01	0.00	0.00	101.11
Line 20 Grt2	32.14	15.47	10.30	23.04	3.66	4.39	0.06	0.11	0.01	0.04	89.22
Line 21 Grt2	37.13	21.18	0.51	21.53	9.17	10.75	0.12	0.02	0.01	0.02	100.44
Line 22 Grt2	37.11	21.30	0.47	21.50	8.73	11.58	0.09	0.00	0.01	0.03	100.81
Line 23 Grt2	37.83	21.11	0.53	21.50	8.65	11.80	0.13	0.00	0.01	0.05	101.60
Line 24 Grt2	0.01	0.02	0.00	0.24	54.08	0.28	0.02	0.00	0.00	0.00	54.65
Line 25 Grt2	0.01	0.02	0.00	0.35	54.07	0.21	0.00	0.05	0.00	0.03	54.74
Line 26 Grt2	37.49	21.33	0.43	20.74	8.42	12.84	0.14	0.03	0.00	0.01	101.42
Line 27 Grt2	29.29	13.94	12.84	15.96	7.06	1.16	7.84	0.16	0.14	0.00	88.37
Line 28 Grt2	38.09	20.96	0.65	19.95	8.60	13.08	0.14	0.03	0.00	0.01	101.50
Line 29 Grt2	16.21	9.51	0.24	9.85	32.40	7.29	0.06	0.06	0.00	0.01	75.61
Line 30 Grt2	37.57	21.01	0.39	19.62	8.06	14.53	0.14	0.02	0.02	0.01	101.35
Line 31 Grt2	35.98	22.80	0.38	19.14	8.14	14.31	0.14	0.02	0.01	0.04	100.96
Line 32 Grt2	35.70	22.23	0.37	18.79	8.11	14.21	0.13	0.08	0.01	0.00	99.62
Line 33 Grt2	36.48	20.99	1.45	19.70	7.94	13.38	0.14	0.03	0.03	0.06	100.19
Line 34 Grt2	37.66	21.01	0.36	19.57	8.58	13.88	0.12	0.00	0.00	0.00	101.18
Line 35 Grt2	37.77	21.28	0.39	19.77	8.81	13.08	0.18	0.05	0.01	0.04	101.38
Line 36 Grt2	36.75	18.87	0.38	17.70	11.10	11.47	3.93	0.03	0.01	0.00	100.25
Line 37 Grt2	40.09	18.36	0.90	19.90	8.24	12.28	0.33	0.12	0.00	0.02	100.23
Line 38 Grt2	37.64	21.18	0.45	20.08	8.67	12.83	0.18	0.04	0.02	0.04	101.13
Line 39 Grt2	37.43	21.31	0.39	20.43	8.25	12.98	0.11	0.04	0.00	0.01	100.96
Line 40 Grt2	37.63	21.20	0.43	20.87	8.26	13.13	0.19	0.00	0.00	0.00	101.70
Line 41 Grt2	37.42	21.29	0.44	20.49	8.68	12.32	0.08	0.03	0.00	0.01	100.77
Line 42 Grt2	37.51	21.18	0.45	21.08	8.47	12.28	0.15	0.02	0.01	0.04	101.20
Line 43 Grt2	37.47	19.75	0.49	20.13	9.87	10.98	2.43	0.04	0.00	0.00	101.15
Line 44 Grt2	33.10	21.81	0.42	22.54	8.93	10.53	0.11	0.04	0.01	0.05	97.53
Line 45 Grt2	36.34	17.68	0.41	18.75	12.63	7.89	5.61	0.02	0.00	0.00	99.30
Line 46 Grt2	31.30	18.21	8.50	21.88	4.99	5.51	0.07	0.12	0.03	0.03	90.63
Line 47 Grt2	37.73	21.20	0.69	23.10	9.27	9.01	0.11	0.03	0.01	0.03	101.16
Line 48 Grt2	27.13	20.28	2.06	21.22	7.37	6.88	0.14	0.35	0.03	0.03	85.49
Line 49 Grt2	37.29	21.43	0.73	23.45	9.96	8.33	0.09	0.00	0.00	0.00	101.28
Line 50 Grt2	37.58	21.19	0.76	23.26	10.09	7.65	0.09	0.00	0.00	0.05	100.67
Line 51 Grt2	37.54	21.11	0.76	22.96	10.23	7.88	0.16	0.00	0.00	0.02	100.65
Line 52 Grt2	37.51	21.19	0.78	22.19	10.39	8.19	0.09	0.00	0.00	0.01	100.34
Line 53 Grt2	37.90	21.48	0.82	22.71	9.81	8.08	0.08	0.02	0.00	0.00	100.91
Line 54 Grt2	35.75	20.95	1.13	19.86	10.45	9.45	0.18	0.06	0.00	0.00	97.84
Line 55 Grt2	37.51	21.11	0.55	19.39	11.04	11.31	0.19	0.08	0.00	0.02	101.20
Line 56 Grt2	37.39	21.03	0.52	17.89	11.76	11.60	0.24	0.00	0.00	0.06	100.49
Line 57 Grt2	37.95	21.45	0.65	19.10	11.11	10.89	0.14	0.09	0.00	0.01	101.40
Line 58 Grt2	37.91	21.46	0.71	19.48	11.48	10.47	0.17	0.03	0.00	0.07	101.78
Line 59 Grt2	98.64	0.04	0.01	0.44	0.08	0.15	0.00	0.02	0.01	0.04	99.43
Line 60 Grt2	38.27	21.76	0.85	22.30	12.23	6.22	0.06	0.01	0.00	0.00	101.69
FD370_m158	26.47	20.26	18.27	20.95	0.05	0.51	0.03	0.06	0.00	0.00	86.59
FD370_m159	37.52	21.46	0.33	17.20	7.88	16.67	0.15	0.00	0.00	0.00	101.21

FD370_m160	49.31	27.86	3.01	2.29	0.00	0.00	0.14	0.17	11.20	0.07	94.05
FD370_m161	37.34	21.23	0.35	18.45	7.66	15.61	0.24	0.03	0.00	0.02	100.92
FD370_m162	37.13	21.03	0.20	11.34	8.04	23.30	0.28	0.04	0.00	0.03	101.37
FD370_m163	37.00	21.31	0.28	14.81	8.09	18.78	0.19	0.00	0.01	0.01	100.49
FD370_m164	0.02	0.01	0.17	0.61	56.17	0.37	0.03	0.00	0.01	0.04	57.43
FD370_m165	36.55	21.20	0.27	12.22	7.69	22.31	0.21	0.05	0.00	0.00	100.48
FD370_m166	36.64	21.21	0.25	11.87	7.63	22.79	0.30	0.02	0.01	0.03	100.72
FD370_m167	36.52	15.65	0.23	9.13	6.21	17.84	0.34	0.00	0.01	0.07	86.01
Line 1 AB2	37.90	21.18	0.89	20.50	10.67	9.72	0.12	0.03	0.01	0.00	101.01
Line 2 AB2	37.78	21.58	0.79	20.05	10.80	10.59	0.19	0.01	0.00	0.06	101.83
Line 3 AB2	37.50	20.88	0.54	18.84	11.26	11.07	0.21	0.00	0.00	0.01	100.33
Line 4 AB2	37.96	21.04	0.60	19.64	11.55	10.52	0.19	0.01	0.00	0.01	101.52
Line 5 AB2	37.83	21.19	0.79	22.39	10.37	8.01	0.10	0.02	0.01	0.00	100.70
Line 6 AB2	37.63	21.50	0.71	22.50	10.99	7.94	0.09	0.04	0.00	0.04	101.43
Line 7 AB2	37.44	21.30	0.76	22.75	10.24	7.76	0.06	0.02	0.02	0.01	100.36
Line 8 AB2	37.67	21.26	0.70	23.09	9.91	7.85	0.05	0.01	0.01	0.00	100.52
Line 9 AB2	37.68	21.39	0.77	23.63	9.91	7.83	0.10	0.02	0.01	0.04	101.38
Line 10 AB2	85.97	2.78	0.07	2.46	1.08	0.74	0.00	0.00	0.00	0.02	93.12
Line 11 AB2	37.47	21.49	0.70	23.37	9.90	8.34	0.14	0.00	0.00	0.04	101.45
Line 12 AB2	37.51	21.29	0.68	23.13	9.87	8.60	0.15	0.00	0.01	0.04	101.27
Line 13 AB2	37.62	21.23	0.61	22.96	9.95	8.86	0.09	0.02	0.02	0.01	101.36
Line 14 AB2	37.56	21.28	0.63	22.60	9.87	9.27	0.12	0.00	0.00	0.03	101.36
Line 15 AB2	37.85	21.34	0.63	23.47	9.02	8.96	0.09	0.00	0.00	0.02	101.39
Line 16 AB2	37.76	21.25	0.62	22.83	9.41	8.96	0.15	0.02	0.00	0.01	101.02
Line 17 AB2	24.29	20.81	12.28	22.09	1.70	2.21	0.07	0.13	0.01	0.00	83.61
Line 18 AB2	37.50	21.05	0.63	23.24	9.11	9.02	0.20	0.02	0.00	0.02	100.78
Line 19 AB2	37.92	21.18	0.58	23.26	9.36	9.41	0.13	0.02	0.00	0.01	101.86
Line 20 AB2	37.72	21.18	0.57	22.78	9.27	9.85	0.15	0.05	0.01	0.00	101.58
Line 21 AB2	37.87	21.26	0.47	22.44	9.28	9.94	0.22	0.00	0.00	0.02	101.52
Line 22 AB2	37.58	21.35	0.47	21.90	9.02	10.88	0.12	0.02	0.00	0.01	101.34
Line 23 AB2	37.46	21.37	0.47	22.30	8.44	11.21	0.13	0.00	0.00	0.03	101.41
Line 24 AB2	37.28	21.29	0.44	21.53	8.79	11.49	0.12	0.03	0.00	0.02	100.98
Line 25 AB2	37.73	21.02	0.45	21.45	8.75	11.52	0.10	0.00	0.00	0.03	101.03
Line 26 AB2	37.72	21.07	0.52	21.10	8.67	12.02	0.10	0.00	0.00	0.02	101.23
Line 27 AB2	31.94	16.63	10.80	21.50	3.30	5.82	0.02	0.11	0.01	0.00	90.12
Line 28 AB2	24.14	18.93	3.93	20.12	7.64	8.52	0.11	0.17	0.01	0.02	83.58
Line 29 AB2	37.65	21.46	0.47	20.93	8.40	12.65	0.11	0.01	0.01	0.04	101.73
Line 30 AB2	30.47	1.89	0.00	0.98	27.90	0.55	33.67	0.05	0.01	0.00	95.51
Line 31 AB2	37.50	21.37	0.46	19.96	8.40	13.36	0.15	0.00	0.00	0.03	101.21
Line 32 AB2	37.79	20.98	0.45	20.04	8.53	12.80	0.09	0.05	0.00	0.04	100.78
Line 33 AB2	37.47	21.34	0.42	20.06	8.95	13.10	0.12	0.00	0.02	0.00	101.46
Line 34 AB2	37.88	21.13	0.43	20.25	8.74	12.53	0.31	0.05	0.00	0.03	101.36
Line 35 AB2	37.34	21.69	0.44	20.65	8.52	12.97	0.11	0.00	0.01	0.00	101.74
Line 36 AB2	38.91	21.30	0.47	20.46	8.30	12.81	0.19	0.05	0.00	0.03	102.51
Line 37 AB2	37.91	20.31	0.66	19.58	9.39	12.86	1.26	0.01	0.00	0.01	101.99
Line 38 AB2	37.31	20.95	0.48	20.40	8.59	12.82	0.14	0.00	0.00	0.00	100.69
Line 39 AB2	37.70	21.06	0.44	20.32	8.56	12.39	0.17	0.01	0.00	0.00	100.66
Line 40 AB2	37.63	21.10	0.42	20.49	8.52	12.51	0.12	0.00	0.00	0.03	100.83
Line 41 AB2	37.61	21.14	0.46	20.80	8.05	12.24	0.16	0.03	0.00	0.00	100.48
Line 42 AB2	37.64	21.50	0.46	20.87	8.48	12.59	0.13	0.05	0.01	0.00	101.72
Line 43 AB2	38.63	20.96	0.52	21.59	8.69	11.39	0.26	0.01	0.00	0.01	102.05
Line 44 AB2	33.08	11.22	0.75	21.81	7.11	10.73	0.12	0.04	0.00	0.00	84.84
Line 45 AB2	37.42	21.20	0.59	22.61	8.99	9.56	0.13	0.04	0.00	0.04	100.58
Line 46 AB2	31.57	20.94	5.97	20.82	5.72	5.98	0.14	0.21	0.01	0.00	91.37
Line 47 AB2	37.42	21.50	0.68	22.92	9.37	8.80	0.11	0.00	0.02	0.00	100.81

Line 48 AB2	34.69	18.39	2.59	22.51	8.73	7.91	0.06	0.09	0.02	0.02	95.02
Line 49 AB2	37.62	21.40	0.78	23.15	9.67	8.08	0.13	0.01	0.00	0.00	100.82
Line 50 AB2	37.51	21.26	0.79	23.45	10.00	7.74	0.15	0.00	0.00	0.04	100.93
Line 51 AB2	37.78	21.45	0.76	22.98	10.14	7.86	0.04	0.04	0.02	0.01	101.08
Line 52 AB2	37.72	21.40	0.73	22.16	10.27	7.68	0.13	0.00	0.00	0.03	100.11
Line 53 AB2	37.93	21.47	0.81	21.59	11.14	8.34	0.09	0.03	0.01	0.01	101.42
Line 54 AB2	44.90	19.21	0.50	16.93	11.05	10.58	0.28	0.00	0.00	0.04	103.50
Line 55 AB2	38.12	20.07	0.53	18.05	12.01	11.19	0.23	0.05	0.01	0.05	100.31
Line 56 AB2	37.47	21.34	0.59	18.32	11.87	10.79	0.20	0.02	0.00	0.00	100.59
Line 57 AB2	36.70	16.68	0.63	18.38	11.27	10.72	0.17	0.09	0.00	0.02	94.66
Line 58 AB2	37.73	21.71	0.92	20.49	11.14	9.38	0.11	0.03	0.01	0.00	101.52
Line 59 AB2	37.67	21.50	0.75	20.06	12.90	7.70	0.09	0.05	0.00	0.02	100.74
Line 60 AB2	37.61	21.82	0.98	22.27	11.25	6.24	0.07	0.03	0.00	0.00	100.27
FD370_m168	96.25	0.02	0.00	0.12	0.09	0.00	0.00	0.02	0.00	0.04	96.55
FD370_m169	38.09	28.56	0.02	5.94	24.08	0.18	0.10	0.02	0.03	0.04	97.06
FD370_m170	26.38	21.20	17.60	20.20	0.11	0.49	0.05	0.01	0.14	0.01	86.19
FD370_m171	30.70	27.47	0.46	7.21	15.79	0.69	0.12	0.11	2.21	0.01	84.76
FD370_m172	52.67	25.76	3.46	2.63	0.23	0.07	0.14	0.19	9.83	0.00	94.97
FD370_m173	29.82	1.67	0.03	0.24	28.66	0.09	33.21	0.03	0.13	0.00	93.88
FD370_m174	0.02	0.00	0.27	0.55	55.23	0.77	0.00	0.00	0.00	0.03	56.86
FD370_m175	38.69	28.44	0.02	5.75	24.07	0.20	0.14	0.00	0.08	0.04	97.42
FD370_m176	52.27	26.08	3.54	2.48	0.05	0.00	0.13	0.22	9.46	0.04	94.26
FD370_m177	26.31	20.80	18.57	19.62	0.18	0.26	0.01	0.10	0.03	0.02	85.91
FD370_m178	49.48	30.49	2.57	2.50	0.01	0.06	0.11	0.25	10.98	0.07	96.51
FD370_m179	36.17	24.75	0.09	8.03	20.74	0.32	0.08	0.00	0.07	0.00	90.26
FD370_m180	38.01	27.30	0.03	6.76	23.64	0.22	0.08	0.06	0.01	0.03	96.14
FD370_m181	0.01	0.02	0.28	0.45	58.21	1.18	0.01	0.00	0.01	0.00	60.17
FD370_m182	95.09	0.01	0.00	0.02	0.04	0.02	0.03	0.00	0.02	0.01	95.24
FD370_m183	38.47	27.63	0.04	6.54	23.02	0.39	0.08	0.00	0.00	0.03	96.20
FD370_m184	52.95	25.11	3.57	3.49	0.01	0.00	0.15	0.15	10.78	0.01	96.20
FD370_m185	37.12	21.20	0.22	11.52	7.55	23.14	0.17	0.06	0.00	0.00	100.98
FD370_m186	37.03	21.38	0.27	14.75	7.35	20.46	0.13	0.05	0.01	0.02	101.46
FD370_m187	37.04	20.20	0.22	11.58	8.64	22.52	1.94	0.00	0.01	0.00	102.15
FD370_m188	30.02	1.24	0.00	0.80	28.38	0.34	33.81	0.00	0.00	0.01	94.61
FD370_m189	53.06	26.38	3.39	3.25	0.00	0.05	0.12	0.18	10.85	0.03	97.29
FD370_m190	53.41	26.79	3.51	3.25	0.00	0.01	0.11	0.17	10.56	0.02	97.84
FD370_m191	53.23	27.22	3.55	3.24	0.00	0.02	0.17	0.05	10.59	0.00	98.08
FD370_m192	53.80	26.50	3.62	3.35	0.00	0.07	0.16	0.16	10.50	0.00	98.17
FD370_m193	50.70	27.01	3.24	2.60	0.00	0.00	0.20	0.22	11.10	0.06	95.12
FD370_m194	53.07	26.22	3.47	3.27	0.00	0.04	0.13	0.18	11.01	0.03	97.42
Line 1 AB3	38.90	21.13	0.79	20.64	10.14	8.91	0.02	0.06	0.00	0.00	100.58
Line 2 AB3	37.19	21.24	0.73	23.13	10.29	7.72	0.13	0.00	0.01	0.00	100.44
Line 3 AB3	37.86	21.48	0.80	23.88	10.38	6.94	0.04	0.02	0.01	0.00	101.40
Line 4 AB3	37.37	21.36	0.61	22.28	10.00	8.55	0.09	0.00	0.00	0.00	100.26
Line 5 AB3	36.87	21.66	0.48	21.84	8.77	10.90	0.11	0.00	0.01	0.00	100.65
Line 6 AB3	38.14	20.70	0.59	23.11	8.97	9.50	0.07	0.03	0.01	0.05	101.16
Line 7 AB3	37.55	21.34	0.49	21.09	9.18	11.69	0.21	0.02	0.00	0.04	101.61
Line 8 AB3	37.28	21.27	0.46	21.38	9.02	11.56	0.13	0.00	0.01	0.06	101.17
Line 9 AB3	37.56	21.02	0.42	20.61	9.30	12.15	0.12	0.00	0.01	0.04	101.23
Line 10 AB3	37.66	21.32	0.43	21.08	7.71	12.63	0.12	0.04	0.01	0.04	101.02
Line 11 AB3	37.86	21.30	0.42	21.02	7.90	12.89	0.06	0.03	0.00	0.00	101.46
Line 12 AB3	36.15	16.66	0.61	18.04	6.97	11.83	0.23	0.06	0.03	0.02	90.60
Line 13 AB3	36.51	22.19	0.37	19.84	8.77	12.91	0.19	0.00	0.00	0.02	100.80
Line 14 AB3	36.73	21.03	0.41	19.97	8.03	13.99	0.16	0.01	0.01	0.01	100.34
Line 15 AB3	37.16	20.90	0.38	19.47	8.10	14.74	0.20	0.06	0.00	0.02	101.01

Line 16 AB3	37.45	21.33	0.37	19.06	9.12	14.07	0.20	0.01	0.00	0.02	101.63
Line 17 AB3	37.89	21.13	0.34	18.98	8.55	14.65	0.15	0.00	0.01	0.00	101.69
Line 18 AB3	37.26	21.18	0.38	19.21	7.99	15.11	0.17	0.03	0.00	0.00	101.32
Line 19 AB3	37.42	21.25	0.35	18.90	8.21	14.70	0.18	0.00	0.01	0.06	101.08
Line 20 AB3	20.71	23.33	0.10	18.06	8.22	15.23	0.14	0.07	0.01	0.03	85.89
Line 21 AB3	34.11	23.80	0.31	17.71	8.25	14.98	0.13	0.03	0.01	0.02	99.35
Line 22 AB3	37.27	21.38	0.35	18.02	7.40	16.79	0.11	0.01	0.00	0.02	101.35
Line 23 AB3	37.05	21.98	0.28	16.49	8.12	17.54	0.10	0.04	0.01	0.00	101.60
Line 24 AB3	36.55	20.50	0.26	13.11	7.44	21.21	0.23	0.06	0.00	0.00	99.37
Line 25 AB3	36.91	21.12	0.24	11.74	7.27	23.81	0.16	0.02	0.00	0.04	101.32
Line 1 AB4	36.89	20.95	0.23	11.77	7.66	22.70	0.32	0.02	0.00	0.00	100.53
Line 2 AB4	36.77	21.24	0.25	13.15	7.45	22.11	0.33	0.05	0.00	0.01	101.35
Line 3 AB4	37.18	21.82	0.30	18.35	8.13	15.90	0.14	0.05	0.01	0.03	101.91
Line 4 AB4	37.37	21.33	0.35	18.95	7.22	16.46	0.14	0.00	0.00	0.00	101.82
Line 5 AB4	36.91	20.07	0.32	17.59	9.15	15.05	1.89	0.04	0.00	0.17	101.19
Line 6 AB4	10.80	18.66	1.31	18.73	5.17	8.76	0.07	0.12	0.04	0.01	63.67
Line 7 AB4	36.71	21.39	2.64	19.56	7.29	13.81	0.17	0.00	0.00	0.03	101.59
Line 8 AB4	36.86	21.07	0.39	19.11	8.18	14.55	0.22	0.02	0.00	0.00	100.39
Line 9 AB4	42.98	12.34	1.52	11.46	10.62	6.96	8.56	0.04	0.02	0.02	94.51
Line 10 AB4	37.34	21.51	0.41	20.00	8.24	13.85	0.14	0.02	0.00	0.01	101.52
Line 11 AB4	94.18	0.26	0.00	0.53	0.12	0.37	0.00	0.00	0.00	0.04	95.51
Line 12 AB4	35.10	13.93	0.39	20.35	8.50	12.92	0.15	0.02	0.00	0.02	91.38
Line 13 AB4	37.34	21.41	0.45	20.92	8.45	12.60	0.12	0.03	0.00	0.00	101.32
Line 14 AB4	94.63	0.03	0.00	0.47	0.03	0.16	0.01	0.00	0.01	0.03	95.37
Line 15 AB4	94.02	0.00	0.00	0.38	0.04	0.15	0.00	0.00	0.00	0.00	94.59
Line 16 AB4	93.70	0.06	0.01	0.33	0.06	0.14	0.03	0.00	0.01	0.00	94.36
Line 17 AB4	34.07	23.69	0.60	21.75	9.53	8.68	0.16	0.13	0.01	0.00	98.62
Line 18 AB4	36.52	20.52	0.62	22.41	10.00	8.59	0.12	0.00	0.00	0.00	98.77
Line 19 AB4	37.15	21.65	0.64	23.41	9.84	8.11	0.16	0.00	0.00	0.01	100.97
Line 20 AB4	37.00	18.03	0.74	23.00	10.10	7.87	0.30	0.06	0.00	0.02	97.11
Line 21 AB4	37.42	21.12	0.70	22.71	10.54	7.76	0.12	0.00	0.00	0.01	100.37
Line 22 AB4	38.06	21.34	0.77	22.95	10.33	7.77	0.07	0.00	0.00	0.05	101.34
Line 23 AB4	95.04	0.03	0.00	0.29	0.05	0.14	0.01	0.00	0.00	0.00	95.54
Line 24 AB4	87.31	2.60	0.08	1.89	1.30	1.21	0.01	0.02	0.02	0.00	94.43
Line 25 AB4	37.57	21.01	0.78	19.55	12.04	9.30	0.21	0.01	0.01	0.04	100.50

Sample FD372

Measurement	SiO_2	Al_2O_3	MgO	FeO	CaO	MnO	TiO_2	Na_2O	K_2O	Cr_2O_3	Sum
FD372_m1	37.85	21.47	0.78	26.75	9.29	4.65	0.08	0.00	0.01	0.03	100.91
FD372_m2	37.16	20.97	0.45	22.81	7.42	10.72	0.12	0.03	0.02	0.07	99.76
FD372_m3	53.06	26.72	3.45	2.98	0.00	0.05	0.18	0.12	9.69	0.00	96.26
FD372_m4	53.25	26.15	3.21	3.80	0.01	0.01	0.14	0.14	9.53	0.00	96.22
FD372_m5	51.99	25.13	3.08	3.77	0.00	0.00	0.16	0.18	9.57	0.10	93.96
FD372_m6	53.62	2.55	15.77	11.34	12.27	0.32	0.06	0.38	0.13	0.00	96.45
FD372_m7	52.26	2.41	12.96	15.13	10.96	0.74	0.07	0.74	0.12	0.00	95.40
FD372_m8	52.57	28.12	3.20	2.49	0.06	0.03	0.24	0.10	9.78	0.01	96.60
FD372_m9	30.27	1.81	0.02	0.46	28.48	0.08	37.54	0.00	0.11	0.08	98.84
FD372_m10	96.08	0.02	0.01	0.15	0.00	0.04	0.05	0.00	0.01	0.00	96.37
FD372_m11	53.70	2.28	15.99	10.90	12.36	0.40	0.00	0.49	0.09	0.00	96.22
FD372_m12	53.53	1.73	14.18	14.58	11.73	0.67	0.01	0.48	0.10	0.00	96.99
FD372_m13	54.70	2.30	16.32	10.87	12.14	0.38	0.03	0.57	0.07	0.04	97.41
FD372_m14	50.45	25.70	3.40	2.61	0.08	0.06	0.14	0.17	8.77	0.02	91.40
FD372_m15	96.43	0.01	0.00	0.15	0.01	0.01	0.00	0.00	0.02	0.00	96.62

FD372_m16	53.99	25.59	3.37	3.89	0.00	0.06	0.16	0.08	9.92	0.11	97.18
FD372_m17	53.62	26.60	3.21	3.59	0.00	0.04	0.17	0.18	9.42	0.00	96.83
FD372_m18	37.28	21.00	0.28	14.49	8.13	19.45	0.28	0.03	0.00	0.03	100.97
FD372_m19	37.63	21.55	0.91	27.60	8.64	4.40	0.11	0.06	0.02	0.00	100.94
FD372_m20	52.89	26.12	3.15	3.68	0.00	0.00	0.16	0.19	9.64	0.00	95.83
FD372_m21	51.40	3.23	11.84	17.04	10.32	0.73	0.11	1.10	0.17	0.03	95.96
FD372_m22	53.88	2.03	16.77	10.64	12.23	0.25	0.03	0.41	0.09	0.00	96.32
FD372_m23	51.22	25.69	3.25	3.88	0.00	0.00	0.19	0.17	10.86	0.01	95.26
FD372_m24	50.59	24.69	3.33	3.56	0.03	0.03	0.21	0.37	10.54	0.01	93.35
FD372_m25	37.92	27.82	0.03	7.15	23.97	0.24	0.06	0.02	0.11	0.00	97.31
FD372_m26	35.92	23.28	0.06	10.34	21.19	0.20	0.06	0.01	0.04	0.00	91.08
FD372_m27	33.43	20.17	0.14	11.62	17.38	0.31	0.01	0.03	0.05	0.01	83.15
FD372_m28	37.94	29.20	0.06	4.68	23.98	0.19	0.27	0.02	0.01	0.02	96.36
FD372_m29	33.82	20.35	0.16	11.49	17.56	0.30	0.02	0.07	0.05	0.02	83.83
FD372_m30	36.74	20.91	0.22	11.29	7.84	23.41	0.20	0.03	0.02	0.02	100.68
FD372_m31	37.11	21.03	0.34	17.77	7.80	16.31	0.13	0.00	0.00	0.00	100.49
FD372_m32	32.80	0.19	0.02	1.30	0.33	0.35	0.32	0.00	0.04	0.03	35.38
FD372_m33	30.08	1.62	0.01	1.07	28.10	0.33	33.15	0.01	0.01	0.01	94.38
FD372_m34	96.33	0.09	0.00	0.68	0.06	0.29	0.03	0.02	0.00	0.01	97.50
FD372_m35	36.86	20.94	0.19	10.77	7.74	24.02	0.19	0.01	0.01	0.02	100.75
FD372_m36	36.74	20.97	0.20	11.02	7.56	24.04	0.25	0.00	0.01	0.02	100.80
FD372_m37	36.86	20.86	0.23	12.08	8.09	22.61	0.23	0.02	0.01	0.02	101.00
FD372_m38	36.95	20.92	0.25	12.96	8.21	21.39	0.26	0.02	0.00	0.01	100.97
FD372_m39	36.69	21.00	0.28	14.51	8.67	19.59	0.20	0.04	0.02	0.05	101.02
FD372_m40	36.98	20.92	0.34	16.15	8.08	18.97	0.20	0.04	0.00	0.00	101.69
FD372_m41	37.22	21.03	0.41	21.23	7.33	13.78	0.11	0.00	0.01	0.06	101.17
FD372_m42	36.98	20.92	0.54	23.66	7.50	10.46	0.29	0.08	0.01	0.03	100.46
FD372_m43	37.43	20.96	0.72	26.84	7.96	6.86	0.14	0.01	0.01	0.02	100.93
FD372_m44	37.67	21.32	0.94	28.26	8.37	4.59	0.10	0.01	0.01	0.00	101.27
FD372_m45	37.84	20.99	0.92	26.41	10.01	4.39	0.07	0.05	0.02	0.00	100.69
FD372_m46	52.34	28.03	3.23	2.72	0.01	0.00	0.14	0.10	9.90	0.01	96.47
FD372_m47	95.46	0.00	0.00	0.06	0.00	0.01	0.02	0.00	0.01	0.00	95.57
FD372_m48	38.73	28.13	0.05	6.42	23.76	0.22	0.14	0.01	0.00	0.04	97.50
FD372_m49	54.19	1.57	15.67	12.36	12.54	0.52	0.04	0.31	0.05	0.00	97.24
FD372_m50	0.00	0.00	0.02	0.17	54.62	0.15	0.01	0.00	0.01	0.00	54.97
FD372_m51	30.11	0.96	0.00	0.85	28.50	0.41	34.45	0.02	0.01	0.05	95.35
FD372_m52	26.76	20.48	17.02	21.07	0.11	1.52	0.04	0.00	0.00	0.01	87.01

Sample FD374

Measurement	SiO_2	Al_2O_3	MgO	FeO	CaO	MnO	TiO_2	Na_2O	K_2O	Cr_2O_3	Sum
FD374_m1	37.47	20.55	0.45	27.76	6.91	7.60	0.12	0.00	0.00	0.49	101.35
FD374_m2	52.47	24.13	2.54	5.00	0.03	0.11	0.14	0.05	9.36	1.04	94.88
FD374_m3	95.86	0.00	0.00	0.00	0.00	0.00	0.04	0.03	0.00	0.03	95.96
FD374_m4	50.54	23.92	2.64	4.62	0.14	0.08	0.21	0.05	8.24	0.77	91.20
FD374_m5	24.04	20.63	6.04	35.18	0.07	1.20	0.07	0.00	0.35	0.41	87.98
FD374_m6	24.11	20.32	5.03	37.55	0.08	1.27	0.03	0.08	0.15	0.53	89.15
FD374_m7	96.99	0.09	0.01	0.68	0.03	0.08	0.00	0.01	0.00	0.04	97.93
FD374_m8	37.15	20.29	0.41	26.22	6.99	8.77	0.11	0.02	0.01	0.60	100.57
FD374_m9	37.01	20.71	0.35	23.77	7.92	10.63	0.16	0.00	0.01	0.65	101.19
FD374_m10	37.10	20.40	0.28	23.67	6.85	11.83	0.08	0.00	0.01	0.59	100.81
FD374_m11	52.56	24.39	2.61	5.05	0.10	0.05	0.11	0.07	8.98	0.75	94.67
FD374_m12	48.64	22.53	2.63	4.49	0.00	0.03	0.14	0.06	10.31	0.93	89.76
FD374_m13	51.95	23.96	2.92	4.91	0.23	0.27	0.11	0.08	7.87	0.57	92.85

FD374_m14	52.91	24.61	2.55	4.77	0.04	0.13	0.18	0.04	9.74	1.10	96.07
FD374_m15	37.51	20.70	0.57	30.55	5.93	5.07	0.04	0.00	0.00	0.45	100.84
FD374_m16	37.44	20.85	0.65	29.95	6.24	5.44	0.14	0.05	0.01	0.54	101.30
FD374_m17	23.86	19.10	8.21	31.62	0.05	0.62	0.08	0.00	0.10	0.27	83.90
FD374_m18	23.53	18.98	8.17	32.62	0.06	0.69	0.13	0.05	0.13	0.23	84.58
FD374_m19	96.73	0.00	0.00	0.37	0.00	0.03	0.01	0.00	0.01	0.05	97.20
FD374_m20	51.35	28.22	2.28	3.85	0.00	0.00	0.23	0.47	10.28	0.10	96.79
FD374_m21	53.39	25.54	2.66	4.49	0.00	0.04	0.17	0.10	10.62	0.91	97.91
FD374_m22	0.00	0.02	0.01	39.34	0.01	8.25	54.37	0.02	0.06	0.02	102.08
FD374_m23	51.52	24.05	2.51	4.51	0.00	0.02	0.09	0.07	10.82	1.30	94.88
FD374_m24	53.78	24.67	2.58	4.86	0.00	0.01	0.08	0.07	10.70	0.81	97.56
FD374_m25	24.45	19.48	8.47	31.49	0.07	0.45	0.08	0.06	0.08	0.14	84.76
FD374_m26	53.49	24.89	2.82	4.86	0.53	0.21	0.13	0.08	7.32	0.05	94.37

Sample FD377

Measurement	SiO_2	Al_2O_3	MgO	FeO	CaO	MnO	TiO_2	Na_2O	K_2O	Cr_2O_3	Sum
FD377_m1	30.32	20.70	26.46	9.99	0.02	0.12	0.00	0.02	0.01	0.16	87.79
FD377_m2	57.13	0.40	21.32	4.36	13.43	0.08	0.00	0.21	0.01	0.07	97.02
FD377_m3	38.13	27.28	2.42	2.51	22.36	0.11	0.03	0.06	0.00	0.04	92.95
FD377_m4	39.25	29.57	0.03	5.65	24.30	0.09	0.02	0.01	0.00	0.01	98.93
FD377_m5	44.94	11.51	16.26	8.42	12.06	0.07	2.30	2.43	0.29	0.09	98.36
FD377_m6	70.71	20.38	0.00	0.12	0.09	0.00	0.00	11.94	0.03	0.01	103.28
FD377_m7	70.86	20.39	0.00	0.14	0.10	0.02	0.00	12.69	0.03	0.00	104.23
FD377_m8	29.98	19.20	27.17	10.21	0.06	0.09	0.03	0.02	0.00	0.15	86.91
FD377_m9	57.61	0.71	21.11	4.61	13.72	0.06	0.00	0.05	0.01	0.01	97.90
FD377_m10	39.32	30.63	0.02	3.84	24.45	0.06	0.04	0.12	0.01	0.00	98.49
FD377_m11	39.59	30.28	0.03	4.59	24.55	0.02	0.09	0.02	0.01	0.12	99.27
FD377_m12	70.42	20.68	0.06	0.20	0.48	0.00	0.00	11.64	0.04	0.01	103.52
FD377_m13	31.61	21.33	25.33	9.68	0.31	0.16	0.03	0.07	0.00	0.03	88.55
FD377_m14	39.12	27.58	3.20	1.60	21.48	0.17	0.10	0.28	0.00	0.00	93.50
FD377_m15	69.45	20.19	0.00	0.09	0.11	0.03	0.00	11.75	0.03	0.00	101.64
FD377_m16	58.21	0.41	21.65	4.68	13.37	0.10	0.03	0.07	0.00	0.05	98.57
FD377_m17	28.59	21.72	25.74	11.08	0.03	0.10	0.01	0.03	0.01	0.08	87.39
FD377_m18	55.03	30.66	3.23	0.70	0.03	0.00	0.07	0.33	9.97	0.01	100.03
FD377_m19	69.87	20.37	0.00	0.14	0.13	0.01	0.00	12.24	0.03	0.00	102.77
FD377_m20	53.58	30.30	3.23	0.78	0.08	0.00	0.05	0.53	9.26	0.00	97.80
FD377_m21	39.25	27.38	3.21	1.68	21.99	0.17	0.08	0.08	0.02	0.00	93.87
FD377_m22	38.78	28.07	0.00	7.50	23.84	0.02	0.05	0.03	0.01	0.00	98.29
FD377_m23	38.10	27.05	3.28	1.38	22.29	0.15	0.04	0.08	0.03	0.00	92.39
FD377_m18b	53.50	31.01	3.48	0.83	0.03	0.00	0.08	0.09	10.12	0.05	99.17
FD377_m18b	53.43	31.01	3.23	0.73	0.04	0.00	0.06	0.25	9.76	0.03	98.53
FD377_m24	42.52	12.17	15.54	8.97	11.86	0.04	3.07	2.51	0.26	0.14	97.09
FD377_m25	29.61	19.80	26.21	10.27	0.03	0.08	0.00	0.00	0.01	0.19	86.21
FD377_m26	29.57	19.40	25.94	10.47	0.07	0.09	0.01	0.03	0.00	0.22	85.80
FD377_m27	57.76	0.40	21.80	4.58	13.51	0.12	0.00	0.03	0.00	0.07	98.25
FD377_m28	57.35	0.38	21.22	4.91	13.31	0.10	0.01	0.17	0.03	0.12	97.59
FD377_m29	43.93	11.78	15.82	8.65	11.85	0.11	2.95	2.70	0.30	0.13	98.21
FD377_m30	43.62	12.12	15.50	8.68	11.90	0.15	3.26	2.67	0.28	0.17	98.34
FD377_m31	43.84	12.02	15.68	8.27	11.95	0.11	2.91	2.44	0.31	0.09	97.62
FD377_m32	57.64	0.63	21.37	4.78	13.32	0.04	0.05	0.18	0.00	0.07	98.09
FD377_m33	57.49	0.46	21.45	4.27	13.41	0.18	0.00	0.02	0.01	0.02	97.30
FD377_m34	48.59	8.57	24.26	2.80	5.36	0.02	0.02	0.07	0.00	0.04	89.72
FD377_m35	38.18	27.25	3.72	1.33	22.31	0.23	0.03	0.13	0.03	0.02	93.23

FD377_m36	39.25	30.19	0.05	5.13	24.33	0.05	0.09	0.03	0.02	0.02	99.15
FD377_m37	55.28	25.87	5.09	1.64	0.20	0.01	0.03	3.95	5.78	0.01	97.85
FD377_m38	53.71	28.14	4.53	1.17	0.13	0.03	0.04	0.63	10.09	0.00	98.47
FD377_m39	54.99	29.27	3.89	1.23	0.19	0.03	0.06	0.20	9.58	0.10	99.54
FD377_m39b	54.36	30.72	3.65	0.97	0.55	0.04	0.05	0.30	9.55	0.05	100.23
FD377_m40	68.85	20.22	0.00	0.13	0.14	0.02	0.00	11.37	0.02	0.03	100.77
FD377_m41	69.62	20.09	0.01	0.15	0.13	0.00	0.02	11.32	0.02	0.01	101.38
FD377_m42	68.38	20.27	0.00	0.12	0.15	0.03	0.01	11.49	0.02	0.00	100.47

Table of samples

Sample	Lithology	Unit	Area	Foliation	Lineation
FD01	Gneiss	Dent Blanche	Allein	186/30	219/20
FD02	Calcschist	Tsaté	Allein	120/28	134/28
FD03	Calcschist	Cimes Blanches	Allein	98/25	122/19
FD04	Greenschist	Tsaté	Allein	47/23	
FD05	Calcschist	Tsaté	Allein	346/15	346/15
FD06	Calcschist	Tsaté	Ollomont	128/20	128/20
FD07	Mylonite	Dent Blanche	Ollomont	77/25	114/22
FD08	Metapegmatite	Dent Blanche	Ollomont	123/66	218/19
FD09	Greenschist	Tsaté	Aosta	54/50	68/12; 106/23
FD10	Calcschist	Tsaté	Aosta	137/50	104/44
FD11	Calcschist	Tsaté	Aosta	140/26	115/24
FD12	Calcschist	Tsaté	Aosta	132/21	132/21
FD13	Calcschist	Tsaté	Aosta	20/37	75/24
FD14	Greenschist	Tsaté	Aosta	178/06	81/01
FD15	Calcschist	Tsaté	Barthelemy	323/45	295/44
FD16	Mylonite	Dent Blanche	Barthelemy	264/10	284/13
FD17	Mylonite	Dent Blanche	Barthelemy	166/09	106/04
FD18	Mylonite	Dent Blanche	Barthelemy	56/21	82/16
FD19	Mylonite	Dent Blanche	Trois Ville	188/22	124/05
FD20	Mylonite	Dent Blanche	Trois Ville	290/34	278/30
FD21	Mylonite	Dent Blanche	Trois Ville	229/20	268/16
FD22	Calcschist	Tsaté	Cignana	291/31	316/28
FD23	Calcschist	Tsaté	Cignana	322/21	0/23
FD24	Calcschist	Zermatt-Saas	Cignana	330/39	312/37
FD25	Quartzite	Cimes Blanches	Cignana	319/10	336/10
FD26	Quartzite	Cimes Blanches	Cignana	269/10	331/08
FD27	Quartzite	Cimes Blanches	Cignana	295/21	335/18
FD28	Quartzite	Cimes Blanches	Cignana	278/20	327/12
FD29	Marble	Cimes Blanches	Cignana	352/14	352/14
FD30	Quartz vein	Tsaté	Cignana	322/44	289/36
FD31	Calcschist	Tsaté	Cignana	288/24	341/14
FD32	Greenschist	Tsaté	Cignana	325/20	315/20
FD33	Greenschist	Tsaté	Cignana	08/08	303/06
FD34	Greenschist	Tsaté	Cignana	66/15	332/02
FD35	Greenschist	Tsaté	Cignana	338/29	296/25
FD36	Calcschist	Tsaté	Cignana	342/24	300/12
FD37	Calcschist	Tsaté	Cignana	274/27	313/21
FD38	Calcschist	Tsaté	Cignana	296/09	293/09
FD39	Calcschist	Tsaté	Cignana	296/29	311/02
FD40	Mylonite	Dent Blanche	Cignana	254/35	304/27
FD41	Mylonite	Dent Blanche	Cignana	244/22	312/16
FD42	Mylonite	Dent Blanche	Cignana	276/21	318/11

FD43	Mylonite	Dent Blanche	Breuil	198/08	142/05
FD44	Mylonite	Dent Blanche	Breuil	199/10	131/02
FD45	Mylonite	Dent Blanche	Breuil	215/10	136/03
FD46	Mylonite	Dent Blanche	Breuil	245/09	320/02
FD47	Calcschist	Tsaté	Breuil	300/29	340/21
FD48	Mylonite	Dent Blanche	Breuil	222/03	312/00
FD49	Greenschist	Tsaté	Zermatt	331/39	252/03; 310/28
FD50	Metasediment	Cimes Blanches	Zermatt	251/19	221/19
FD51	Quartzite	Cimes Blanches	Zermatt	338/19	359/17; 276/14
FD52	Calcschist	Tsaté	Zermatt	00/30	09/28
FD53	Marble	Tsaté	Zermatt	340/20	00/18
FD54	Calcschist	Tsaté	Zermatt	342/22	302/22
FD55	Greenschist	Tsaté	Zermatt	322/39	343/34
FD56	Calcschist	Tsaté	Zermatt	326/13	320/15
FD57	Calcschist	Tsaté	Zermatt	338/15	326/23
FD58	Calcschist	Tsaté	Zermatt	311/28	280/25; 326/27
FD59	Metabasite	Zermatt-Saas	Zermatt	303/41	259/31
FD60	Metabasite	Zermatt-Saas	Zermatt	289/36	260/30
FD61	Metabasite	Zermatt-Saas	Zermatt		
FD62	Metabasite	Zermatt-Saas	Zermatt	309/28	245/14
FD63	Metasediment	Cimes Blanches	Zermatt	303/25	268/14
FD64	Metasediment	Cimes Blanches	Zermatt	292/19	224/10
FD65	Calcschist	Cimes Blanches	Zermatt	278/17	278/17; 218/10
FD66	Calcschist	Cimes Blanches	Zermatt	300/33	258/25; 324/28
FD67	Metabasite	Zermatt-Saas	Zermatt		
FD68	Metabasite	Zermatt-Saas	Zermatt	271/37	239/34
FD69	Calcschist	Tsaté	Zermatt	265/27	265/27
FD70	Calcschist	Tsaté	Zermatt	263/27	244/25
FD71	Calcschist	Tsaté	Zermatt	238/28	180/13
FD72	Calcschist	Tsaté	Zermatt	288/18	319/20
FD73	Calcschist	Tsaté	Zermatt	333/36	346/35
FD74	Calcschist	Tsaté	Zermatt	334/12	334/12
FD75	Metasediment	Cimes Blanches	Zermatt	284/12	276/13
FD76	Metasediment	Cimes Blanches	Zermatt	284/27	278/18
FD77	Metasediment	Cimes Blanches	Zermatt	277/19	299/17
FD78	Calcschist	Tsaté	Zermatt	349/23	285/12
FD79	Calcschist	Tsaté	Zermatt	06/15	293/08; 30/24
FD80	Quartzite	Cimes Blanches	Zermatt	316/18	312/17; 02/12
FD81	Metasediment	Cimes Blanches	Zermatt	264/21	299/16; 264/21
FD82	Metabasite	Zermatt-Saas	Zermatt	326/49	247/09; 259/25
FD83	Calcschist	Cimes Blanches	Zermatt	279/15	252/13
FD84	Calcschist	Frilihorn	Zermatt	272/23	276/21
FD85	Metasediment	Frilihorn	Zermatt		
FD86	Calcschist	Frilihorn	Zermatt	289/29	249/14
FD87	Greenschist	Tsaté	Zermatt	316/30	304/29; 234/05
FD88	Calcschist	Tsaté	Zermatt	276/23	287/22
FD89	Calcschist	Tsaté	Zermatt	302/17	324/20

FD90	Calcschist	Tsaté	Zermatt	333/18	303/17
FD91	Calcschist	Tsaté	Zermatt	267/22	329/08
FD92	Gneiss	Dent Blanche	Arolla	318/34	292/31; 279/31
FD93	Gneiss	Dent Blanche	Arolla	302/43	302/43
FD94	Gneiss	Dent Blanche	Arolla	300/32	276/24
FD95	Quartzite	Dent Blanche	Arolla	346/40	281/18
FD96	Gneiss	Dent Blanche	Arolla	335/31	291/23; 326/34
FD97	Gneiss	Dent Blanche	Arolla	318/38	284/36
FD98	Gneiss	Dent Blanche	Arolla	257/19	257/19
FD99	Gneiss	Dent Blanche	Arolla	285/49	235/30
FD100	Metasediment	Tsaté	Arolla	146/77	63/41
FD101	Gneiss	Dent Blanche	Arolla	266/28	286/18
FD102	Calcschist	Tsaté	Arolla	222/35	146/08; 166/16
FD103	Calcschist	Tsaté	Arolla	193/32	129/22; 108/08
FD104	Calcschist	Tsaté	Arolla	152/13	115/12
FD105	Calcschist	Tsaté	Arolla	136/30	161/24
FD106	Metasediment	Tsaté	Arolla	185/49	156/52
FD107	Metasediment	Tsaté	Arolla	40/22	03/18
FD108	Metasediment	Tsaté	Arolla	53/16	16/16
FD109	Metasediment	Tsaté	Arolla		
FD110	Gneiss	Dent Blanche	Arolla	106/30	178/14; 72/27
FD111	Gneiss	Dent Blanche	Arolla	306/23	256/11
FD112	Gneiss	Dent Blanche	Arolla	316/62	252/19
FD113	Gneiss	Dent Blanche	Arolla	333/22	317/22
FD114	Gneiss	Dent Blanche	Arolla	317/17	308/15; 357/13
FD115	Gneiss	Dent Blanche	Arolla	64/18	54/19
FD116	Greenschist	Tsaté	Arolla	110/37	107/35
FD117	Gneiss	Dent Blanche	Arolla	279/41	223/33
FD118	Gneiss	Dent Blanche	Arolla	272/23	272/23
FD119	Gneiss	Dent Blanche	Arolla	330/36	299/30; 239/05
FD120	Gneiss	Dent Blanche	Arolla	329/39	274/23
FD121	Gneiss	Dent Blanche	Arolla	303/71	301/70
FD122	Greenschist	Tsaté	Arolla	109/33	135/27
FD123	Gneiss	Dent Blanche	Arolla	94/22	127/19
FD124	Gneiss	Dent Blanche	Arolla	49/24	24/22; 330/05
FD125	Calcschist	Tsaté	Arolla	316/26	316/26
FD126	Greenschist	Tsaté	Arolla	177/17	249/06; 142/17
FD127	Greenschist	Tsaté	Arolla	158/46	146/45
FD128	Calcschist	Tsaté	Arolla	167/28	148/26
FD129	Gneiss	Dent Blanche	Arolla	180/61	273/05
FD130	Gneiss	Dent Blanche	Arolla	204/56	281/13
FD131	Gneiss	Dent Blanche	Arolla	182/55	272/00
FD132	Gneiss	Dent Blanche	Arolla	178/59	264/08
FD133	Gneiss	Dent Blanche	Arolla	184/63	272/10
FD134	Gneiss	Dent Blanche	Arolla	179/60	268/06
FD135	Calcschist	Tsaté	Zermatt	256/34	254/33
FD136	Marble	Frilihorn	Zermatt	266/34	237/29

FD137	Greenschist	Tsaté	Zermatt	221/22	248/19; 175/14
FD138	Greenschist	Tsaté	Zermatt	285/40	314/36
FD139	Mylonite	Dent Blanche	Zermatt	199/40	135/21
FD140	Mylonite	Dent Blanche	Zermatt	188/37	123/21
FD141	Mylonite	Dent Blanche	Zermatt	186/30	235/19
FD142	Mylonite	Dent Blanche	Zermatt	174/37	226/33; 125/24
FD143	Mylonite	Dent Blanche	Zermatt	226/31	173/20
FD144	Eclogite	Zermatt-Saas	Zermatt		
FD145	Metasediment	Tsaté	Zermatt	311/43	06/26
FD146	Mylonite	Dent Blanche	Zermatt	282/31	293/29
FD147	Mylonite	Dent Blanche	Zermatt	308/29	325/26
FD148	Mylonite	Dent Blanche	Zermatt	298/20	332/16
FD149	Mylonite	Dent Blanche	Zermatt	262/19	312/12
FD150	Mylonite	Dent Blanche	Zermatt	274/26	339/12
FD151	Metabasite	Zermatt-Saas	Zermatt	272/43	242/41
FD152	Metasediment	Zermatt-Saas	Zermatt	306/59	255/46
FD153	Metabasite	Zermatt-Saas	Zermatt	298/46	249/31
FD154	Metabasite	Tsaté	Zermatt	312/52	314/46
FD155	Calcschist	Tsaté	Zermatt	326/17	311/22
FD156	Calcschist	Tsaté	Zermatt	352/23	330/21
FD157	Metasediment	Tsaté	Zermatt	128/57	128/57
FD158	Metasediment	Tsaté	Zermatt	281/47	330/34
FD159	Mylonite	Dent Blanche	Zermatt	333/08	330/04
FD160	Mylonite	Dent Blanche	Zermatt	316/20	41/03; 312/25
FD161	Mylonite	Dent Blanche	Zermatt	354/18	39/09
FD162	Mylonite	Dent Blanche	Zermatt	307/05	307/05
FD163	Mylonite	Dent Blanche	Zermatt	268/20	303/15; 241/16
FD164	Metasediment	Cimes Blanches	Zermatt	327/31	250/09; 00/25
FD165	Metasediment	Cimes Blanches	Zermatt	270/43	225/33
FD166	Metasediment	Cimes Blanches	Zermatt	265/44	290/42
FD167	Metasediment	Cimes Blanches	Zermatt		
FD168	Metasediment	Cimes Blanches	Zermatt		
FD169	Garnet calcschist	Zermatt-Saas	Zermatt		
FD170	Garnet calcschist	Zermatt-Saas	Zermatt		
FD171	Calcschist	Tsaté	Zermatt	284/32	314/30
FD172	Quartzite	Cimes Blanches	Zermatt	284/31	284/31
FD173	Metabasite	Zermatt-Saas	Zermatt	294/30	249/20; 313/26
FD174	Metabasite	Tsaté	Zermatt	259/24	212/16
FD175	Garnet calcschist	Zermatt-Saas	Zermatt	278/30	206/16
FD176	Garnet calcschist	Zermatt-Saas	Zermatt	242/35	188/25
FD177	Eclogite	Zermatt-Saas	Cignana	274/33	260/32
FD178	Metasediment	Zermatt-Saas	Cignana	297/39	266/38
FD179	Metasediment	Zermatt-Saas	Cignana	344/37	281/26
FD180	Eclogite	Zermatt-Saas	Cignana	334/29	274/17
FD181	Serpentinite	Zermatt-Saas	Torgnon	256/15	253/15
FD182	Quartzite	Etirol-Levaz	Torgnon	349/34	64/06
FD183	Gneiss	Etirol-Levaz	Torgnon	332/39	44/14

FD184	Gneiss	Etirol-Levaz	Torgnon	330/33	277/20
FD185	Eclogite	Etirol-Levaz	Torgnon		
FD186	Eclogite	Zermatt-Saas	Cignana	284/31	271/24
FD187	Quartzite	Cimes Blanches	Cignana	343/55	282/38; 352/53
FD188	Quartzite	Cimes Blanches	Cignana	330/44	333/44
FD189	Quartzite	Cimes Blanches	Cignana	346/55	336/44
FD190	Eclogite	Zermatt-Saas	Cignana	264/34	306/22
FD191	Eclogite	Zermatt-Saas	Cignana	263/32	246/30
FD192	Eclogite	Zermatt-Saas	Cignana	188/39	262/12
FD193	Metasediment	Zermatt-Saas	Cignana	04/38	302/22
FD194	Metasediment	Zermatt-Saas	Cignana	04/29	294/26
FD195	Gneiss	Dent Blanche	Cignana	288/12	330/10
FD196	Gneiss	Dent Blanche	Cignana	314/02	322/02
FD197	Gneiss	Etirol-Levaz	Torgnon	202/43	252/31
FD198	Gneiss	Etirol-Levaz	Torgnon	199/48	117/09
FD199	Gneiss	Etirol-Levaz	Torgnon	212/40	283/15
FD200	Gneiss	Etirol-Levaz	Torgnon	126/35	151/37
FD201	Gneiss	Etirol-Levaz	Torgnon		
FD202	Gneiss	Etirol-Levaz	Torgnon		
FD203	Eclogite	Etirol-Levaz	Torgnon		
FD204	Gneiss	Etirol-Levaz	Torgnon	250/24	208/25
FD205	Gneiss	Etirol-Levaz	Torgnon	215/35	286/12
FD206	Gneiss	Dent Blanche	Moiry	253/51	344/01
FD207	Gneiss	Dent Blanche	Moiry	163/42	181/46
FD208	Gneiss	Dent Blanche	Moiry	170/61	170/61
FD209	Calcschist	Tsaté	Zinal	112/30	146/28
FD210	Calcschist	Tsaté	Zinal	112/30	156/23
FD211	Gneiss	Dent Blanche	Zinal	207/38	272/33
FD212	Gneiss	Dent Blanche	Zinal	206/46	289/07
FD213	Gneiss	Dent Blanche	Zinal	210/57	289/16
FD214	Gneiss	Dent Blanche	Zinal	186/46	160/43
FD215	Gneiss	Dent Blanche	Zinal	243/42	312/22
FD216	Gneiss	Dent Blanche	Zinal	260/22	319/12
FD217	Gneiss	Dent Blanche	Zinal	226/24	151/06
FD218	Gneiss	Dent Blanche	Zinal	233/18	159/04
FD219	Gneiss	Dent Blanche	Zinal	269/35	341/13
FD220	Quartzite	Dent Blanche	Zinal	259/38	
FD221	Gneiss	Dent Blanche	Zinal	246/41	186/23
FD222	Gneiss	Dent Blanche	Zinal	260/18	198/20
FD223	Gneiss	Dent Blanche	Zinal	238/41	320/07
FD224	Gneiss	Dent Blanche	Zinal	246/40	322/12
FD225	Gneiss	Dent Blanche	Zinal	230/31	149/03; 212/30
FD226	Greenschist	Tsaté	Tournalin	271/16	336/04
FD227	Greenschist	Tsaté	Tournalin	168/26	117/18
FD228	Greenschist	Tsaté	Tournalin	249/13	300/08
FD229	Quartz layer	Tsaté	Tournalin	261/08	299/06
FD230	Calcschist	Tsaté	Tournalin	118/14	130/13

FD231	Metasediment	Cimes Blanches	Tournalin	74/18	141/07
FD232	Metasediment	Cimes Blanches	Tournalin	112/22	148/16
FD233	Metasediment	Cimes Blanches	Tournalin	102/19	144/21
FD234	Gneiss	Etirol-Levaz	Torgnon	09/49	286/08
FD235	Greenschist	Tsaté	Torgnon	346/53	340/53
FD236	Gneiss	Etirol-Levaz	Torgnon	285/13	277/11
FD237	Gneiss	Etirol-Levaz	Torgnon	279/32	254/29
FD238	Gneiss	Etirol-Levaz	Torgnon	256/29	268/27
FD239	Gneiss	Etirol-Levaz	Torgnon	308/21	240/08
FD240	Gneiss	Etirol-Levaz	Torgnon	192/38	110/06
FD241	Eclogite	Zermatt-Saas	Cignana	319/40	265/20
FD242	Metasediment	Zermatt-Saas	Cignana	163/48	80/14
FD243	Metasediment	Zermatt-Saas	Cignana	68/17	96/14
FD244	Eclogite	Zermatt-Saas	Cignana	318/22	269/16
FD245	Greenschist	Zermatt-Saas	Cignana	217/12	155/08
FD246	Calcschist	Zermatt-Saas	Cignana	92/39	328/33
FD247	Metagabbro	Etirol-Levaz	Torgnon	321/30	262/09
FD248	Metabasite	Etirol-Levaz	Torgnon	244/69	312/12
FD249	Metabasite	Etirol-Levaz	Torgnon	239/32	300/22
FD250	Eclogite	Zermatt-Saas	Cignana	324/52	324/52
FD251	Quartz layer	Zermatt-Saas	Cignana	315/19	292/17
FD252	Quartz layer	Zermatt-Saas	Cignana	256/23	289/18
FD253	Metasediment	Zermatt-Saas	Cignana	69/13	121/13
FD254	Greenschist	Zermatt-Saas	Cignana	208/32	142/09
FD255	Greenschist	Zermatt-Saas	Cignana	244/04	293/02
FD256	Greenschist	Zermatt-Saas	Cignana	64/16	68/15
FD257	Greenschist	Zermatt-Saas	Cignana	81/13	89/11
FD258	Gneiss	Etirol-Levaz	Torgnon	291/25	283/25
FD259	Gneiss	Etirol-Levaz	Torgnon	270/30	279/28
FD260	Gneiss	Etirol-Levaz	Torgnon		
FD261	Metabasite	Etirol-Levaz	Torgnon		
FD262	Metabasite	Etirol-Levaz	Torgnon		
FD263	Metasediment	Zermatt-Saas	Cignana	02/32	274/04
FD264	Metasediment	Zermatt-Saas	Cignana	313/27	300/25
FD265	Metasediment	Zermatt-Saas	Cignana	350/35	356/28
FD266	Calcschist	Zermatt-Saas	Cignana	356/31	304/18
FD267	Calcschist	Zermatt-Saas	Cignana	337/28	320/24
FD268	Gneiss	Dent Blanche	Breuil	306/31	306/31
FD269	Gneiss	Dent Blanche	Breuil	256/33	304/25
FD270	Gneiss	Dent Blanche	Breuil	270/63	326/47
FD271	Gneiss	Dent Blanche	Breuil	279/51	330/37
FD272	Gneiss	Dent Blanche	Breuil	284/46	312/40
FD273	Gneiss	Dent Blanche	Breuil	268/46	320/32
FD274	Garnet calcschist	Zermatt-Saas	Cignana	323/50	304/46
FD275	Garnet calcschist	Zermatt-Saas	Cignana	318/46	332/44
FD276	Greenschist	Zermatt-Saas	Cignana	306/35	322/32
FD277	Calcschist	Tsaté	Cignana	247/16	199/11

FD278	Calcschist	Tsaté	Cignana	248/10	326/02
FD279	Metasediment	Cimes Blanches	Dix	356/59	88/01
FD280	Metasediment	Cimes Blanches	Dix	342/79	69/10
FD281	Metasediment	Cimes Blanches	Dix	340/63	274/27
FD282	Quartzite	Cimes Blanches	Dix	201/08	286/01
FD283	Quartzite	Cimes Blanches	Dix	226/16	270/12
FD284	Quartzite	Cimes Blanches	Dix	149/47	101/36
FD285	Quartzite	Cimes Blanches	Dix	162/48	94/18
FD286	Quartzite	Cimes Blanches	Dix	161/33	98/16
FD287	Gneiss	Dent Blanche	Arolla	353/25	288/11
FD288	Gneiss	Dent Blanche	Arolla	344/38	281/20
FD289	Gneiss	Dent Blanche	Arolla	325/42	274/18
FD290	Gneiss	Dent Blanche	Arolla	354/40	288/04
FD291	Greenschist	Tsaté	Arolla	13/40	96/06
FD292	Gneiss	Dent Blanche	Arolla	336/43	272/19
FD293	Gneiss	Dent Blanche	Arolla	336/41	285/26
FD294	Gneiss	Dent Blanche	Arolla	303/21	284/16
FD295	Gneiss	Dent Blanche	Arolla	347/46	285/26
FD296	Gneiss	Dent Blanche	Arolla	350/55	60/26
FD297	Gneiss	Dent Blanche	Arolla	352/56	75/10
FD298	Gneiss	Dent Blanche	Arolla	342/60	57/24
FD299	Gneiss	Dent Blanche	Arolla	04/20	98/04
FD300	Metagabbro	Tsaté	Arolla		
FD301	Metagabbro	Tsaté	Arolla		
FD302	Metagabbro	Tsaté	Arolla		
FD303	Metagabbro	Tsaté	Arolla		
FD304	Metagabbro	Tsaté	Arolla		
FD305	Metagabbro	Tsaté	Arolla		
FD306	Metagabbro	Tsaté	Arolla		
FD307	Gneiss	Dent Blanche	Zinal	125/12	135/11
FD308	Gneiss	Dent Blanche	Zinal	105/13	139/07
FD309	Gneiss	Dent Blanche	Zinal	48/65	326/08
FD310	Gneiss	Dent Blanche	Zinal	214/43	128/12
FD311	Gneiss	Dent Blanche	Zinal	182/22	146/18
FD312	Gneiss	Dent Blanche	Zinal	231/15	151/03
FD313	Gneiss	Dent Blanche	Zinal	202/82	288/18
FD314	Metagabbro	Tsaté	Zinal		
FD315	Metagabbro	Tsaté	Zinal		
FD316	Metagabbro	Tsaté	Zinal		
FD317	Mylonite	Dent Blanche	Breuil	36/13	306/01
FD318	Mylonite	Dent Blanche	Breuil	46/11	133/01
FD319	Mylonite	Dent Blanche	Breuil	86/09	120/09
FD320	Mylonite	Dent Blanche	Breuil	98/12	119/16
FD321	Mylonite	Dent Blanche	Breuil	95/14	
FD322	Calcschist	Tsaté	Breuil	256/13	311/09
FD323	Greenschist	Tsaté	Breuil	13/24	310/12
FD324	Greenschist	Tsaté	Breuil	339/04	314/01

FD325	Mylonite	Dent Blanche	Breuil	05/13	318/06
FD326	Mylonite	Dent Blanche	Breuil	296/11	317/08
FD327	Mylonite	Dent Blanche	Breuil	359/16	311/10
FD328	Eclogite	Etirol-Levaz	Torgnon		
FD329	Eclogite	Etirol-Levaz	Torgnon		
FD330	Gneiss	Dent Blanche	Torgnon	340/23	318/21
FD331	Gneiss	Dent Blanche	Torgnon	257/17	317/04
FD332	Marble	Cimes Blanches	Bonatchiesse	329/52	240/02
FD333	Quartzite	Cimes Blanches	Bonatchiesse	314/38	238/12
FD334	Marble	Cimes Blanches	Bonatchiesse	320/38	242/12
FD335	Calcschist	Tsaté	Moiry	154/25	91/13
FD336	Quartz layer	Tsaté	Moiry	194/13	267/04
FD337	Quartz layer	Tsaté	Moiry	177/27	259/07
FD338	Quartzite	Cimes Blanches	Moiry	172/18	117/09
FD339	Quartzite	Cimes Blanches	Moiry	155/34	110/25
FD340	Metabasite	Etirol-Levaz	Torgnon		
FD341	Metabasite	Etirol-Levaz	Torgnon		
FD342	Garnet micaschist	Etirol-Levaz	Torgnon		
FD343	Eclogite	Etirol-Levaz	Torgnon		
FD345	Eclogite	Etirol-Levaz	Torgnon		
FD346	Calcschist	Tsaté	Becca d'Aver		
FD347	Calcschist	Tsaté	Becca d'Aver	180/12	116/11
FD348	Serpentinite	Tsaté	Becca d'Aver		
FD349	Mylonite	Dent Blanche	Ollomont	97/18	117/25
FD350	Mylonite	Dent Blanche	Ollomont	91/25	118/22
FD351	Mylonite	Dent Blanche	Ollomont	86/22	123/17
FD352	Calcschist	Tsaté	Becca d'Aver	136/17	122/17
FD353	Marble	Frilihorn	Becca d'Aver	183/15	137/07
FD354	Marble	Frilihorn	Becca d'Aver	165/28	124/25
FD355	Metasediment	BACS	Becca d'Aver		
FD356	Metasediment	BACS	Becca d'Aver	187/22	118/07
FD357	Metasediment	BACS	Becca d'Aver	152/13	96/15
FD358	Metasediment	BACS	Becca d'Aver	236/16	316/03; 282/11
FD359	Metasediment	Tsaté	Becca d'Aver	235/25	293/15
FD360	Calcschist	Tsaté	Becca d'Aver	246/28	314/08
FD361	Metasediment	BACS	Becca d'Aver	164/27	106/15
FD362	Metasediment	BACS	Becca d'Aver	201/35	201/30
FD363	Greenschist	Tsaté	Becca d'Aver	184/31	100/02
FD364	Calcschist	Tsaté	Becca d'Aver	204/34	118/02
FD365	Calcschist	Tsaté	Becca d'Aver	194/33	124/13
FD366	Calcschist	Tsaté	Becca d'Aver	173/28	136/23
FD367	Calcschist	BACS	Becca d'Aver	166/23	131/18
FD368	Calcschist	BACS	Becca d'Aver	145/28	118/29
FD369	Calcschist	BACS	Becca d'Aver	203/38	138/15
FD370	Metasediment	BACS	Becca d'Aver	356/02	304/01
FD371	Metasediment	BACS	Becca d'Aver	205/17	109/03
FD372	Metasediment	BACS	Becca d'Aver		

FD373	Metasediment	BACS	Becca d'Aver	161/30	106/22
FD374	Metasediment	BACS	Becca d'Aver	181/37	129/25
FD375	Metagabbro	Tsaté	Arolla		
FD376	Metagabbro	Tsaté	Arolla		
FD377	Metagabbro	Tsaté	Arolla		
FD378	Metagabbro	Tsaté	Arolla		
FD379	Metagabbro	Tsaté	Arolla		

Sample locations

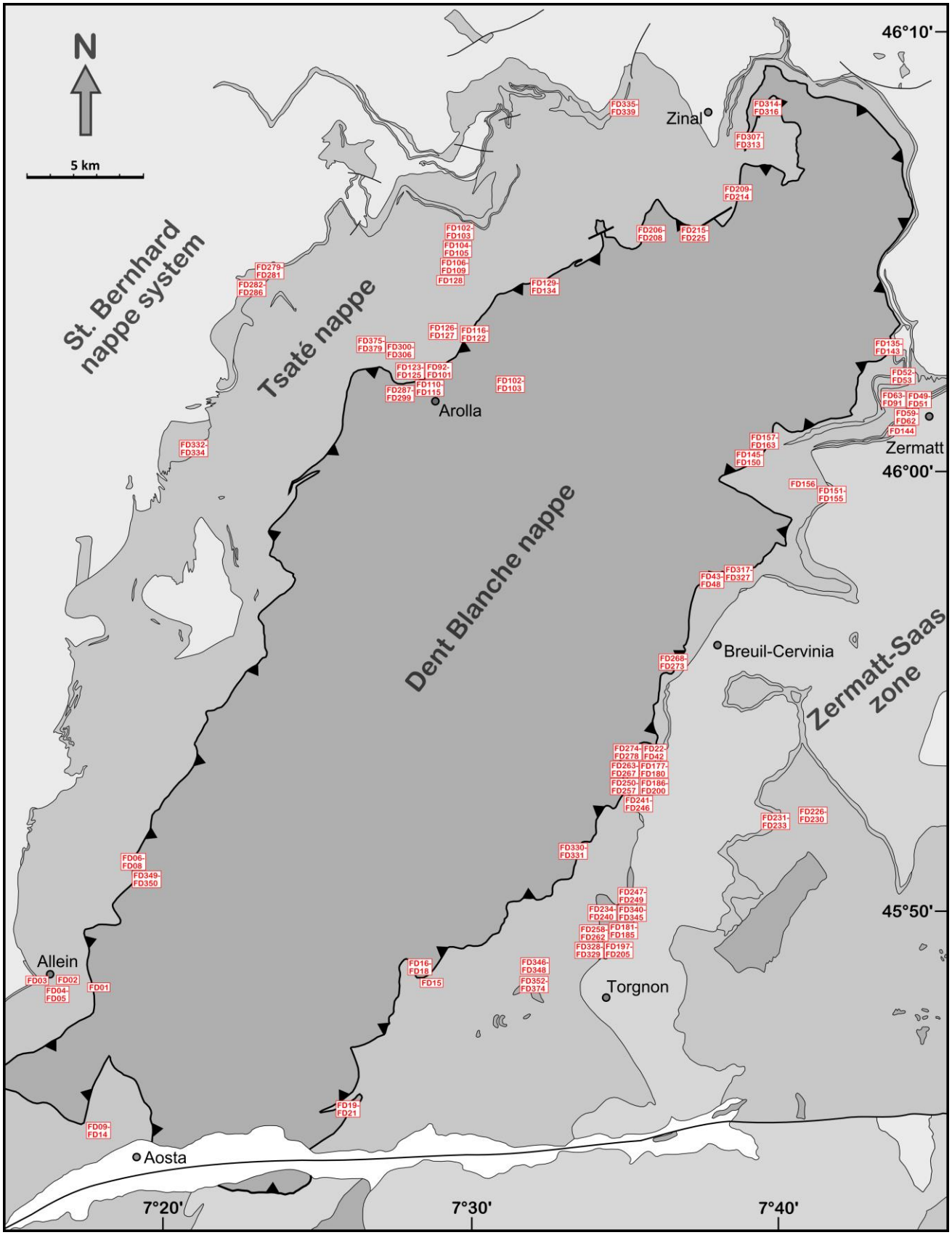

Map with approximate locations of samples taken for further microstructural and petrological investigations.
Note that locations of samples FD164 – FD176 are outside the depicted area east of Zermatt near Oberrothorn.